An Investigation into Nucleic Acid Binding Compounds

By

Fraser Scott

A thesis submitted to the WestCHEM, Department of Pure and Applied Chemistry, University of Strathclyde in part fulfilment of regulations for the degree of Doctor of Philosophy

January 2013

DECLARATION OF COPYRIGHT

This thesis is the result of the author's original research. It has been composed by the author and has not been previously submitted for examination which has led to the award of a degree.

Acknowledgements

I would like to express my graditiude to my supervisor Prof. Colin Suckling for his support and encouragement throughout the time of my PhD. The guidance and expertise he has provided has been invaluable in the completion of this thesis. I would also like to thank Dr. Colin Gibson for the advice he provided over the course of my PhD.

The people of lab TG416 have made every day a joy to work through and for this I would like to thank everyone I have had the pleasure to work alongside. At the very beginning of my PhD I had help settling in and would like to thank Dr. David Breen, Craig McInnes and Donna MacMillan for their help in this. A special thank you must go Dr. Abedawn Khalaf for his continous support and advice.

Finally I would like to thank all of my family and friends for supporting me and keeping me sane.

Contents

List of Abbreviations

AaR	aminoacyl-tRNA synthetase
A	adenine
AIR	5-aminoimidazole ribonucleotide
A. thaliana	*Arabidopsis thaliana*
BOC	di-*tert*-butyl-dicarbonate
C	cytosine
CMV	cytomegalovirus retinitis
DCC	*N,N'* -dicyclohexylcarbodiimide
DCM	dichloromethane
DIC	*N,N'* –Diisopropylcarbodiimide
DMF	*N,N'*-dimethyl formamide
DMSO	dimethyl sulfoxide
DNA	deoxyribonucleic acid
E. coli	*Escherichia coli*
EPI	efflux pump inhibitor
G	guanine
GTP	guanosine triphosphate
h	hour
HBTU	*O*-(benzotriazol-1-yl)-*N,N,N',N'*-tetramethyluronium hexafluorophosphate
hERG	human ether-a-go-go gene
HMP-P	hydroxymethylpyrimidine monophosphate
HMP-PP	hydroxymethylpyrimidine pyrophosphate
Hp	3-hydroxy-*N*-methylpyrrole
HPβCD	hydroxypropyl-β-cyclodextrin
HPLC	high performance liquid chromatography
HR-MS-FAB	high resolution mass spectrometry fast atom bombardment
h	hours

Im	*N*-methylimidazole
K_d	dissociation constant
LB	Lysogeny broth
M63	A minimal medium used for cultivation of bacteria
MD	molecular dynamics
MIC	minimum inhibitory concentration
Mins	minutes
MGB	minor groove binder
mRNA	messenger ribonucleic acid
MRSA	methicillin-resistant *Staphylococcus aureus*
NMM	*N*-methylmorpholine
NMR	nuclear magnetic resonance
OTPP	oxythiamine pyrophosphate
PDB	protein database
PFP	pentafluorophenol
PreQ0	7-cyano-deazaguanine
PreQ1	7-aminomethyl-7-deazaguanine
PT	pyrithiamine
PTPP	pyrithiamine pyrophosphate
Py	*N*-methylpyrrole
Q	queuosine
QueA	*S*-adenosylmethionine:tRNA ribosyltransferase-isomerase
QueF	$preQ_0$ oxidoreductase
RNA	ribonucleic acid
RMSD	root mean squared deviation
rRNA	ribosomal ribonucleic acid
s.e.	standard error
T	thymine
TEA	triethylamine
TFA	trifluoroacetic acid

TGT	tRNA-guanine transglycosylase
Thz-P	thiazole monophosphate
TLC	thin layer chromatography
TP	thiamine monophosphate
TPP	thiamine pyrophosphate
t pr	t probability
tRNA	transfer ribonucleic acid
U	uracil
UTR	untranslated region
Y	a pyrimidine base; cytosine or guanine

Biological Assays

Throughout this thesis a number a different assays were carried out against a range of organisms. For convienience the name and an appropriate classification of the organism (relative to this thesis) is presented below.

Name	**Classification**
EMRSA 16	Gram-positive bacterium
SMRSA 106	Gram-positive bacterium
Escherichia coli ATCC.8739	Gram-negative bacterium
Trypanosoma brucei	Parasite
Mycobacterium marinum ATCC BAA535	Gram-positive bacterium
Klebsiella pneumoniae NDM-1 ATCC BAA-2145	Gram-negative bacterium
Klebsiella pneumoniae ATCC -13883	Gram-negative bacterium
Pseudomonas aeruginosa ATCC-27853	Gram-negative bacterium
Leishmania	Parasite

Abstract

Antibiotic reistance has become a major cause for concern in recent times and as such there is increased demand for new drugs that can obviate this issue. The vast majority of drugs exert their therapeutic effects by interfering with protein function; few drugs target the nucleic acid structures of DNA or RNA. Since these structures are underutilised as drug targets by comparison to proteins, it is desirable to design new antibiotics that target them. This allows new mechanisms of action to be explored and thus assists in circumventing the problem of antibiotic resistance.

The Suckling group have been developing molecules that bind to the minor groove of DNA for many years and, when this PhD commenced, a panel of these were under preclinical investigation by an industrial collaborator. An investigation into the optimisation and scale up of these compounds will be discussed within this thesis. It will be revealed that one of the initial panel of lead compounds has been chosen to progress to Phase I clinical trials against both *Clostridium Difficile* and Methicillin-resistant *Staphylococcus aureus* (MRSA) and as such the investigation into suitable formulations will be discussed. Whilst a lead candidate had been selected this did not deter further investigation into minor groove binding compounds and this thesis also investigates modifications to these compounds that can lower affinity to the hERG ion channel, a major pharmaceutical anti-target. Whilst a range of our compounds display significant activity against Gram positive bacteria, very few have significant activity against Gram negative species. In order to investigate this, a series of compounds has been synthesised, based on known Gram negative active compounds, and these have been tested for activity against *Pseudomonas aeruginosa*. The proposed reason for the lack of activity, efficient cell efflux, was investigated by using an efflux pump inhibitor in the antibacterial assay and the results of this will be discussed.

Very few drugs target RNA and because of this there is still much basic science to be learned about using RNA as drug target. This thesis has focused on obtaining more information on a recently discovered RNA element, known as a riboswitch, and their use as drug targets. In achieveing this two riboswitches have been selected to be investigated: the thiamine pyrophosphate riboswitch and the

PreQ1 riboswitch. The suitability of each of these riboswitches as drug targets has been explored; however, in the case of the thiamine pyrophosphate riboswitch a set of novel modulators of this riboswitch have been prepared and shown by our collaborators to inhibit the growth of Gram negative bacteria. This is the first time that the TPP riboswitch has been shown to be a potential drug target.

1 Introduction

1.1 Introduction: Nucleic Acids

1.1.1 Nucleic Acid Structure

The nucleic acids are one of the three major classes of biological macromolecule along with carbohydrates and proteins. There are two classes of nucleic acids: deoxyribonucleic acid (DNA) and ribonucleic acid (RNA). DNA is the store of genetic information in all cellular life, along with some viruses, and has two functions: to direct its self replication and to undergo transcription which is the synthesis of molecules of RNA, called messenger RNA (mRNA), that are complementary to the DNA. RNA has a more varied role. The above mentioned mRNA is translated into a protein at the ribosome (rRNA) which is its self a catalytic RNA structure. The appropriate amino acids for the protein are delivered to the ribosome during protein synthesis by transfer RNAs (tRNAs). This relationship between DNA, RNAs and proteins is illustrated in figure 1. Additionally, many viruses often use RNA instead of DNA as their source of genetic information.

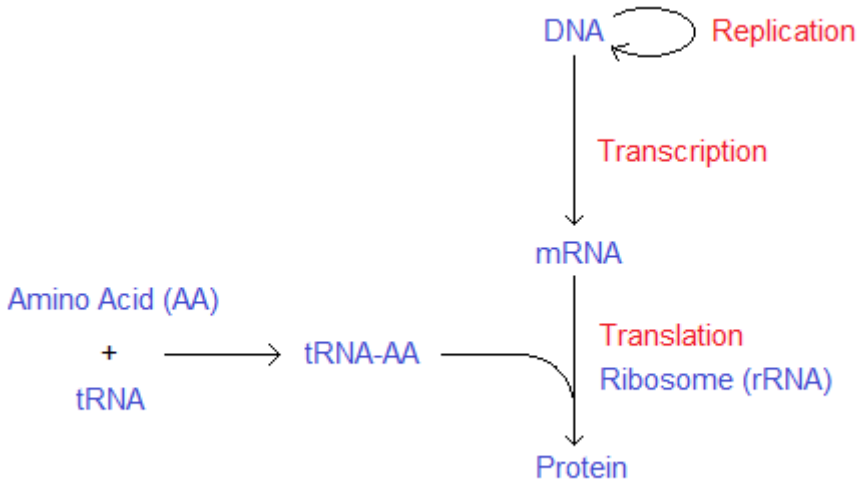

Figure 1: The relationship between DNA, RNAs and protein. Biological molecules, blue. Names of processes, red.

All of the processes illustrated in figure 1 are mediated by a variety of proteins. The unwinding and winding of DNA, required for both replication and transcription, is controlled by topoisomerases which must bind to the DNA in order

to exert their effects. Transcription of DNA to mRNA also uses proteins known as transcription factors that can upregulate or downregulate the transcription of specific genes by binding to regions of DNA. The process of attaching an amino acid to its respective tRNA is also carried out by a protein called an aminoacyl-tRNA synthetase.[1]

Nucleic acid structures are linear polymers of nucleotides and these nucleotides are composed of a phosphate group, a pentose sugar and a nitrogenous base. The two types of nucleic acids are differentiated by the pentose sugar incorporated into their nucleotide: RNA has a ribose sugar whereas DNA has a deoxyribose sugar. The structure of each of these pentose sugars is shown below (fig. 2).

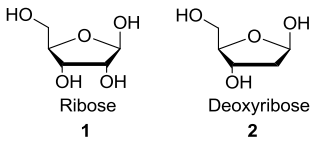

Figure 2: Structure of deoxyribose.

Attached to the pentose sugar is one of five nitrogenous bases: adenine (A), cytosine (C), guanine (G), thymine (T) or uracil (U). A and G are from a set of heterocyclic molecules called purines whilst C, T and U are from one called pyrimidines. DNA uses only A, T, C and G in its structure whereas RNA uses U instead of T. Their structures are shown below (fig. 3).

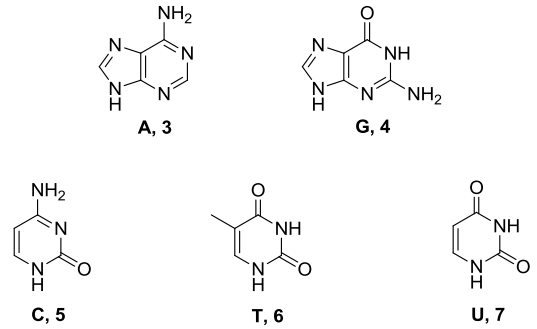

Figure 3: Purines (A and G) and pyrimidines (C ,T and U) which constitute the bases of DNA and RNA.

When the ribose sugar and one of the nitrogenous bases are joined they form a structure known as a nucleoside (fig. 4).

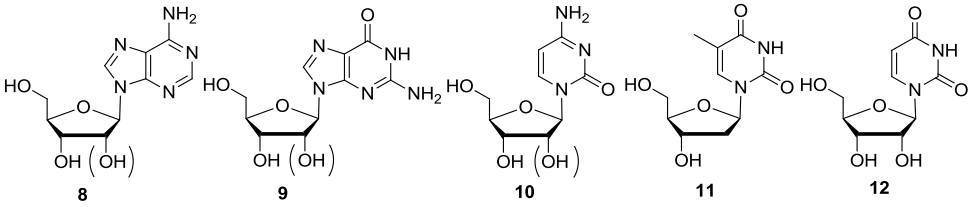

Figure 4: The structure of the nucleosides of DNA (or RNA).

With the addition of one final component, the phosphate group, the building block of DNA and RNA is obtained: the nucleotide (fig. 5).

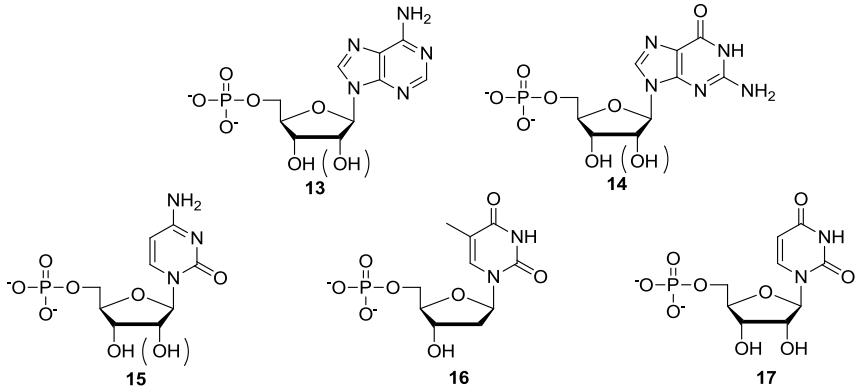

Figure 5: The structure of the five nucleotides of nucleic acids.

The structre of the nucleic acids RNA and DNA are polymers of the above nucleotides. In the final polymeric structre the phosphate of one nucleotide is attached to the free hydroxyl group of the next, and so on, forming a sugar phosphate backbone (fig. 6). The phosphodiester groups of these polynucleotides are acidic so that at physiological pH of 7.4, nucleic acids are polyanions and thus counter ions are often needed for stabilisation.

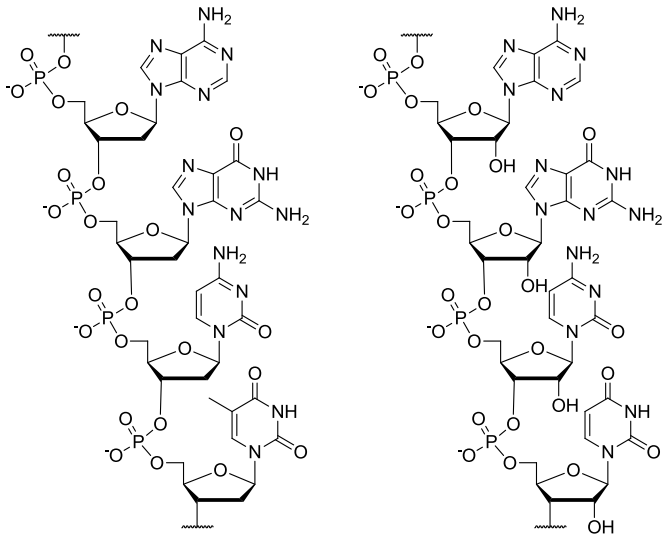

Figure 6: Segments of nucleic acids: DNA on the left; and, RNA on the right.

Extended segments of nucleic acids do not exist as linear chains; instead, they interact with either another molecule of nucleic acid or they interact intramolecularly. These interactions are hydrogen bonds between the bases of the nucleotides and are governed by the Watson-Crick base pairing rules. It is found that G forms three hydrogen bonds with C and A forms two hydrogen bonds with T, or U if RNA is the nucleic acid in the configurations shown below (fig. 7).

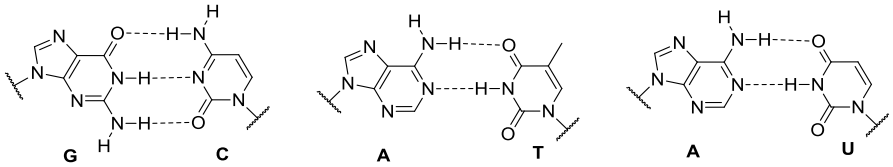

Figure 7: Watson-Crick base pairing.

These Watson-Crick base pairs are not the only types of hydrogen bonding interaction to be found between bases; however, they are the interactions that predominate in DNA. In RNA a much wider assortment of hydrogen bonding patterns are observed, for example, Hoogsteen base pairing occurs between the N7 position and the C6 amino group of an A which bind to the Watson-Crick face of T or U. To form a G/C Hoogsteen base pair the C must be protonated. (fig. 8).

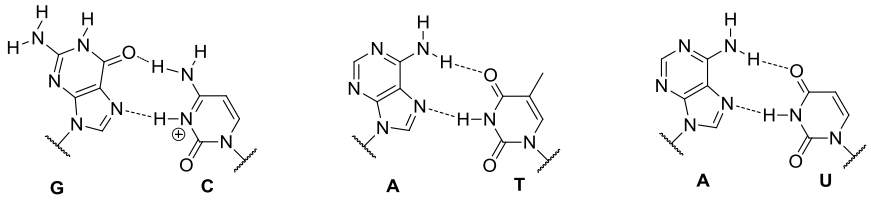

Figure 8: Hoogsteen base pairing.

Base pairing allows the formation of stable secondary and tertiary structures of the nucleic acids. In particular, the non Watson-Crick base pairs are important for RNA's ability to form a wide variety of secondary structures.[2]

1.1.2 DNA Structure and Function

The predominant form of secondary structure encountered in cellular DNA is the double helix; however, there exist several forms of this, the most common being the B-form DNA helix. This is the form of DNA that was elucidated by Watson and Crick from Rosalind Franklin's famous X-ray diffraction experiments in 1953 (fig. 9).[3]

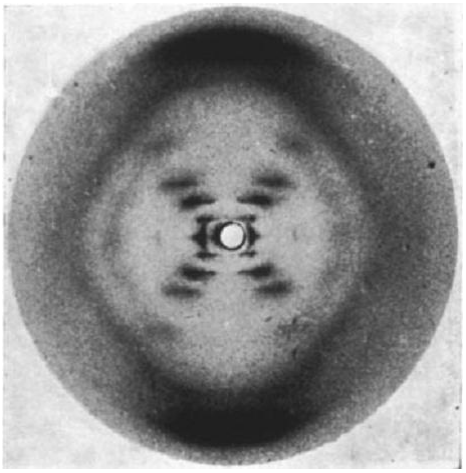

Figure 9: An X-ray diffraction photograph of vertically oriented sodium salt of DNA in the B-form helical conformation (Reproduced with permission, see appendix 1).

This form of DNA consists of two DNA strands, in opposite directions to each other, which wind around a common axis with a right handed twist to form a double helix with a diameter of about 20 Å. The bases of the nucleotides are stacked within the core of the helical structure, which provides stabilising π-π interactions

and the sugar-phosphate backbone occupies the exterior of the helix, such that the repulsions between the anionic phosphates are minimised. Each base on one strand is hydrogen bonded to its complementary base on the opposite strand, based on strict Watson-Crick base pairing rules, and the plane of this two base platform is almost perpendicular to the axis of the double helix. It is found that one turn of the helix contains ten base pairs which is equivalent to 34 Å per turn, given a thickness of 3.4 Å per base pair (fig. 10).[1]

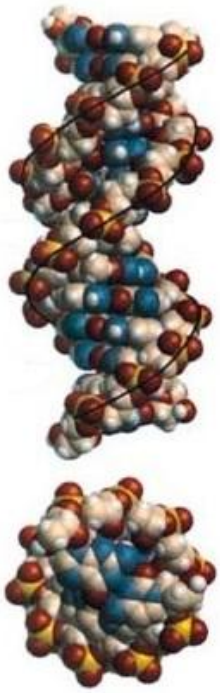

Figure 10: B-form DNA helix. Side view, top; top down view, bottom (reproduced with permission, see appendix 2).[5]

This B-form DNA helix can only be maintained if the Watson-Crick pairing rules are strictly adhered to; however, the ordering of these base pairing units is inconsequential to the overall topology of the B-form helix. This is because the position of its C1' atom is identical for an A/T or G/C base pair and thus the geometry of the sugar-phosphate backbone would be the same. Any other combination of bases, or non-Watson-Crick hydrogen bonding pattern would result in a distortion of the B-form DNA helix (fig. 11). This is somewhat of an oversimplification as the sequence of A/T or G/C runs in a B-form helix can lead to

regions of local distortion in topology; however, the average structure still remains that of B-form helix due to the geometric similarity of the A/T or G/C base pairs. The local conformation of DNA is thus irregular in a sequence specific manner which is important for recognition by biological macromolecules.

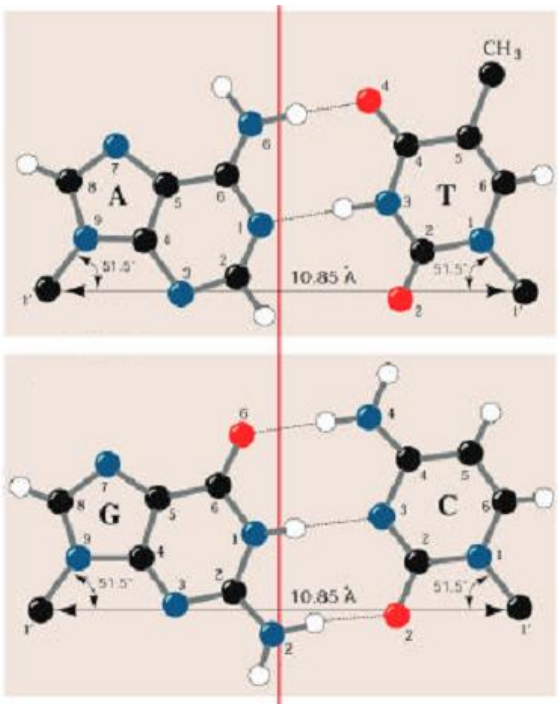

Figure 11: Arrangement of base pairs that results in identical geometries of base pairs. The line joining the C1' atoms is the same length, 10.85 Å for both base pairs. This line makes the same angle, of 51.5°, with the glycosidic bonds to the bases (reproduced with permission, see appendix 2).[5]

The most important topological feature of the B-form DNA helix are the two grooves that the spiralling sugar-phosphate backbone makes along the double helix. These grooves are unequal in size; the major groove is about 22 Å wide and the minor groove about 12 Å wide (fig. 12). This disparity in size makes the sequence of bases more accessible to biological macromolecules in the major groove and thus these tend to interact here, for example transcription factors, which are proteins involved in the regulation of transcription, interact with the edges of the bases via complexation to the major groove.[1]

B-DNA form is the most common under the conditions found in cells; however, A-form DNA and Z-form DNA are also encountered. A-form DNA is a wider and flatter helix still with a right hand twist. It has 11 base pairs per turn,

one turn covers 28 Å, and the base pairs themselves are tilted by 20°. This has the effect of giving the structure a deep major groove and a very shallow minor groove with a hole down the centre of the helix (fig. 12). It has been found to occur in DNA-RNA hydrid structures and also in protein-DNA complexes. Whilst the A-form DNA helix retains a very similar structure to B-form, Z-form DNA is rather distinct as it is a left-handed helix. This helix, has 12 base pairs per turn, is significantly stretched in comparison to the others as one turn takes place over 45 Å and the base pairs are tilted by 7°. The helix has a deep major groove but no noticeable minor groove. This more unusual structure can be recognized by specific Z-DNA binding proteins and is thought to be involved in the regulation of transcription.[1]

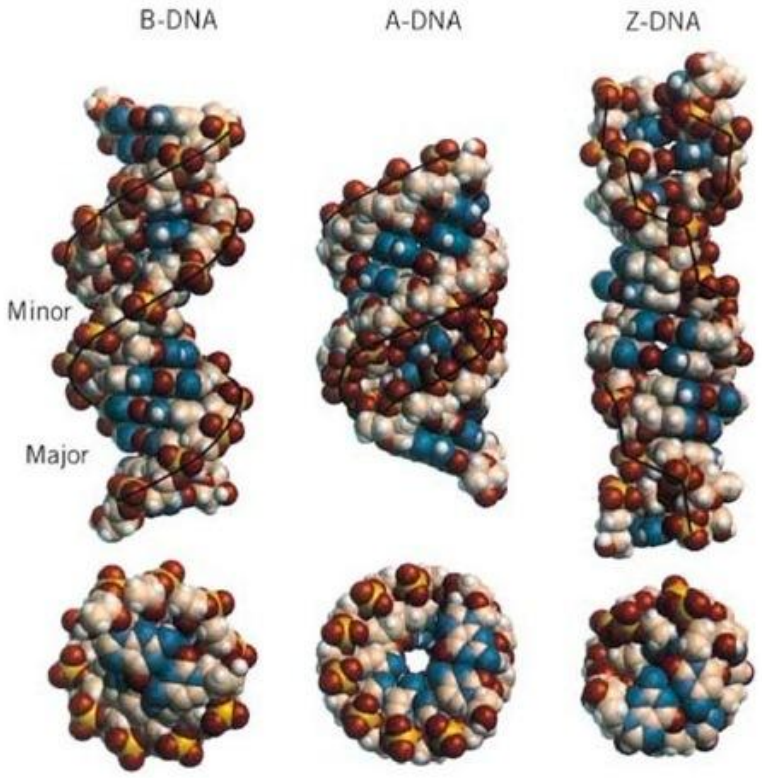

Figure 12: Contrasting structures different DNA helices. Side view, top; top down view, bottom (reproduced with permission, see appendix 2).[5]

1.1.3 Targeting DNA With Small Molecules

There are two modes in which small molecules can bind to DNA: non-covalent and covalent. A covalent interaction results in the formation of an adduct

between the DNA and small molecule and thus a permanent change to the DNA. These can be exemplified by DNA alkylating compounds.

Alkylators are strongly electrophilic compounds that are irreversible inhibitors of transcription and translation. Nucleophilic substitution reactions at the DNA bases occurs at the most reactive sites: those that are both nucleophilic and exposed in the grooves of the DNA helix. The N7 atom of guanine and the N3 atom of adenine fulfil both of these criteria. Sulfur mustard **18a** is a highly toxic nerve gas that was used during the First World War (fig. 13). Although too toxic for use in cancer therapy, it led to the development of a series of compounds known as nitrogen mustards that signalled the beginning of modern cancer chemotherapy. Mechlorethamine **18b** was the first of these compounds to be used in the treatment of advanced Hodgkin's disease (fig. 13).[4]

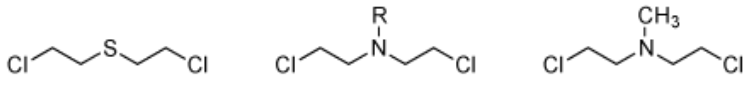

Figure 13: Structures of sulfur mustards and nitrogen mustards.

The mechanism of action of the mustards begins with the formation of an electrophilic aziridinium ion **19** by displacement of chloride. The aziridinium ion **19** is then attacked by a nucleophilic DNA base and then this happens once again to cross-link two strands of DNA (fig. 14).

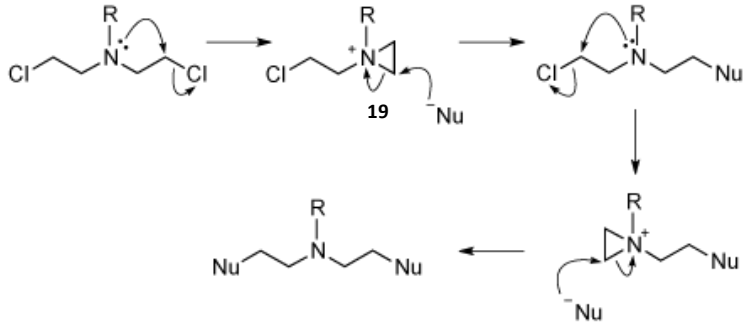

Figure 14: Mechanism of action of mustards.

Noncovalent interactions are reversible interactions with DNA and there are conceptually three distinct types of possible interaction: small molecules may stack themselves between the base pairs, termed intercalation; they may interact with the functional groups of base pairs on the floor of the minor groove, termed minor groove binding and they may do the same in the major groove, termed major groove binding.

Intercalators tend to be flat aromatic or heteoaromatic molecules such that they can slide between the base pairs and afford some stabilisation to the DNA helix without disrupting the base pairing. The insertion of the intercalator Amsacrine **20** (fig. 15), a drug used to treat leukaemia, serves to lengthen the DNA helix by approximately 3 Å causing a slight unwinding of the DNA. This change in topology can prevent replication and transcription by reducing association between the DNA other macromolecules such as DNA polymerase, RNA polymerase and transcription factors. It has also been demonstrated to inhibit topoisomerases, which are involved in the winding and unwinding of DNA, by stabilising the topoisomerase-DNA complex.[4]

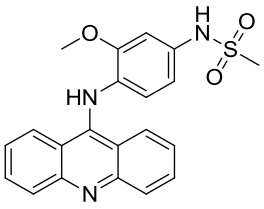

Amsacrine, **20**

Figure 15: Amsacrine, a DNA intercalator.

The major groove of B-form DNA helix is 22 Å wide which allows many biological macromolecules to interact with DNA through complexation to the major groove. However, the major groove is too large to give rise to give rise to favourable interactions with small molecules. Whilst the major groove of DNA is regarded to be too open for significant interactions between it and small molecules, the minor groove is more hospitable. Molecules which interact through binding to the minor groove, called minor groove binder (MGBs) are discussed in detail in section 1.2.[5]

1.1.4 RNA Structure and Function

RNA, like DNA, uses a much smaller set of basic building blocks compared to proteins and has the capacity to form a regular helix containing a major and minor groove. However, the stability of an RNA helix is much less than that of DNA and as a consequence a regular RNA helix is often disrupted by regions of mismatched or unpaired bases which allows RNA to adopt more complex three dimensional structures more akin to proteins. This wider array of structures gives rise to regions of RNA that can interact with other RNAs, proteins, small molecules and even form tertiary structures through intermolecular interactions. It is this diverse structure that allows RNA to be directly involved with transcriptional regulation,[6] translational regulation,[7] protein function,[8] and even catalysis,[9] each of which, until fairly recently, were all thought to be controlled by exclusively by proteins. The central dogma of molecular biology, in which RNA is viewed as only an intermediary between DNA and proteins, is no longer an accurate model.

The feature of RNA that gives rise to the differences in secondary structure between it and DNA is the presence of a hydroxyl group on the 2' carbon of the ribose sugar. The extra steric bulk causes the B-form RNA helix that would be formed to be much less stable and so an A-form RNA helix is the preferred helical structure. Given the lower stability of A-form helices over B-form helices then perturbations in the helix structure of RNA are common.

In contrast to the major and minor grooves of DNA, those of RNA do not form regions in which there are optimal binding sites for small molecules. The major groove of RNA is narrow and deep and the minor groove is shallow. These structural features prevent a fully base-paired RNA helix from providing a particularly hospitable environment for small molecule binding (figure 16).[10]

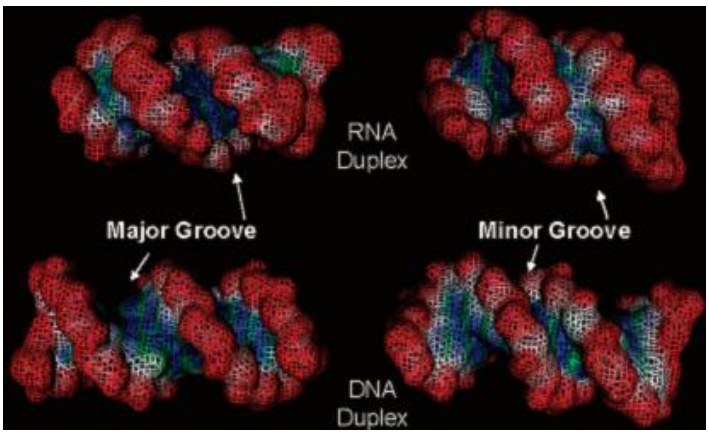

Figure 16: Contrasting topologies of DNA and RNA (Adapted with permission from (*Chem. Rev.*, 2008, 108, 117-1224). Copyright (2012) American Chemical Society).[12]

Small molecules could in principle bind in the major groove of RNA in which the discriminatory edges of the bases are projected and as such this is the information rich groove. Computational studies have demonstrated this groove to have a higher negative potential than the minor groove and so positively charged molecules would prefer to bind here. These pieces of information might indicate that the major groove could be used to bind small molecules; however, it has been demonstrated that in the A form helix, the major groove of RNA is only 4Å wide thus preventing access to small molecules. The minor groove, whilst more accessible, has the presence of the 2' hydroxyl as its only discriminatory feature and so is difficult to use as a target for small molecules to specifically bind to.[11]

Due to the less stable nature of A-form RNA, perturbations in the structure are common. These perturbations create a number of types of secondary structure: hairpin loops, internal loops and bulged regions (figure 17). The un- or mispaired bases that result in these secondary structures serves to widen the major groove and thus expose potential binding pockets for small molecules. This ability to bind small molecules is crucial to RNAs function as aptamers which will be discussed fully in section 1.3.[10]

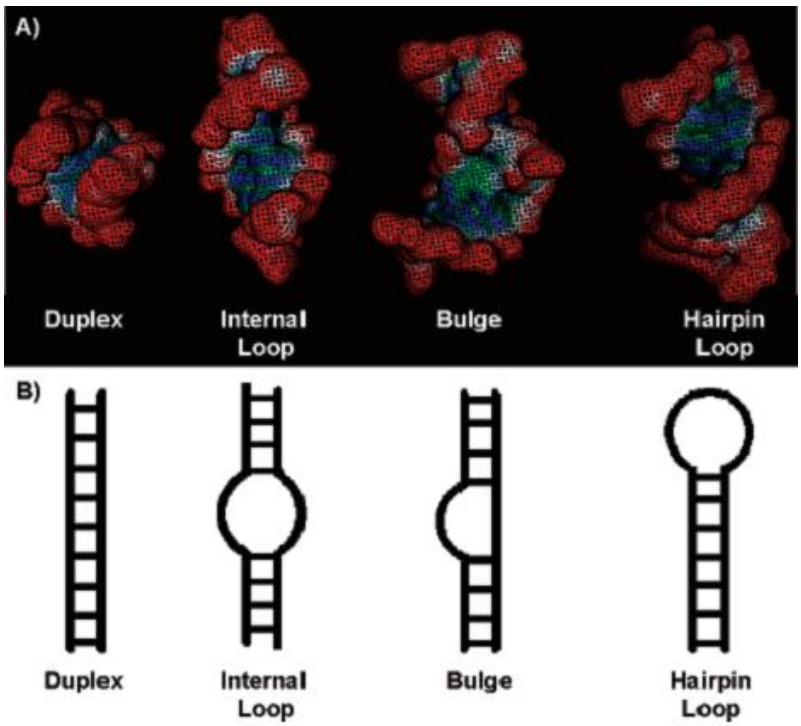

Figure 17: A) surface representation and B) schematic representation of RNA secondary structures (Adapted with permission from (*Chem. Rev.*, 2008, 108, 117-1224). Copyright (2012) American Chemical Society).[12]

1.1.5 Targeting RNA With Small Molecules

Presently, all RNA binding drugs target the ribosome, which is the RNA construct that is responsible for protein synthesis from an mRNA substrate. The prokaryotic ribosome consists of two subunits: the 30S, termed the small subunit, and the 50S, termed the large subunit. These are primarily composed of ribosomal RNA (rRNA); however, there are a number of proteins involved in this structure but they do not take part in the catalytic process. The 30S subunit carries out the responsibility of ensuring the correct transfer RNA (tRNA) molecule is recognised so the appropriate amino acid is added into the protein chain. The 50S subunit serves to catalyse the peptide bond formation between amino acids.[12]

The region within the 30S subunit that binds the tRNA molecule and hence carries out the proof reading duty is called the 16S A site. Here, binding of the correct tRNA molecule induces residues A1492 and A1493 to adopt an extrahelical

conformation; binding of an incorrect tRNA molecule does not afford the same shift in conformation (fig. 18).[13]

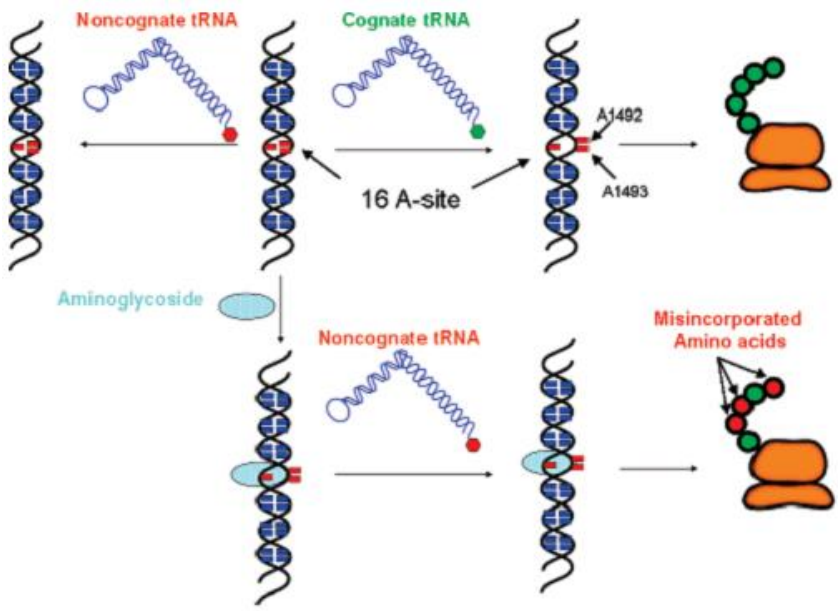

Figure 18: Formation of extrahelical conformation by tRNA binding and aminoglycoside binding and result on growing amino acid chain at the ribosome (Adapted with permission from (*Chem. Rev.*, 2008, 108, 117-1224). Copyright (2012) American Chemical Society).[12]

The aminoglycoside class of antibiotics exert their effects by binding to the 16S A site, inducing the extrahelical conformation and thus allowing incorrect tRNA molecules to be read as though they are the intended tRNA (fig. 18 and 19). This leads to the synthesis of dysfunctional proteins.[14]

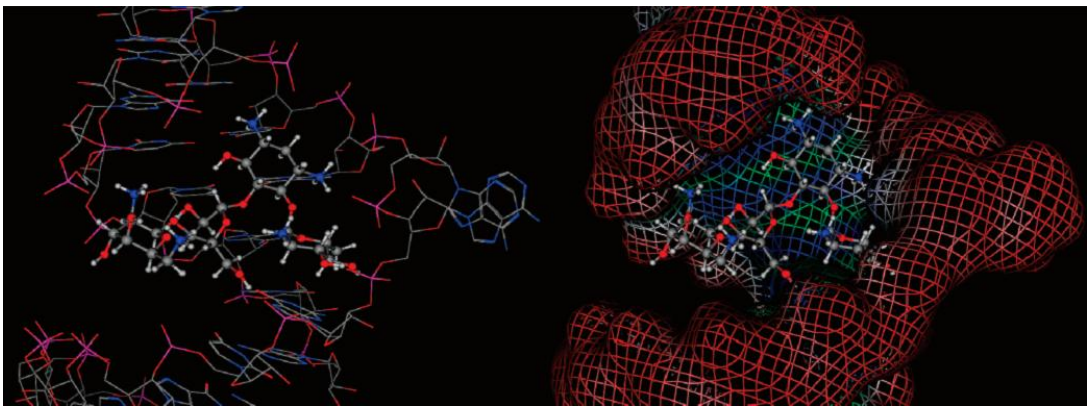

Figure 19: Induction of extrahelical conformation by an aminogycoside, paromomycin (*Chem. Rev.*, 2008, 108, 117-1224). Copyright (2012) American Chemical Society).[12]

The aminoglycosides are class of molecule that consist of amino-modified poly sugars. A number of examples are shown in figure 20. They are extensively used in evaluating RNA as a target due to their ability to bind to a wide range of RNA structures. This promiscuity derives from the non-specific way in which the aminoglycosides bind; the positively charged amino groups of an aminoglycoside are electrostatically attracted to the negatively charged RNA. Binding strength often correlates with the number of amino groups present in an aminoglycoside. Whilst this promiscuity allows the rapid identification of a molecular architecture that can bind a specific RNA target, attaining selectivity is very problematic.[12]

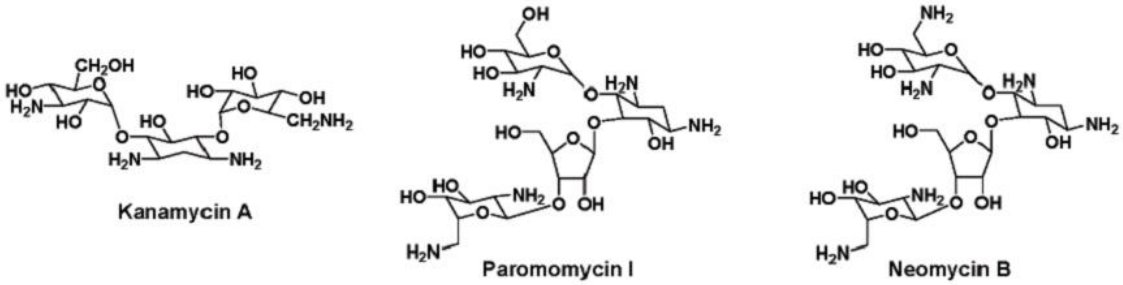

Figure 20: A selection of aminogycosides.[12]

Another class of antibiotic that is thought to bind to rRNA is the oxazolidinones, the first of which to reach the clinic was Linezolid **24** (fig. 21). This class of compound is purported to bind to the 23S rRNA, which is a feature of the 50S subunit of rRNA, and blocks the binding of charged tRNA into the subunit.[12]

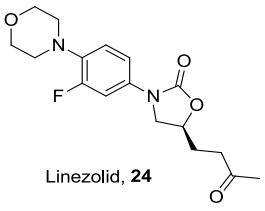

Figure 21: Linezolid, 24.

The above classes of RNA binding antibiotics interfere with the interaction between tRNA and rRNA but the process of charging a tRNA with its amino acid

can also be inhibited. Without the necessary charged tRNAs protein synthesis is inhibited and cell death can ensue. Instead of inhibiting the aminoacyl-tRNA synthetases (AaRs) that attach an amino acid to its tRNA, which has had some attention as a drug target, the tRNA itself can be considered a possible target. Neomycin **23**, an aminoglycoside (fig. 20), has been shown to inhibit the charging of the tRNA for phenylalanine.[15]

Inhibiting the production of one protein by stopping the translation of its respective mRNA has great utility as a therapeutic intervention given the potential selectivity. As such, the ability to target the mRNA strand itself becomes of interest. An mRNA strand can be conceptually separated into three regions: the 5'-untranslated region (UTR), the coding region and the 3'-UTR (fig. 20). The 5'-UTR contains the ribosomal binding site, the coding region contains the sequence of bases to get translated and the 3'-UTR contains elements involved with controlling the half-life of the mRNA.

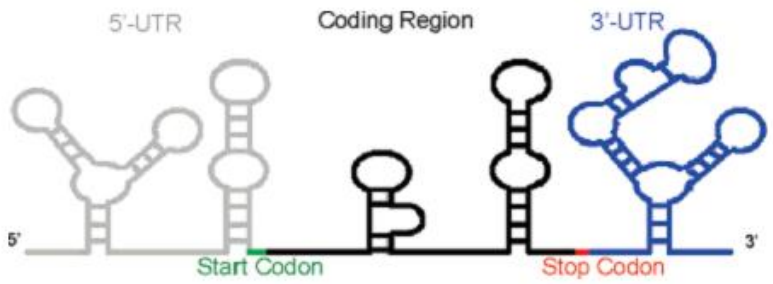

Figure 20: The structure of an mRNA strand (*Chem. Rev.*, 2008, 108, 117-1224). Copyright (2012) American Chemical Society).[12]

Formivirsen is a marketed antiviral drug used in the treatment of cytomegalovirus retinitis (CMV). It is a 21 member oligonucleotide which has nuclease resistant phosphorothioate linkages. Its sequence of bases is complementary to a section of the coding region of a viral mRNA strand that is translated into the transcription factor IE2. Thus formivirsen can bind to this mRNA strand preventing the synthesis of this transcription factor and lead to the death of the virus; this strategy is termed anti-sense therapy. Due to formivirsen being a very large, highly

charged molecule it suffers from bioavailabilty problems and, as such, it is administered as an intraocular injection.[16]

In Gram positive bacteria many of the proteins involved in amino acid biosynthesis and transport, including the previously mentioned AaRs, have their expression regulated by an RNA element known as the T box. This structure is found within the 5'-UTR and consists of a conserved sequence of 14 nucleotides that is involved with the binding of noncharged tRNAs. When there is a low concentration of a specific charged tRNA, the anticodon loop of the uncharged tRNA binds to a complementary bulge region in the 5'-UTR, whilst the 3' end of the uncharged tRNA interacts with a bulge region of an antiterminator stem loop, stabilizing it, and thus allows translation to proceed. In high concentrations of charged tRNA, this cannot occur as the amino acid, attached to the 3'end, blocks the interaction between the bulge region of the antiterminator stem loop and the tRNA which allows the more stable terminator stem loop to form and thus halts translation (fig. 21).[17]

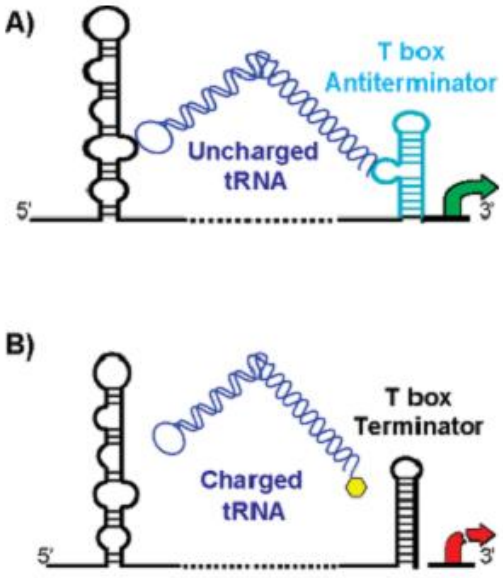

Figure 21: Regulation of T box by tRNAs. A) Formation of antiterminator stem loop allows translation to proceed. B) Inhibition of translation (*Chem. Rev.*, 2008, 108, 117-1224). Copyright (2012) American Chemical Society).[12]

An array of aminoglycosides has been assessed for their ability to stabilize to the T box antiterminator, and hence prevent synthesis of amino acids. Affinities in

the range of 8.5 to 790 μM were observed. However, given the promiscuity problems with the aminoglycosides it is likely that other small molecule inhibitors that mimic the action of the tRNA would need to be sought for T box to serve as a drug target.[18]

There does exist an as yet largely unexplored feature of mRNA that would not have the problem of either molecules binding indiscriminately to RNA structures, as the aminoglycosides, or of attempting to recreate the interactions of a large molecule to RNA in a small molecule, as in antisense therapy or tRNA and T box as targets. Riboswitches are regulatory elements found in the 5'-UTR of mRNA that have evolved to bind specific small molecule metabolites. Modification of these natural metabolites could be a route to modulate activity of these riboswitches without the drawbacks of the other methods. Riboswitches will be discussed in more detail in section 1.3.

This thesis investigates anti-infective compounds that bind to either DNA or RNA and bring about their effects through inhibition of the critical functions of each. The next sections will discuss in more detail the particular DNA and RNA targets under investigation.

1.2 Introduction: Minor Groove Binders

1.2.1 General Overview

The complex sequence of bases contained in DNA, which allows for the storing of all genetic information, significantly contributes to the attractiveness of DNA as a therapeutic target of numerous disease states. If a molecule can be designed to interact with only a specific sequence of bases then only the biological functions which rely on that sequence of bases are subjected to modulation and hence selectivity can be achieved. It has been shown that interactions with the major groove results in little overall change in the structure of DNA; however, interactions with the minor groove have been shown to significantly alter the structure.[5] Thus through designing small molecules that bind to the minor groove of DNA, called minor groove binders (MGBs), it is thought that the concomitant conformational change in DNA can interfere with biological functions, such as gene expression or DNA replication, and hence afford a drug candidate.

As with many drugs, MGBs were initially isolated as natural products. The first MGBs to be discovered were distamycin **25** and netropsin **26** (fig. 24), which are derived from *Streptomyces distallicus* and *Streptomyces netropsis* respectively.[19]

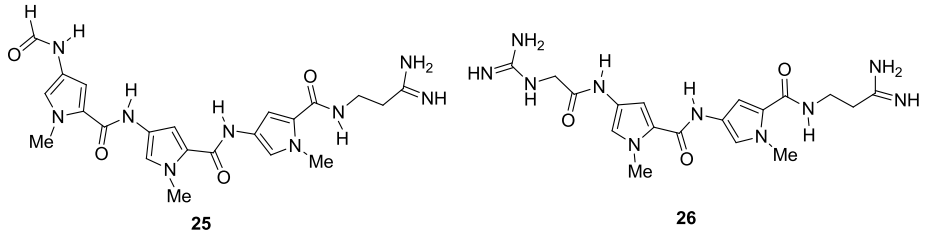

Figure 24: Distamycin, 25, and netropsin, 26.

Although these compounds, **25** and **26**, show significant antibacterial and antiviral activity, they are considerably cytotoxic.[5] Their structures have thus been used as a starting point in order to optimise their properties for the development of a viable drug. The main feature of these compounds that is retained is the sequence of heterocyclic rings (usually five membered) joined by amide links. The *N*-terminus is

usually referred to as the head group and the *C*-terminus is usually referred to as the tail group because of its flexibility in most MGBs. It is therefore appropriate to consider the following to be a general structure for MGBs (fig. 25).

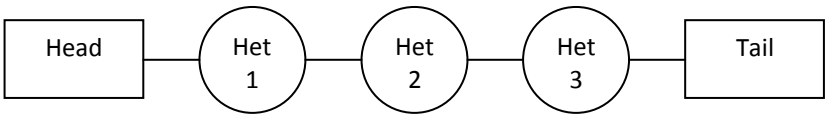

Figure 25: General MGB structure.

The binding of an MGB to the minor groove of DNA involves various bonding interactions and structural features of the molecules. The structures of distamycin, **25**, and netropsin, **26**, show one and two positively charged areas respectively. These are able to undergo ionic interactions with the negatively charged phosphate groups in the sugar phosphate backbone and can thus lead to stabilisation of a DNA/MGB complex.[20] There are a few potential problems with this interaction; first let us consider bioavailability. Highly polar molecules find it difficult to traverse the phospholipid bilayer that constitutes the cell membrane due to its hydrophobic nature. So it would be expected that both distamycin, **25**, and netropsin, **26**, having an amidine tail group, of pK_a around 12, would fail to penetrate the membrane and thus display poor biological activity, yet they do enter the cell interior and are toxic.[21] This could be due to some feature of their structure being similar to an endogenous molecule which requires active transport into the cell.[22] Given that they both contain an amidine group, it is plausible that the transporter involved may be the arginine transporter. The structural similarities allow both distamycin, **25**, and netropsin, **26**, to gain entry via this route. However, other MGBs may not have this structural similarity and thus it would be important to consider the effects of the inclusion of significantly charged areas on any MGB. Additionally, it has been demonstrated that positively charged molecules can pass membranes at an increased rate compared with negatively charged or neutral. This is due to the attraction between the negatively charged phospholipids that constitute biological membranes and the positively charged molecules.[22] The second important consideration with the ionic interaction pertains to the mode of binding. Netropsin, **26**, binds to the minor groove in a 1:1 complex where as distamycin, **25**, binds in a 2:1 complex (fig. 26).

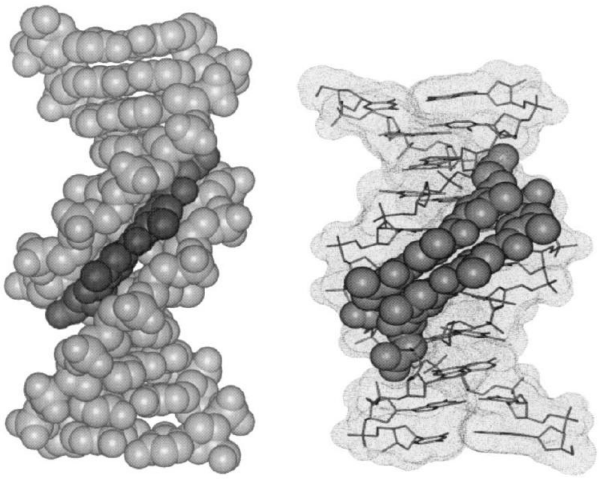

Figure 26: Binding modes of netropsin, 2, left, and distamycin, 1, right (Reproduced with permission, see appendix 2).[5]

In this 2:1 complex the two distamycin, **25**, molecules sit side by side and anti-parallel within the minor groove but they do not completely overlap. At the site of binding the two molecules are displaced by approximately one pyrrole ring and this allows a reading frame of 4 DNA bases to be achieved as apposed to only 3 for an MGB binding to DNA as a monomer. (fig. 27).[5]

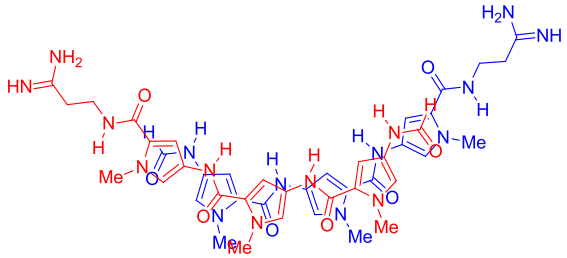

Figure 27: Displaced overlap of distamycin, 25, molecules.

Netropsin, **26**, is prevented from binding in a similar mode to distamycin, **25**, due to the repulsion between the positively charged head and tail groups that would result in attempting to form this 2:1 complex. The conformational change that the DNA undergoes during the 2:1 binding is significantly greater than that of the 1:1 binding as an extra molecule must be accommodated. This enhanced conformational change should have a more profound effect on the disruption of cellular activities and lead to a more effective drug. Therefore, in designing MGBs it is important to try and

retain this 2:1 binding (see linked dimers in section **1.2.2.1**).[5] In fact, this does not solely relate to the ionic interaction as if the head group and tail group of an MGB are particularly cumbersome then 1:1 binding may be more favourable, so size of the head and tail are also significant considerations.

Hydrophobic interactions also play a vital role. When the MGB is bound within the minor groove then the methyl groups on the pyrrole rings are able to interact with the walls of the minor groove. This hydrophobic contact between the MGB and the methylene and methines of the deoxyribose backbone can thus lead to further stabilisation of the DNA/MGB complex.[23]

The planar crescent shape of the MGB is also important. There is an approximate match between the curvature of these MGBs and that of the minor grove which facilitates a snug insertion of the MGB and in turn maximises favourable interactions.[24] Indeed, a recent study by Khedkar *et al*. has shown that distamycin derivatives without coplanarity lose significant antibacterial activity in comparison to their coplanar analogues.[25]

Perhaps the most significant interaction to be considered is the series of hydrogen bonds that are formed between the MGB and the bases of DNA. When distamycin, **25**, or netropsin, **26**, bind to the minor groove they are sufficiently embedded to allow hydrogen bonding to occur between the amide NH's and the terminal amidinium moieties of the MGB and the edges of the DNA base pairs, which form the floor of the minor groove. More specifically, as both distamycin, **25**, and netropsin, **26**, bind preferentially to sequences of A:T, it is the N3 of adenine and the O2 of thymine that are involved in these hydrogen bonds. The hydrogen bonding pattern that is observed for these two molecules is not the same; this is due to their differing modes of binding. Netropsin, **26**, has been shown to display bifurcated hydrogen bonding, in which the hydrogen bonds of the NH's span two base pairs and the molecule reads both strands simultaneously whereas, the hydrogen bonds of the NH's in the 2:1 complex of distamycin are directed towards only one base, thereby enabling each strand of DNA to be read by only one molecule of the dimer (fig. 28).[5]

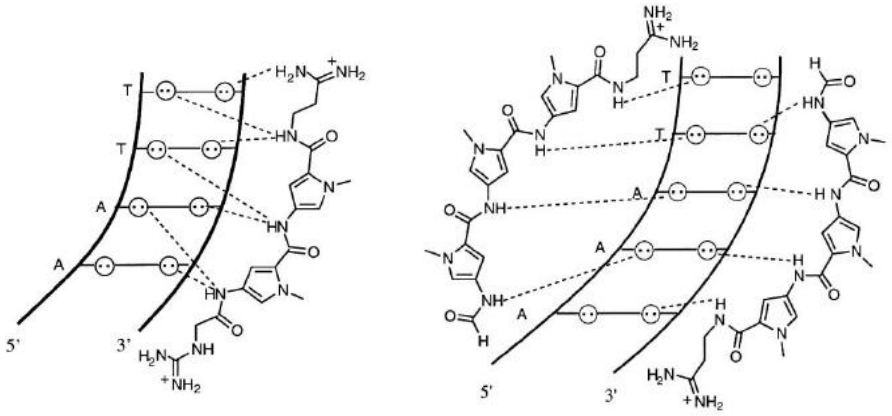

Figure 28: Hydrogen bonding patterns of Netropsin, 26, (left) and Distamycin, 25, (right) (Reproduced with permission, see appendix 2).[5]

Both distamycin, **25**, and netropsin, **26**, bind preferentially to regions rich in the bases A and T. This is primarily due to steric repulsion. Attempts to bind adjacent to C or G brings about unfavourable steric interactions between the amino group of guanine, which points into the minor groove, and H3 of the pyrrole ring (fig. 29).[26]

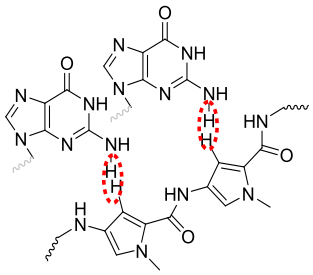

Figure 29: Steric repulsion between guanines of DNA (above and distamycin (below).

This specificity is also partly due to the electrostatic potential of C/G regions being more positive than A/T regions and thus unfavourable ionic interactions occur with the positive regions of both distamycin, **25**, and netropsin, **26**.[5] Hydrophobic interactions also contribute as the minor groove of A/T regions has a somewhat narrower width than that of G/C; this results in a better contact of the methyl groups of the distamycin and netropsin with the wall of the groove in regions of high A/T density.[5]

In order to build in tolerance for C/G regions of the DNA strand and inevitably to allow specific sequences of DNA to be MGB targets then some

structural changes would need to be carried out on distamycin **25** and netropsin **26**. In a 1:1 DNA/MGB complex like that of netropsin **26**, each heterocycle can read one pair of bases, for example, the methyl pyrrole has preference for A/T or T/A. However, in the 2:1 DNA/MGB complex like that of distamycin **25**, then each MGB molecule reads a separate strand of DNA, in other words each pair of overlapping heterocycles in the MGB has a preference for different DNA base pairs, and as a result more specific sequence selectivity is achieved. Much work has been carried out on replacing the pyrrole rings in the structure of distamycin **25** with alternative but similar moieties, primarily by Dervan *et al.*, and now there exists a variety of heterocycles that can be used to create strong binding affinity for specific sequences of DNA.[5] It is even possible to be selective in binding between an A/T base pair or a T/A pair and similar for G/C. Table 1 shows the pairing rules, whilst figure 30 gives the structure of each heterocycle.

Heterocycle 1	Heterocycle 2	Preference
Py	Py	A/T or T/A
Py	Hp	A/T
Hp	Py	T/A
Py	Im	C/G
Im	Py	G/C

Table 1: Table of DNA base binding preferences for different heterocycle pairs.

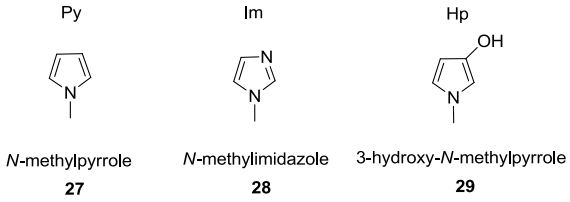

Figure 30: Structures of MGB heterocycles.

The introduction of the *N*-methylimidazole, **28**, allows for the recognition of C/G base pairs as the additional nitrogen not only removes the steric clash with the amino group of guanine but also facilitates a new hydrogen bond to it. Similarly, the 3-hydroxy-*N*-methylpyrrole, **29**, allows for the selective recognition of thymine over

adenine by the formation of a hydrogen bond between the additional hydroxyl and O2 of thymine.[27]

Although all base pairs can be recognised with these three heterocycles, this did not arrest the search for further replacements and many heterocycles and their pairing rules are known. One such development is witnessed in the molecule thiazotropsin A, **30**, (fig. 31), developed by Suckling *et al* at Strathclyde.[28] In this molecule an *iso*-propylthiazole has replaced one of the standard methyl pyrroles. Studies have shown the existence of a hydrogen bond between guanine and the thiazole nitrogen thus producing a preference for G/C pairs in DNA. The increased size of the alkyl chain is also important as G/C regions in the minor groove are wider and thus this can afford better hydrophobic interactions.[5]

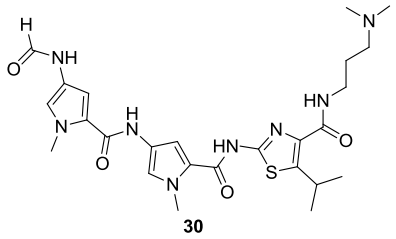

30

Figure 31: Thiazotropsin A

1.2.2 Further Developments

1.2.2.1 Linked Dimers

The paradigm for MGB development is to design distamycin analogues that capitalise on the formation of the 2:1 complex; this enables an increase in the specificity of the target sequence. A logical extension of this concept leads to the development of linked dimers. In these, the two molecules can be covalently tethered head to head, **31**, (fig. 32), head to tail, **32**, (fig. 33) or internally, **33** and **34**, (fig. 34).

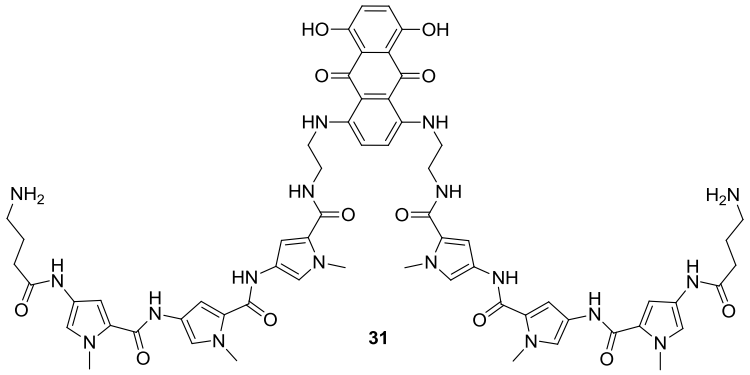

Figure 32: NetMitox, a head-to-head bis-lexitropsin.

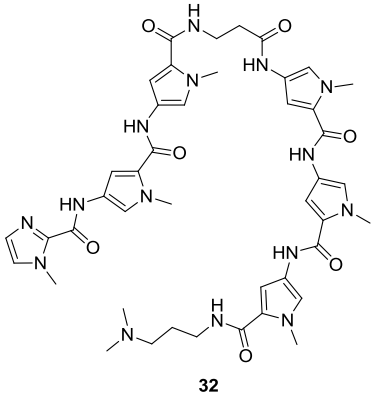

Figure 33: A head-to-tail bis-lexitropsin.

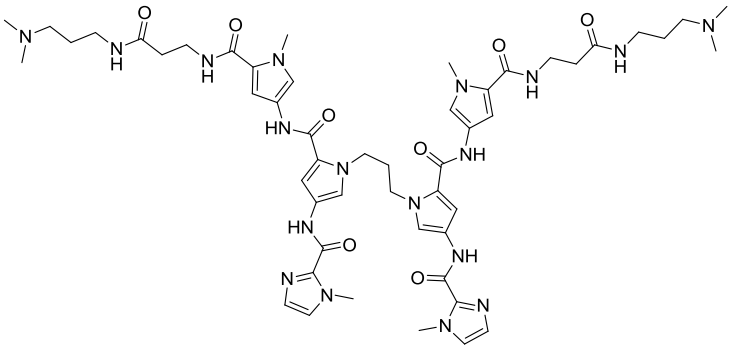

33

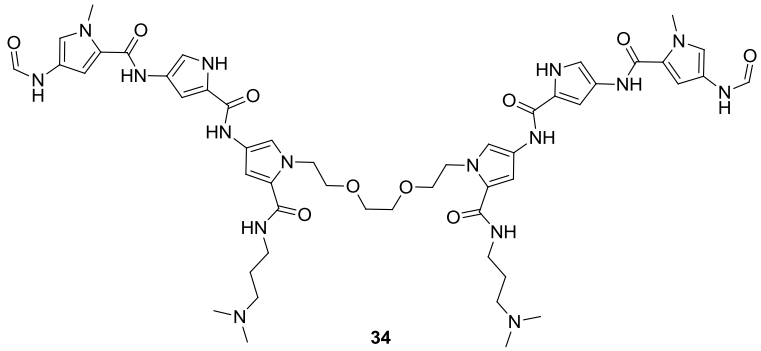

34

Figure 34: Stapled bis-lexitropsins. Tethered through central pyrroles, top and through tail group pyrroles, bottom.

These linked dimers are known to have far superior binding affinities and selectivity than their analogous 2:1 complex monomers. For example, compound **33** has an equilibrium association constant (K_a) of $9.3x10^6$ against the sequence 5'-TGTCA-3', whereas, the analogous unlinked dimer has a K_a of less than $1x10^5$.[29, 30, 31]

1.2.2.2 Reactive Moiety Hybrids

Drug molecules with the capacity to alkylate DNA find use in the fight against cancer. Uramustine, **34**, (fig. 35) is an inexpensive alkylating agent that has applications in this field. This anticancer property stems from the molecule's ability to crosslink DNA by alkylation of the N7 of guanidine. The tertiary amine of uramustine **34** acts as an intermolecular nucleophile, attacking the halogenated

carbon and forming a highly reactive aziridinium cation. Alkylation ensues by the N7 of guanine opening the strained aziridinium ring. The tertiary amine can attack the remaining halogenated carbon and the process repeats for another guanine, thus cross linking the DNA strand.[4]

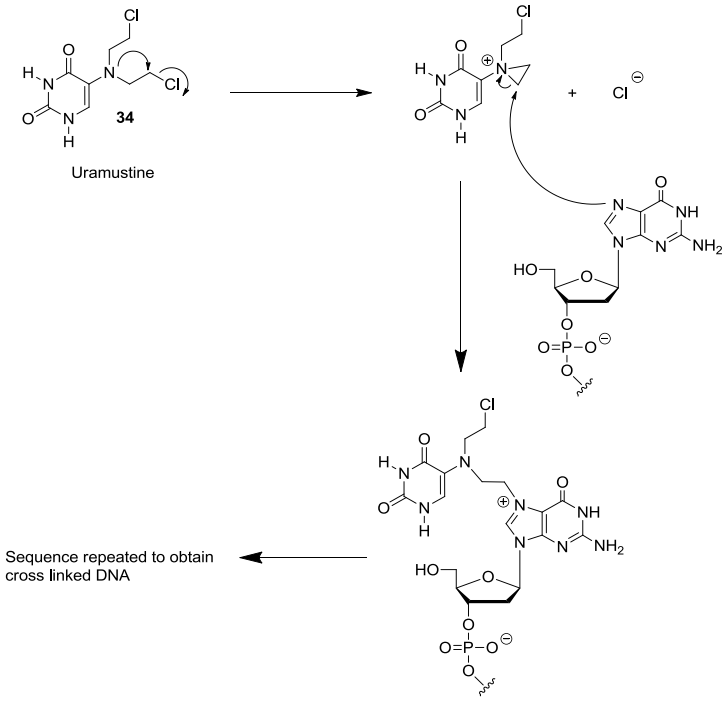

Figure 35: Mechanism of guanine alkylation by uramustine.

5-fluorouracil, **35**, is another agent used in the treatmeant of cancer. Its activity is brought about via the covalent binding to thymidylate synthase and as such, prevents the synthesis of DNA. Once inside the body, 5-fluorouracil **35** is converted to its active form by a series of reactions that leave it tethered to a DNA nucleotide (fig. 36).

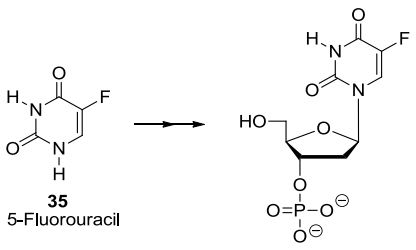

Figure 36: Activation of 5-Fluorouracil.

The complex between the now active drug molecule, thymidylate synthase and its cofactor (*N*5,*N*10-methylene tetrahydrofolate) facilitates the formation of two covalent bonds. If the normal substrate of this reaction pathway, uracil, were present then there would be a hydrogen in place of the fluorine atom, this would be lost and thus the enzyme could detach. However, since fluorine cannot leave as a positive ion, the reaction stops leaving the thymidylate synthase covalently bonded to the drug and inactivated (fig. 37).[4]

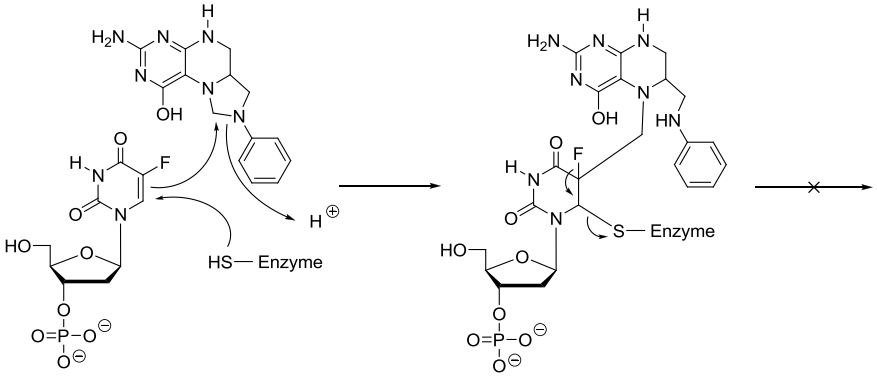

Figure 37: Inhibition of thymidylate synthase by the activated 5-Fluorouracil.

One of the main issues with the majority of these anticancer drugs is the unfortunate lack of target specificity thus introducing an array of unwanted and often severe side effects to the recipient of the treatment.[4] Previously mentioned has been the sequence specificity that distamycin, **25**, and its analogues possess so it should come as no surprise that work has been carried out on investigating the effectiveness of hybrid molecules arising from distamycin and known anticancer agents. With the reactive moiety tethered to the MGB chain, transport to the target site becomes more efficient due to the MGBs affinity to DNA. It is also possible that cell uptake will be increased as a result of the hybrid molecule being more lipophilic than the unhybridised anticancer agent.[32]

Work carried out by Baraldi *et al.*[32] has focused on the effect of attaching uramustine to distamycin (fig.38).

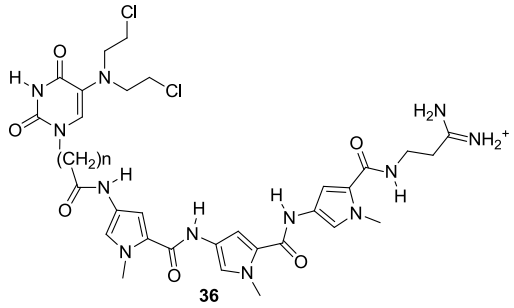

Figure 38: Uramustine/distamycin hybrid.

It has been found that this hybrid molecule, **36**, has an enhanced activity compared to either distamycin, **25**, or uramustine, **34**, alone. The length of the alkyl linker was shown to have an effect on the activity also. As n was increased from 1 through to 6 then an increase in activity was observed. This has been attributed to an increase in the lipophilicity of the molecule.

It does appear that distamycin, **25**, and its analogues have the potential to facilitate the creation of more active anticancer molecules, although this method of creating a hybrid does not always produce the desired result.

Further work carried out by Baraldi *et al.* has looked at the distamycin hybrid analogue, **37**, of the anticancer agent, 5-fluorouracil **35** (fig. 39).[32]

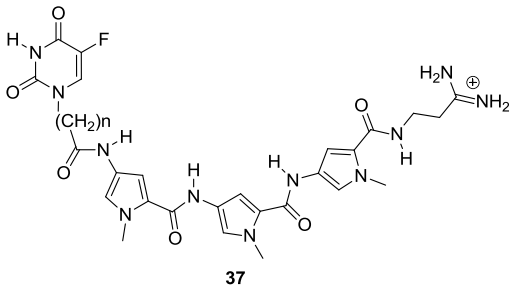

Figure 39: 5-fluorouracil/distamycin hybrid, 37.

The research carried out by this team showed that this hybrid was ineffective as the activities for the compounds where n is 1 through to 6 were all lower than distamycin itself.

Adopting a different approach to the modification of distamycin, Brostallicin, **38**, is an α-bromoacrylamide containing anti cancer drug currently in phase II clinical trials (fig. 40).

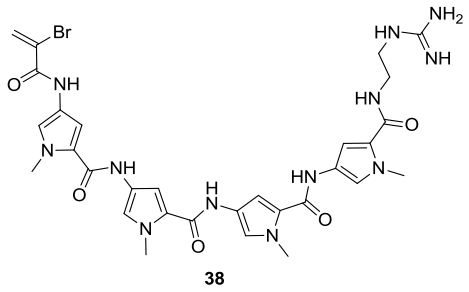

Figure 40: Brostallicin.

Like both the 5-fluorouracil **35** and uramustine **34** minor groove binder analogues above, it contains an alkylating reactive moiety; however, Brostallicin **38** has been found to interact reversibly with AT rich sequences of DNA and is found to be unreactive in *in vitro* DNA alkyation assays. This indicates that direct DNA alkyation is not the mechanism of action. It is thought that an intracellular reactive nucleophilic species, glutathione **39**, reacts with the reactive moiety of Brostallicin. This bromo compound is then converted into the chloro analogue and it is this species that eventually leads to the alkyation of DNA (fig. 41).[33, 34]

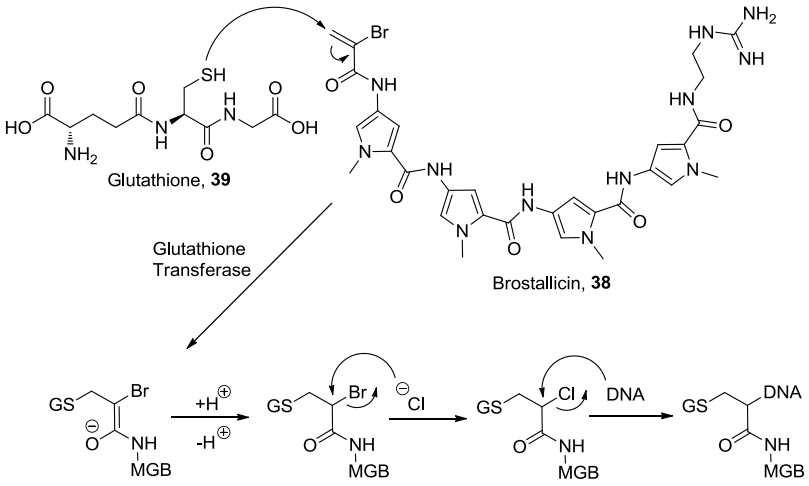

Figure 41: Activation of Brostallicin.

Brostallicin **38** is thus an example of a drug which is intracellularly converted into its active form. This approach is often utilised and will be of relevance in section **3.3.3.**

1.2.3 Design Concepts at Strathclyde

Mentioned previously was the design of a novel heterocycle, *iso*-propylthiazole, with a preference to bind to C/G regions of DNA. This falls in line with the general design concept at Strathclyde which is to increase the lipohiphilicity of the MGBs to attain potent anti-bacterial agents. The thinking behind this is two-fold: by increasing the lipophilicity of the molecules we increase the cell permeation capabilities and can achieve enhanced activity; the increased lipophilicity is also likely to improve the hydrophobic interactions between the MGB and DNA, again leading to enhanced activity.[28]

In addition to the replacement of the pyrrole rings with larger alkyl chains, c.f. thiazotropsin A, **30**, a number of other strategies have been employed. The peptide links have been replaced with more lipophilic isosteres such as alkene and diazo links; the formyl head group of distamycin, **25**, has been replaced with much larger aromatic moieties; and, the guanidinium tail group has been replaced with moieties that are less ionised at physiological pH. Ultimately, this has led to the development of the following set of lead compounds (fig. 42) that are being investigated by the University of Strathclyde and an external partner company due to their excellent profile of activity against Gram positive activity or in the case of BP4, its Gram negative activity.

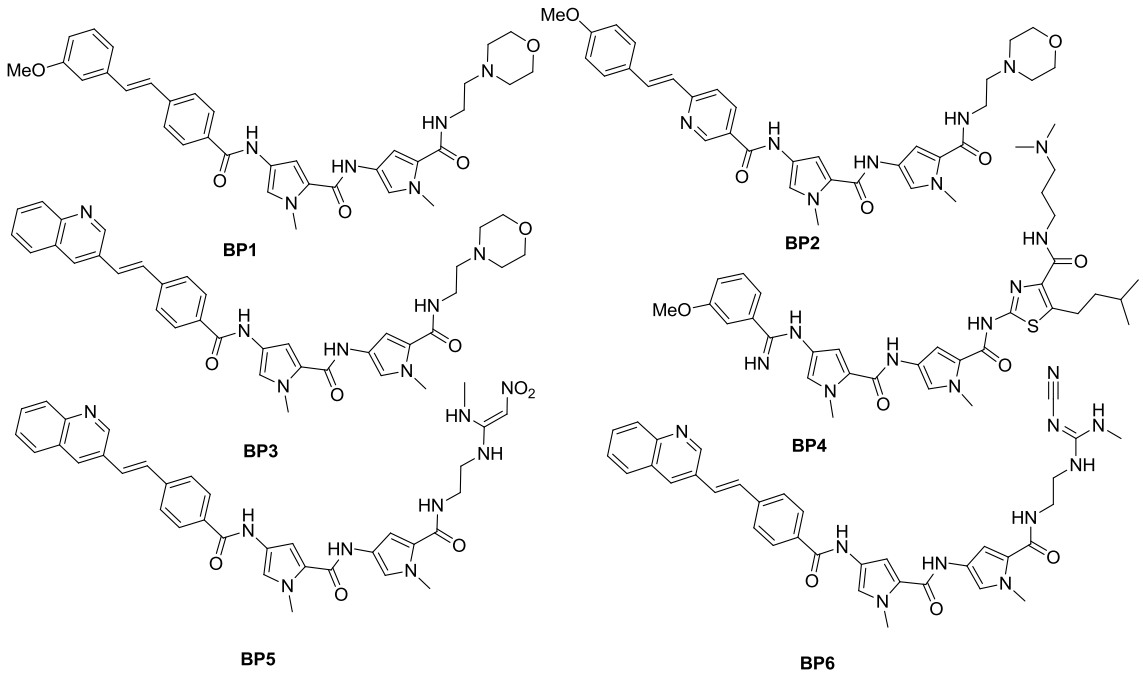

Figure 42: Lead MGBs.

1.2.3.1 The hERG Ion Channel

For any drug discovery programme to be successful then strong binding to the target is necessary; however, specificity is also important. Off-target interactions need to be avoided as these are often the cause of unwanted side effects and one particularly important case is human ether-a-go-go (hERG) ion channel. This is relevant to the MGBs because some aspects of the hERG binding preferences match the structures of our MGBs.

The hERG gene codes for a protein that is found in potassium ion channels. These ion channels are particularly important as they are involved in the generation of the electrical current that maintains the correct rhythm for the heart beat. Mutations in these ion channels can cause a disorder called long QT syndrome in which sudden death may occur due to the arrhythmic contraction of the ventricles in the heart. Furthermore, it has been found that a number of clinically successful drugs have been found to interact with and inhibit the hERG protein, and thus the potassium ion channel, leading to cases of induced (acquired) long QT syndrome. These drugs were swiftly removed from the market and hERG is now a major pharmaceutical anti-target.[35]

The crystal structure of the hERG protein has not yet been solved and as such its structure is only inferred through homology models. Despite this, a number of tactics, relevant to our MGBs, are available in order to attenuate hERG activity: pK_a consideration and fluorine incorporation. Molecules that contain basic nitrogen atoms, as in the morpholino nitrogen in the tail group of **BP1**, **BP2** and **BP3**, are known to have a high likelihood of inhibiting hERG. **BP5** and **BP6** were specifically designed to include a non-cationic tail group in the hope of circumventing this possibility. It has also been observed that the inclusion of a fluorine atom in a molecule can reduce hERG activity; however, the reason for this remains unknown. This tactic for attenuating hERG activity has not yet been exploited in our MGBs.[36,37]

1.2.3.2 Targeting Gram negative Bacteria

The six lead MGBs are particularly effective against a wide spectrum of Gram positive bacteria (MICs of 0.25 - 2.5 µg/ml); however, they display very little activity against Gram negative bacteria. **BP4** is our most active Gram negative compound, hence its inclusion in the lead compound set; however, it is one among few to have Gram negative activity. Since a number of Gram negative bacteria lead to infections of clinical relevance, *Escherichia coli* or *Pseudomonas aeruginosa* for example, then it is important to further investigate the lack of activity our compounds display for Gram negative bacteria and see if it can be improved upon.

1.2.3.2.1 Differences between Gram positive and Negative Bacteria

The main difference between Gram positive and Gram negative bacteria is in the structure of their cell wall/membranes. Gram positive bacteria have only one phospholipid membrane which is surrounded by a thick layer of peptidoglycan based cell wall; in contrast, Gram negative bacteria have an inner membrane, a periplasmic space, a thinner peptidoglycan layer and then another, outer membrane (fig. 43).

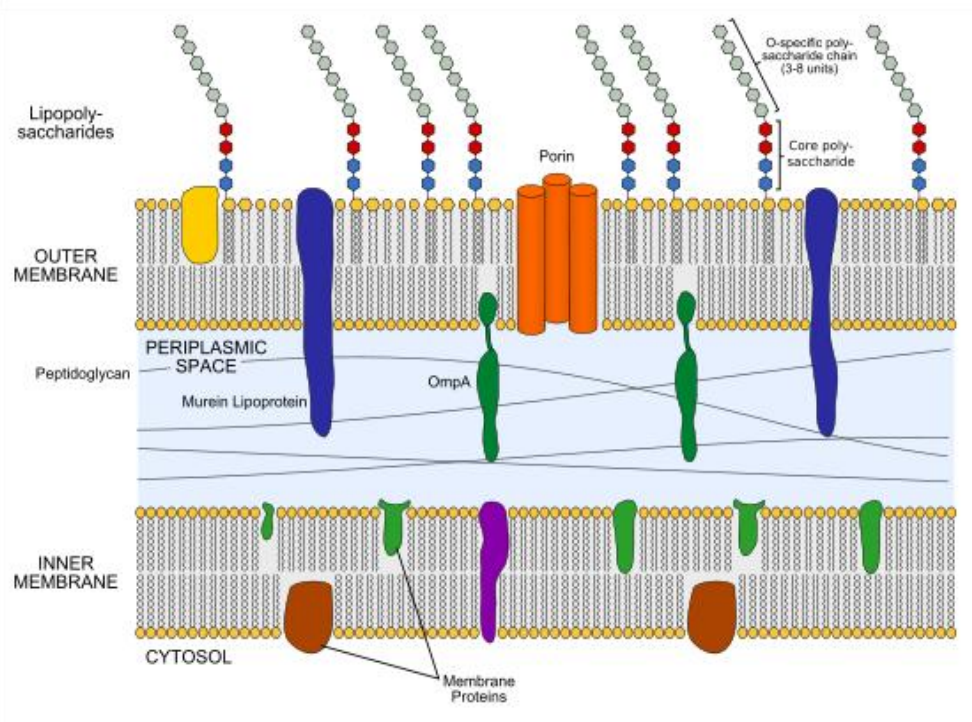

Figure 43: Gram negative bacterial cell wall (reproduced with permission, see appendix 3).[40]

The outer membrane makes Gram negative bacteria more difficult to target with antibiotics than Gram positive bacteria for several reasons. Firstly, an external constituent of the membrane is a very polar lipopolysaccharide, which makes reaching the cell wall surface proper difficult for large hydrophobic molecules.[38] A second important constituent of the outer membrane is a protein known as porin. Porins usually exist as trimers with each monomer made up of a large β-barrel (fig. 44). Two types of these transmembrane protein complexes exist: general and specific porins. The general porins allow passive transport of hydrophilic solutes through the membrane up to an exclusion size of around a molecular weight of 500-600. Specific porins are similar but only allow passage of a particular solute molecule or class of molecule.

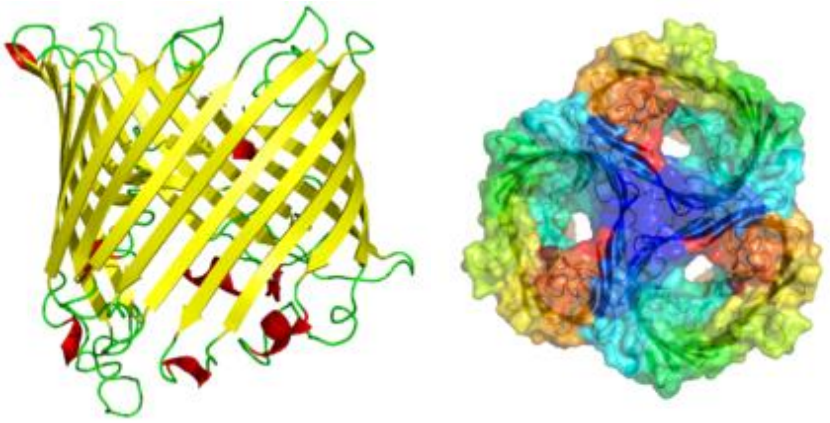

Figure 44: Porin monomer, left; porin trimer, right (reproduced with permission, see appendix 3).[40]

Solutes attempting to pass through a porin find that the diameter of the channel decreases from around 2 nm at the enterance to about 0.9 nm half way along the channel and then expands back to around 2 nm at the exit. This reduction in diameter is caused by a section of loop secondary structure that extends into the centre of the channel (fig 45). A number of critical residues exist on this loop and on the walls of the porin channel. There are two acidic residues on the loop: an aspartic acid and a glutamic acid. Near the wall of the channel there are three basic arginine residues (fig. 45).

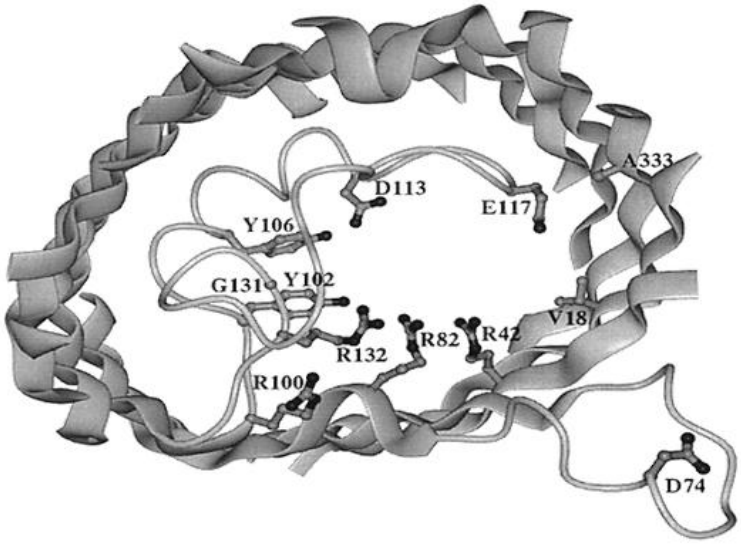

Figure 45: Structural features found inside a porin channel (reproduced with permission, see appendix 3).[41]

Interestingly, mutation of the gene that codes for porin proteins is a common way for bacteria to gain antibiotic resistance. This may be through subtle modification to a specific porin to prevent passage of an antibiotic that is fortuitously taken up or through the narrowing of the general porin apertures.[39]

Bacterial membranes also possess transport pumps which are transmembrane proteins that can actively transport various substrates out of cells. These are particularly significant as over expression of these transport pumps is another mechanism through which bacteria can gain antibiotic resistance due to many drug molecules being efficient substrates for these transport pumps.

There are a number of families of transport pumps, each having a particular subset of substrates that they are effective against; however, two in particular are worth commenting on, the major facilitator superfamily and the resistance nodulation cell division superfamily.

The major facilitator superfamily is the group of efflux pumps which predominate in Gram positive bacteria. Almost all of these consist of a bundle of 12 transmembrane α-helices connected by loops of hydrophillic residues (fig. 46). There are three mechanisms through which these transporters function: uniporters transport one type of substrate and are powered by the substrate gradient; symporters move two or more substrates in the same direction and are powered by the electrochemical gradient of one substrate; and antiporters move two or more substrates in opposite directions. The major facilitator superfamily, as a whole, is responsible for the translocation of many substrates including nucleosides, amino acids, sugars and many drugs; however, individual members of this family are particularly specific for their respective substrates.[40]

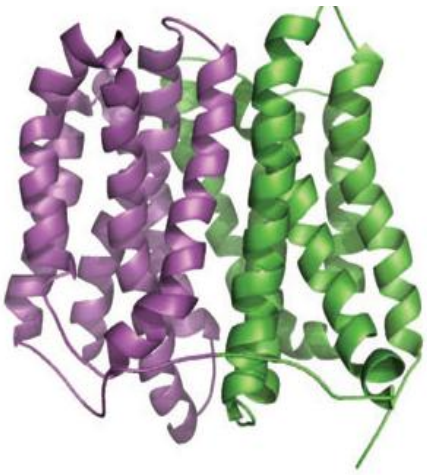

Figure 46: Major facilitatory super family efflux pump structure (reproduced with permission, see appendix 4).[40]

The resistance nodulation cell division superfamily is the group of transport pumps that dominate Gram negative bacterial efflux systems. These transmembrane proteins are reported to be the main feature that differentiates Gram negative bacteria from Gram positive bacteria in terms of the difficulties in overcoming their resistance and the challenges associated with their treatment in the clinic. These efflux pumps are proficient at pumping out many molecules which could prove to be detrimental to the health of the bacterial cell which explains the smaller spectrum of antibiotics that are effective against them. Gram negative bacteria can also acquire resistance by over expressing the genes for these efflux pumps much the same as the major facilitator superfamily of the Gram positive bacteria.[41]

These pumps are composed of three separate regions: an outer membrane protein; an inner membrane proton antiporter; and, a periplasmic membrane fusion protein. A representation of this tri-partite structure can be seen in figure 47.

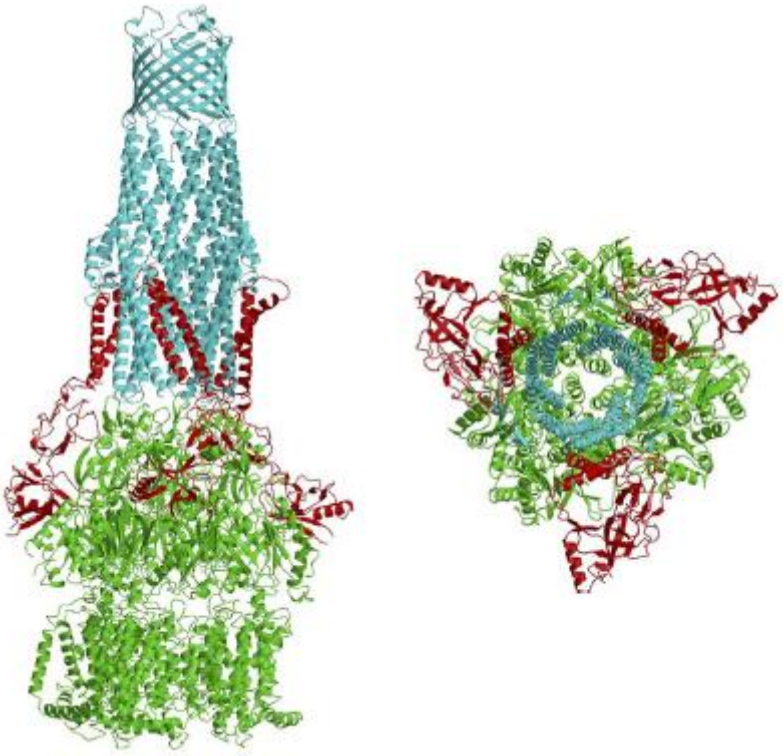

Figure 47: Resistance nodulation cell division pump. Homotrimer TolC, Blue; ArcA, Red; trimeric AcrB, Green (reproduced with permission, see appendix 3).[41]

The three domains are only complexed transiently when actively pumping out unwanted molecules; in fact, the outer membrane protein can interact with various inner membrane proton antiporters to extrude a wider spectrum of molecules. Drugs such as the aminoglycosides, tetracyclines and β-lactams are known to be efficiently effluxed by these pumps.[41]

1.2.3.2.2 Towards Attaining Gram Negative Activity In Our MGBs.

Hoeschst 33258, **40**, is a bis-benzamidazole dye that binds to the minor groove of DNA where it is known to interfere with the complexation of topoisomerase I.[42]

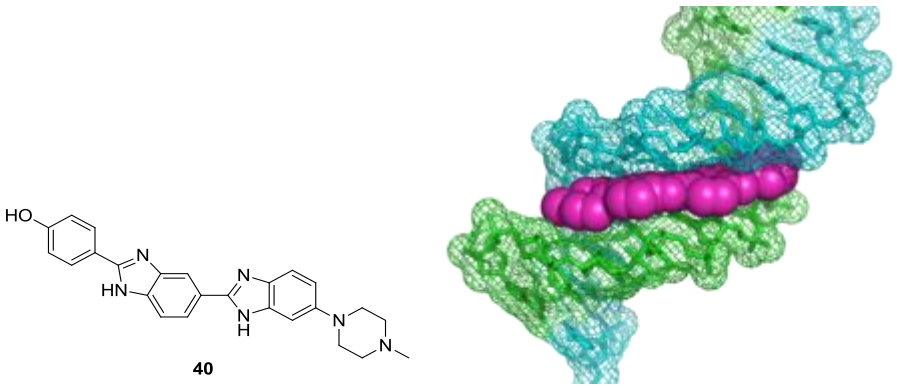

Figure 48: Hoeschst 33258, 40, left; Hoeschst inserted into DNA (reproduced with permission, see appendix 2).[5]

It is however considerably cytotoxic and, as such, it is not ideal as an antibiotic. A number of Hoechst 33258 analogues have been synthesised by Bansal *et al* and of these one, DMA, **41**, was shown to have reduced cytotoxicity and activity against both Gram positive and Gram negative bateria. This is demonstrated by inhibition of growth of *S. aureus* at 16 µM and *E. coli* at 2 µM. [43]

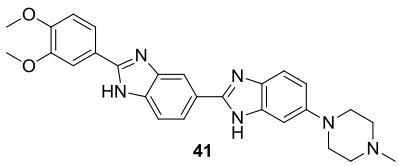

Figure 49: Modified Hoechst 33258.

This is important to consider as our current MGB design does not give a satisfactory activity profile against Gram negative bacteria. A number of similarities can be seen between our MGB paradigm and the structure of DMA, **41**. Each possess conjoined heterocycles giving the resulting molecule a degree of curvature; both the *N*-methylpiperazine of DMA and our *N*-methylmorpholine are weakly basic tail groups and each has a head group with hydrogen bonding capabilities. There are too, a number of notable differences which, when taken into consideration alongside the function of porins, could allude to why our MGBs display poor activity against Gram negative bateria. Hoechst analogues are comfortably under a molecular weight of 500, whereas, our MGBs typically exceed a molecular weight of 600. This is largely due to a greater number of heterocycles in our approach and has the further consequence of giving our MGBs a more pronounced curvature by comparison. One

can envisage the difficulties a large, cresent shaped molecule may have in attempting to pass through the narrow channel of a porin. Adding to this challenge is the flexibility of our ethyl morpholine tail group; given normal thermal energy this part of the molecule would be sampling a large volume of conformational space, further impeding passage through the porin.

1.2.4 Project Aims for MGBs

The panel of lead compounds that had been identified at the start of this project had to be further investigated to assess their commercial suitability. Ultimately, the goal was to get a lead compound from preclinical development into phase I clinical trials for treatment of *Clostridium difficile* and MRSA infections as preliminary data had suggested excellent activity against these bacterial species. In order to move the compounds forward to this stage a number of the chemical and physicochemical properties of these compounds need to be investigated so as to ensure a smooth transition into clinical trials and to reveal any potential problems.

Over many years the Suckling group have produced in excess of 200 MGBs; however, as the full synthesis can involve as many as 13 steps and as very little material is required for the initial screening of biological activity, most of the syntheses yielded around 10-30 mg of MGB. These quantities are much too little to embark upon an investigation into the properties of the lead compounds and, as such, a large scale synthesis was required to be undertaken, including optimisation, to yield enough of each compound for full biological evaluation, physical chemical property determination and stability studies.

The lead compounds were to be qualitatively assessed for solubility in relevant, pharmaceutically acceptable solvent systems. They were also to be subjected to stability studies including an assessment of stability to mouse liver microsomes. The information gained from these assessments was essential to move the MGB antibacterial project forward from the preclinical development stage and was used to inform both the company that is assisting in this project and the contract research organisations (CRO) they employ.

Given the importance of hERG as a pharmaceutical anti-target we sought to expand our collection of potential anti-hERG compounds. A number of novel structures were designed and synthesied taking advantage of current anti-hERG strategies.

The low Gram negative activity of our MGBs was also investigated. Multiple design strategies led to the synthesis of a large panel of novel compounds. The activity of these against a clinically relevant strain of *Pseudomonas aeruginosa* was investigated and so too was the involvement of porins and efflux pumps in the activity of these compounds.

1.3 Introduction: Riboswitches

1.3.1 General Overview

A riboswitch is part of an mRNA molecule that post-transcriptionally regulates gene expression through the specific recognition of a small molecule metabolite. Proteins that are produced from genes controlled in this manner are responsible for the production of the metabolite sensitive to the riboswitch; therefore, this gene expression control mechanism is an example of a negative feedback loop.[44] This is true for almost all riboswitches containing mRNAs although there are a few that activate gene expression. The presence of riboswitches is now firmly established in the bacterial realm; bioinformatic investigations suggest that approximately 2% of mRNAs in *Bacillus subtilis* are regulated by riboswitches.[45] There is one type of riboswitch, the TPP riboswitch, which has been found in plants and fungi and has been proposed to exist in some species of archaea.[46] Notably, no riboswitches have been proposed or discovered in the human genome; hence, they are attractive drug targets due to their intrinstic selective toxicity.

The riboswitch is usually found in the 5'-UTR of an mRNA, the region that participates in ribosome binding, and can be considered as two distinct structural units, the aptamer domain and the expression platform.[47] The aptamer domain binds the small molecule metabolite with high specificity and affinity and this module of the riboswitch is highly conserved throughout all species for a particular riboswitch.[48] A specific tertiary structure is required for metabolite binding to take place and this is formed by the juxtaposition of different secondary structures. Within this binding site the metabolite is often involved in an extensive array of contacts to bring about the aforementioned specificity.[49] For example, the *S*-adenosylmethionine (SAM) riboswitch displays a 75 fold decrease in affinity when one methylene group is removed from the methionine side chain (fig. 50); this observation is of interest with respect to our results with the thiamine riboswitch in which the length of an alkyl chain has been varied (section **3.3.3**).

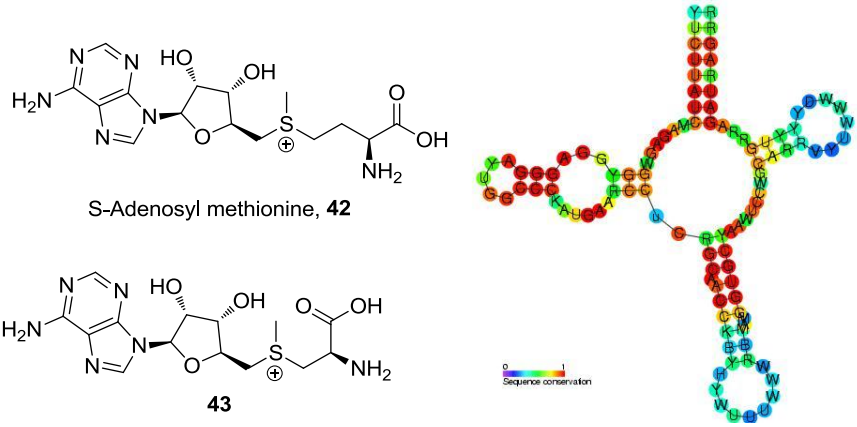

Figure 50: The SAM riboswitch (least to most conserved nucleotides; blue to red) and ligands (reproduced with permission, see appendix 4).[40]

Another example of this specificity is seen in the purine riboswitches in which the specificity for guanine or adenine is due to the interactions with only one pyrimidine at position Y74: the guanine riboswitch has C74; whereas the adenine riboswitch has U74.[50] It is important to note that metabolites are significantly buried within their aptamer domains and it appears as though the RNA undergoes most, if not all, of the conformational rearrangement associated with the binding event.[51]

The other principal domain of the riboswitch, the expression platform, undergoes a major allosteric conformational change, induced by metabolite binding in the aptamer domain, which ultimately leads to gene regulation by a number of different routes. The expression platform of a riboswitch is much less conserved and thus a particular riboswitch will always have the same aptamer domain but different expression platforms may be coupled to this across different species or genera.[52,53] The expression platform may exert its effect in a number of ways and the following illustrate the more common of these. Premature transcription termination may be caused by the formation of rho-independent transcription termination hairpins. These are C/G rich stem-loop structures that are up to 20 bases in length and are followed by a chain of uracil bases (fig. 51). The RNA polymerase complex binds to the stem-loop very tightly causing a momentary stall in the polymerase's transcriptional activity, which coincides with the transcription of the chain of uracil bases. Since uracil-adenine interactions are weak, the DNA-RNA duplex is destabilised resulting in its dissociation from RNA polymerase.[54]

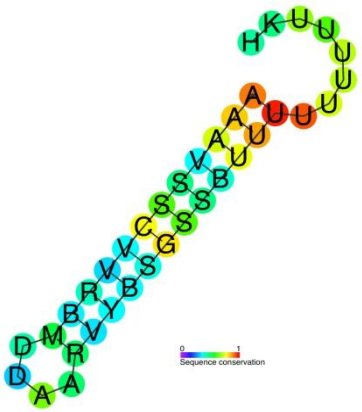

Figure 51: rho-independent transcription termination hairpin (least to most conserved nucleotides; blue to red) (reproduced with permission, see appendix 4).[39]

The Shine-Delgarno (SD) sequence (consensus sequence AGGAGG) is located approximately 8 bases upstream of the AUG start codon and helps to recruit the 16S subunit of the ribosome to the mRNA in order for translation to occur.[55] This sequence is only found in prokaryotic organisms; the eukaryotic analogue being the Kozak sequence (consensus sequence (gcc)gccRccAUGG).[56] The expression platform of some riboswitches sequesters this sequence leading to inhibition of translation (fig. 52).

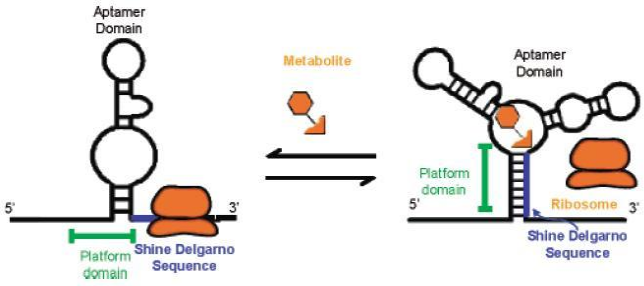

Figure 52: Sequestration of the Shine-Delgarno sequence (reproduced with permission, see appendix 2).[12]

The final example of an expression platform is when the riboswitch also acts as a self-cleaving ribozyme. The presence of a significant concentration of the metabolite will allow binding to the aptamer and eventual scission of the mRNA preventing translation.[12]

It is noteworthy that the modular nature of riboswitch structure is such that replacement of the aptamer domain with one from an unrelated riboswitch still

allows the retention of the control of gene expression albeit with the system sensitive to the new metabolite.[12]

1.3.2 Importance of Riboswitches to Drug discovery

The most recently approved antibacterial drug, linezolid, targets the ribosome and demonstrates the usefullness of RNA as a clinically recognized antibacterial drug target. Many other RNA structures also have been investigated as potential drug targets (see section 1.3); however, these examples illustrate the association between the ligand and the RNA structure to be fortuitous and not a natural function of the RNA. Consequently, the modification of these ligands can be troublesome as they possess little selectivity in their binding.

Riboswitches have evolved specifically to interact with small, low molecular weight ligands and this makes riboswitches a very different target than other RNA structures. The recognition capabilities of a riboswitch for its cognate ligand approach the level of selectivity and complexity that is seen in protein-drug interactions. Therefore, it is possible that compounds that target riboswithces could be designed to be highly selective and not bind to other cellular targets.

Given that bacterial resistance is becoming increasingly problematic an entirely new biological target is, in the form of riboswitches, most welcome. Whilst they have much potential, their only recent discovery means that a lot of work is needed to understand the basic science of riboswitches before they become validated targets for drug discovery.

1.3.3 Riboswitches: PreQ1 Riboswitch

1.3.3.1 Biological Role of Q-base

There are 64 combinations of 3 bases that give rise to the codons of an mRNA strand; however, most organisms have less than 45 tRNAs and thus some tRNA molecules must base-pair with more than one codon. The Wobble Hypothesis, proposed by Francis Crick, states that the 5' base on the anti-codon is not subjected to as strict a spatial confinement as the other two and thus can participate in non-Watson-Crick base pairing. This "wobble" in the third position of the codon allows for some tRNA to read multiple codons e.g. UCU, UCA, UCG, UCC all code for the amino acid serine.[57]

In addition to the normal RNA nucleosides, tRNAs are known to utilise over one hundred modified nucleosides which have influence over the folding and stability of the tRNA and are involved with the codon-anticodon interactions. One such nucleoside is queuosine (Q) **44** which is a hypermodified guanosine analogue (fig. 53), originally identified in *E. coli* and found in bacteria, plants and animals, though is notably absent from yeast and plant leaf cells.[58]

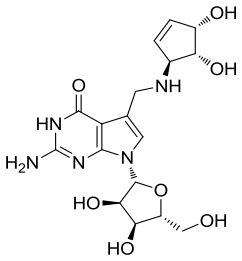

44

Figure 53: Queuosine.

This nucleoside is found in the 5' position (position 34, fig. 54) of the anticodon of the tRNAs associated with histidine, aspartic acid, asparagine and tyrosine and is necessary for the "wobbling" of these tRNAs. It is also known to improve the accuracy of translation. Q is found across both prokaryotic and eukaryotic genera; however, its *de novo* synthesis only occurs in bacteria, leaving eukaryotic organisms to acquire it from alternative sources.[58]

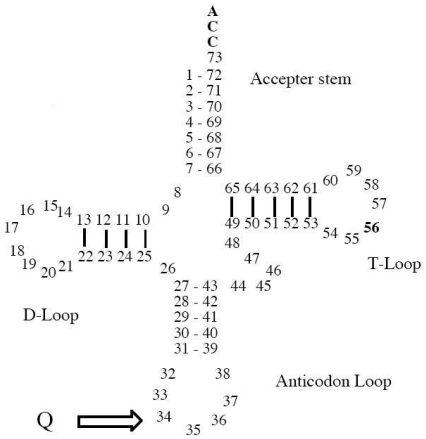

Figure 54: General tRNA schematic showing position of Q (reproduced with permission, see appendix 5).[58]

1.3.3.2 Bacterial Synthesis of Q

It is thought that the first enzyme in the bacterial biosynthesis of Q is GTP cyclohydrolase I which has as its substrate GTP **45**. This molecule is the precursor to the essential cofactors tetrahydropterin (BH4) **47** and tetrahydrofolate (THF) **48** each of which also employs GTP cyclohydrolase I as the first enzyme in their biosynthesis to afford the transformation into 7,8-dihydroneopterin triphosphate **46** (fig. 55).[59]

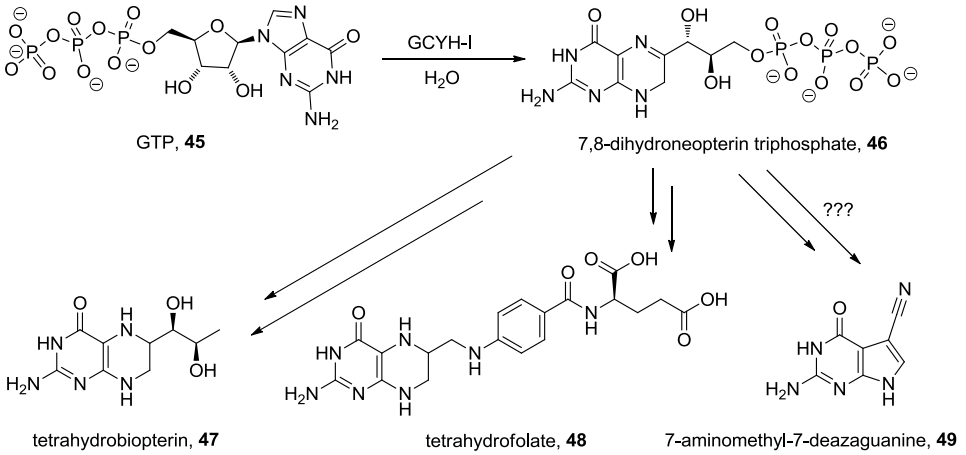

Figure 55: Biological Pathways of GTP.[40]

The first known intermediate in the biosynthetic pathway after GTP is 7-cyanodeazaguanine ($preQ_0$) **49** and this undergoes a reduction of the nitrile group to 7-aminomethyl-7-deazaguanine (preQ1) **50** by $preQ_0$ oxidoreductase (QueF) which is an NADPH dependant enzyme. The enzyme tRNA-guanine transglycosylase

(TGT) then inserts the preQ$_1$ base **50** into tRNA, with concomitant removal of guanine, whereupon it is tethered through the primary amine to a ribose derivative by *S*-adenosylmethionine:tRNA ribosyltransferase-isomerase (QueA) forming epoxyqueuosine. An unidentified enzyme then converts the epoxide to the alkene with the resultant production of Q (fig. 56).[59,60]

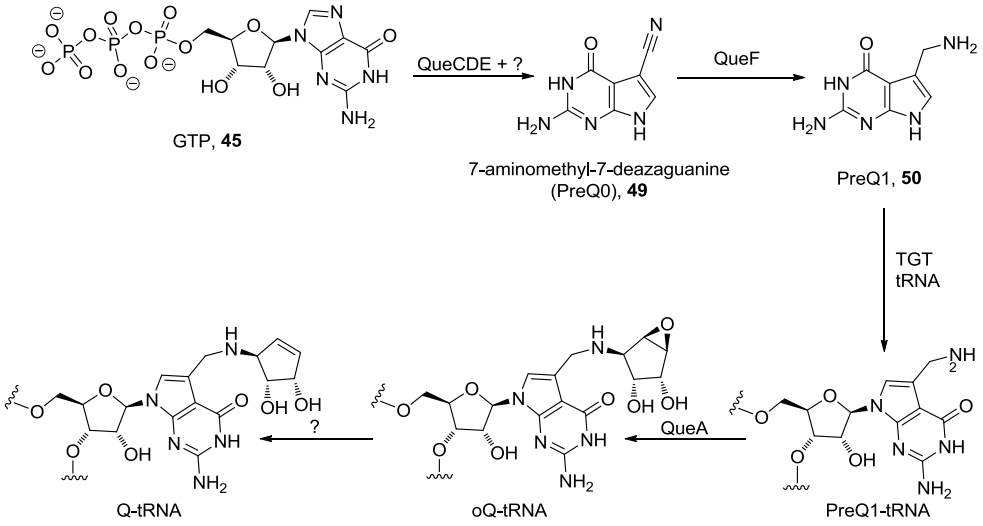

Figure 56: Biosynthesis of Q-tRNA in Bacteria.

1.3.3.3 Eukaryotic Synthesis of Q

Since eukaryotic organisms cannot biosynthesise Q, **44**, it must be salvaged from food consumption and enteric bacteria as the free base. The first step in this process involves a specific cellular membrane uptake mechanism whereby queuine **51** is moved from the extracellular space into the cytosol of the cell. The queuine **51** is then incorporated into the already formed tRNA by queuine-tRNA ribosyltransferase (QTR) which is the eukaryotic version of the prokaryotic TGT. Eukaryotic organisms also possess a queuine salvage pathway which allows the queuine-5'-monophosphate, that is produced during normal tRNA turnover, to be recycled back into the free queuine base **51** enabling its re-incorporation into tRNA (fig. 57).[61,62]

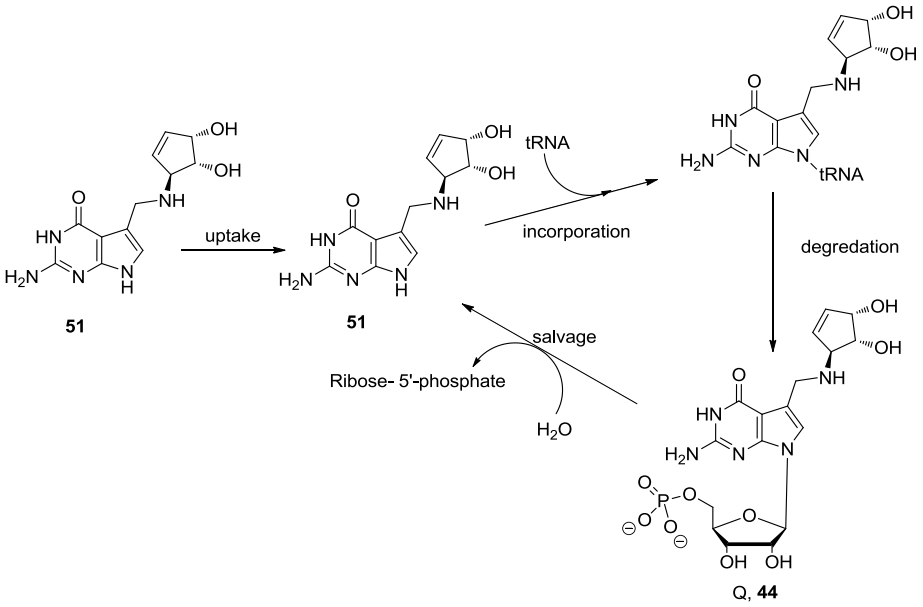

Figure 57: Biosynthesis of Q-tRNA in Eukaryotes.

1.3.3.4 The PreQ1 Riboswitch

In a large number of Gram positive bacteria, the 5'- untranslated region of genes associated with the biosynthesis of PreQ1 **50**, which is the last small molecule in the pathway that ultimately forms Q **44** in the tRNA, contains a conserved sequence which is now known as a class I preQ1 riboswitch. There also exists a class II variant but this is structurally distinct and less well investigated; all further references to the preQ1 riboswitch will be describing the class I and therefore class II shall be omitted from the name.[63] The class I preQ1 riboswitch is further split into two classifications: type I, which exerts regulatory control through translational termination; and type II which does so through transcriptional termination. This work is focused on the type II variant and again this nomenclature shall be omitted in the following discussion for brevity.

This riboswitch enables the regulation of preQ1 **50** biosynthesis through its recognition and binding at the aptamer domain, once sufficient quantities of the metabolite have been generated, and subsequent "activation" of the expression platform. Since the expression platforms of riboswitches are known to be much less conserved, in comparison to the aptamer domain, then the biological mechanism

through which the expression platform operates to bring about the down regulation of the genes may differ from species to species. The preQ1 riboswitch isolated from *Bacillus subtilis* has been subject to the most investigation and consequently the details presented below refer to this species.

The aptamer domain of the preQ1 riboswitch is rather unusual amongst the other riboswitches as it requires only 34 nucleotides to afford ligand recognition, this is about 2.5 times less than the ligand related purine riboswitches. Despite its small structure it is able to achieve remarkable selectivity in binding; preQ1 **50** binds with a K_d of 20 nM, the precursor preQ0 **49** binds with a K_d of 100 nM and the riboswitch is able to discriminate against guanine binding. In the absence or low concentrations of preQ1 **50** the riboswitch aptamer forms a stem-loop structure (P1A, fig. 58) with another stem-loop structure (the antiterminator, fig. 58) towards the 3' end. In the presence of a significant concentration of preQ1 **50** the aptamer domain forms an alternative conformation, known as a psuedoknot, which sequesters a segment of the antiterminator enabling a terminator stem-loop to form and thus preventing transcription (fig. 58). It has been demonstrated that once the nucleotides for the antiterminator stem-loop have been transcribed and then adopted their secondary structure, the presence of preQ1 **50** will not induce the formation of the psuedoknot motif.[63, 64]

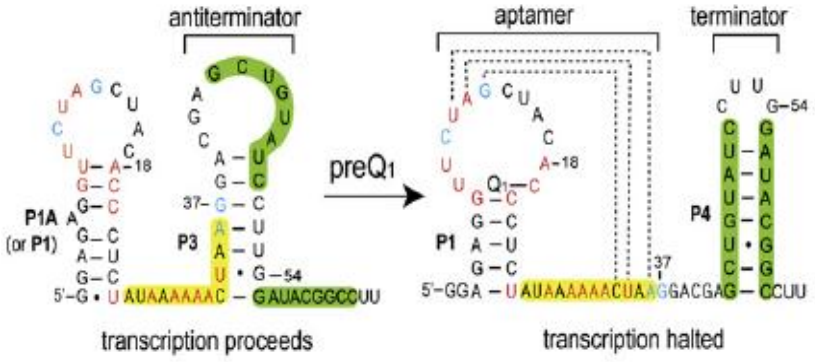

Figure 58: Formation of terminator stem-loop (reproduced with permission, see appendix 6).[65]

Phylogenetic analysis had originally predicted that the structure of the aptamer domain of the preQ1 riboswitch was a single stem-loop; however,

subsequent X-ray crystallography and NMR investigation have revealed that it is an H-type psuedoknot. This more complex 3D configuration allows for a variety of interactions that enable the aptamer to discriminate against similar ligands to PreQ1 **50**. H-type psuedoknots are composed of two stem sections (P1 and P2, fig. 59) separated by three loop regions (L1, L2 and L3, fig. 59), typically L1 is uracil rich and L3 is adenine rich.[65]

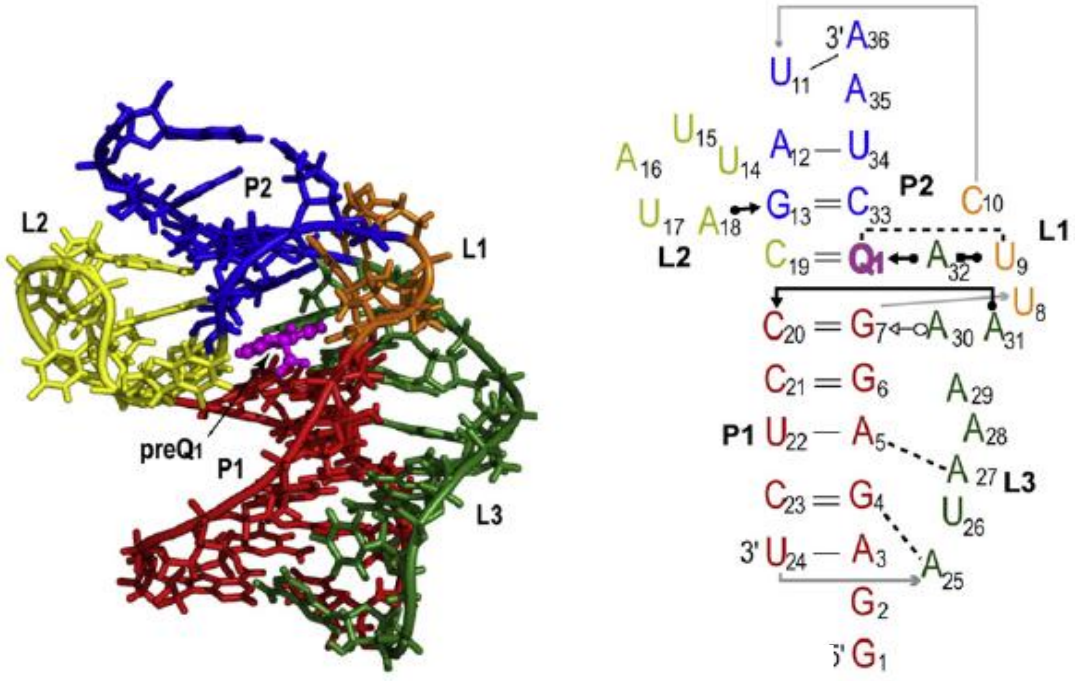

Figure 59: 3D structure of PreQ1 Riboswitch (left) and 2D representation (right) (reproduced with permission, see appendix 6). [65]

The 3' end of the adenine rich L3 is base paired to G13, A12 and U11 thus forming P2 which stacks on top of P1. PreQ1 **50** is sandwiched between P1 and P2 and forms a base quadruple with C19 by a Watson-Crick interaction and with A9 and U32 through its sugar edge (fig. 60).[65]

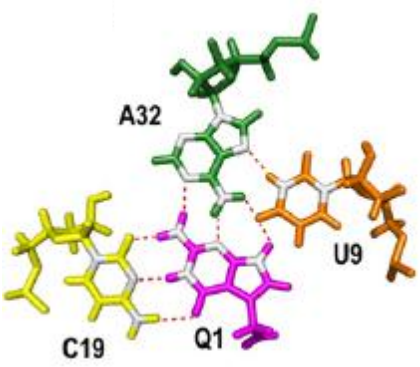

Figure 60: Interactions of PreQ1 with the Riboswitch (reproduced with permission, see appendix 6).[65]

In order to afford further stability to the preQ1 binding pocket there is a further base quadruplex below and a base triple above the preQ1 base quadruplex. The base triple is formed between G13, A18 and C33 and the further quadruplex is formed by the G7-C20 base pair interaction with A30 and A31 (fig. 61).[65]

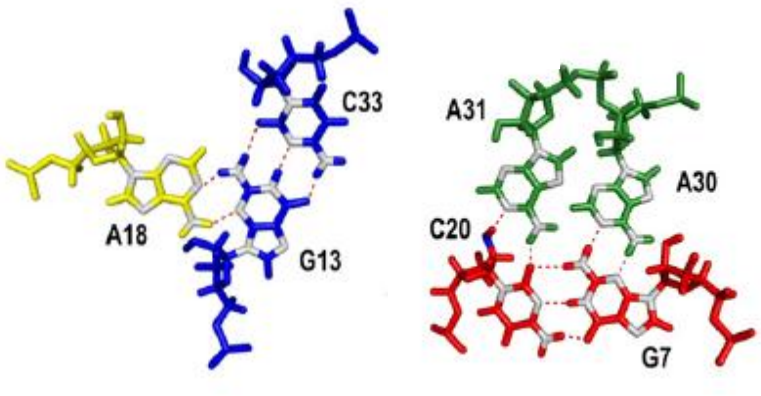

Figure 61: Base triple above preQ1 (left) and base quadruplex below (right) (reproduced with permission, see appendix 6).[65]

The Watson-Crick base pair to C19 is of great importance as it has been shown that if this residue is mutated to uracil then the aptamer will discriminate against PreQ1 **50** in favour of 2,6-diaminopurine. Similarly demonstrated has been the importance of the bases A31 and A32; if these are mutated to guanines then the aptamer fails to fold in the presence of PreQ1 **50**.

The specificity attained by this riboswitch is clearly related to the extensive network of hydrogen bonds that are formed between it and PreQ1. All of the

available H-bond donors and acceptors of the ring system and of the atoms directly attached to it are utilised. An X-ray crystal structure determination of preQ1 **50** bound to the aptamer has suggested that the alkylamino group hydrogen bonds to G7, the sugar of G13 and a water molecule (fig. 62); however, a solution state NMR study has suggested that there are only van der Waals contacts between the amino group and G7.[63, 64] Both of these are backed up by PreQ0 **49** displaying a 5-fold reduced strength of binding due to the alkylamino being replaced by a nitrile group.[65]

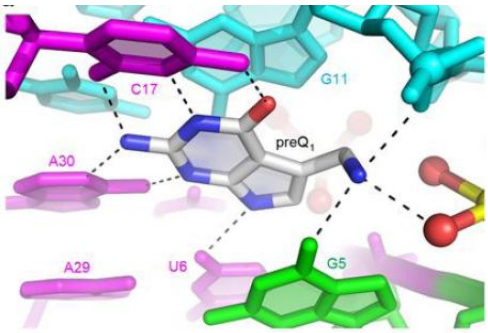

Figure 62: Hydrogen bonds of preQ1 in the riboswitch (reproduced with permission, see appendix 6).[65]

1.3.3.5 Project Aims in the PreQ1 Riboswitch Field

The ultimate aim was to design and synthesise PreQ1 **50** analogues that can bind to the riboswitch; however, in order to do so an assay to assess binding was first required to be established. This has been carried out by our collaborators at the University of Bonn and to set up the assay they required samples of both PreQ1 **50** and PreQ0 **49**; these have been synthesised.

The Suckling group have much experience in synthesising PreQ1 **50** like molecules and as such there is a large library of relevant compounds available to be screened for activity examples of which can be seen in figure 63. This set of compounds includes a variety of substitution patterns around the pyrrolopyrimide ring system. There are some 2 substituted thio compounds, **59** and **60**, some diamino compounds, **61** and **62**, and some fused furan compounds also, **61**.

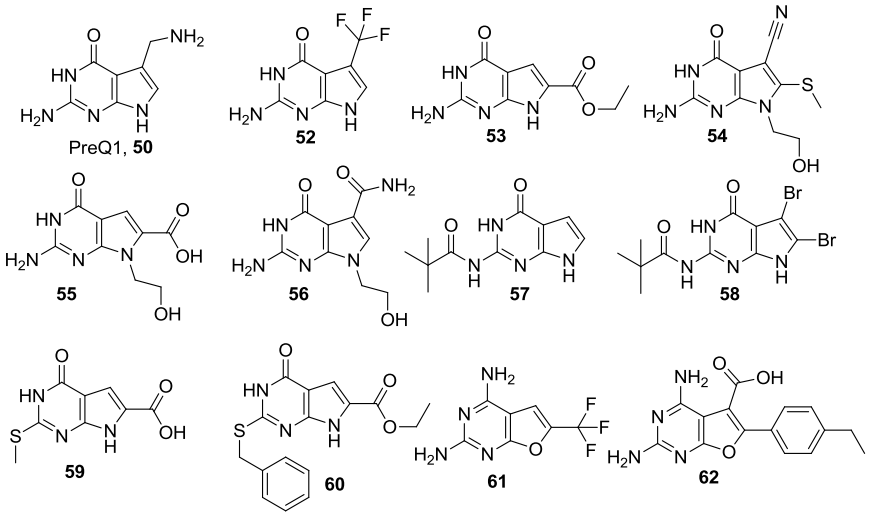

Figure 63: Examples of PreQ1 type compounds in our library.

Another aim of this investigation into the PreQ1 riboswitch was to gain further insight into the interactions of PreQ1 **50** with its riboswitch in order to direct which molecules from our library should be selected for screening. To achieve this, a molecular dynamics study was completed to provide some insight.

1.3.4 Introduction: Riboswitches: TPP Riboswitch

1.3.4.1 Biological Role of TPP

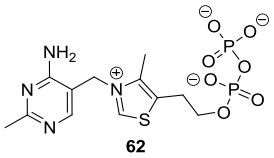

Figure 64: Thiamine pyrophosphate (TPP).

Thiamine pyrophosphate, **62**, (TPP, fig. 64) is an essential biological molecule that acts as a coenzyme for a large number of enzymes. These enzymes include pyruvate decarboxylase, which is associated with the formation of alcohol during anaerobic fermentation, transketolase which effects the transformation of a ketose into an aldose by a 2-carbon unit transferral and pyruvate dehydrogenase, which is involved in the synthesis of acetyl-CoA. Each of these enzymes is responsible for the catalysis of carbon-carbon bond-forming or bond-breaking reactions adjacent to a carbonyl group and the role of the TPP coenzyme in each case is that of an electron sink. In order to illustrate the general chemical mechanism of this coenzyme, the catalytic cycle for pyruvate decarboxylase is discussed (fig.65).[66]

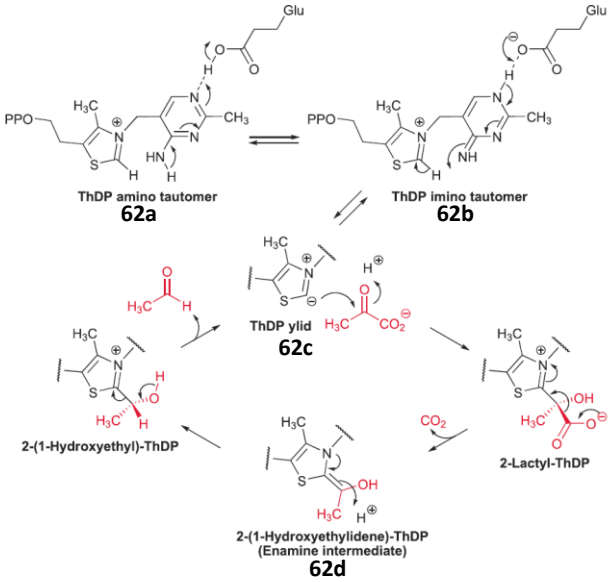

Figure 65: Catalytic cycle of TPP dependent enzymes; that for pyruvate decarboxylase shown (reproduced with permission, see appendix 7).[67]

The first step involves the conversion of the amino tautomer of the aminopyrimide **62a** into its imino tautomer **62b** through assistance of a nearby glutamic acid residue (fig. 66). Once in this form the exocyclic imino nitrogen deprotonates the C2 carbon of the thiazolium ring, thereby returning to the amino tautomer. The resulting ylide **62c** then nucleophilically attacks the keto group of pyruvate, effecting a decarboxylation, and leading to the formation of an enamine intermediate **62d**. The enamine can then attack a number of electrophilic species depending on the particular enzyme. For pyruvate decarboxylase, the enamine is protonated and the expulsion of acetaldehyde regenerates the ylide.[66]

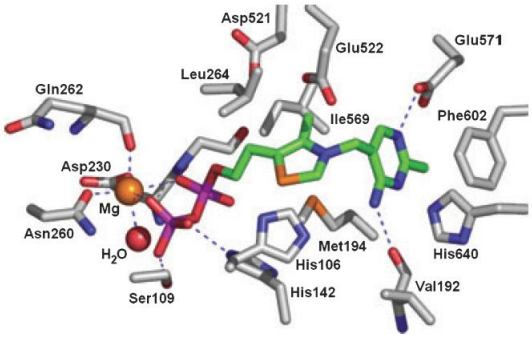

Figure 66: Binding site of pyruvate dehydrogenase showing catalytically required Glu (Glu571) (reproduced with permission, see appendix 7).[67]

1.3.4.2 Biosynthesis of TPP

Bacteria are able to synthesise TPP *de novo* by a long and complex route involving multiple genes. This route can vary considerably between species but follows a general trend: 5-aminoimidazole ribonucleotide (AIR) is converted into hydroxymethylpyrimidine monophosphate (HMP-P) and subsequently to the diphosphate (HMP-PP). Thiazole monophosphate (Thz-P) is synthesised from precursors tyrosine or glycine, cysteine, and deoxy-D-xylulose-5-phosphate. HMP-PP and Thz-P are then condensed to form thiamine monophosphate (TP) with the pyrophosphate of the HMP-PP acting as the leaving group during the reaction. TP is finally phosphorylated by the appropriate kinase to yield TPP. At a number of stages during this biosynthetic pathway there are precursor salvage routes present (fig. 67).[67]

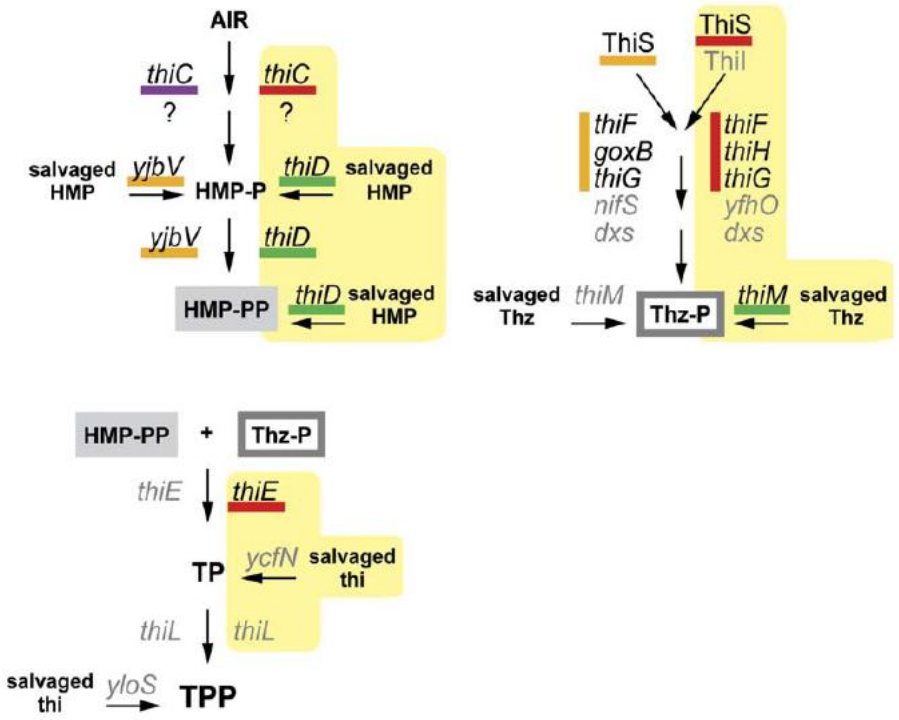

Figure 67: The biosynthesis of TPP in bacteria. Genes in yellow boxes are from *B. Subtillus*, those not are from *E.coli* (reproduced with permission, see appendix 8).[69]

In fungi *de novo* synthesis also occurs but it is much less well studied and currently only a few genes have been attributed to TPP **62** biosynthesis. Fungi are also able to import thiamine and intracellularly convert it into TPP **62** via a thiamine phosphokinase enzyme. Higher eukaryotic organisms are unable to carry out the full biosynthesis of TPP **62** and must rely on this import mechanism as their only source of TPP **62**.[67]

1.3.4.3 Pyrithiamine

In the late 1930's a number of groups became interested in synthesising the pyridinium isostere of thiamine, **63**, pyrithiamine, **64**, (PT, fig. 68), and this was eventually achieved in 1941 by Tracy and Elderfield.[66]

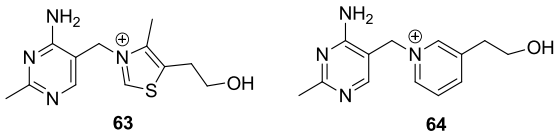

Figure 68: Thiamine, 63, Pyrithiamine, 64.

When administered to a newly weaned mouse a 0.17 mg dose was shown to retard growth the cause of which was discovered to be thiamine deficiency. Pyrithiamine, **64**, has been used widely in the following years to induce symptoms of thiamine deficiency in mice and it has also been shown to be toxic to many species of bacteria, fungi and algae.

The similarity to the endogenous thiamine, **63**, allows PT, **64**, to be phosphorylated to pyrithiamine pyrophosphate (PTPP) through the same biological mechanism that produces TPP, **62**. This generated the notion that PTPP brought about its effects through mimicking TPP, **62**, as a coenzyme where the inability to produce an ylid resulted in enzyme inhibition. Enzyme studies showed that PTPP was only a modest inhibitor of apo-transketolase and apo-pyruvate decarboxylase suggesting that the anti-thiamine effects were not due to competititive binding. In addition, a number of thiamine biosynthesising organisms that one would expect to upregulate their thiamine, **63**, production upon administration of PT, **64**, were found not to. Furthermore, PT, **64**, was shown to disrupt thiamine biosynthesis, through an unknown mechanism, resulting in a decrease in the production of thiamine. These observations are all neatly explained now that TPP riboswitches have been identified.[67]

1.3.4.4 The TPP Riboswitch

The TPP riboswitch is the only riboswitch to be found, thus far, in all kingdoms of life, and is the only one to date that has been found in plants.[67] Like all other riboswitches, it is found in the mRNA of many of the genes responsible for the biosynthesis of the cognate ligand, its transport and salvage of the precursors required for its synthesis, and thus forms a negative feedback loop. In bacteria and archaea the riboswitch tends to be found in the 5'-UTR of these genes whereas, for fungi and plants it can be found in the 5'-UTR, the 3'-UTR, or the introns of these genes. The expression platform is similarly diverse. Gram positive bacteria have shown examples of the riboswitch acting as a transcription terminator by forming a rho-independent transcription termination stem-loop. Gram negative bacteria indicate that it can suppress the initiation of translation by sequestering the Shine-Delgarno

sequence; and, in eukaryotic organisms the riboswitch can be found to regulate the splicing of the mRNA by acting as a ribozyme (fig. 69).[68]

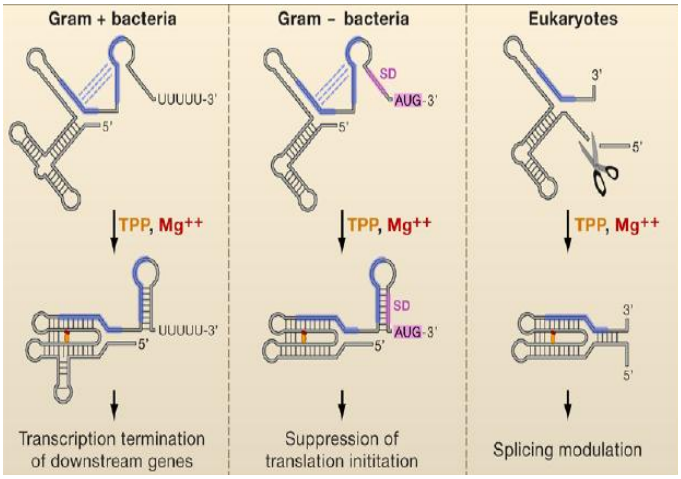

Figure 69: The expression platforms of the TPP riboswitch (reproduced with permission, see appendix 8).[69]

The TPP riboswitch displays a dissociation constant of around 50 nM and this level of affinity can only be achieved through extensive, and specific, interactions with the cognate ligand. An investigation into the conserved sequences of TPP riboswitches across all phyla has suggested that the minimum receptor domain is a secondary structure composed of five helical regions (P1 to P5) and three regions of mostly unpaired nucleotides (J2/3, J2/4 and J4/5, fig. 70). The nucleotides in the J regions, are almost universally conserved throughout all TPP riboswitches.[69, 70]

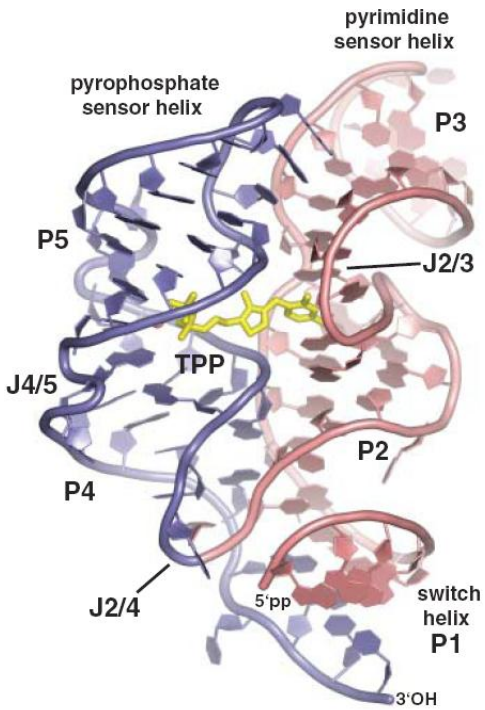

Figure 70: The 3D structure of the TPP riboswitch from *A. thaliana* (reproduced with permission, see appendix 8).[69]

A three way junction can be seen between helices P1, P2 and P4 along with bulge J2/4 and the bulges J2/3 and J4/5 connect helices P2 with P3 and P4 with P5, respectively. Overall, the structure is composed of two larger helical regions each interacting with a different region of the TPP **62** molecule: one is composed of P2 and P3 and this is termed the pyrimidine sensor helix; the other is composed of P4 and P5 and is termed the pyrophosphate sensor helix. The binding sites in each of the sensor helices form deep pockets so as to tightly bind their respective regions of TPP **62**.[70]

In the pyrimidine binding pocket of both an *E. coli* crystal structure and that of *A. thaliana* crystal structure can be seen three hydrogen bonds between the pyrimidine of TPP and two nucleotides of the riboswitch. Two of these are from a base pair with a conserved guanine and the other from a hydroxyl from the ribose of another guanine (fig. 71).

In the pyrophosphate binding pocket for the *E. coli* crystal structure there are two magnesium ions that coordinate to the RNA, TPP and several water molecules.

There are also a number of water-mediated and direct RNA-TPP hydrogen bonds that assist in binding. In the crystal structure for *A. thaliana* there is only one magnesium ion and no waters in the pyrophosphate binding site; in this case the hydrogen bonds occur directly between TPP **62** and the RNA (fig. 71).[70, 71] The understanding of the interactions between the pyrophosphate moiety and the riboswitch are crucial for the project goals as will be revealed later.

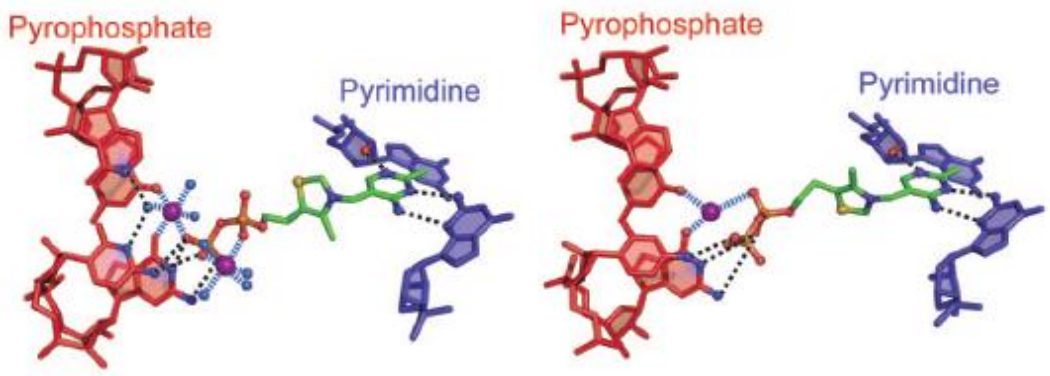

Figure 71: Interactions of TPP with the sensor helices of an *E.coli* and a *A. thaliana* crystal structure (left and right, respectively) (reproduced with permission, see appendix 9).[69]

Despite these differences in binding interactions, the overall shape of the riboswitch and the positioning of the nucleotides that interact with TPP are remarkably similar in both the prokaryotic and eukaryotic riboswitches (fig. 72).

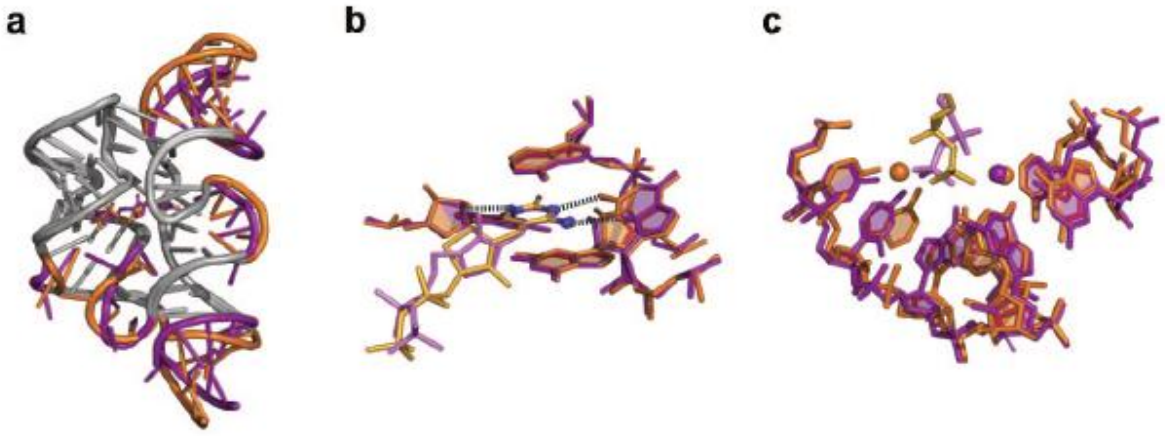

Figure 72: Overlay of riboswitches from *E.coli* (orange) and *A.thaliana* (purple). a) entire construct, b) pyrimidine binding pocket and c) pyrophosphate binding pocket (reproduced with permission, see appendix 9).[70]

The presence of the magnesium ions in the riboswitch structure is essential for its proper functioning; this is no different to any other polynucleotide structure as counter ions are ubiquitously required to stabilise the polyanionic backbone inherent in these structures. The association constant of TPP **62** to its riboswitch from *Aspergillus oryzae* was shown to decrease with decreasing concentration of magnesium ions. Moreover, replacement of the magnesium ions by sodium or potassium ions, by exposing the riboswitch to high concentrations of these, showed that the TPP **62** did not bind tightly in comparison to magnesium ion exposure. This suggests that the interactions are not just electrostatic but specific to the coordination capacity of the magnesium in the environment of the pyrophosphate binding region.[71, 72]

It must be noted that the thiazolium moiety of TPP **62** interacts very little, if at all, with the riboswitch. This fact allows the analogue pyrithiamine **64** to bind to the riboswitch once it is intracellularly phosphorylated; the pyridinium replacement makes similarly few interactions.[73] This importance of this structural tolerance is crucial to the goal of this project.

Another crucial interaction within the riboswitch structure is that at the three way junction of P1, P2 and P4. Four nucleotides, including those from distant regions in the primary sequence, form an interaction platform (fig. 73) which stabilises the kink in junction J2/4 between both sensor helices. This interaction platform is thought to be important as it allows for the correct folding of the helix P1 which is coupled to the "off" state of the gene for all types of expression platform.[70]

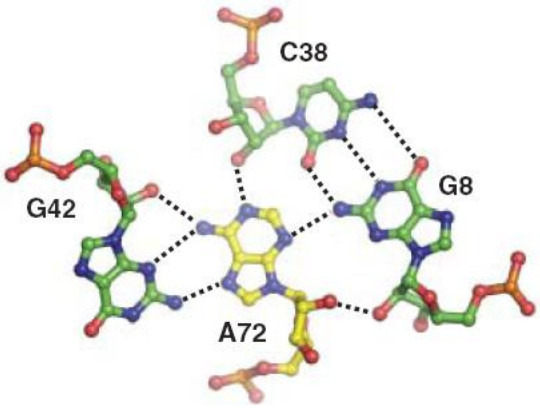

Figure 73: The interaction platform of *A. thaliana* (reproduced with permission, see appendix 8).[69]

The importance of this interaction platform is further exemplified in that it is mutations in this region, specifically A72, that are responsible for pyrithiamine resistance in *Aspergillus oryzae*. Similar resistance in bacteria is thought to be caused by mutations in both A72 and C38 (*A. thaliana* numbering). It has been shown that these mutations do not affect the binding of TPP **62** or PTPP to the riboswitch, as the sensory regions are unaffected by the mutation, instead the concomitant allosteric change in P1 to effect the gene regulation does not occur.[67]

The sequence of events during the operation of this riboswitch can be expressed thus: TPP **62** binds to both sensory helices parallelising their relative orientations (1, fig. 74); the interaction platform is assembled as a consequence (2); and this leads to a decrease in the entropic penalty associated with the formation of P1 (3).

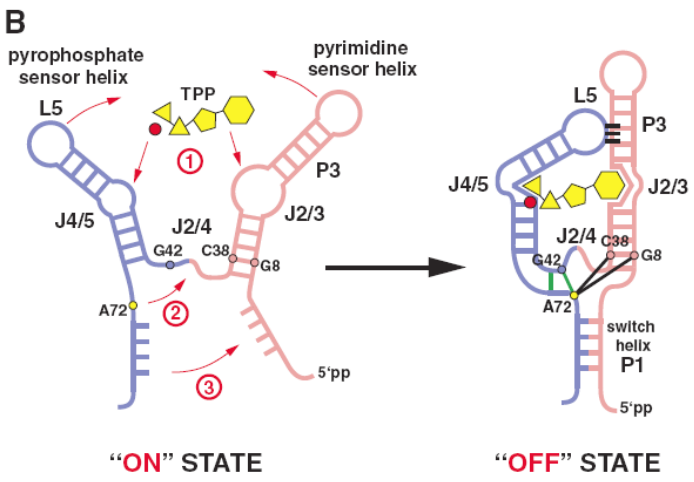

Figure 74: The switching off of the TPP riboswitch (reproduced with permission, see appendix 9).[70]

1.3.4.5 Project Aims in the TPP Riboswitch Field

It will be the aim of this project to investigate analogues of TPP, **62**, that can bind to and switch off genes associated with the TPP riboswitch. The most important feature of the analogues is a suitable isostere for the pyrophosphate moiety of TPP, **62**, as it is widely known that highly charged molecules will have considerable issues relating to bioavailability. Additionally, as very little is known about non-natural ligands binding to this riboswitch, thus molecules were also designed with a view to gaining more insight into the biology of the system.

Firstly, an *in silico* study was carried out on the TPP riboswitch in order to direct further sysnthesis. From here a library of TPP **62** analogues was designed and synthesised and their biological effects have been evaluated.

Chapter 2 Results and Discussion: MGBs

2.1 Results and Discussion: Minor Groove Binders

To achieve the intended outcome of advancing the lead compound set from preclinical development a number of factors needed to be investigated. First, a suitable formulation for the compounds needed to be found that was acceptable for an animal model toxicology study and acceptable for clinical trials. The stability of the compounds in solution was also investigated as if they are to be administered as drugs then it is important to insure they are not undergoing chemical changes either before administration, say as a solution for injection, or whilst in the blood or gastrointestinal tract depending on the route of administration. The metabolic stability of these compounds was also of great interest as if they were metabolised to inactive metabolites and excreted then they would unlikely be taken forward to clinical studies. Several studies were carried out to investigate these different stabilities. For the above to be achieved, sufficient material was required to be synthesised, much more than usually synthesised in our lab, and thus an investigation into scale up was also carried out.

2.2 Lead Compound Scale Up

2.2.1 Precursor Synthesis

The most troublesome step in the synthesis of the MGBs was the final step involving the coupling of the head group to the tail group dimer as the yields were particularly low, around 30 %, and purification was carried out by HPLC, a technique not appropriate for manufacture at scale. This step was chosen to be further investigated for optimisation but before this could be carried out many of the precursors had to first be synthesised.

An intermediate required for the synthesis of each of **BP1**, **BP2** and **BP3** is the morpholino tail dimer **68** and this was synthesised according to scheme 1.

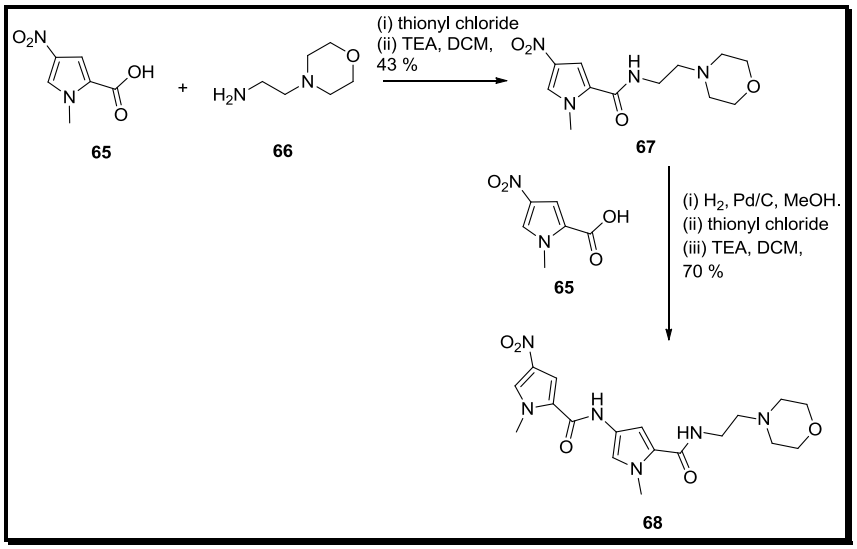

Scheme 1

Across the six lead compounds there are only four different head groups (fig. 75).

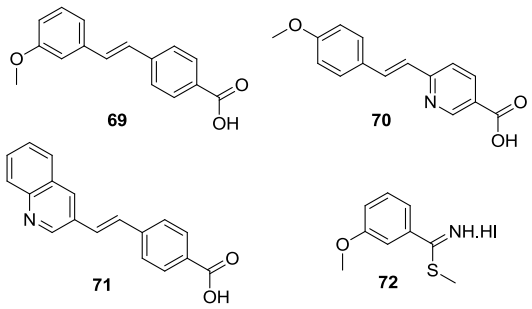

Figure 75: MGB head groups.

Compounds **69 – 71** were prepared using a similar method that was established method in our lab (scheme 2 and 3).

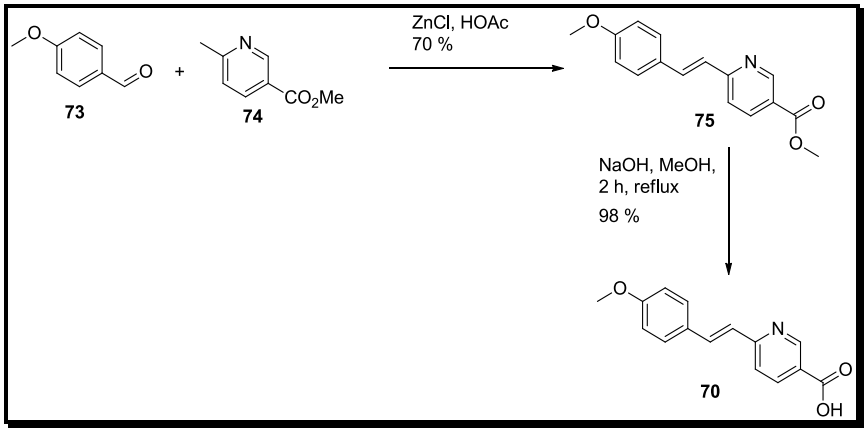

Scheme 2

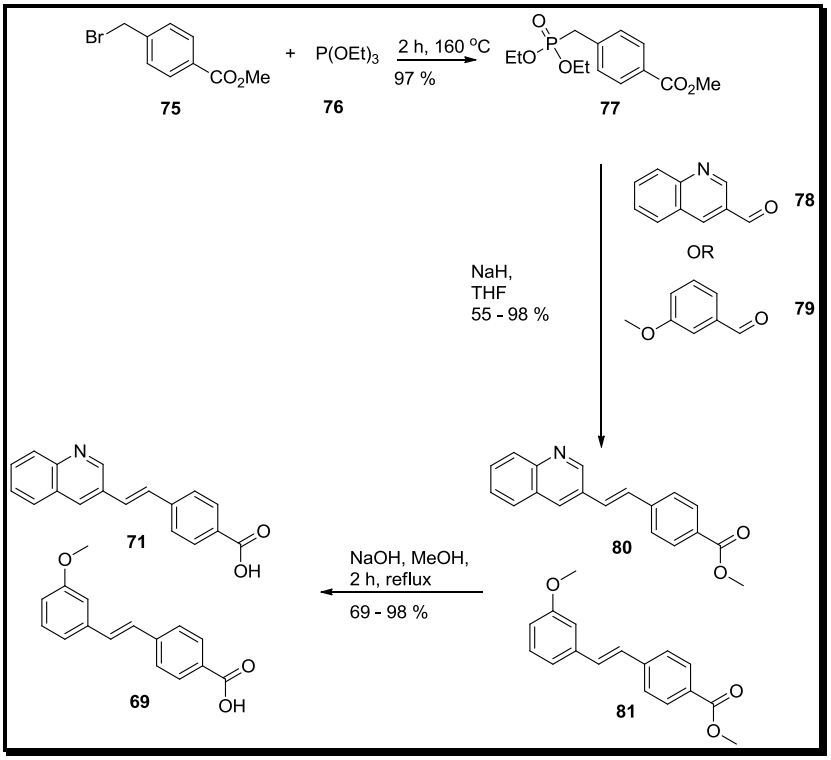

Scheme 3

The final head group to be synthesised was compound **72** and our lab's original synthesis of this afforded an overall yield of 3%. In light of the large quantities now required it seemed appropriate to revise this method. Starting from the commercially available 3-methoxybenzamide, **82**, a conversion into the corresponding thioamide, **83**, was afforded by the use of Lawesson's reagent (scheme 4). Initial purification was carried out by column chromatography after the solvent had been removed under reduced pressure; however, subsequent

investigation revealed that the desired material could be obtained in pure form by recystallisation of the reaction residue from acetone/water. Consistent yields of approximately 70% could be obtained using both column chromatography and recrystallisation. The thioamide was then reacted with methyl iodide, as per the original synthesis in order to afford compound **72** in 72% yield (scheme 4).

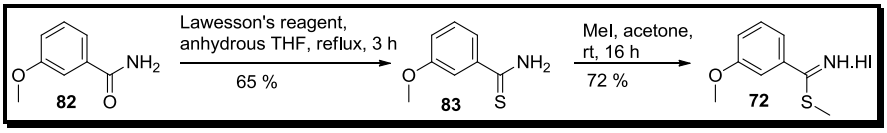

Scheme 4

Compound **72** was thus prepared in an overall yield of 47%, over two steps, which is a significant improvement over 3%.

2.2.2 Investigation Into Head Group Coupling

The final step for compounds **BP1**, **BP2** and **BP3**, and a step in the synthesis of compounds **BP5** and **BP6**, involves an amide coupling of the carboxylic acid of the head group to the amine of the rest of the MGB. Traditionally, this has been done on a small scale by HBTU coupling followed immediately by HPLC purification, with yields in the region of 30%. Purification by HPLC does not lend itself to large scale synthesis and thus an alternative coupling procedure was sought; it was thought that alternative active esters of the head groups could be prepared and stored prior to use. Firstly, the pentafluorophenol (PFP) esters were investigated using compound **70** as this was available in highest quantity. Compound **70** was converted to the acid chloride using of thionyl chloride, and after removal of solvent under reduced pressure it was reacted immediately with pentaflurophenol in anhydrous DCM, using NMM to quench the resultant acid (scheme 5). No product was observed by mass spectrometry or NMR and thus an alternative coupling agent was sought to afford the active ester.

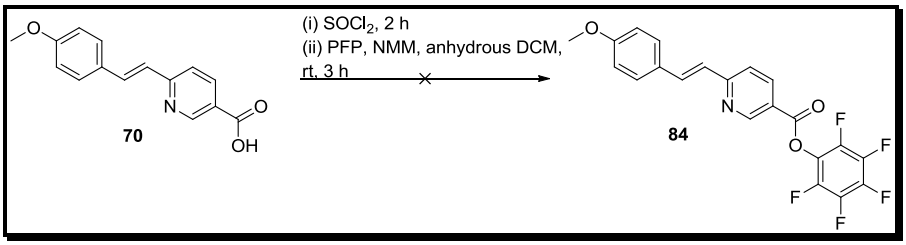

Scheme 5

Both DCC and DIC were used and the reaction conditions for both involved dissolving the carboxylic acid, **70**, in anhydrous DCM, adding the respective coupling agent and stirring for 30 mins, followed by the slow addition of PFP and monitoring by TLC (scheme 6). The reaction mixtures were then washed with saturated potassium carbonate and the solvent removed under reduced pressure to yield a solid material. Subsequent washing with ether yielded the active esters in pure form. The average yield for the DCC reaction was approximately 45%; whereas, that for the DIC was around 50%.

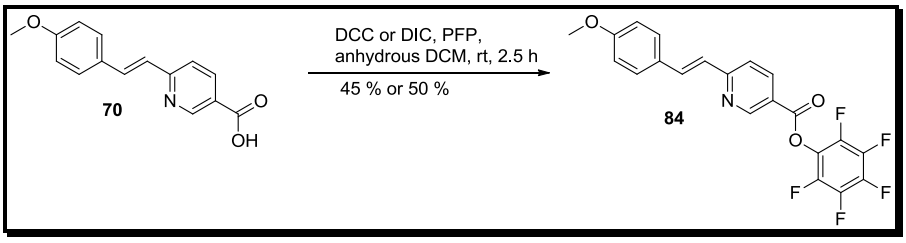

Scheme 6

The yield of 50% was deemed somewhat low and as such it was decided to try an alternative to this active ester in the form of the pivalic anhydride. Compound **70** was reacted with pivaloyl chloride at room temperature in anhydrous DCM using TEA as the base to quench the acid formed *in situ* (scheme 7). NMR revealed that the reaction had produced a mixture of the active anhydride, **85**, and pivalic acid, **86**, and no simple workup procedures could remove the pivalic acid thus column chromatography would need to be used in purification.

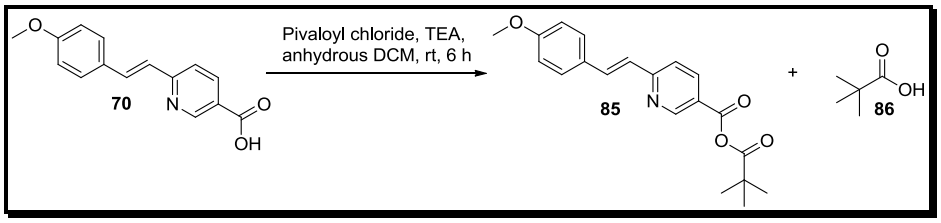

Scheme 7

Since the PFP active ester approach avoided the need for chromatographic purification and the scaling up potential of the reactions was important, this active anhydride method was abandoned. The PFP active ester approach employing DIC was thus the method of choice to produce a storable, active head group for coupling and as such compounds **69** and **71** were similarly reacted to generate the respective active esters, **87** and **88**, in similar average yields (scheme 8).

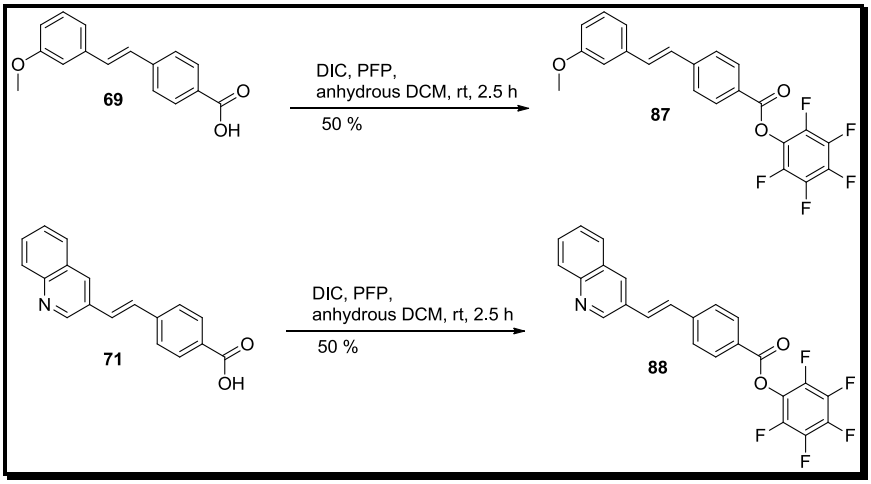

Scheme 8

2.2.3 Final Couplings to Generate Target Compounds

With a stock of the morpholino dimer **68** and the active pentafluoro phenol esters, **84**, **87** and **88**, of each of the head groups in hand the assement of the final couplings was carried out. The nitro group of the morpholino dimer **68** was reduced to the amine by hydrogenation and once the catalyst and solvents were removed, this was dissolved in DMF. To this was added 1 equivalent of the necessary pentafluoro phenol ester, either **84, 87** or **88**, and the reaction mixture heated for 2 h at 50 ^{o}C then left at room temperature for a further 16 h. After removal of the DMF under reduced

pressure, the resulting residue was treated with ethyl acetate containing 5% methanol and saturated solution of potassium carbonate. This resulted in the precipitation of the desired compounds, **BP1, BP2** or **BP3**, in yields of 52 – 72 % (scheme 9).

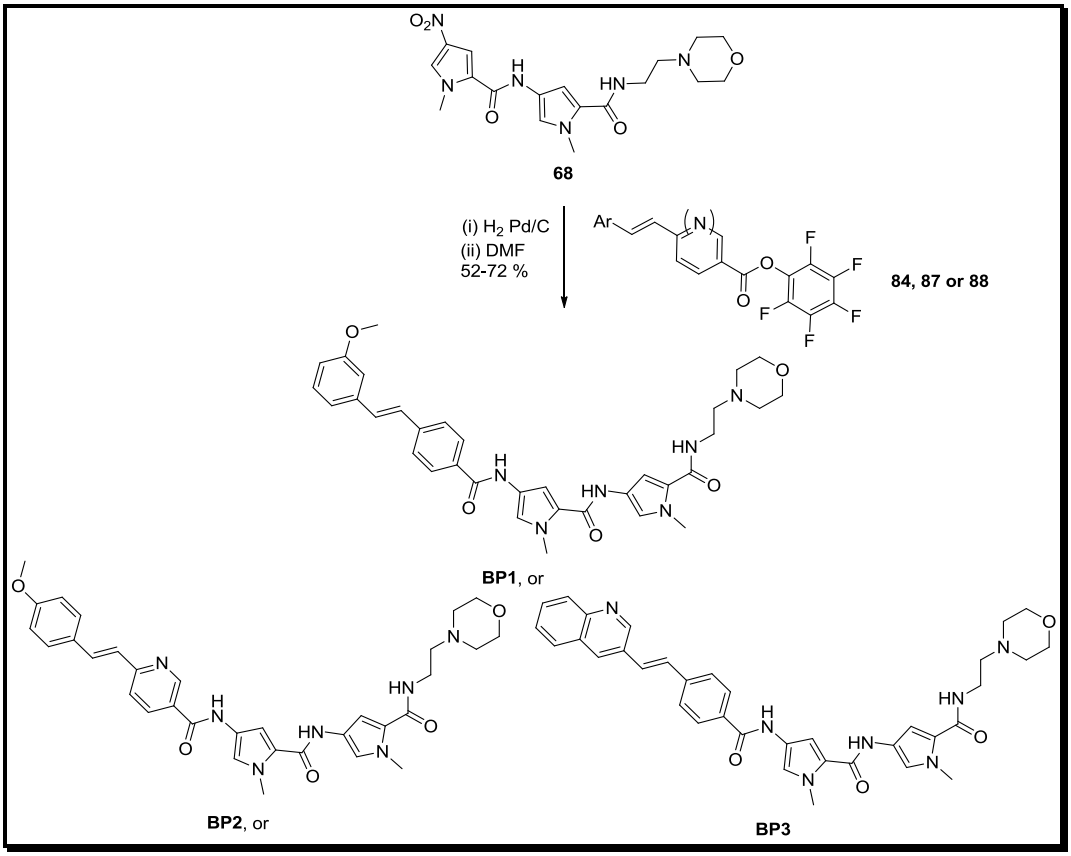

Scheme 9

This method was a definite improvement on previous methods as HPLC purification had always been used in the final step. The reason for this was largely due to the quantities involved; around 10 – 30 mg of final MGB were only ever synthesised previously. In light of this it was decided to try the original HBTU syntheses on a larger scale to see if the product could precipitate without the need for purification.

As for the pentafluorophenyl ester couplings, the nitro group of the morpholino dimer **68** was reduced to the amine by hydrogenation and once the catalyst and solvents were removed, this was dissolved in DMF. To this was added the carboxylic acid of the head group, either **69, 70 or 71**, 2 equivalents of HBTU

and the reaction mixture was left at room temperature for 16 h. The same work up procedure as for the active ester couplings produced the desired compounds, **BP1, BP2** or **BP3**, in similar yields and without the need for further purification (scheme 10).

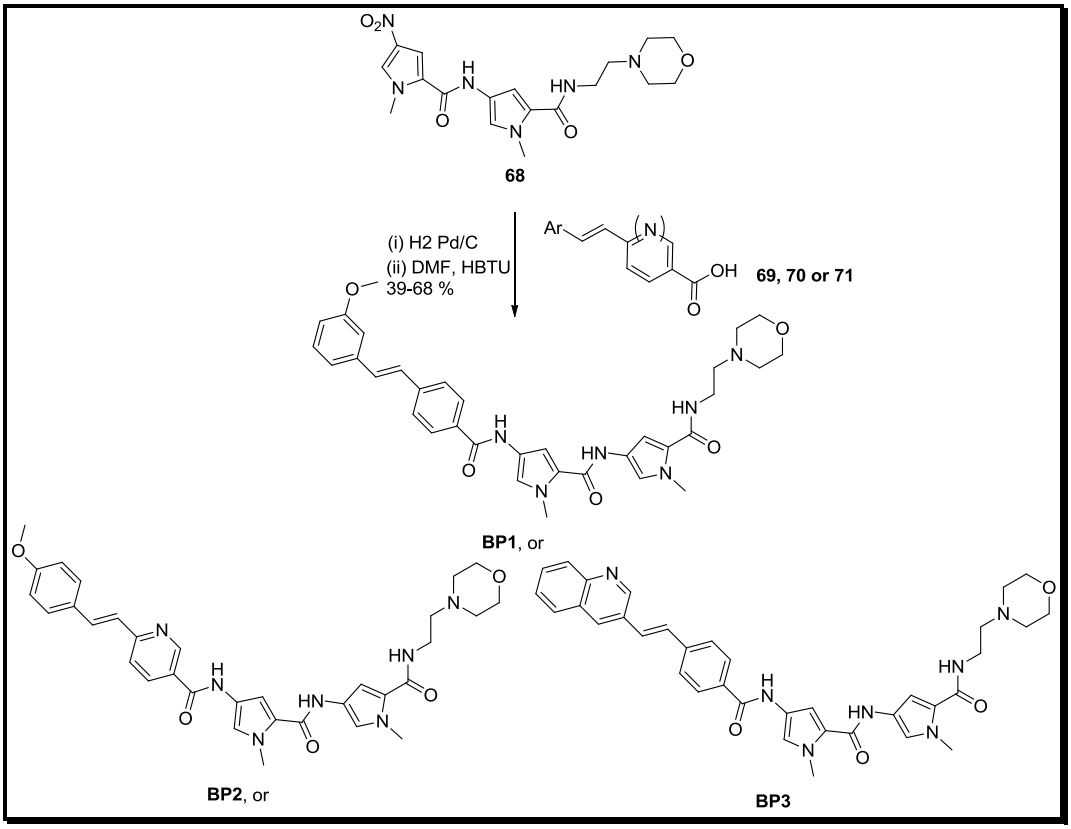

Scheme 10

Comparatively, the HBTU coupling method is now preferred as it has one step less in the total synthesis due to no requirement to prepare an active ester of the head group.

With the above efforts in optimising the reactions complete, enough of the lead compounds were syntheisied in order to carry out the initial solubility studies and stability studies. Eventually, the synthetic methods were handed over to a Contract Research Organisation who provided the compounds for the later solubility studies. In the case of **BP3**, this investigation into synthetic procedures for scale up has contributed towards production on the kilogram scale.

2.3 Solubility and Stability Investigation

2.3.1 Solubility Studies

Physiological conditions are aqueous with a pH of 7.4 and as our compounds are potential drugs the solubility of these in a similar system is of great importance. There are, however, a number of pharmaceutically acceptable vehicles of administration and, as such, each compound was subjected to series of solubility tests with different applicable solvent systems. These solvent systems may include dipolar aprotic or protic solvents, such as DMSO or propylene glycol, respectively. Other excipients that are often used are cyclodextrins that are able to form inclusion complexes with many drug molecules.

Compounds **BP1**, **BP2** and **BP3** were used as the free bases and **BP4**, **BP5** and **BP6** as the TFA salts (structures can be found on page 35). The TFA salts were used for the latter compounds as these were prepared by HPLC purification in which the solvent system contained TFA. A summary of these is shown in the table that follows (table 2).

mg/mL	**Compound**					
Solvent	**BP1**	**BP2**	**BP3**	**BP4(2TFA)**	**BP5(TFA)**	**BP6(TFA)**
Propylene Glycol	N/A	N/A	N/A	13.4	10.4	11.2
Cyclodextrin/pH 6 Buffer[1]	N/A	10.4[2]	N/A	N/A	N/A	N/A
Cyclodextrin/pH 5 Buffer[1]	N/A	10.4[2]	N/A	N/A	N/A	N/A

Table 2: Data indicate the minimum solubility achieved in mg/mL. N/A indicates that solubility was not observed in the tested solvent system. [1]The cyclodextrin was hydroxypropyl-β-cyclodextrin which was used at a concentration of 33.6 M in a pH 6 or 5, 10 mM Citrate Bufffer. [2]This level of solubility was only observed after sonication and 4 hours of standing.

The lack of solubility observed for the free bases led to the assessment of their solubility as HCl salts. The HCl salt form was chosen over the TFA salt as the former is more pharmaceutically acceptable. These data are shown in table 3.

mg/mL	Compound		
Solvent	**BP1(HCl)**	**BP2 (2HCl)**	**BP3(2HCl)**
Propylene Glycol	12.2	12.8	11.6
Cyclodextrin/pH 6 Buffer[1]	10.2	12.2	11.4

Table 3: Data indicate the minimum solubility achieved in mg/mL. . [1]The cyclodextrin was hydroxypropyl-β-cyclodextrin which was used at a concentration of 33.6 M in a pH 6, 10 mM Citrate Bufffer.

The HCl salts of compounds **BP1**, **BP2** and **BP3** display far improved solubility profiles compared with their free bases. The solubility of the HCl salts of **BP1**, **BP2** and **BP3** along with the TFA salts of **BP4**, **BP5** and **BP6** were then investigated using a system closer to that of the physiological system. These data are presented in table 4.

Compound	Solvent System	Conc	Soluble?	Comments
BP1	pH 7.4 10 mM phosphate buffer	2 mg/mL	No	Precipitation seen after 3h from that which did dissolve
	pH 7.4 10 mM phosphate buffer with 25% DMSO	20 mg/mL	Yes	
BP2	pH 7.4 10 mM phosphate buffer	2 mg/mL	No	Precipitation seen after 3h from that which did dissolve
	pH 7.4 10 mM phosphate buffer with 25% DMSO	20 mg/mL	Yes	
BP3	pH 7.4 10 mM phosphate buffer	2 mg/mL	No	Precipitation seen after 3h from that which did dissolve
	pH 7.4 10 mM phosphate buffer with 25% DMSO	20 mg/mL	Yes	
BP4	pH 7.4 10 mM phosphate buffer	2 mg/mL	No	
	pH 7.4 10 mM phosphate buffer with 25% DMSO	20 mg/mL	No	1.5 mg/ml in 50% DMSO
BP5	pH 7.4 10 mM phosphate buffer	2 mg/mL	No	
	pH 7.4 10 mM phosphate buffer with 25% DMSO	20 mg/mL	No	1 mg/ml in 75% DMSO
BP6	pH 7.4 10 mM phosphate buffer	2 mg/mL	No	
	pH 7.4 10 mM phosphate buffer with 25% DMSO	20 mg/mL	No	1 mg/ml in 75% DMSO

Table 4: Solubility studies on Lead compounds.

Compounds **BP1**, **BP2** and **BP3** clearly display a much better solubility profile in comparison to the others and this is largely due to their common feature of the morpholine tail group.

Across the spectrum of distamycin analogues it has been found that a basic tail group is an important feature, more specifically a nitrogenous one.[74, 75] The amidine functional group on the tail of distamycin **25** has pK_a of 12.4, and so at physiological pH is significantly protonated. [74] This is simultaneously a benefit and a

burden to the molecule: whilst it is true that the charge will hinder the molecules' ability to pass through the cell membrane, it will also confer to the molecule the required solubility in the gut wall and thus favourably increase its pharmacokinetics related to oral administration.[4] In the case of distamycin **25**, an active transport mechanism that recognises the guanidine to allow cell uptake is likely to be available and so the positive charge does not detrimentally affect the activity as the molecule circumvents the need for membrane solubility. Contrariwise, other MGBs may not have an active transport mechanism available to them and hence the ionic character of the molecule and thus the pK_a of the tail group are of paramount importance.

With a predicted pK_a of around 8 the morpholine tail group is only weakly basic and thus is partially ionised at physiological pH allowing easy equilibration between the ionised and non-ionised states.[76] This provides both the necessary solubility in the ionised form and the membrane crossing capability of the non-ionised form.[4]

Compounds **BP5** and **BP6** are rather insoluble in the tested solvent systems and this is due to their tail groups: these were specifically designed to be non-ionic in order to combat possible cell membrane permeability but now suffer in terms of solubility as their pK_as have been significantly increased. Compound **BP4** displays a slightly better solubility profile but it too is fairly insoluble.

Since the scale up of the lead compounds was complete it was possible to submit a sample of each to the formulation unit in the Strathclyde Institute of Pharmacy and Biomedical Sciences (SIPBS) to have their pK_as measured. The data are shown in table 5.

Compound	**BP1**	**BP2**	**BP3**	**BP4**	**BP5**	**BP6**
pK_a 1	NA	3.49	4.38	8.44	NA	NA
pK_a 2	6.04	5.26	6.02	9.12	4.04	4.05

Table 5: pKas of our lead compounds

It can be seen from table 5 that **BP1**, **BP2** and **BP3** each display pKas much lower than expected. This illustrates an important point that will be expanded upon in later in this section: many of these MGBs self-associate in aqueous media. It is believed that this self-association is the cause of the lower than expected pK_as. Moreover, recent studies on **BP4** within the department suggest that it does not show appreciable self-association which is in line with it having expected pK_a values.

At this point in the project the company that were working with the University of Strathclyde to further develop the lead compounds selected **BP3** as their lead molecule due to its excellent activity against both MRSA and *Clostridium difficile*. It was shown to be superior to vancomycin, the industry standard antibiotic, against both of these bacteria with MICs in the 0.1-1 µM range. More generally, BP3 was found to inhibit the growth of 87 % of all Gram positive isolates tested compared with 43 % for vancomycin.

The toxicity of the compound in an animal model had to be investigated and to do this a concentration of 100 mg/mL had to be achieved. *C. difficile* is a gut borne infection and thus an acceptable route of administration is an oral dosage. **BP3** has two protonisable sites and is thus soluble in the acidic environment of the stomach which allows a concentration of 100 mg/mL to be achieved for the oral route of administration. However MRSA is a systemic infection, which means that either the compound has to be absorbed through the gut wall and into the blood steam, if using an oral route of administration, or a parenteral administration can be used. It was found that BP3 is very poorly absorbed through the gut wall which is good for *C. difficile* treatment, as the compound can stay concentrated in the gut, but means that an oral route of administration for MRSA is rather difficult.

The company was keen on achieving a parenteral formulation that was as close to physiological pH as possible; however, with a high concentration of 100 mg/mL it was found that **BP3** would not remain in solution at pH 7.4. In neutral conditions **BP3** is predominantly uncharged and previous investigations in the Suckling group have shown that **BP1**, a close analogue of **BP3**, exists as dimers in solution, even at very low concentration. Further physical chemical investigations

have shown that these dimers aggregate, in an unknown manner, which can lead to the formation of gels and precipitation. Previously it was mentioned that the pK_as of these MGBs are much lower than expected and it is believed that self-association is the cause of this phenomenon. This aggregation can be easily demonstrated by viewing the NMR spectra of BP3 in *d*-DMSO and D_2O (fig 76 and 77 respectively). It can be seen that the signals in the *d*-DMSO spectrum are sharp; whereas, in the D_2O spectrum the signals are much broader which is an indication of significant aggregation.

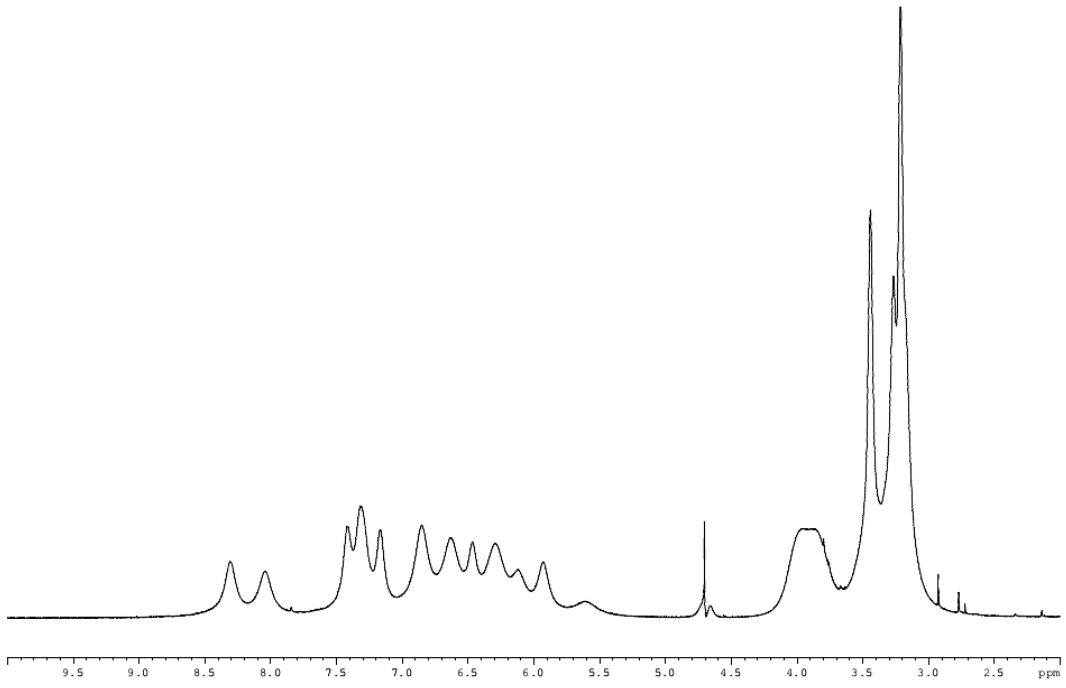

Figure 76: ^{1}H NMR of BP3 in D_2O.

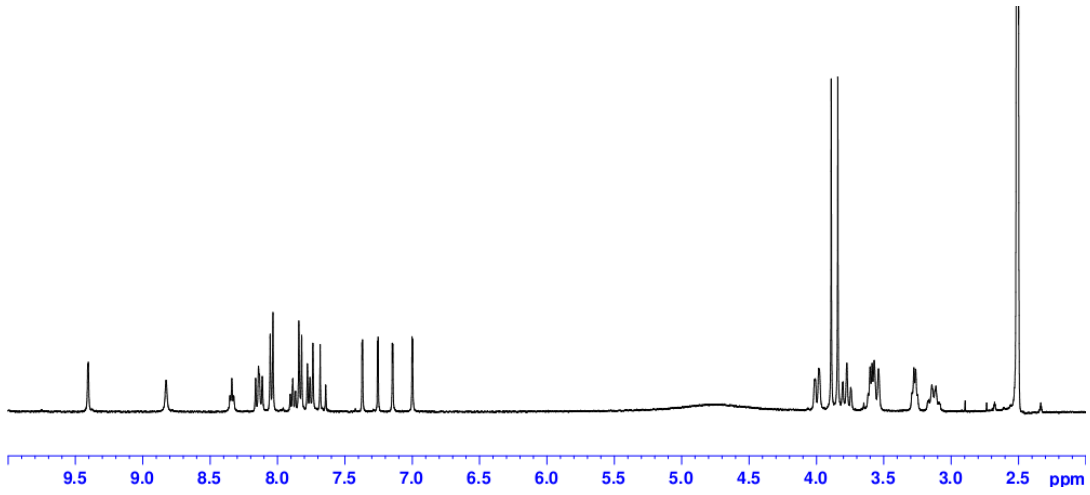

Figure 77: ^{1}H NMR of BP3 in *d*-DMSO.

It was thought that aggregation of these dimers could be prevented by introducing additives to the formulation and perhaps enable a concentration of 100 mg/mL to be achieved. Glucose, mannitol, sucrose, glucose-6-phosphate and hydroxypropyl-β-cyclodextrin (HPβCD) were chosen as the additives. HPβCD was chosen as it is a well established solubiliser used in pharmcuetical formulations and it was hoped that part of **BP3** may be able to be encapsulated within the cyclodextrin preventing further aggregation. The three sugar molecules were chosen to investigate whether or not they could form hydrogen bonds to the inner curve of **BP3** dimers (fig. 78). If they did, then this too may prevent further aggregation of the dimers through added steric bulk of the sugars. Glucose-6-phosphate was chosen as it too could interact with the MGB dimers. In this case it could be possible that the negatively charged phosphate groups on the sugar could interact with the positive charges on the MGB tail groups.

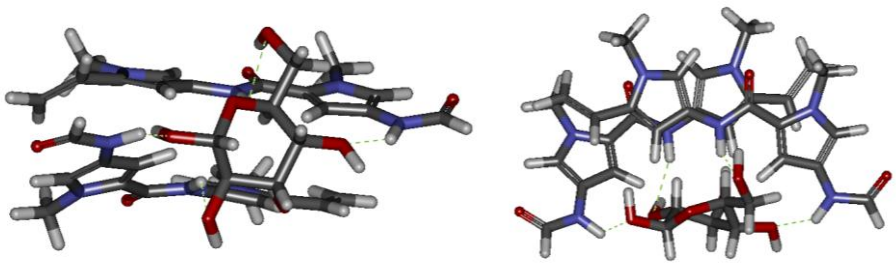

Figure 78: Proposed interactions of a sugar molecule with the central region of an MGB dimer. Simple Chem3D illustration.

It is not normal practise to adopt this type of molecular approach when investigating additives for use in formulations; however, given our molecular understanding of the physicochemical properties of MGBs due to their self-association, it was appropriate.

At this time the stock of **BP3** was insufficient to carry out this additive study so it was decided to use **BP2** instead and it was used as the HCl salt. It was also decided that it was more important to observe if there were any effects due to the additives rather than trying to achieve the desired concentration and pH in case precipitation occurred. The additives were investigated at final concentrations of 1% 2.5% and 5% weight/volume, **BP2** was at a final concentration of 12.5 mg/mL and the pH of the solutions was maintained at 3. The effects of the additives on the time for the solution to gel are shown below in table 6.

Additive	Conc	0 hrs	2 hrs	18 hrs	32 hrs	104 hrs
None	NA					
Glucose	1%					
	2.5%					
	5%					
Mannitol	1%					
	2.5%					
	5%					
Sucrose	1%					
	2.5%					
	5%					
Glucose-6-phosphate	1%					
	2.5%					
	5%					
HPβCD	1%					
	2.5%					
	5%					

Table 6: Effects of additives on pH 3 12.5 mg/mL solution of BP2. Fully in solution, green; Gelling/Precipitation, red; Slight gelling, amber.

Some very interesting qualitiative information can be gleaned from these data. Sucrose had no noticeable effect on the formation of gels whereas, both glucose and mannitol could significantly hinder the formation of gels for up to 32 hours. Higher concentrations of glucose-6-phosphate also prevented the onset of gel

formation. The most effective additive from this study was the cyclodextrin,which can prevent the formation of a gel for at least 32 hours and even after 104 hours the solution had not fully gelled.

After a sufficient quantity of **BP3** was available, the above solubility study was repeated. As the additives were believed to be interacting with an MGB dimer, subsequent solubility studies used a 2:1 molar ration of MGB to additive. Our industrial partner expressed particular interest in assessing the solubility of the free base at a concentration of 100 mg/mL with the additives and so an initial attempt was made to achieve this concentration in water adjusted to pH 4 with HCl. Unfortunately, the free base of **BP3** did not show any signs of solubility. In order to retrieve some information from this experiment it was decided to include an organic solvent, *N*-methylpyrolidine (NMP), to afford solubility. This is a dipolar, aprotic solvent that is miscible with water. To this end, solutions were prepared that consisted of a 1:1 mixture of NMP: pH4 water and in this was **BP3**, at a final concentration of 100 mg/mL and an additive at a concentration that gave a 2:1 molar ratio between **BP3** and additive. A further four additives, chosen on a similar basis to the others, were investigated also. The results are presented in table 7.

Additive	0 hrs	1 hrs	2 hrs	3 hrs	5 hrs	70 hrs
None (10)						
Mannitol (1)						
Glucose (2)						
Sucrose (3)						
HPβCD (4)						
L-Tartaric Acid (5)						
DL-Tartaric Acid (6)						
Glucose-6-phosphate (7)						
Meso Tartaric Acid (8)						
D-(+)-Mannose (9)						

Table 7: Effects of additives on 100 mg/mL solution of BP3 in 1:1 mixture of NMP and pH 4 water. Fully in solution, green; Visible tubidity, yellow; Slight precipitation, amber; Significant precipitation, red; complete precipitation, red and crossed.

It is clear from table 7 that these additives are able to influence the onset of precipitation in comparison to the control. The following all cause a shortening of the precipitation free period: mannitol, glucose, sucrose, HPβCD, DL-tartaric acid, meso

tartartic acid and D-mannose. L-tartaric acid displays a similar profile to the control and glucose-6-phosphate is able to remain fully in solution for at least an extra two hours. Presented below are two photographs showing the test solutions after the 70 hour period.

Figure 79: Final appearance of vials after additive solubility study. Numbers correspond to those in table 2.

It was desirable to find a formulation that did not contain any organic solvent and as such the above solubility study was repeated but using the HCl salt of **BP3** instead. The pH of a 100 mg/mL solution of **BP3**, as the HCl salt, was measured to be 1.4 and this was determined to be sufficiently low to warrant adjustment. Unfortunately, any attempt to increase the pH, by using a NaOH solution, led to noticeable turbidity in the solution. The solubility study was thus carried out at a pH of 1.4 and table 8 displays the results.

Additive	0 Mins	30 Mins	60 Mins
None			
Mannitol			
Glucose			
Sucrose			
HPβCD			
L-Tartaric Acid			
DL-Tartaric Acid			
Glucose-6-phosphate			
Meso Tartaric Acid			
D-(+)-Mannose			

Table 8: Effects of additives on a pH 1.4 100 mg/mL solution of BP3. Fully in solution, green; Significant increase in viscosity, amber; Formation of gel, red.

At such a high concentration, and with no organic solvent present, the time for gelling to occur was particularly short. Despite this, the glucose-6-phosphate

additive solution was observed to be the last in the test set to fully gel. The presence of the additives has been demonstrated to be a useful tool towards obtaining a suitable formulation for **BP3**.

2.3.2 NMR Studies

The solubility studies revealed that the presence of additives in the MGB solution can effect a change in the physical properties of the solution. The rate of gelling and the amount of precipitation are clearly of great importance in the effort to find a suitable formulation and, as such, understanding this effect is significant too. It was decided to take the empirical study of the effects of additives further therefore in order to discover if the proposed hypothesis that the of additives were interacting with the MGB dimers, and thus preventing further aggregation, was correct diffusion ordered spectroscopy NMR (DOSY) was utilised.

DOSY is a technique that is able to measure the translational diffusion of molecules in solution. This diffusion is governed by many factors including the shape and size of the molecular species under scrutiny. If the additives are able to interact with the MGBs then the extent of aggregation should alter and the species in solution should have a different diffusion coefficient and thus be detectable through using DOSY. Again, using our knowledge of MGB self-association has led us to employ a technique that has not previously be used in efforts towards a drug formulation.

Three of the most promising addivitives were chosen for investigation based upon the previous solubility studies: mannitol, L-tartaric acid, and glucose-6-phosphate. Given that our hypothesis was that of two molecules of MGB were interacting with one molecule of additive, the solutions that were assessed consisted of 7 mM of MGB and 3.5 mM of additive, made up in D_2O. As a control, a solution containing 7 mM of MGB in D_2O was used.

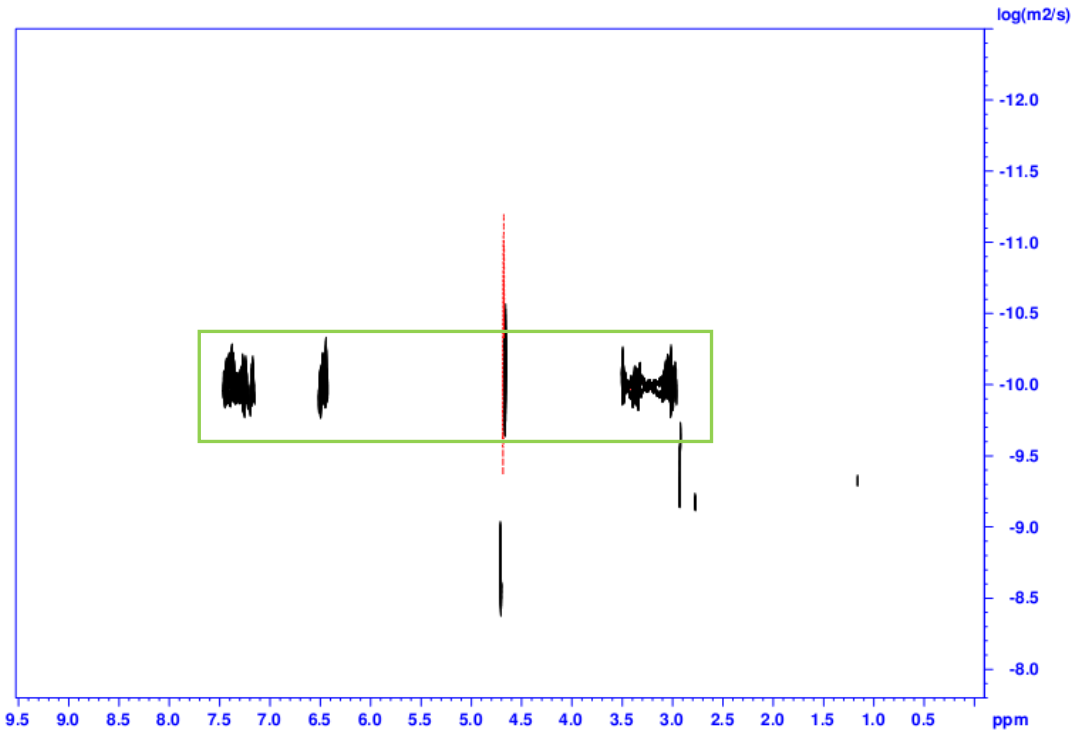

Figure 80: DOSY spectrum of 7 mM BP3 in D_20.

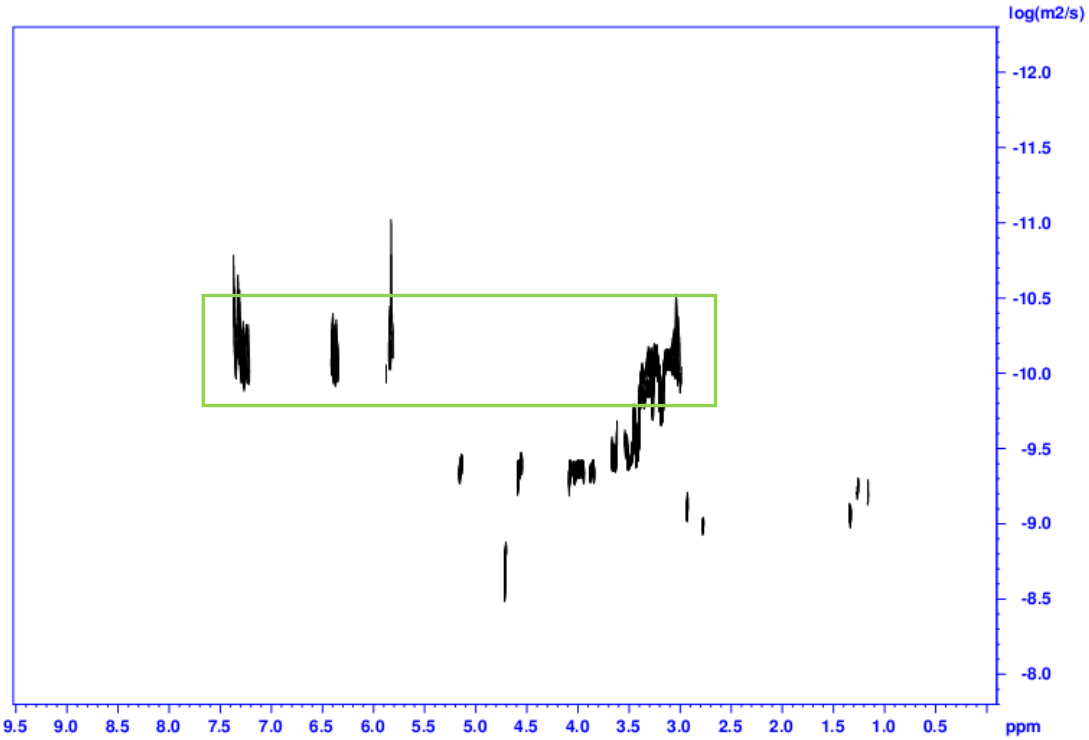

Figure 81: DOSY spectrum of 7 mM BP3 and 3.5 mM mannitol in D_20.

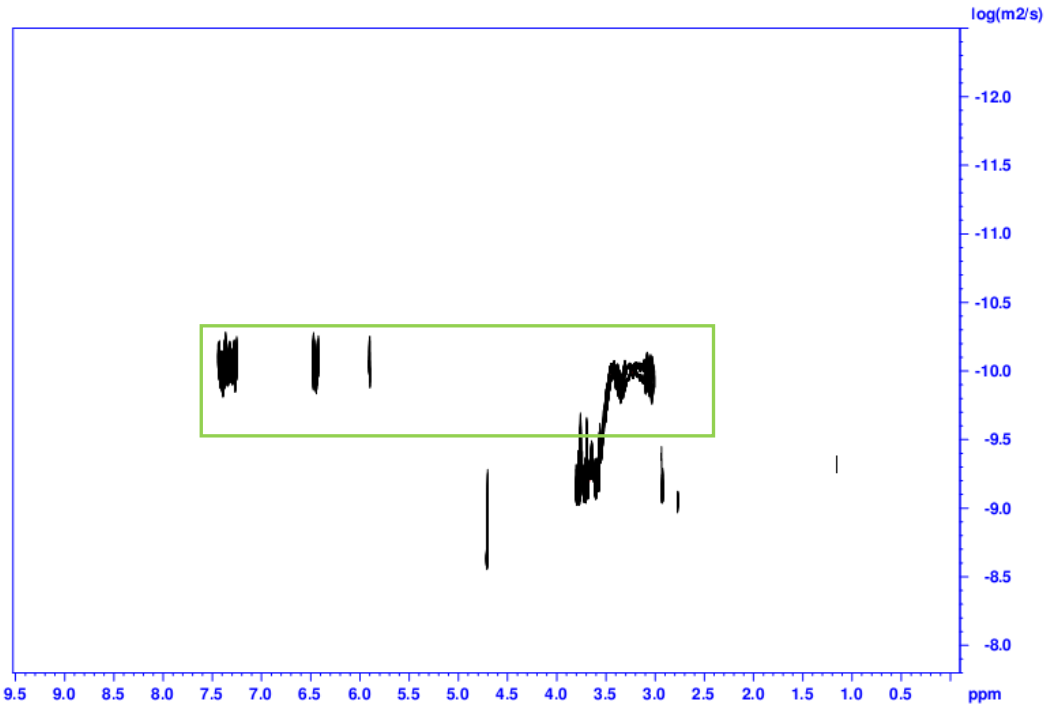

Figure 82: DOSY spectrum of 7 mM BP3 and 3.5 mM glucose-6-phosphate in D_20.

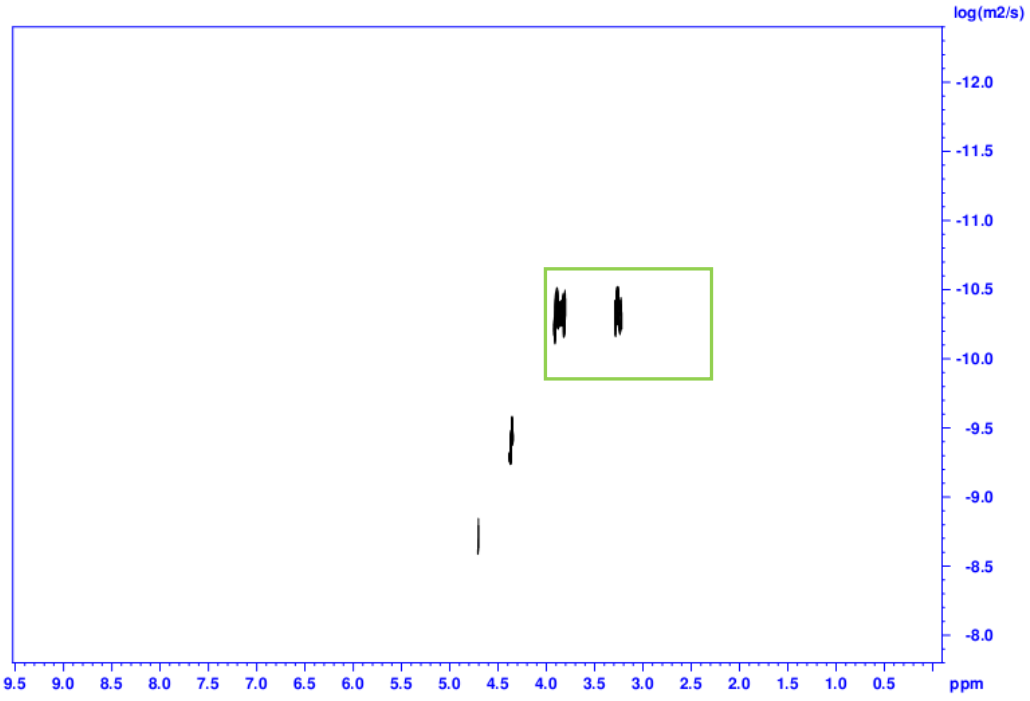

Figure 83: DOSY spectrum of 7 mM BP3 and 3.5 mM tartaric acid in D_20.

For the solutions containing additives, figures 81-83, there can be seen two sets of diffusion coefficients from each experiment: one relating to the motion of the

MGB, boxed in green, and one to the motion of the additive. If the additive was interacting with the MGB and forming a complex with a high binding constant then they would be tumbling in solution as one and as such only one diffusion coefficient would be expected. A diffusion coefficient of around 10^{-10} is indicative of a large aggregate; whereas, one of around 10^{-9} is more expected for non aggregated species. Further evidence to the lack of interaction comes from comparison to the control solution as the single diffusion coefficient, of around $10^{-10.4}$indicating a large aggregate, for this is the same as the diffusion coefficients observed for the MGB in each of the solutions with additives. If there were interactions then the diffusion coefficient would likely change.

Effects on the solubility properties of the MGBs in solution when using additives have been observed; however, these cannot be attributed to a sustained interaction between an MGB dimer and the additive as shown by the DOSY experiments. It is possible that the effects on physical properties are due largely to the kinetics of the system. A greater number of solute molecules have been introduced to the system and so it reasonable to assume that the probability of two MGB dimers finding each other has decreased. This association of MGB dimers would be the first step in forming higher order aggregates and thus reducing the frequency of these collisions would delay the onset of the concomitant physical changes, either gelling or precipitation.

2.3.3 Further Solubility Studies

Acceptable formulations can include organic solvents; however, the concentration allowed varies significantly depending on the particular organic solvent. It was decided to investigate the use of NMP at a pharmaceutically acceptable concentration of 10% and of particular interest was the highest pH that could be achieved in this solvent system. As the highest achievable pH of a given solvent system, without precipitation occurring, would be dependant on the concentration of MGB it was decided to investigate both 50 mg/mL and 25 mg/mL in addition to the 100 mg/mL concentration.

The pH of the 100 mg/mL solution in water was measured to be 1.4. This could be increased to 2.2 using NaOH solution; any further increase caused significant turbidity in the solution. This solution remained free flowing for at least an hour. For a 50 mg/mL concentration of the HCl salt of **BP3**, this could be increased to a pH of 3.5 without immediate precipitation. This solution did start to precipitate within 20 mins. Heating it caused complete dissolution; however, this too would precipitate within a further 20 mins. Similarly, the 25 mg/mL solution was investigated. The pH of this could be increased to 4.3 without significant precipitation. This did form a gel within the 20 mins though. With heating it became completely free flowing and then gelled again. These solutions can be seen in figure 84.

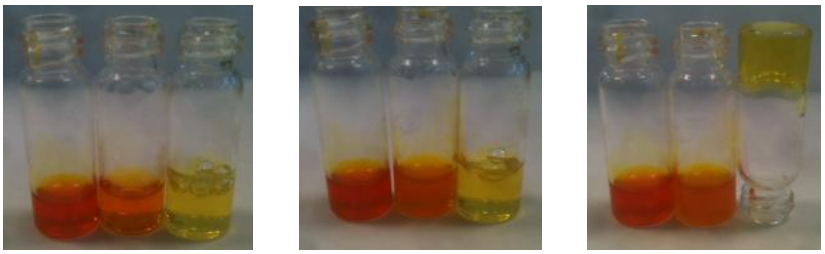

Figure 84: Aqueous solutions of the HCl salt of BP3 in 10% NMP. 100 mg/mL, 50 mg/mL, 25 mg/mL; left vial to right vial. Left panel shows solutions after 5 mins, then after 15 mins in the central panel and after 25 mins in the right panel. The 50 mg/mL solution appears noticeably turbid in the central panel. 25 mg/mL solution has clearly gelled in the final panel.

It is interesting to note that **BP3**, and others, possess a self-indicating property. As the pH is increased the MGB is moving from a predominantely di-cationic state through to mono-cationic with concomitant change of colour from red to yellow.

The reason that a 100 mg/mL concentration of **BP3** was of initial interest was that the toxicological study, in an animal model, had to be carried out at a dose five times higher than that intended for clinical use. A 20 mg/mL concentration was initially of interest; however, a formulation at 5 mg/mL became the likely target concentration. Since the concentration required for the toxicological study was now 25 mg/mL, the final solution from the last mentioned solubility study became of interest. It was known that a concentration of 25 mg/mL of **BP3** could be achieved at pH 4.3 but this caused gellation very quickly. The additive studies had demonstrated

that the gellation time could be increased and so including an additive in the proposed formulation may allow the solution to be free flowing long enough for it to be administered. The choice of additive remained. The final round of additive studies demonstrated the superior effects of glucose-6-phosphate; however, the NMR studies had revealed that these additives were not interacting as hypothesised. As such, HPβCD was further investigated as an additive in this solvent system as, unlike glucose-6-phosphate, it is an approved additive for formulations. An aqueous solution of 25 mg/mL **BP3** was prepared with 10 % v/v NMP and 16% w/v HPβCD. This concentration of HPβCD was chosen as it was the maximum amount that could be safely administered to humans in one day. This solution was found to have a pH of 4.3 and did not form a gel over a 2 hour period. It did become noticeably more viscous; however, was still able to be taken up by syringe. Gentle heating from holding a vial of the solution in a hand allowed it to return to a free flowing state.

The various solubility studies that have been carried out have demonstrated a number of key features. pH has been identified as a particularly constraining parameter of **BP3** solubility in terms of achieving a suitable formulation; low pHs must be used if a high concentration of **BP3** is desired. This does not have toThe pH should not be too low such that the formulation is not appropriate for administration into an animal model, or humans, as demonstrated by the final suggested formulation of 25 mg/mL with a pH of 4.3. Whilst it was discovered that the hypothesised mechanism of additives in the formulation was not due to stong and specific interactions with the MGBs, there were significant benefits to be found that warrant their inclusion. Additives can help to impart some tolerance to the use of higher pHs; there is a balance to be found between an increase in pH decreasing the time to gel formation and the use of an additive increasing the time to gel. Ulitmately, a potential formulation composed of an aqueous solution of 25 mg/mL **BP3** with 10 % v/v NMP and 16% w/v HPβCD has been found and this has been used to adivse both the company and its CROs in order to move **BP3** into the clinical stage of development against MRSA.

2.3.4 Molecular Dynamics Study

The solubility studies clearly demonstated the complex physicochemical properties these compounds possess and, as such, this aggregation was further investigated. It was known from previous NMR studies carried out on **BP1** that it forms at least dimers at low concentration in aqueous solution. It was decided to see if a molecular dynamics simulation could be used to reproduced this dimerisation and to investigate whether any further information could be obtained.

The Accelerys software suite was used to prepare a .pdb file containing two molecules of **BP1** at a distance of at least 17 Å from each other and in no particular orientation. This can be seen in figure 85.

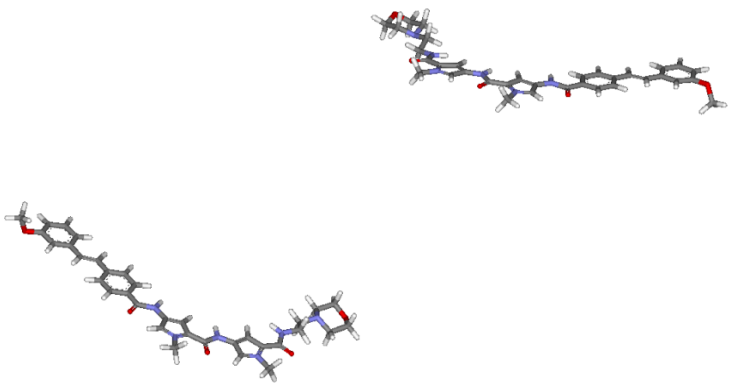

Figure 85: Initial position of two BP1 molecules.

This .pdb file was imported into the AMBER molecular software package[76] and solvated in a box of water. This system was minimised, equilibrated and run according to standard methods developed in our group.[78] This simulation has been provided as a .mpeg file on the disc provided. Within 5 ps the two BP1 molecules are observed to interact and very swiftly form the expected dimer. This dimer then exists for the rest of the simulation without the molecules dissociating from each other. An image of the average structure of this system (with water molecules hidden) is shown in figure 86.

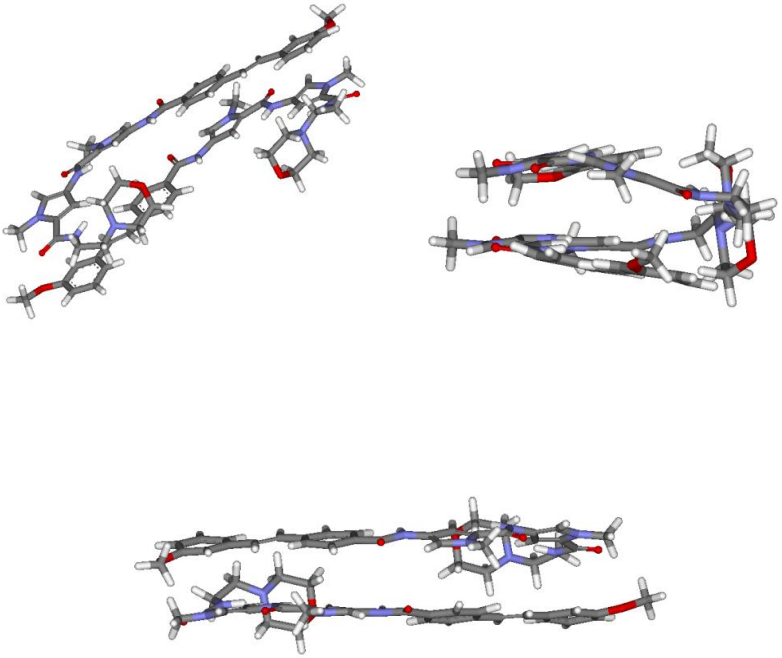

Figure 86: Various views of the average structure of the BP1 dimer.

The Suckling group has previously published a .pdb file (1RMX),[28] obtained from an NMR experiment, in which an MGB, **30**, has bound as a dimer to a short sequence of double stranded DNA. This is shown in figure 87 along with the structure of MGB **30**.

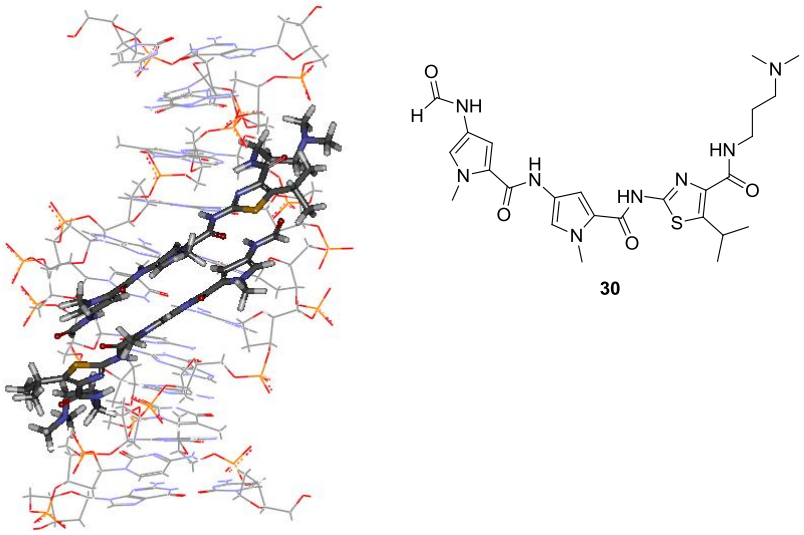

Figure 87: The structure of 30 and a diagram of it bound as a dimer to a short segment of DNA.

A side by side comparison of the dimer obtained from the MD simulation and that which was extracted from the DNA complex is shown in figure 88.

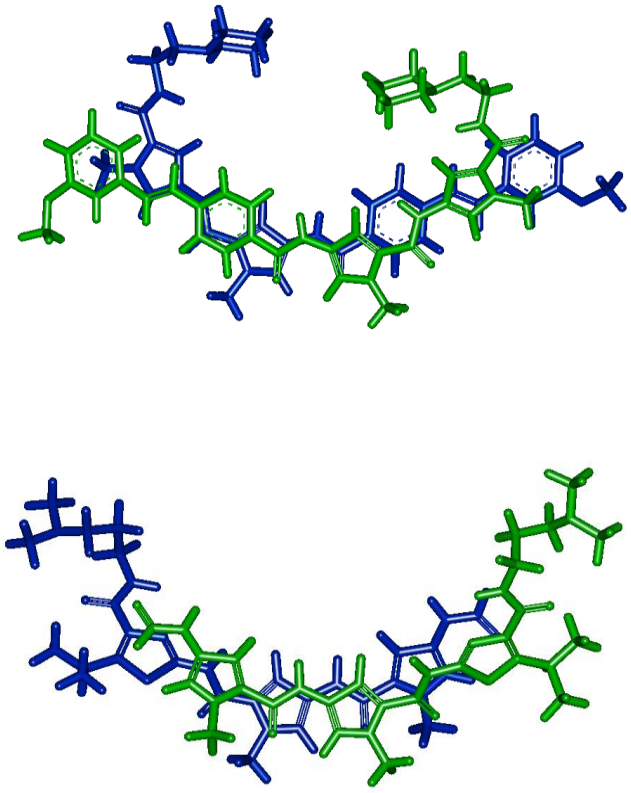

Figure 88: A comparison of the MGB dimers. BP1 dimer obtained from the MD simulation, top. 30 dimer from the NMR experiment, bottom.

This is very informative. Firstly, it has been established that the AMBER molecular simulation package can be used to reproduce the observed dimerisation. Secondly, figure 88 shows that the overlap of the MGB dimers is very similar in both those of the MD study and those bound to DNA. This is quite significant as it is the first evidence which indicates that the dimers that bind to DNA are the same arrangement of molecules that exist before the complexation of the dimer to DNA.

2.3.5 Stability in Solution

The potential drug candidates are polyamides and thus might be expected to be susceptible to hydrolysis. In order to ascertain the stability of our lead compounds

to similar conditions as would be expected in the body it was decided to monitor their HPLC traces over time when 2 mg/mL solutions were incubated at 37.5 ^{o}C in pH 7.4 10 mM phosphate buffer. An HPLC injection was made at 0 h, 2 h, 4 h and 24 h. For compounds **BP1**, **BP2** and **BP3** a slight decrease in the size of the compound peak was observed over the four hour time scale and an almost complete disappearance observed by 24 hours. In addition to this, by 24 hours some smaller extra peaks had presented themselves (fig. 89).

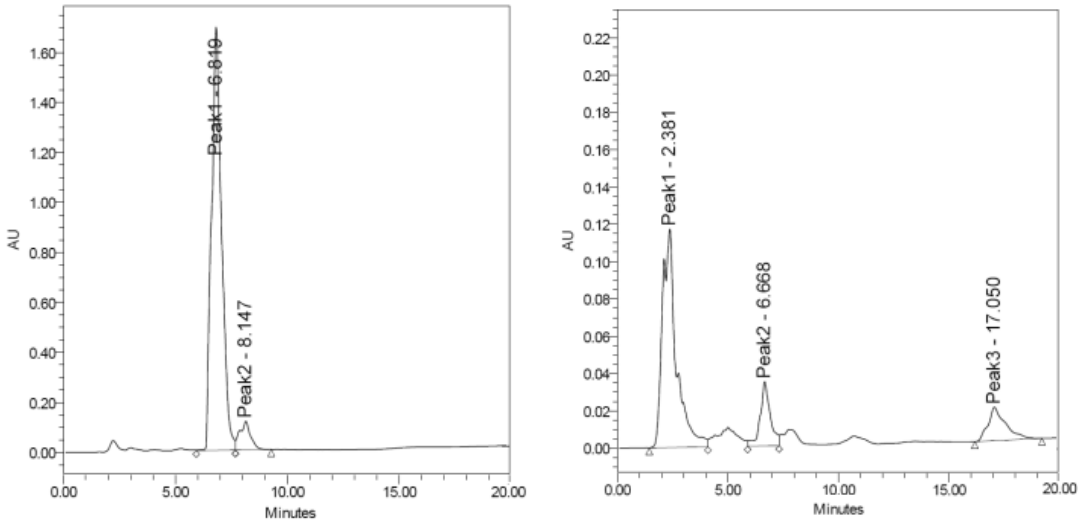

Figure 89: Comparison of example HPLC traces at 1 h (left) and 24 h (right), note the different scales on the y-axis. This trace is for BP3.

Analysis of each peak by mass spectrometry did not reveal any well defined mass except for that of the MGB itself; furthermore, performing mass spectrometry on an aliquot of the solution after 24 h showed only the mass of the compound to be present at significant concentration. Reference to the previous solubility table will show that these compounds are not particularly soluble in buffer alone and thus the decrease in peak size has been attributed to precipitation of the compounds and not products of degradation.

Compounds **BP4** and **BP5** were similarly analysed; however, with their more problematic solubility profiles each 2 mg/mL solution of buffer was adjusted to 10% DMSO in order to afford partial solubility. These showed similar decreases in peak size of the compound of interest, although not to the same extent as before, and no

new peaks were observed over the 4 hour period; however, the HPLC trace at 24 hours showed the complete disappearance of the compound peak. Again, this reduction of peak height is attributed to compound precipitation.

At this point in time our industrial sponsors had indicated that oral administration of compounds **BP2** and **BP3** may be of interest and as such it was deemed necessary to test the stability of these compounds in a pH 3 citrate-phosphate buffer. The procedure was the same as previous except with the alternate buffer. In these cases both compounds appeared stable over the time of the experiment as very little decrease in peak size was observed and no new peaks were seen to appear. Evidently, the low pH has obviated the precipitation issue through significant protonation of the compounds.

2.3.6 Metabolic Stability with Mouse Liver Microsomes

Drugs that enter the body are subjected to a wide range of enzymes which may metabolise the drug in order for it to be excreted by the kidneys. For this excretion to occur the drug needs to be polar; therefore, the enzymes involved in this metabolic process will catalyse various chemical reactions on the drug molecule so that it becomes more polar. The enzymes primarily responsible for this metabolism are from a group of enzymes known as cytochrome P_{450}s and these increase the polarity of drugs by hydroxylation. Other enzymes can also assist in the metabolic process such as esterases which can hydrolyse esters. Most of the reactions involved in metabolism can be found to take place in the cells of the liver and this is the reason that mouse liver microsomes have been used in determining our lead compounds metabolic stability.[4]

Compounds **BP1**, **BP2** and **BP3** all contain numerous amide links and thus these are the most obvious site of metabolic action to be expected. Each compound also contains an alkene-linked head group and these could undergo epoxidation by P_{450} enzymes and perhaps further modification to the diol by epoxide hydrolases. The tail groups contain the tertiary amine morpholine and it is possible that this may be converted into the *N*-oxide by the P_{450}s as well. Similarly, compounds **BP2** and **BP3**

contain a nitrogenous heterocycle in the head group structure and this too could be converted to the *N*-oxide. The methoxy groups of compounds **BP1** and **BP2** may undergo dealkylation to form the corresponding phenols.[4]

Each compound was incubated in a water bath at 37.5 ^{o}C with the mouse liver microsomes (both male and female) using the supplier's recommended procedures and an aliquot of each was removed and analysed by mass spectrometry at 0 h, 6 h and 20 h. Over this 20 hour period no peaks consistent with any expected metabolites were observed and the compound peak remained throughout. In order to further prove the metabolic stability of these compounds, the concentrations present in the incubated mixture at 20 hours was subjected to HPLC analysis, the results of which are summarised below (Table 9).

Compound	% Compound Conc after 20h Incubation with Male Microsomes	% Compound Conc after 20h Incubation with Female Microsomes
BP1	90 ± 9	92 ± 9
BP2	99 ± 8	93 ± 8
BP3	90 ± 10	101 ± 10

Table 9: Stability of Lead compounds to mouse liver microsomes.

It can be seen from the above table that no significant loss of the compounds are observed after the 20 hour incubation period thus confirming the required metabolic stability.

During the acquisition of the data required to produce the calibration curves for this HPLC analysis further support of the previously expounded precipitation properties of these compounds was observed. The diagram below (fig. 90) shows the traces of three injections of the same standard over 120 mins and during this time it can clearly be seen that the concentration of the compound in solution is decreasing; this made obtaining the calibration curves quite problematic as each standard had to be made and injected immediately into the HPLC system.

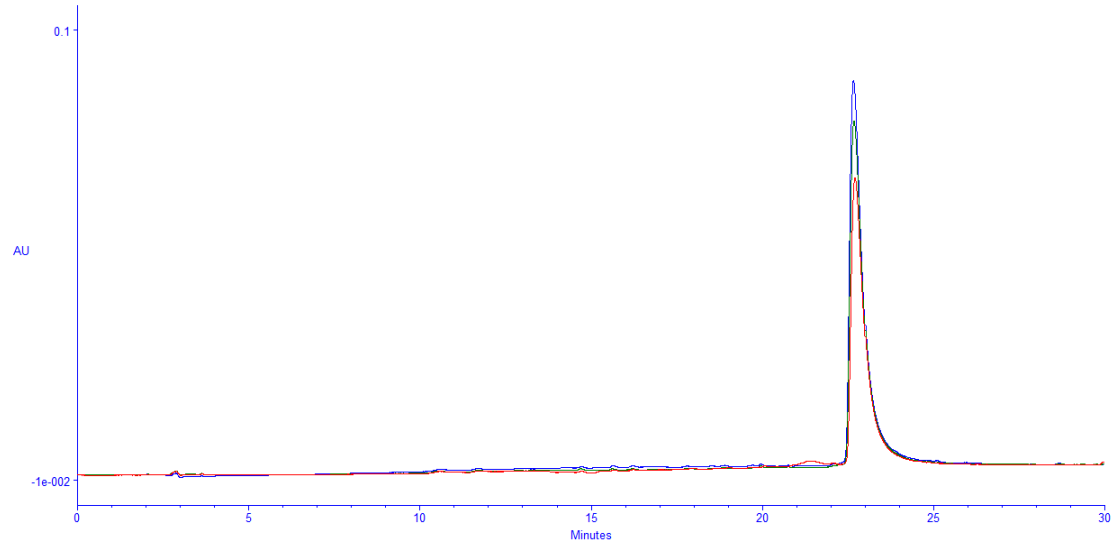

Figure 90: HPLC trace overlay demonstrating decrease in concentration with time. 0 mins shown in blue, 60 mins in green and 120 mins in red.

Our commercial sponsors indicated that **BP3** was of great interest and as such it was decided to enhance the HPLC protocol used to determine the concentration of the compound after microsomal incubation. This was achieved by increasing the injection volumes from 20 µL to 100 µL and also increasing the number of data points to 3 at each concentration during the generation of the calibration curve giving a correlation coefficient of 1.000. This allowed the precision of the system to be improved to < 6% for each concentration and subsequent sample injection determined the concentration of compound remaining after microsomal incubation to be 97 ± 5.5 % for male and 100 ± 5.5 % for female microsomes. These data fully underpin the assertion that **BP3** is stable to metabolism by mouse liver enzymes.

2. 4 Further Synthetic Development

2.4.1 Anti-hERG Compound Synthesis

Although **BP3** continued in development, the overall research programme required further background studies to understand broader issues of structure-activity to be studied. The importance of avoiding hERG activity in drug candidates led us to undertake further synthesis in order to expand on our original two anti-hERG compounds, **BP5** and **BP6**, which had been designed to have strongly dipolar but

unprotonated tail groups. This substitution was based upon the successful transformations of histamine in the classical development of H2 antagonists such as Zantac.[4] The intended compounds (fig. 50) would similarly involve tail group modifications that would be predicted to have the capacity to attenuate hERG activity. However, instead of replacing the protonisable amine nitrogen with a non-cationic isostere, as in **BP5** and **BP6** (see pare 35), the tail groups would include fluorine, known for its anti-hERG effects and *N*-oxide analogues of the three lead compounds. The tail group of **89** would unlikely be protonated at physiological pH as it is an amide; additionally, the *N*-oxidised morpholines of **90** – **92** will impart greater lipophilicity. Both of these observations are in line with the anti-hERG hypothesis.

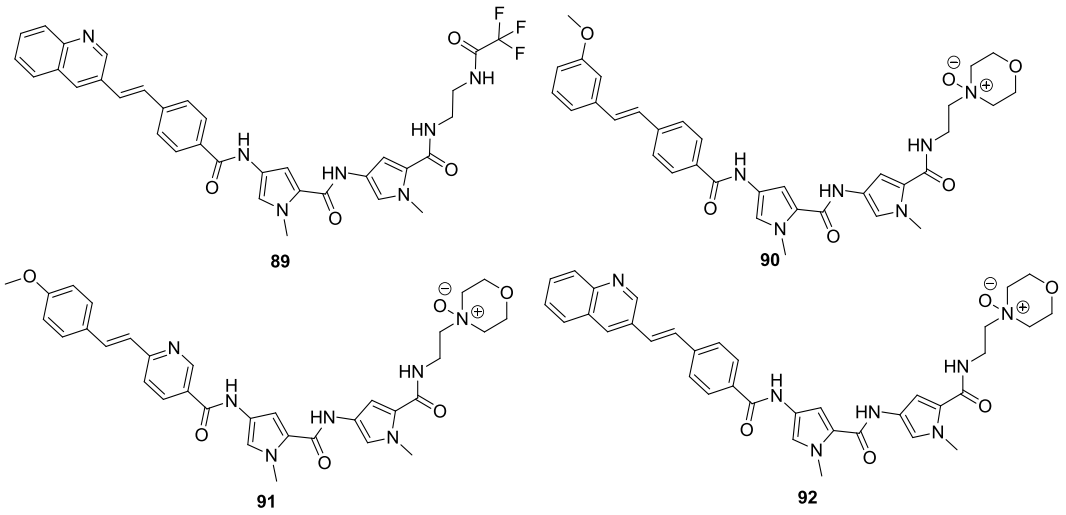

Figure 91: Proposed anti-hERG compounds.

The synthesis of compound **89** involved a late stage diversification (scheme 11), directly in line with the synthesis of **BP5** and **BP6**. Fortunately, a key building block, **93**, was available due to the scale up work on **BP5** and **BP6** that was being carried out by another member of the team.

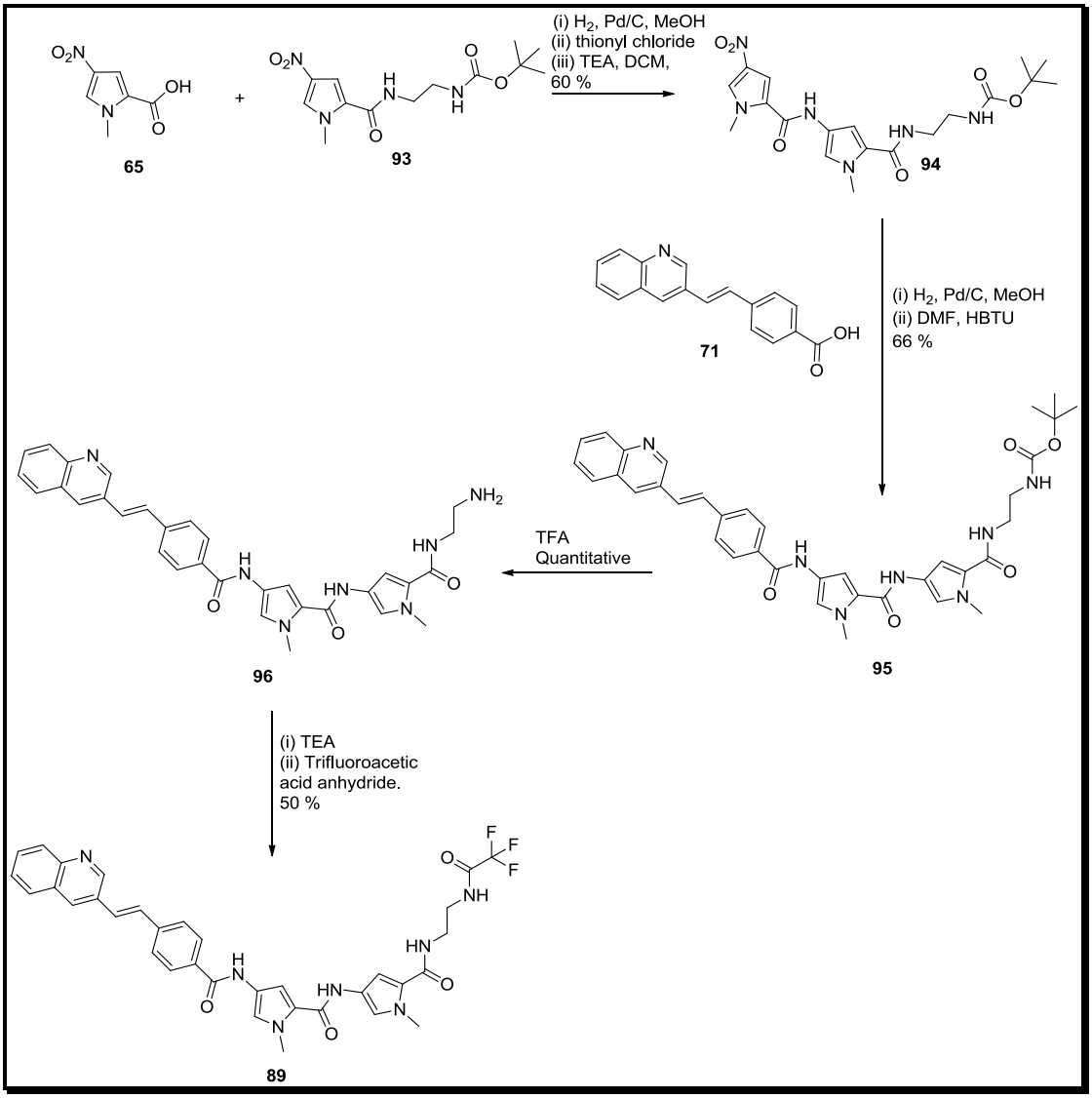

Scheme 11

The nitro compound **93** was reduced to the amine by hydrogenation over palladium on charcoal, whilst simultaneously forming the acid chloride of compound **65** by reflux in thionyl chloride. The acid chloride and the amine were reacted together to form the BOC protected dimer **94**. Previous experience within the group has shown the aminopyrroles to be susceptible to atmospheric oxidation and hence they are not isolated. The BOC protected dimer **94** was then similarly reduced using hydrogenation over palladium on charcoal and used in an HBTU mediated coupling reaction with compound **71** to form the BOC protected tetramer **95**. **95** was deprotected using TFA to obtain the amino tail group in compound **96,** which could

be used to introduce late-stage tail group diversity. The previous syntheses of **BP5** and **BP6** did not isolate compound **96**; as such, it was a novel compound for biological evaluation.

Synthesis of the trifluoroacetamide tail group compound, **89,** was achieved by reacting the amino tail group compound, **96**, first with 2 eq of triethylamine to obtain the free amine, and then with TFA anhydride in a yield of 50 %.

The *N*-oxide analogues were prepared directly from the respective lead compounds **BP1**-**BP3**. This was achieved by reaction with 1 equivalent of mCPBA in DMF followed by HPLC purification.

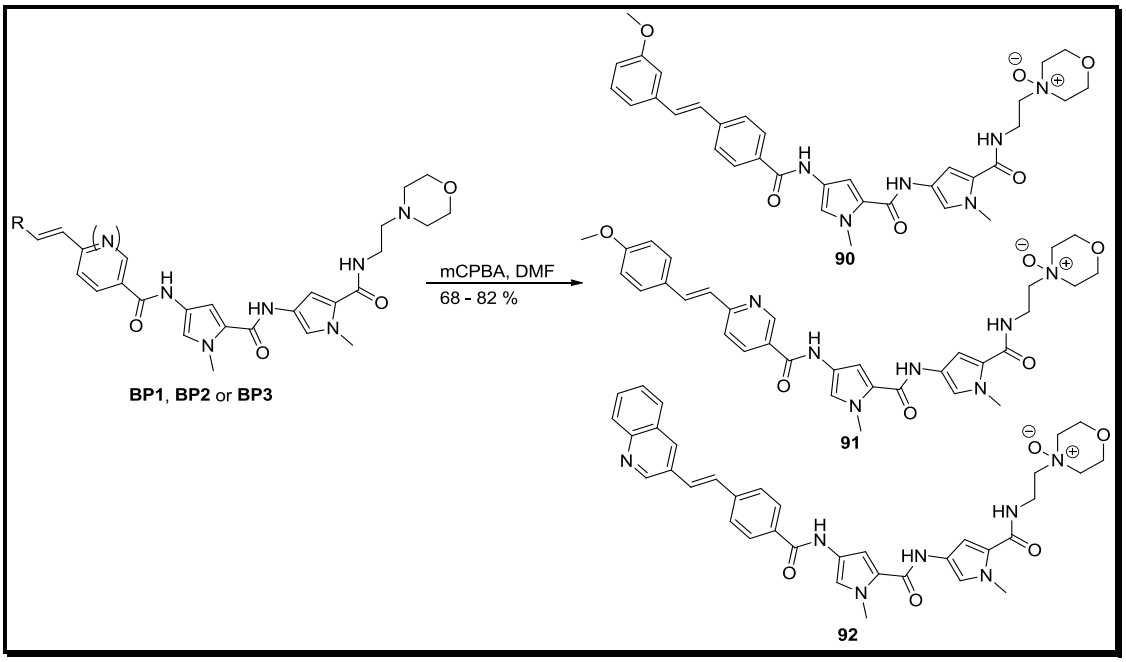

Scheme 12

These four anti-hERG compounds were tested for their minimum inhibitory concentrations (MICs) against our normal set of pathogenic species and also for their effectiveness in binding to the hERG ion channel. The data are presented in the table below in which the column labelled % displacement astemizole refers to the compounds ability to displace the highly hERG-active compound, astemizole, from the ion channel.

	MIC (μM)								
Compound	**EMRSA 16**	**SMRSA 106**	***E.coli ATCC.8739***	***T.b.brucei***	***M.marinum ATCC BAA535***	***K.pneumoniae NDM-1 ATCC BAA-2145***	***K.pneumoniae ATCC -13883***	***P.aeruginosa ATCC-27853***	**% Displacement *Astemizole***
BP1	NA	NA	NA	**0.78**	**25**	NA	NA	NA	65
BP2	**3.12**	**3.12**	NA	**0.78**	**100**	NA	NA	NA	58
BP3	**0.78**	**0.78**	NA	**0.19**	NA	NA	NA	NA	64
90	NA	NA	NA	**6.25**	**50**	NA	NA	NA	45
91	**25**	**12.5**	NA	**1.56**	NA	NA	NA	NA	44
92	**100**	**NA**	NA	**3.12**	NA	NA	NA	NA	48
89	**6.25**	**12.5**	NA	**1.56**	NA	NA	NA	NA	24

Table 10: MIC values of compounds in μM. NA signifies not active.

The *N*-oxide analogues showed a slight reduction in their ability to displace astemizole from the hERG ion channel, which indicates that they are less hERG active. Unfortunately, the modification of the tail group has led to a significant decrease in activity for **91** and eradication of activity for **92**. Compound **89**, with the trifluoro acetamide tail group, showed the greatest decrease in hERG activity whilst at the same time it retained some activity against Gram positive bacteria and *Trypanosoma brucei*. These activities are not clinically significant; however, they do demonstrate that modification of our lead compounds can potentially cause a reduction in hERG binding whilst retaining activity.

2.4.2 Gram Negative Active Compounds

Not only is it of interest to optimise our compounds properties with respect to their initial potential to treat Gram positive bacterial infections, it is also of interest to expand the range of conditions that MGBs can be used to treat. A major disease target is infection by Gram negative bacteria and several strategies were considered to tackle the poor activity our MGBs display against these. Ultimately, the compound synthesis was leading to an assessment of activity against *Pseudomonas aeruginosa*; however, some of the compounds were submitted for assessment against a number of other species to further our understanding.

2.4.2.1 Truncated MGBs

It has been mentioned (section 1.2.3.2.2) that our lead compounds may be too large in order to pass through the porins of Gram negative bacteria and hence give a poor activity profile. To investigate this idea it was decided that the previously mentioned Hoeschst compound, **DMA 41** (see page 42), would be used as a template to design truncated analogues of our lead compounds. Figure 92 shows a comparison of the size of **DMA**, in green, to **BP1**, in blue, used as an example of our larger MGB structures and a truncated analogue of it, in red. It can be seen that the amount of curvature is dramatically reduced in truncating this MGB, in addition to reducing the overall length of the molecule.

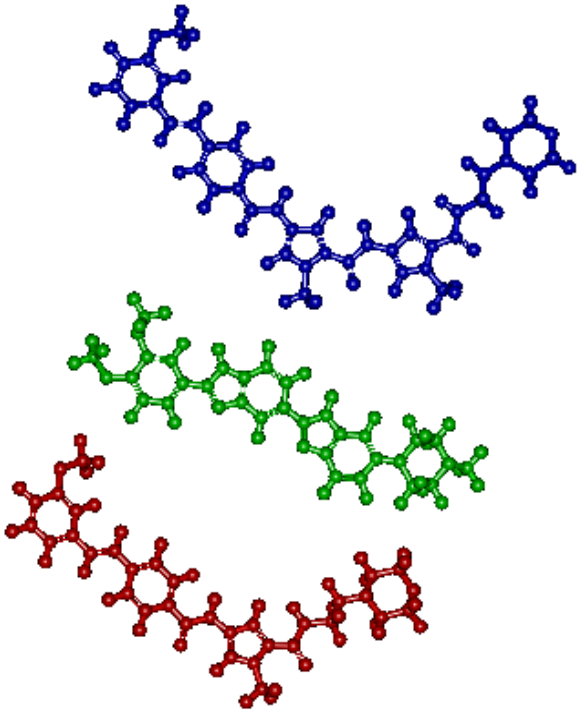

Figure 92: Comparison of the size of DMA, green; BP1, blue; truncated BP1, red.

In order to assess whether or not our truncated MGB strategy may prove successful a panel of six compounds was devised (fig. 93). These compounds all possess one pyrrole less than our standard MGBs and five of these have less flexible, but still weakly basic, tail groups. Two compounds, **102** and **103**, still have the

standard ethyl morpholine tail group in order to observe the effect of just removing a pyrrole from our MGBs.

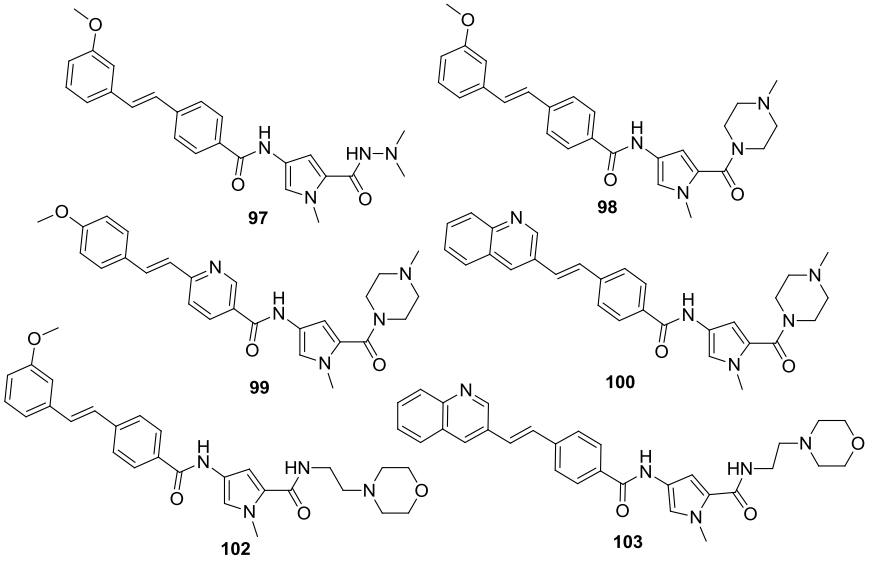

Figure 93: Panel of truncated MGBs.

The synthesis of these compounds was in line with our standard MGB synthesis. Firstly the tail group monomer was constructed by forming the acid chloride of the nitro pyrole **65** and reacting this with 2 eq of either *N*,*N*-dimethyl hydrazine, **105**, or *N*-methylpiperazine, **104**, to form **107** and **106**, respectively (scheme 12). The extra equivalent of amine was used to quench the HCl formed during the reaction. The ethylmorpholine tail group monomer, **67**, was available from previous syntheses and so all three tail group monomers were thus ready to be coupled to their respective head groups.

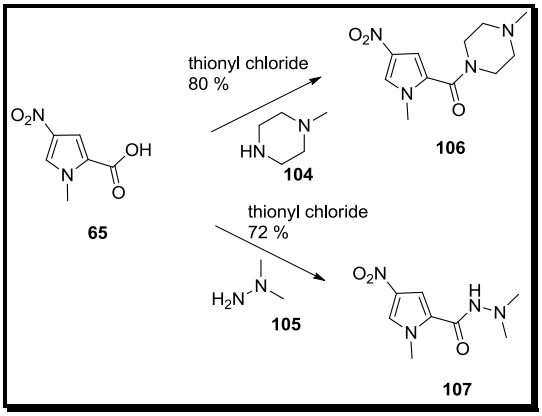

Scheme 13

Due to the availability of the pentafluorophenyl active esters of the required head groups, this method of coupling was employed over the HBTU method. The nitro group of the tail group monomer, **67**, **106**, or **107**, was reduced to the corresponding amine, utilising a Pd over charcoal hydrogenation, and subsequently reacted with the required pentafluorophenyl active ester, **84**, **87** or **88**. This yielded all the required truncated MGBs, **97-103**, which were purified by HPLC (scheme 14).

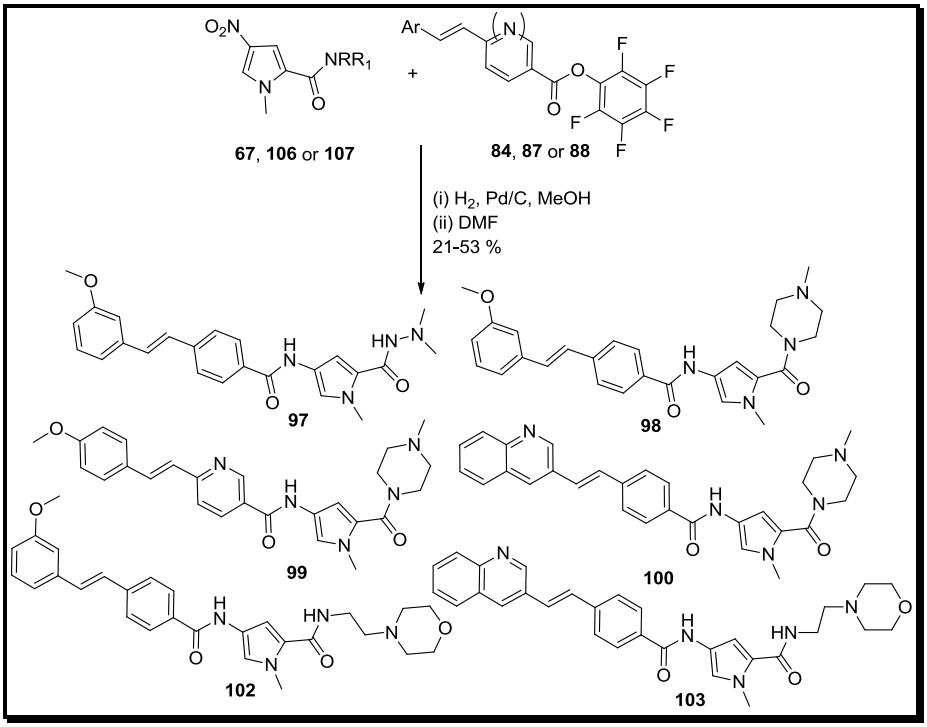

Scheme 14

These compounds were submitted for our standard panel of biological screens; however, the results were not particularly enlightening with regard to our proposed hypothesis (table 11).

	MIC (µM)							
Compound	**EMRSA 16**	**SMRSA 106**	***E.coli ATCC.8739***	***T.b.brucei***	***M.marinum ATCC BAA535***	***K.pneumoniae NDM-1 ATCC BAA-2145***	***K.pneumoniae ATCC -13883***	***P.aeruginosa ATCC-27853***
97	NA	NA	NA	NA	NA	NA	NA	NA
102	NA	NA	NA	**6.25**	**12.5**	NA	NA	NA
103	NA	NA	NA	**3.12**	NA	NA	NA	NA
99	NA	NA	NA	**25**	**100**	NA	NA	NA
100	NA	NA	NA	**6.25**	**12.5**	NA	NA	NA
98	NA	NA	NA	**6.25**	**12.5**	NA	NA	NA

Table 11: MIC values of compounds in µM. NA signifies not active.

It can be seen from the table of activities that none of the compounds displayed any activity against the collection of Gram negative bacteria in the screen. This would lead to the question of whether or not the truncation strategy produced compounds effective at penetrating the cell wall; are they still to large? If significant Gram positive activity was retained in this panel of compounds then it could be concluded that the truncation strategy was not successful; however, the Gram positive activity has been significantly reduced as these compounds only display some activity against *Mycobacterium marinum* and no longer any against the two MRSA strains. Assuming that the molecular target is similar for Gram positive and Gram negative bacteria, and it is only accessibility to the target that is the limiting case for Gram negative bacteria, then it is conceivable that these truncated compounds may well enter the cell of Gram negative bacteria but perhaps they no longer bind to DNA.

Why do these compounds only display limited anti-bacterial activity? The parent compounds of the truncated series, namely **BP1**, **BP2** and **BP3**, are thought to bind to DNA as dimers, and indeed exist in solution like this too (see section 2.3.1).

In an effort to reduce their size, to aid porin passage, it is quite possible that their ability to dimerise has been hindered: smaller size, smaller intermolecular attractions. This line of argument may not follow through to a lack of DNA binding though as, for example, netropsin and the modified Hoechst 33258 analogue, DMA, both bind to DNA as a 1:1 complex and still remain active. The process of generating the set of lead compounds **BP1**, **BP2** and **BP3** involved optimising the structural features that gave good activity and, in doing so, maintained 2:1 binding. It seems plausible that the set of molecular requirements that give rise to good activity for 2:1 binding MGBs may be different from those required for 1:1 binding MGBs. The act of truncating our lead set of MGBs may shift potential DNA binding from 2:1 to 1:1 yet leave the resulting compounds in a section of molecular space that is not amenable to activity for 1:1 binding MGBs.

Although Gram negative bacteria are notorious for their efflux pumping potential, Gram positive bacteria also possess efflux capabilities. The truncation strategy may have given rise to a group of compounds that gram positive bacteria are able to recognise as undesirable and able to remove via their efflux pumps. Perhaps more generally, these truncated compounds may have other biological transport issues related to their physical chemical properties that the parent set do not.

This panel of compounds has raised more questions than answers with regards to our first anti-Gram negative strategy; however, it is clear that these compounds have little antibacterial activity.

Activity against another species of interest was also investigated and table 11 shows noteworthy activity against *T. brucei*. Compound **97** is inactive and points to the dimethylhydrazine tail group not being tolerated. Although not of great significance these activities do provide some evidence against the previous speculative argument that the likely 1:1 binding of these molecules cannot afford a biologically significant event leading to activity in bacteria. The argument for reduced antibacterial activity due to poor biological transport becomes more likely; indeed, the parasite that these show some activity against will likely have a very different spectrum of biological transport mechanisms.

Given the activity against the parasite *T. brucei*, it was thought prudent to have assessed the activity of these compounds against three strains of *Leishmania*: *donovanni*, *mexicana* and *major*. Figure 94 shows the % growth suppression of the compounds, compared to amphotericin B as a positive control, at a concentration of 12.5 µM.

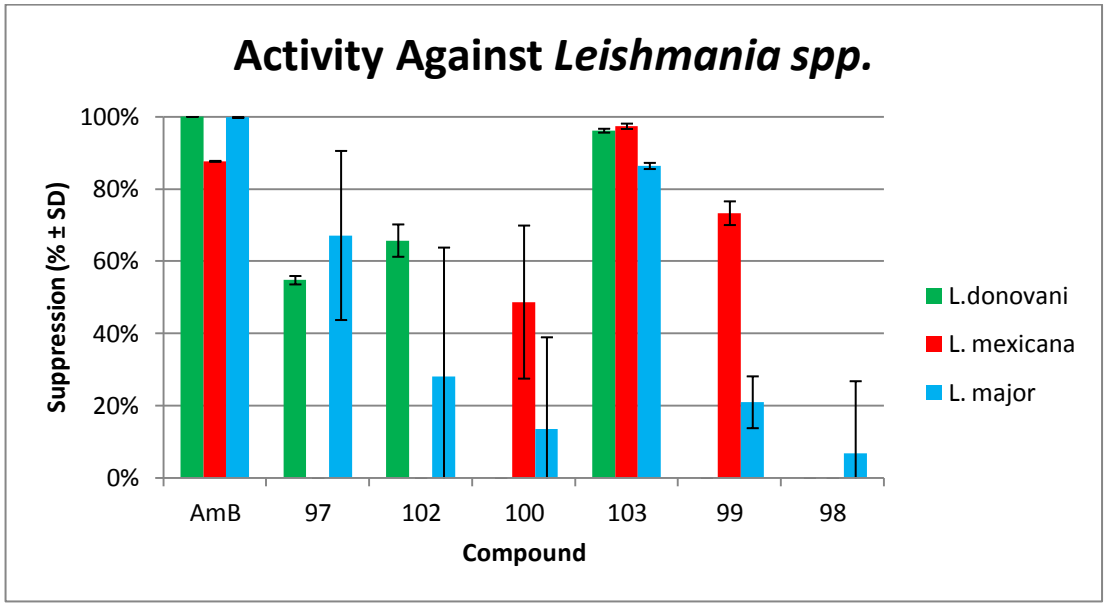

Figure 94: Activity of truncated MGBs against Leishmania spp. AmB is the control amphotericin B.

Only one, **103**, shows significant activity worth further investigation; however, the variation in activities is interesting. What can be seen is that there is differences between the activities between different species such as **97** and **102** showing some suppression of growth for *L. donovani* and *L. major* and none for *L. mexicana* compared to **99** and **100** showing some suppression against *L. mexicana* and *L. major* but none against *L. donovani*. This again could be explained by variation in biological transport mechanisms between species.

2.4.2.2 Netropsin Analogues

Given that our initial design strategy yielded inconclusive information with regards to the transport of our lead set of compounds and ultimately no improvement in Gram negative activity a new approach was sought. It was still desirable to design smaller molecules than our initial lead compounds as, although no conclusive

evidence was obtained from the previous panel of truncated compounds, hindered porin passage is still a likely problem to be avoided. With this in mind attention was shifted to netropsin **26**. This natural product is known to have good Gram positive activity and, unlike distamycin **25**, from which our lead compounds are optimised, it is known to possess some Gram negative activity.[79] Thus instead of simply omitting a central pyrrole from the lead compounds to generate smaller structures of interest a panel of compounds retaining the key features of the already smaller netropsin **95** was designed (fig. 95).

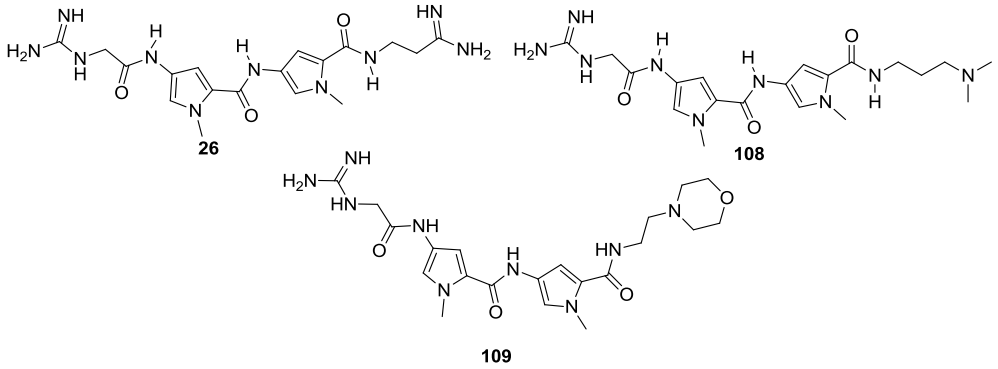

Figure 95: Netropsin 26, and two analogues.

The most noticeable difference between the structures of distamycin **25** and netropsin **26** is the replacement of the formamide pyrrole head group of distamycin **25** with a guanidine acetamide moiety. This guanidine, with a pK_a of around 13, will be almost exclusively protonated at physiological pH and hence give rise to a different pharmacokinetic and pharmacodynamic profile. For this reason the guanidine acetamide moiety was kept constant in this panel of compounds and it was decided that the tail group would be altered by using known moieties from our library of compounds that can give rise to some activity. The panel of compounds thus contains netropsin itself, **26**, an analogue with the dimethylaminopropyl tail group, **108**, and an analogue with the morpholinoethyl tail group, **109**. The tail groups in this set display a decreasing trend in p*K*a: the amidine of netropsin, **26**, pK_a around 14, the dimethyl aminopropyl of **108**, pK_a around 10 and the morpholinoethyl of **109**, pK_a around 7.5.

These compounds were synthesised by standard routes and the required tail group dimers were either synthesised previously for the scale up of our lead compounds, in the case of **26**, or already available in large enough quantities from our compound library for the next step to be carried out, in the cases of **108** and **109**. The nitro group of the tail group dimer, **68**, **111**, or **112**, was reduced to the corresponding amine, utilising a Pd over charcoal hydrogenation, and subsequently reacted with the guanidine acetic acid using HBTU as the coupling agent (scheme 15).

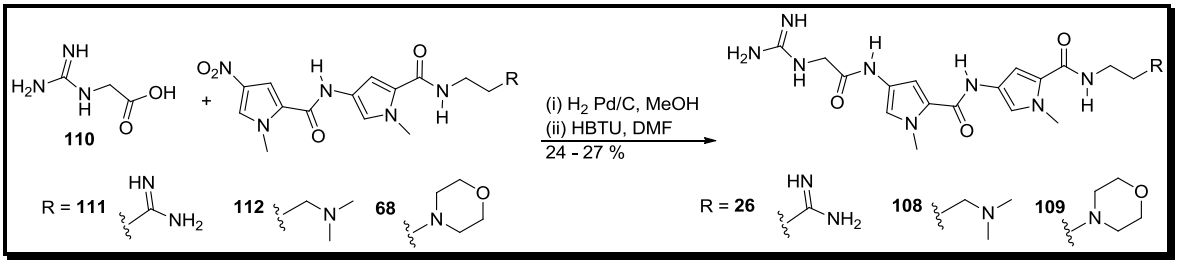

Scheme 15

In addition to the *P.aeruginosa* screen (see section 2.4.2.6), these compounds were evaluated against a number of other clinically relevant species and the results are seen in table 12.

	MIC (µM)							
Compound	**EMRSA 16**	**SMRSA 106**	***E.coli ATCC.8739***	***T.b.brucei***	***M.marinum ATCC BAA535***	***K.pneumoniae NDM-1 ATCC BAA-2145***	***K.pneumoniae ATCC -13883***	***P.aeruginosa ATCC-27853***
26	NA	NA	NA	NT	NA	NA	NA	NA
108	NA	NA	NA	NT	NA	NA	NA	NA
109	NA	NA	NA	NT	NA	NA	NA	NA

Table 12: NA is not active; NT is not tested. NA signifies not active.

It is quite clear that design behind these compounds did not enable any Gram negative activity. It is interesting to note that not even netropsin **26** displayed any activity in this screen; however, most of the species in the screen are clinically relevant strains. This means that they already possess many resistances to known antibiotics due to various mutations in their genenome.

2.4.2.3 Cephalosporin analogues

The cephalosporin antibiotics are a class of β-lactam that were originally isolated from the fungus *Acremonium*. They possess a β-lactam ring and share their mechanism of action with the β-lactams. By inhibiting essential steps in cell wall biosynthesis they are able to cause lysis of the bacterial cell. There are currently at least 5 generations of these compounds and all share the common structural motif shown in figure 96.

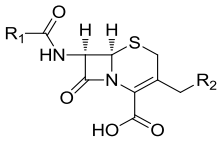

Figure 96: General structure of cephalosporins.

The first generation of cephalosporins possessed simple functional groups around this core such as **113** and **114** in figure 97. The spectrum of activity of these first generation compounds was largely limited to Gram positive bacteria only. The developments of the second (**115**) and third generations (**116** and **117**) lead to increased activity against Gram negative bacteria whilst in many cases reducing Gram positive activity (fig. 97). The most characteristic feature of the third generation is the inclusion of the 2-aminothiazole group. Many of this generation are also able to pass through the blood-brain barrier.[80]

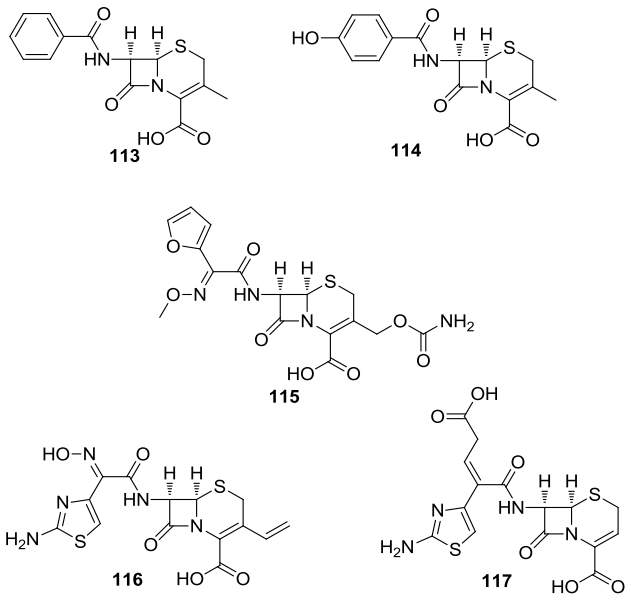

Figure 97: Examples of first, second and third generation cephalosporins.

The fourth generation possess more Gram negative activity still and this has been attributed to their zwitterionic nature; along with the carboxylic acid that is retained throughout the series, this generation contain a positively charged nitrogen centre (fig. 98).[80]

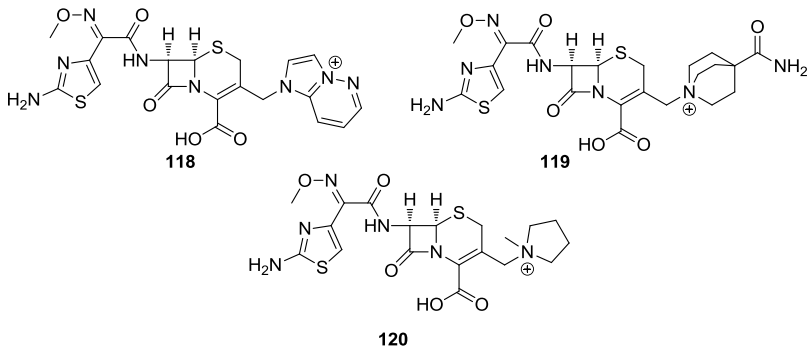

Figure 98: Examples of fourth generation cephalosporins.

Given that the netropsin-like head group strategy did not yield any Gram negative active compounds it was decided to try and incorporate an aspect of the 4th generation cephalosporins into these more netropsin-like compounds. Due to synthetic ease, the desired zwitterionic character was added into the compounds by modifying the head group. The succinate moiety was chosen as it possesses similar flexibility to the netropsin head group and the terephthalate moiety was chosen as it

was more rigid and perhaps more distamycin-like. The synthetic route chosen for these allowed the intermediate compounds with methyl esters of the head groups to be isolated and compared for activity too (fig. 99).

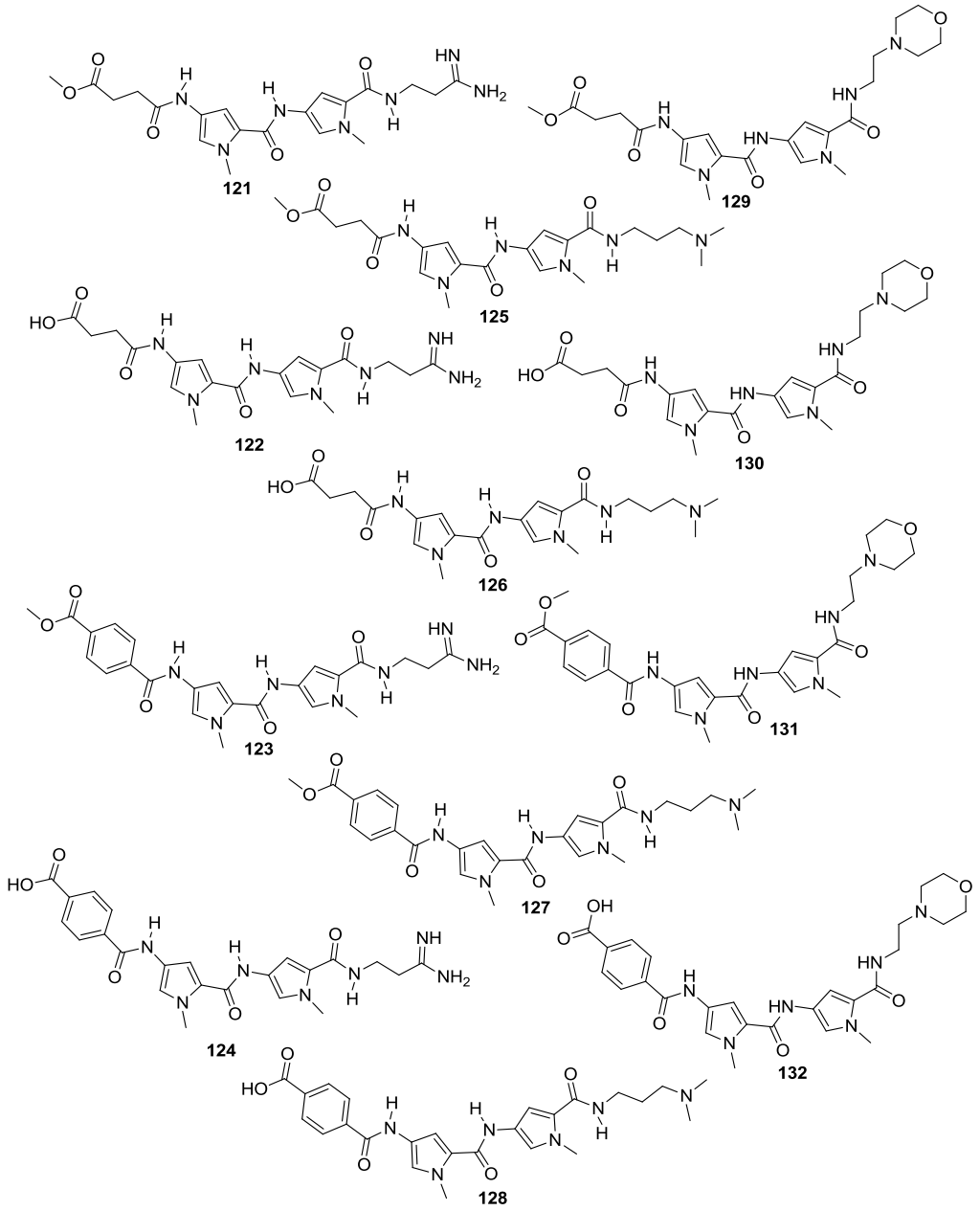

Figure 99: Netropsin like carboxylic acid containing structures and their methyl esters.

The syntheses of this panel of compounds began with an HBTU coupling of the appropriate monomethyl ester, **133** or **134**, to the hydrogenated tail group dimer,

68, **111** or **112** (scheme 16). This yielded six testable compounds after HPLC purification.

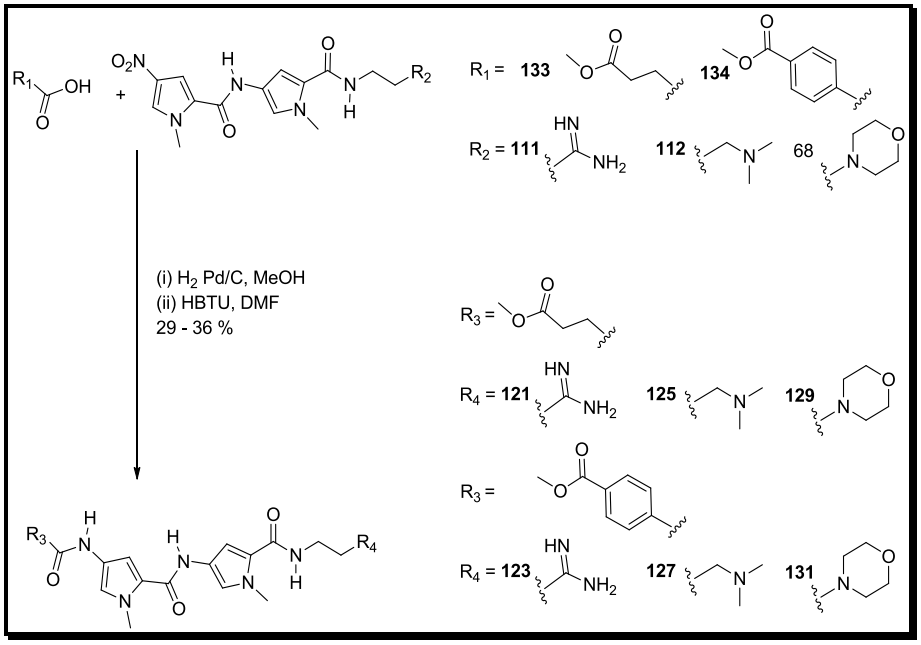

Scheme 16

The monomethyl esters, **121**, **123**, **125**, **127**, **129** and **131**, were then hydrolysed by way of LiOH solution to yield a further six testable compounds, again after purification by HPLC (scheme 17).

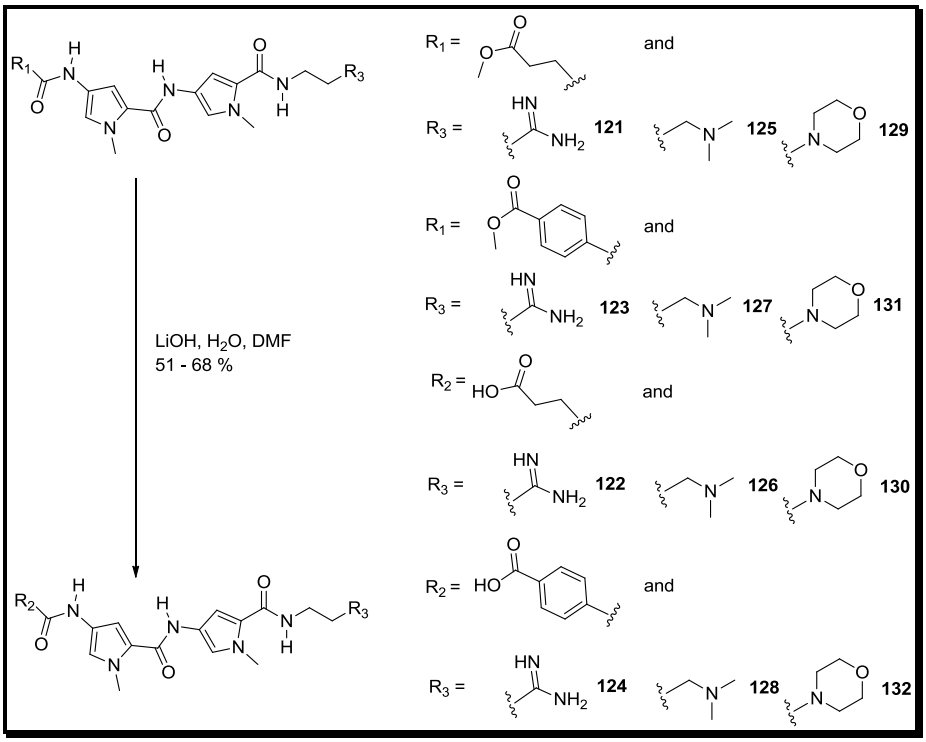

Scheme 17

Results from a general screen of these compounds are still pending; however, their performance in the *P. aeruginosa* assay is discussed in section **2.4.2.6**.

2.4.2.4 BP4 analogues

BP4 (page 35), our hit Gram negative compound, is quite distinct from the paradigm of the lead Gram positive compounds, **BP1**, **BP2** and **BP3**. **BP4** contains a more basic dimethylaminopropyl tail group compared to the morpholino ethyl of the others. **BP4** has a thiazole as the first heterocycle adjacent to the tail group and this adds an extra degree of lipophilicity than the pyrrole of the other lead compounds. There is also an isopentyl substituent on this thiazole adding further lipophilicity. The other lead compounds do possess an alkene containing head group for enhanced lipophilicity but this is at the other end of the molecule and perhaps the location of the lipophilic region is significant. The thiazole also imparts more CG base pair tolerance which might bind to different types of DNA targets than those for the Gram positive active MGBs. The head group of **BP4** contains an amidine moiety, which is significantly basic and thus will be predominantly protonated at physiological pH.

From the above description, a set of **BP4** analogues was designed to probe the significance of the structural features of **BP4** and with a view of exploring simple structure activity relationships (fig. 100).

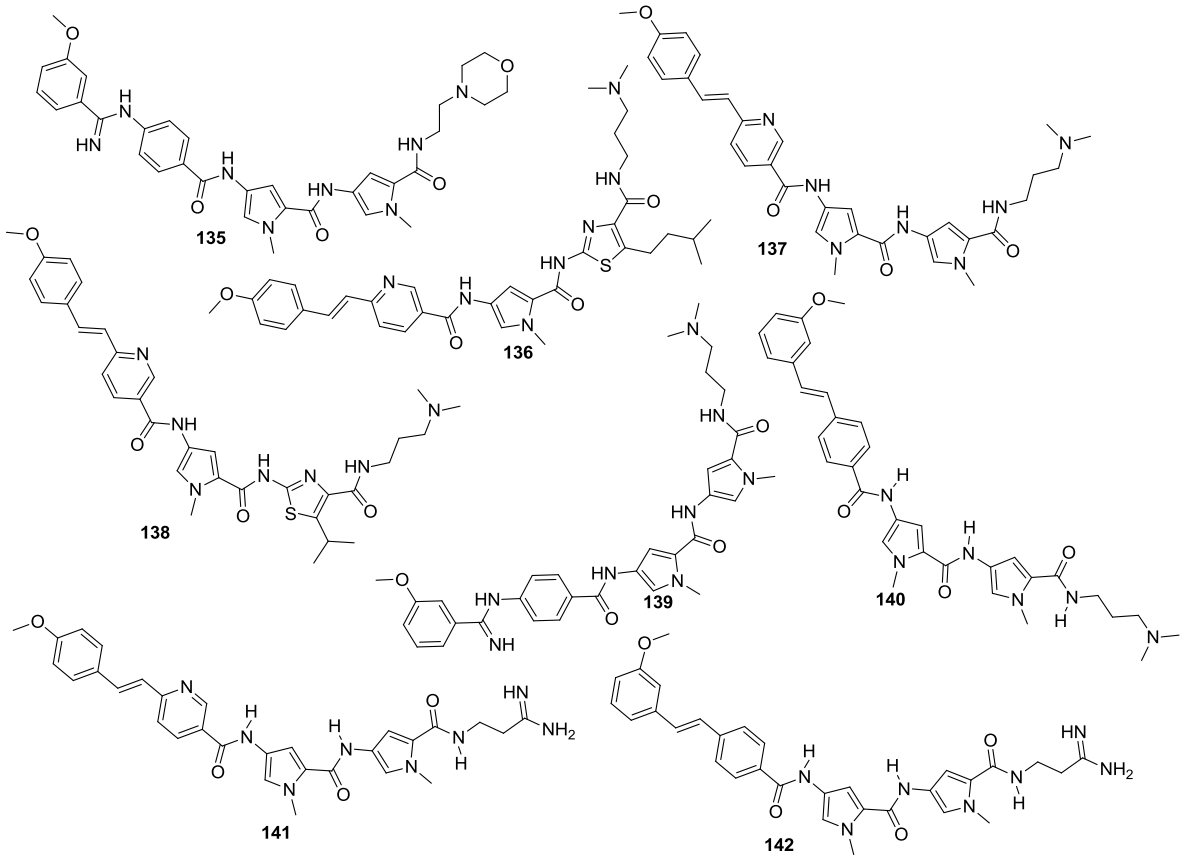

Figure 100: BP4 analogues.

The synthesis of these compounds was achieved by the hydrogenation of the appropriate tail group dimer and subsequent coupling with the required head group using HBTU as the coupling agent (scheme 18 to 21).

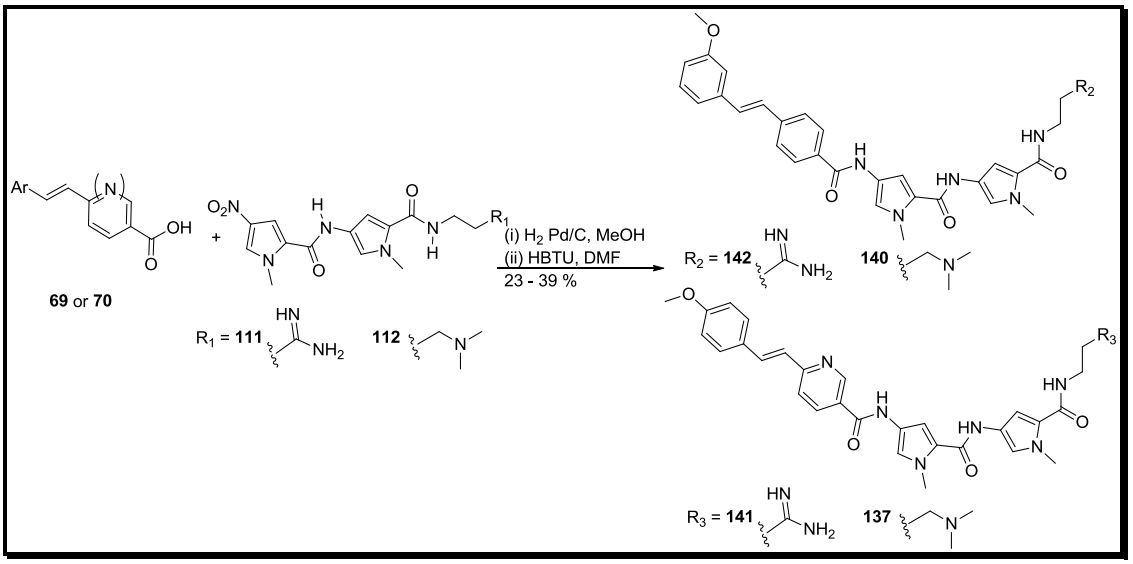

Scheme 18

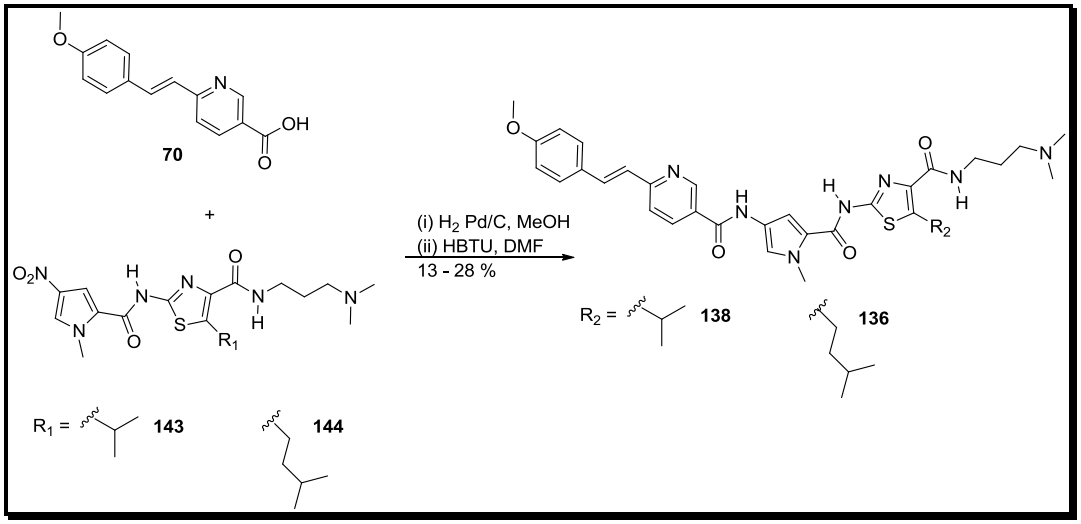

Scheme 19

To synthesise **135** and **139** the head group **146** had to be prepared first. This was done by reacting **72**, prepared previously for the synthesis of **BP4**, with *p*-aminobenzoic acid **145** (scheme 20).

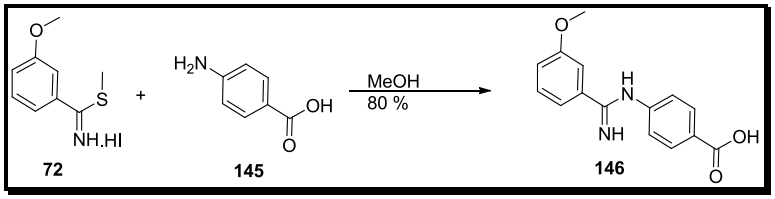

Scheme 20

135 and **139** were synthesised by the hydrogenation of the appropriate tail group dimer, **68** or **112**, and subsequent coupling with the head group, **146**, using HBTU as the coupling agent (scheme 21).

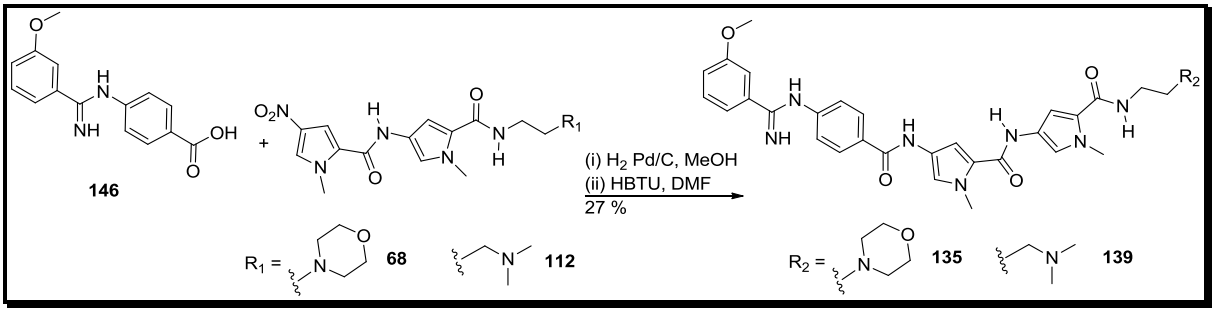

Scheme 21

Results from a general screen of these compounds are still pending; however, their performance in the *P. aeruginosa* assay is discussed in section 2.4.2.6.

2.4.2.5 Cephalosporin II: Methylated analogues

The 4th generation cephalosporins possess a quaternary nitrogen centre and thus are permanently positively charged compared to the distribution of charged molecules that would be present at physiological pH in the compounds prepared thus far. With this in mind it was decided to take the three lead compounds, **BP1**, **BP2** and **BP3**, and prepare the analogues in which the nitrogen of the morpholine has been methylated, compounds **147**, **148** and **149** (fig. 101).

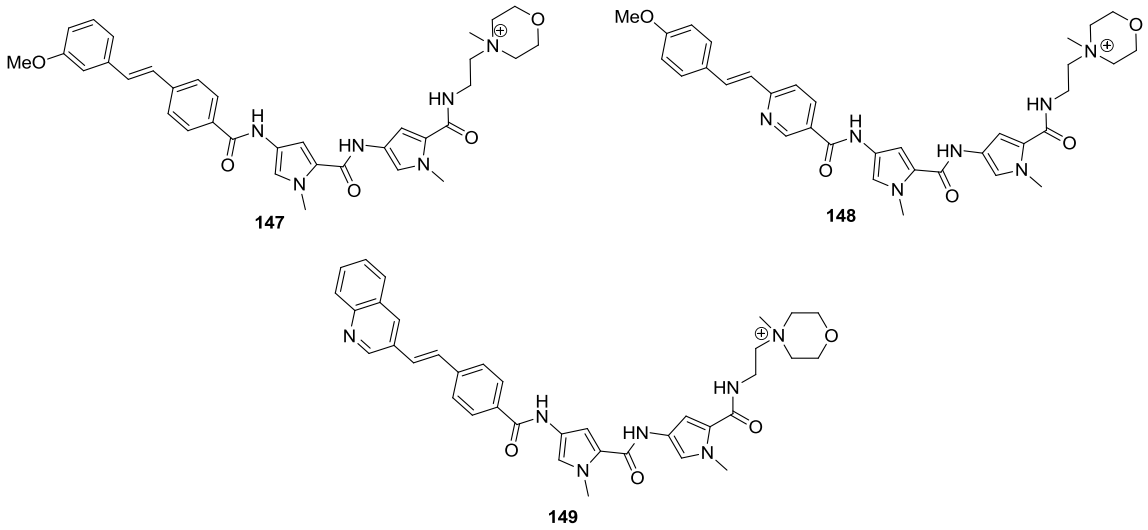

Figure 101: Methylated analogues of BP1, BP2 and BP3.

To synthesise these, the parent compound, **BP1**, **BP2** or **BP3**, was reacted with dimethyl sulfate and subjected to HPLC purification.

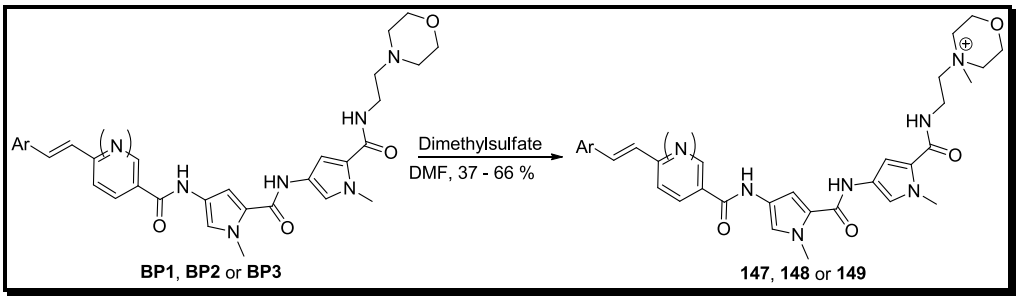

Scheme 22

This panel of compounds was submitted for the normal biological screens and the results are provided in table 13 below along with those for the parent compounds for comparison.

	MIC (μM)							
Compound	**EMRSA 16**	**SMRSA 106**	***E.coli ATCC.8739***	***T.b.brucei***	***M.marinum ATCC BAA535***	***K.pneumoniae NDM-1 ATCC BAA-2145***	***K.pneumoniae ATCC -13883***	***P.aeruginosa ATCC-27853***
BP1	NA	NA	NA	**12.5**	**25**	NA	NA	NA
BP2	**50**	NA	NA	**0.78**	**100**	NA	NA	NA
BP3	**1.56**	**0.78**	NA	**0.19**	NA	NA	NA	NA
147	**6.25**	**6.25**	NA	**1.56**	**12.5**	NA	NA	NA
148	NA	**50**	**100**	**0.78**	NA	NA	NA	NA
149	**0.39**	**0.39**	NA	**<0.19**	**100**	NA	NA	NA

Table 13: MIC values of compounds in μM. NA signifies not active.

The results from the three Gram positive strains indicate that methylation can have a significant effect on the activity of these MGBs. **BP1** went from inactive to displaying activities worthy of comment, albeit not of clinical significance. **BP2** remained fairly inactive against these species upon methylation. Methylated **BP3**, like methylated **BP1**, displayed an increase in activity compared to its parent compound.

The four Gram negative strains that were tested against show a similar story; as for all previous compounds, no activity was found with the exception of methylated **BP2**. This has had an MIC of 100 μM against *E. coli* and, whilst this is weak, it is an increase in activity. The lack of activity for the other methylated compounds again serves to demonstrate that a specific molecular architecture may be required to achieve Gram negative activity in MGBs.

For the parasite that the compounds were tested against, *T. brucei*, there was again a slight increase in activity for the methylated **BP1** and methylated **BP3** but no significant change for **BP2**. Given the relatively good biological profile of these compounds against *T. brucei*, they were also screened against the three species of *Leishmania*, as previous compounds were, and figure 102 displays the results.

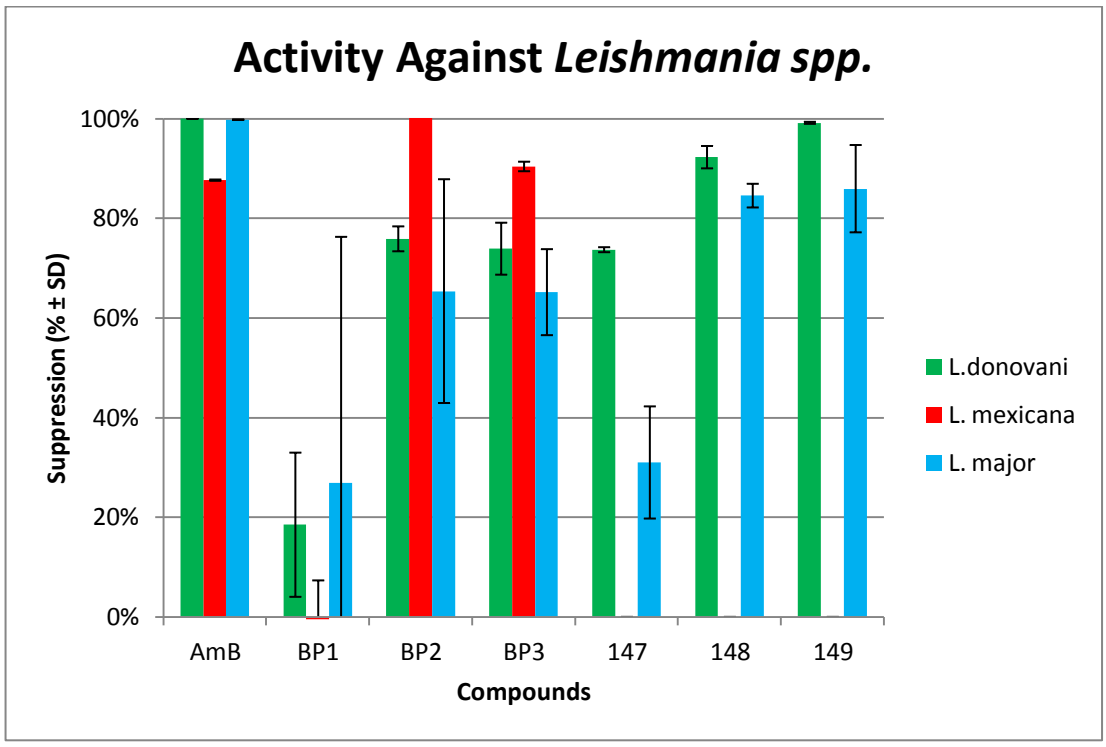

Figure 102: Activity of BP1, BP2, BP3 and their methylated analogues. AmB is amphotericin B.

All the methylated analogues showed a slight increase in activity against *L. donovani* and *L. major* compared with the parent compounds, an interesting trend but their activities are not high enough to warrant further investigation. What was more interesting was the complete lack of activity against *L. mexicana* for all the methylated compounds. This is further evidence that the biological transport properties of the MGBs are a significant factor for activity.

Given that methylation imparted an increase in activity for one compound against one species of Gram negative bacteria it was thought that methylation of the lead Gram negative compound **BP4**, to yield **150** (fig. 103), might be a worthwhile pursuit.

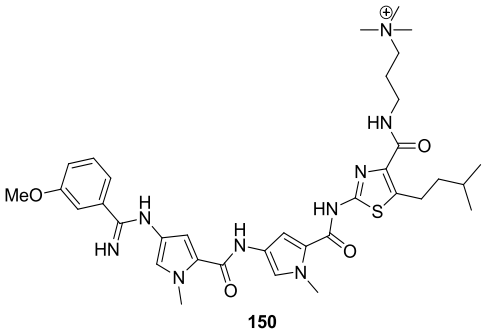

Figure 103: Methylated BP4.

The starting compound had been purified by HPLC and was isolated as the TFA salt so the first step in producing **150** was to obtain the free base of **BP4**. **BP4** was dissolved in DMF and 1 equivalent of TEA was added after which 1 equivalent of dimethyl sulfate was added. The methylated product **150** was purified by HPLC.

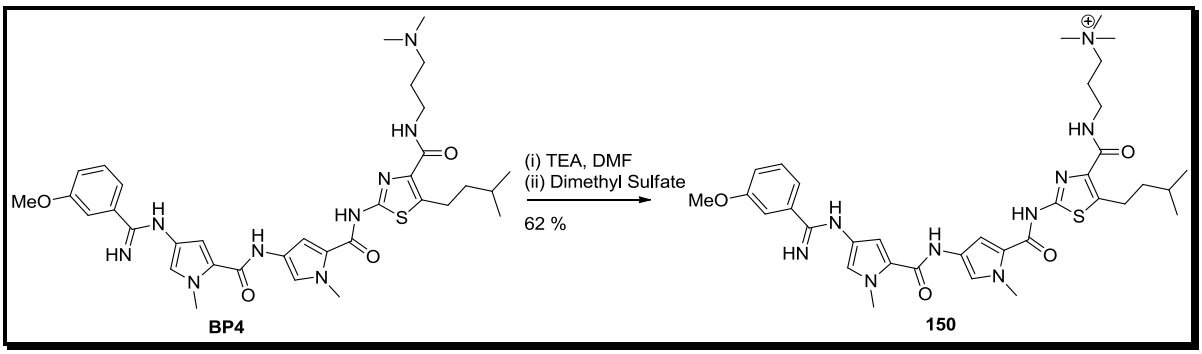

Scheme 23

This compounds activity in the general screen is also still pending; however, its activity against one clinically relevant strain of Gram negative bacteria, *Klebsiella pneumonia* NDM-1 (ATCC BAA-2145), was found to be 25 µM. This is significant for two resons: firstly, it validates the idea of methylation of the tail group being a potential strategy for further development; and secondly, this strain is known to be resistant to a wide range of antibiotics. It was first isolated in 2008 and has quickly gained the title of "Superbug" due to its wide range of resistances.[81]

The activities of these compounds against *P. aeruginosa* are discussed in the next section.

2.4.2.6 Is the problem Efflux pumps?

With the exception of one compound, **150**, little success had been achieved in gaining Gram negative activity. It was considered that given that most of the compounds designed so far were active against Gram positive bacteria, the most likely source for inactivity against Gram negative bacteria was due to either poor influx to the cell or efficient efflux from the cell. A synthetic approach had been tried with the truncated MGBs in order to establish if the compounds were penetrating the cell wall; however, this was unsuccessful and a more biological approach was undertaken.

Phenylalanine-arginyl β-naphthylamide (PAβN) **151** (fig. 104) is a molecule that exihibits a broad spectrum of bacterial efflux pump inhibition, in particular against the resistance nodulation cell division superfamily. It has been demonstrated that through administering PAβN alongside antibiotics that have lost activity due to increased expression of bacterial efflux pumps that the activity can be restored.

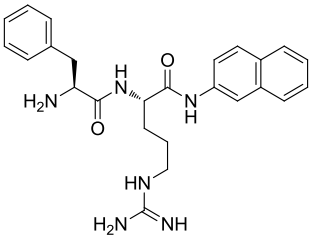

151

Figure 104: Phenylalanine-arginyl β-naphthylamide (PAβN).

A selection of compounds from our library, including all the lead compounds BP1-6, and all the compounds synthesised thus far in the search for Gram negative active compounds, was assembled to be screened against *Pseudomonas aeruginosa* along with the efflux pump inhibitor (EPI) phenylalanine-arginyl β-naphthylamide (PAβN). The structures from this selection that have not appeared thus far are shown in figures 105-107. If efflux pumps are preventing some of these compounds from being active against this Gram negative bacterium then when co-administered with the EPI a significant increase in activity should be seen.[82]

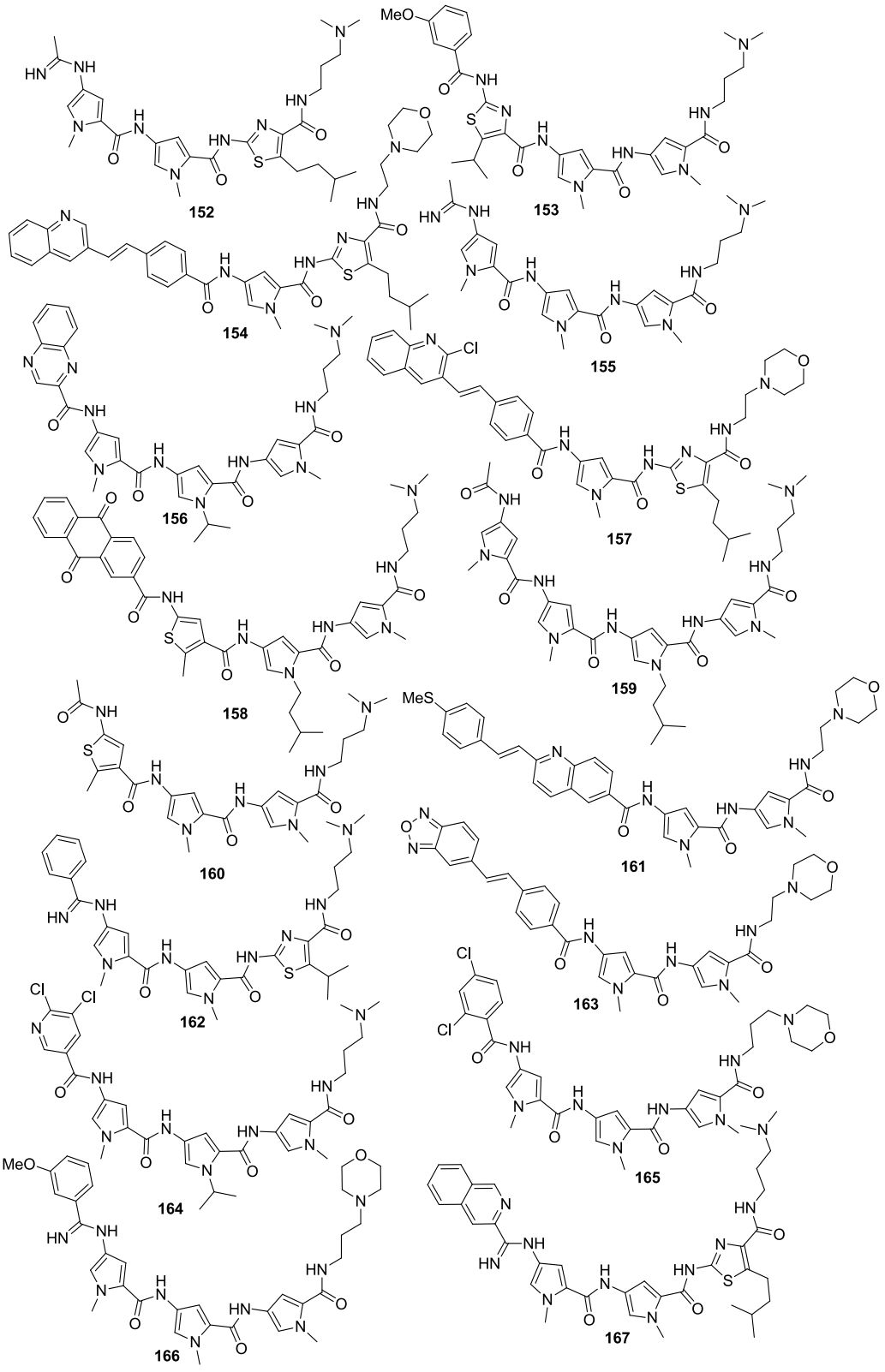

Figure 105: Compounds for *P. aeruginosa* screen.

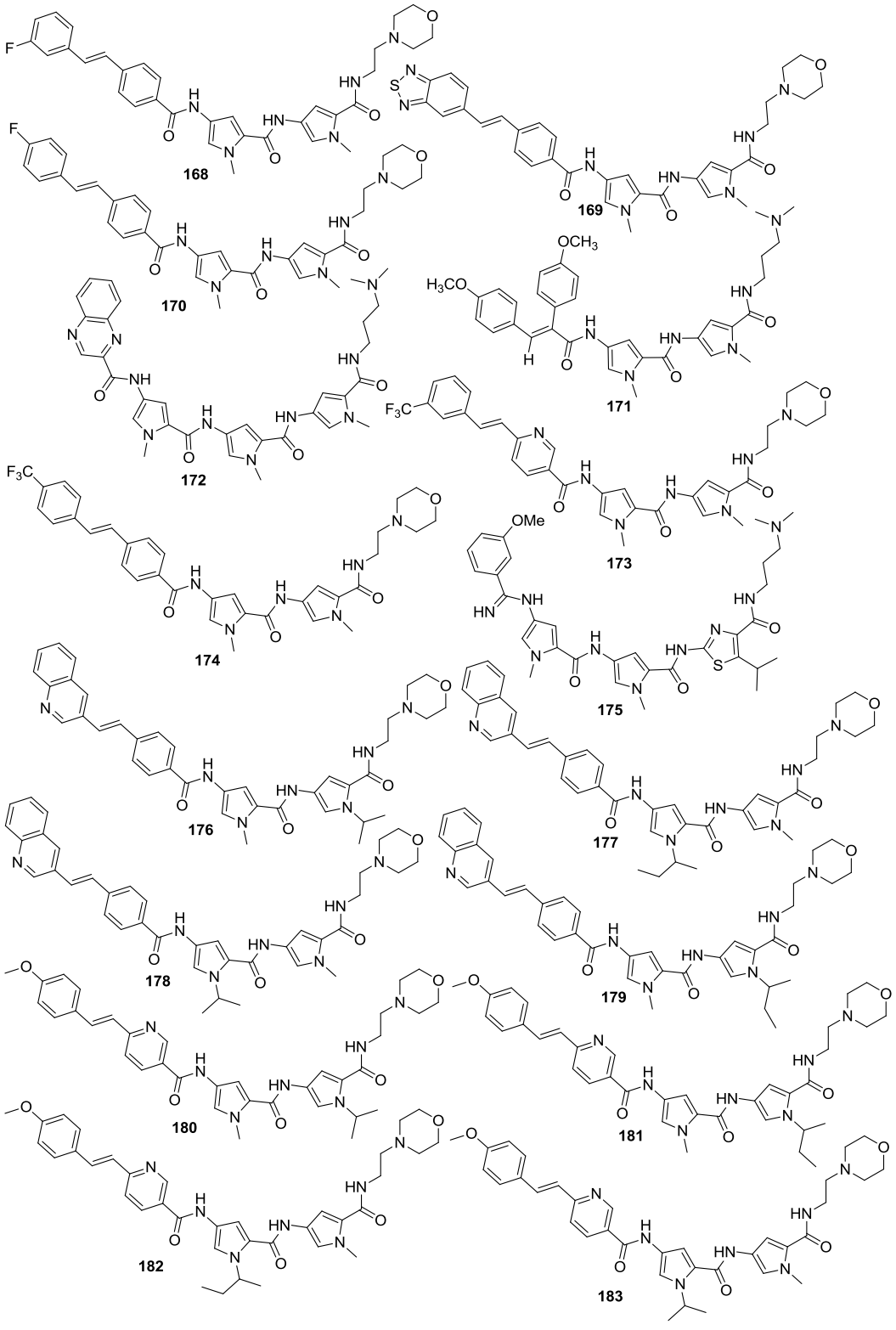

Figure 106: Compounds for *P. aeruginosa* screen.

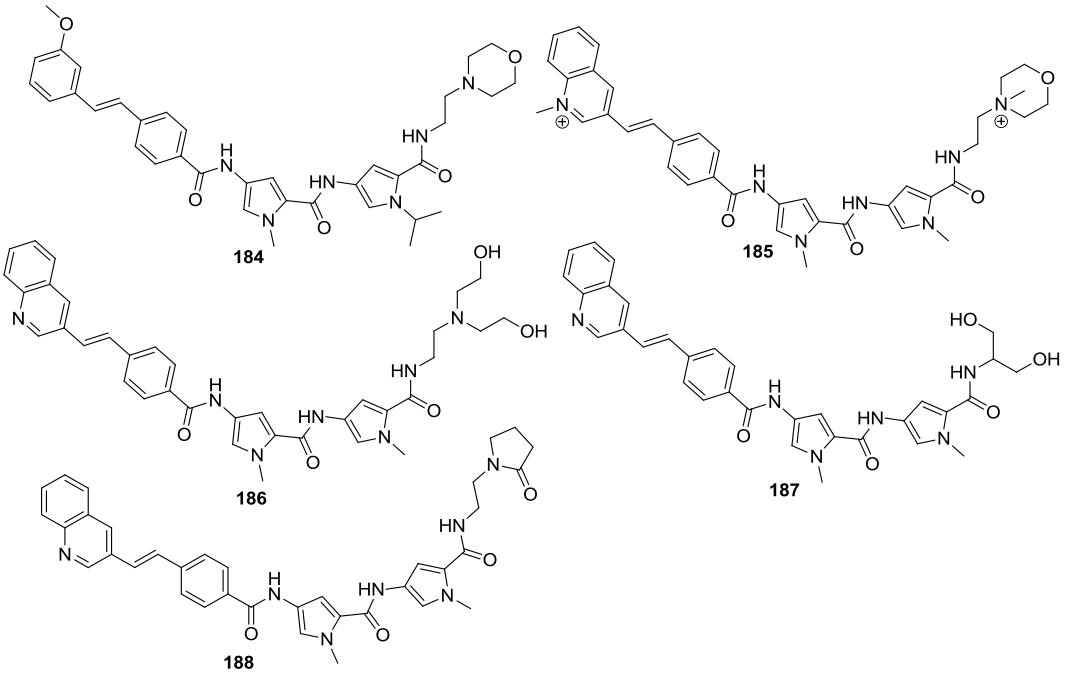

Figure 107: Compounds for *P. aeruginosa* screen.

The initial activity, that without the EPI, of the first batch of compounds was tested by Hazniza Adnan, a microbiology PhD student in the Strathclyde Institute of Pharmacy and Biomedical Sciences (SIPBS). The compounds in this batch were all shown to be inactive (the same set of compounds are shown in figure 108 although this is for the data with the EPI present). The remaining compounds that were to be screened without the EPI and the screening of all compounds with the EPI present was carried out by this researcher and the results that were obtained from this are shown below. Figure 108 displays the growth of the first batch of compounds in the presence of the EPI. Figure 109 shows the growth in the presence and absence of the EPI for the second batch of compounds. The positive control for these experiments is the known gram negative active compound gentamycin and the negative control is the assay run without any compound.

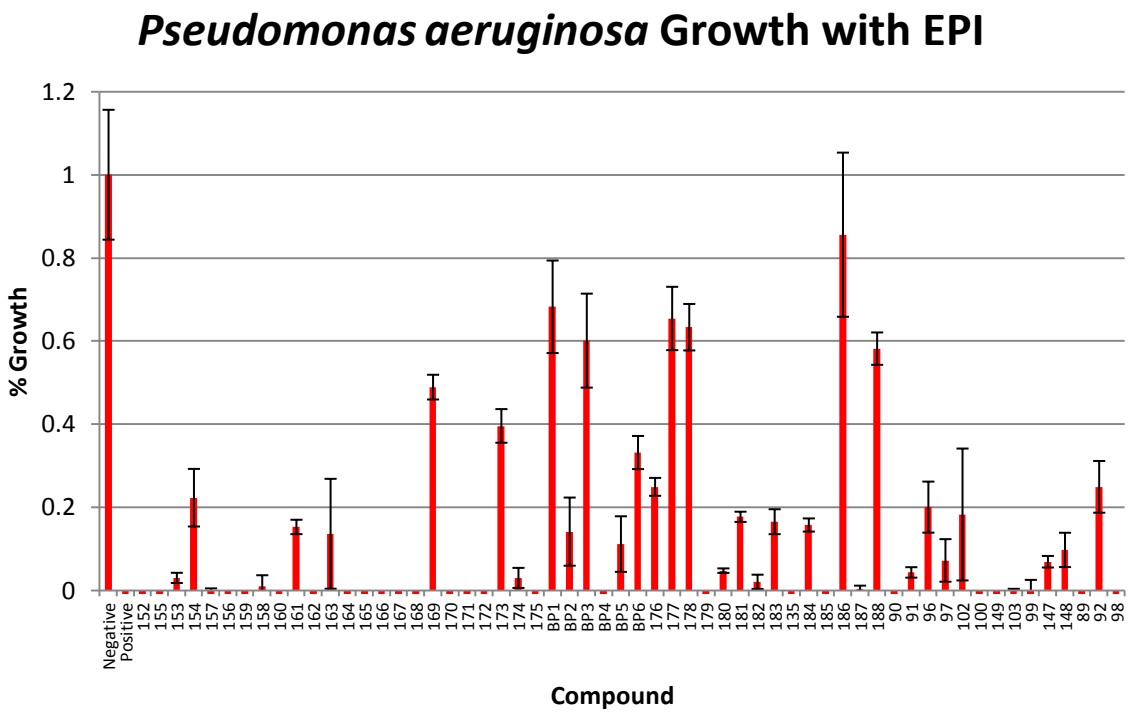

Figure 108: % Growth of compounds from figures 105 – 107 measured at a concentration of 30 µg/mL and an EPI concentration of 80 µg/mL.

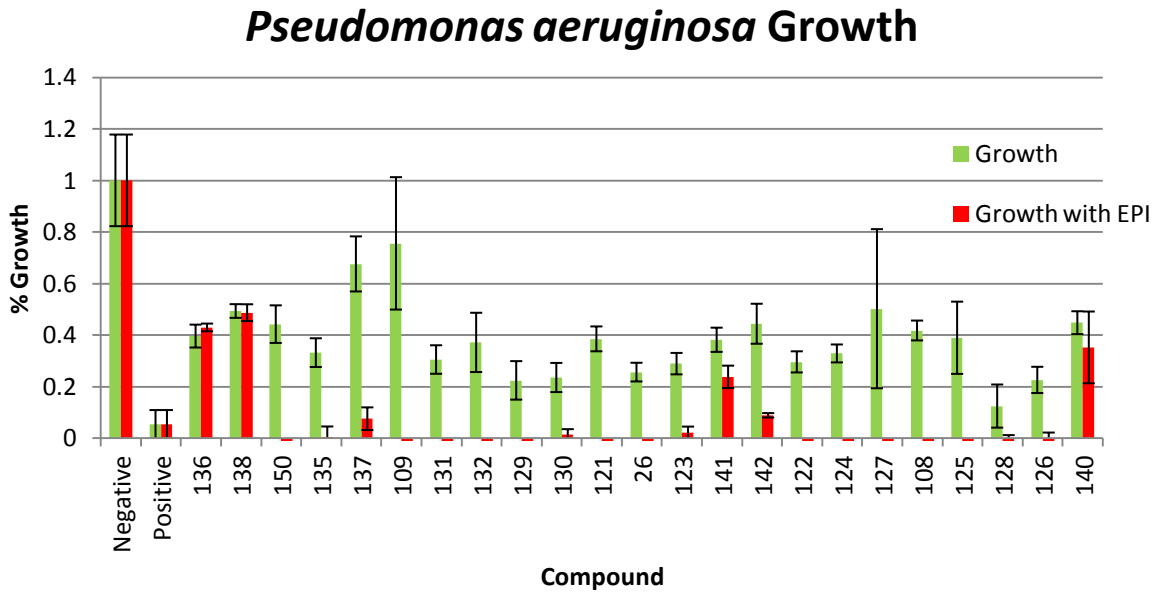

Figure 109: % Growth of other MGB compounds not in figures 105 – 107 at a conc of 30 µg/mL. Growth shown in the absence and presence of an EPI with a concentration of 80 µg/mL.

Beginning with figure 109 it can be seen that these too displayed no significant activity at this concentration without any EPI present. The experiments including the EPI, figures 108 and 109, revealed that around 60% of the tested compounds completely inhibited the growth of the bacteria when efflux from the cell was inhibited.

A number of the truncated MGBs were found to have activity when tested with the EPI. These are compounds **98**, **99**, **100** and **103** and this set includes the three compounds with the *N*-methyl piperazine tail group with each of the different head groups from the lead compounds BP1, BP2 and BP3. The fact that some of these truncated MGBs showed activity serves to discount the previous argument that this class of compounds cannot bind to DNA to bring about a significant biological event leading to activity. More likely becomes the possibilty that in truncating the MGBs, they are now substrates for Gram positive efflux pumps.

All of the netropsin-like compounds from sections **2.4.2.2** and **2.4.2.3** showed activity when the EPI is used. It is significant that these compounds display positively charged, neutral and negatively charged head groups with a tail groups of varying basicity. Those with the negatively charged head groups are of particular interest as they are the first examples of zwitterionic MGBs with antibacterial activity that have been produced by the research group at Strathclyde.

Considering the whole data set, some general observations can be made. For the larger MGBs, any containing an alkene link in the head group tend to remain inactive even in the presence of the EPI. This is true unless the head group also possesses a halogen at its terminal end, for example **168** and **170** or compare **154** to **157**. It might not just be the electron withdrawing characteristic of the halogen that is necessary as the CF_3 analogues of **168** and **170**, **173** and **174**, do not show any activity. Additionally, alkene linked head group containing compounds in which there has been an alteration to the nitrogen of the tail group may give rise to some activity: the *N*-oxide compound **90** shows some activity; also the BP3 analogue without this nitrogen **187**, which can be compared to **186**, shows some activity. The reason why alkene-containing compounds show poorer activities is unlikely to be

related to the overall lipophilicity of the molecules as some of the active compounds possess isopentyl thiazoles, which are highly lipophilic sub-units. It is more likely that there exists a combination of lipophilicity with other properties such as shape or flexibility that give better activity.

The compounds that remain inactive during co-administration with the EPI probably possess other biological transport issues that could be to do with influx to the cell or efflux since there are different barriers and different pumps genetically specified in different species.

In order to refine the set of compounds which are active in the presence of the EPI the set was subjected to the same assay but with a 10-fold dilution so that the concentration was now 3 µg/mL. The data are presented in figure 110 below.

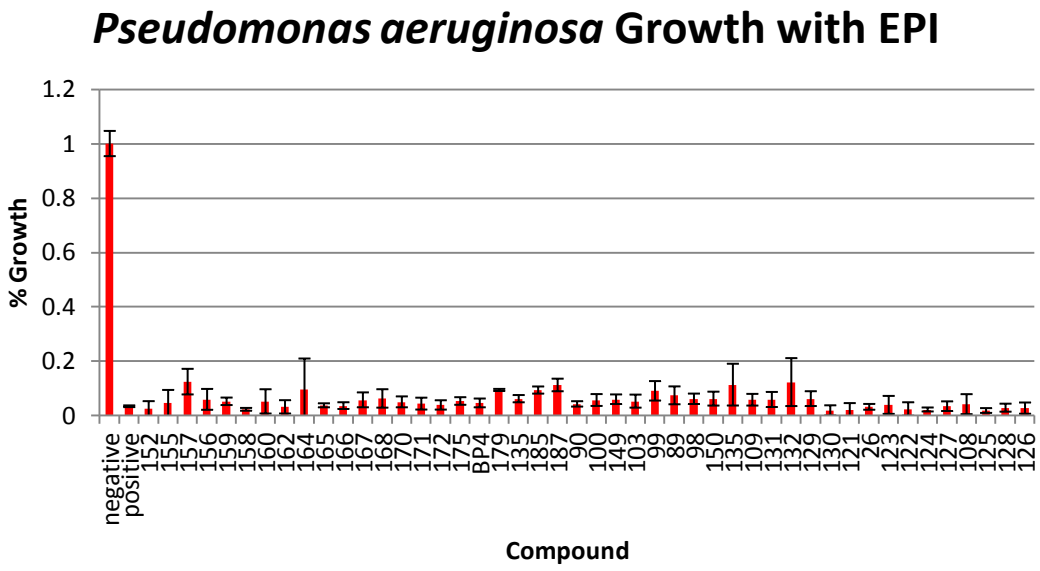

Figure 110: % Growth of MGB compounds at a conc of 3 µg/mL and an EPI concentration of 80 µg/mL .

At this lower concentration all the compounds are still significantly effective at inhibiting bacterial growth. Whilst this is good as it shows that this panel of compounds can display activities at a concentration more in line with that expected of a lead compound, it does not assist in reducing the size of the data set. In order to discern the structural features of the MGBs within the data set the assay was repeated

once more but with a reduced EPI concentration of 20 µg/mL. This is shown in figure 111 below.

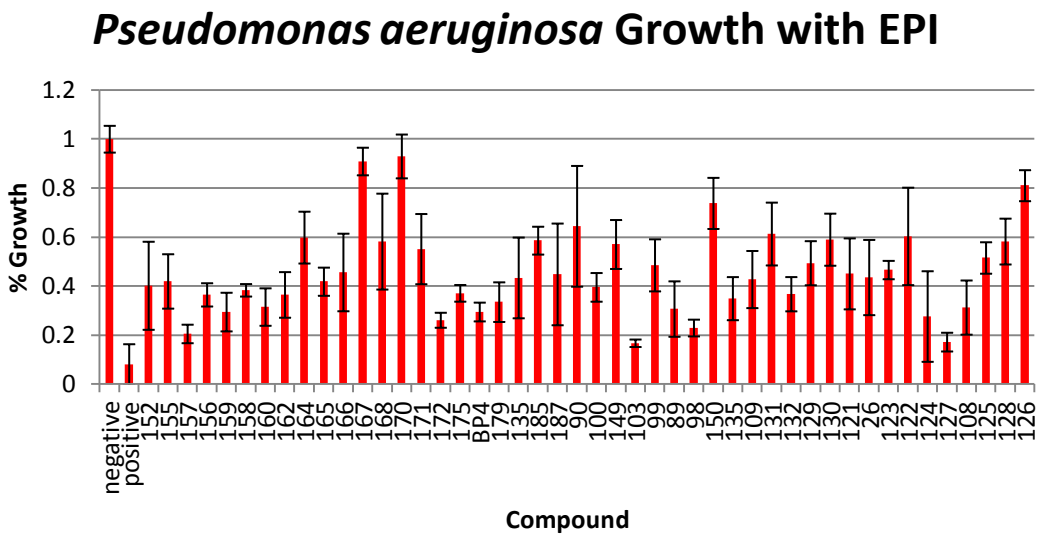

Figure 111: % Growth of other MGB compounds at a conc of 3 µg/mL with an EPI concentration of 20 µg/mL.

This last assay has highlighted a number of features of the data set with the most active compounds from this assay being compounds **157**, **103**, **98** and **127**.

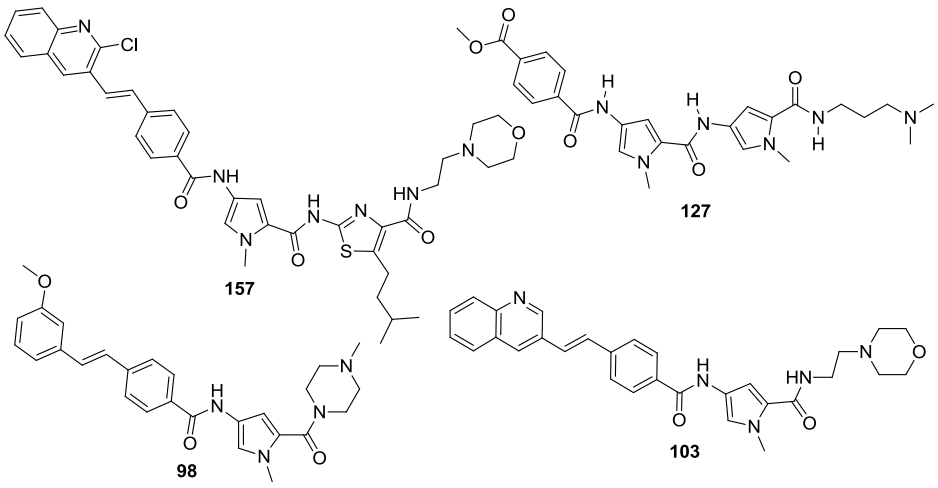

Figure 112: Most active compounds from *Pseudomonas aeruginosa* assay.

Compound **157** is the only compound from the initial screen that has both an alkene containing head group and is of the larger MGB variety. Compounds **103**, **98** and **127** are all of shorter MGB structure: **103** and **98** are from the truncated MGB panel and **127** is from the netropsin like panel. This suggests that the shorter MGBs are more promising structures for future synthetic efforts.

These results challenging Gram negative bacteria in the presence and absence of an EPI suggest new approaches to the design of broader spectrum MGBs than those currently known. There now exists a set of compounds, with varied subsets, that should be active if only one feature can be solved: cell efflux. This should help to facilitate further design and synthesis.

2.5 Conclusion

Efforts to improve the synthesis of the lead compound set have been successful. There is now a synthesis, involving minimal work up in the final step, which can be used to produce larger quantities than previously obtained. This is evident from the successful prepation of material for solubility and stability testing. Furthermore, the new synthetic procedures have been used to allow a CRO to produce the chosen clinical candidate, **BP3**, on a kilogram scale.

Whilst investigating the solubility and stability of the MGBs our understanding of their physicochemical properties, such as self-association, has been increased. This investigation has also revealed that there are not any potential issues for **BP3** being further developed; phase I clinical trials are scheduled this year for its use against *C. difficile* and, now with the discovery of a suitable formulation, this path is planned for use against MRSA.

Some novel compounds have also been developed that investigate strategies for reducing affinity towards the hERG ion channel. These include a late stage diversification of some of our lead compounds, in the formation of *N*-oxides, and also inclusion of a trifluoroacetamide tail group.

An array of novel compounds were designed and synthesised to enable a greater understanding of our compounds lack of Gram negative activity. These compounds, along with a large number from our compound library, were screened against the Gram negative bacterium *P. aeruginosa*. The significance of avoiding efflux pumps has been identified as crucial if activity is to be attained in our MGBs.

2.6 Future Work

The efflux pumps of Gram negative bacteria have been identified as being the reason for our compounds lack of activity in these bacteria. In order to capitalise on this discovery MIC values for our compounds against *P. aeruginosa* with the EPI need to be obtained as this should further narrow the spectrum of compounds of interest. It would also be of interest to repeat the assay using a different EPI to observe if the spectrum of efflux inhibition is the same. This will allow a synthetic strategy to be designed that can explore structural features that might prevent the rapid efflux of the MGBs.

The University of Strathclyde has access to a *P. aeruginosa* mutant library in which individual genes that code for various components of efflux pumps are not present. It is planned for the smaller panel of compounds that have been identified to be screened against this mutant library to provide further evidence for the involvement of efflux pumps in Gram negative resistance to our MGBs.

Chapter 3 Results and Discussion: Riboswitches

3.1 Results and Discussion: Riboswitches

Compounds that act as drugs and bind to RNA are far fewer in number than those that bind to the more traditional protein targets; moreover, the ribosome is the major target of those that do bind RNA structures. The fairly recent discovery of riboswitches has opened up a potential new avenue of investigation for the design of antibiotics. Since they are still a recent discovery there is a need for investigation into the basic science of riboswitches and their interactions with their cognate ligands. Only with this will riboswitches become validated drug targets. The details of our investigations into the PreQ1 riboswitch and the TPP riboswitch now follow.

3.2 PreQ1 Riboswitch

The Suckling group has much experience in synthesising compounds similar in structure to PreQ1 hence it being chosen as target. There was thus a large library of compounds that were available which could be screened but before this could be begun it was necessary to have a robust assay method of determining the activity of a compound and our collaborators at the University of Bonn were to do this. Our compound library was quite large and we were interested in filtering the number of compounds to be screened. It was thus advantageous to understand as much about the target as possible in order to eliminate some compounds. There was also a basic science drive as compared to proteins, which have been used as targets for drug design for decades, very little is known about how riboswitches bind their natural ligands.

3.2.1 Synthesis of PreQ1

In order for our collaborators at the University of Bonn to set up a binding assay for the PreQ1 riboswitch, they required of us a small quantity of both PreQ0 and PreQ1. Our research group frequently uses PreQ0 as an intermediate for other projects and some of this was made available by both Dr. David Breen and Dr. Judith Huggan; hence, PreQ1 was the only molecule left to be synthesized for the assay to be established.

To this end a synthesis very closely aligned to that of Klepper *et al.* was employed.[83] Instead of the initial oxidation of the hydroxypropylphthalimide (scheme 24) by way of *Dess-Martin* periodinane, a Swern oxidation was carried out (76% yield); the remaining synthetic steps were kept the same. The aldehyde **190** was converted to the α-bromoketone *in situ* and cyclised with 2,6-diaminopyrimidine-4-one to form the phthalimide protected PreQ1 **191** in a yield of 85%. The phthalimide was cleaved using hydrazine to yield the crude PreQ1; however, Klepper *et al* had reported issues with purification and hence the PreQ1 in the crude mix was BOC protected **192** to allow purification by column chromatography giving a yield of 31%. The TFA salt of PreQ1 **50** was then obtained quantitatively by hydrolysis with TFA.

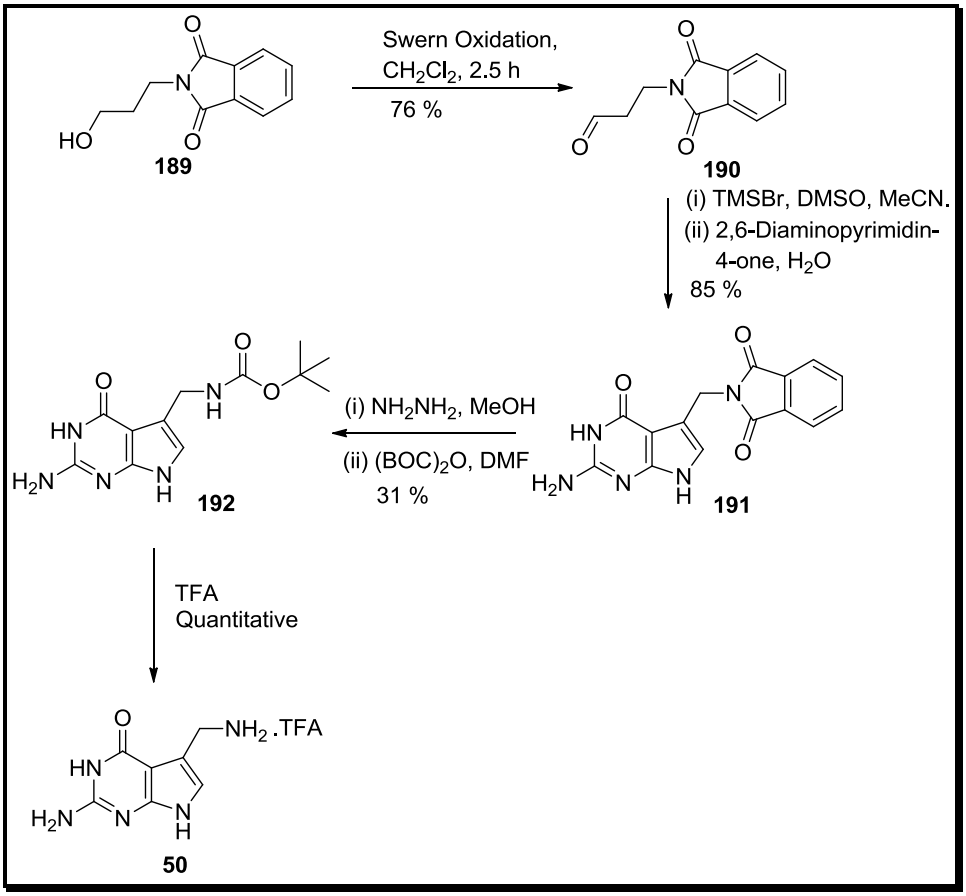

Scheme 24

3.2.2 Molecular Dynamics of PreQ1

In order to be able to direct the choice of molecules from our compound library to be screened and ultimately synthesise a number of relevant molecules targeting the PreQ1 riboswitch it was though necessary to further investigate the aptamer domain. To achieve this, two molecular dynamics simulations were carried out on the aptamer domain of the PreQ1 riboswitch from *Bacillus subtilis*, PDB file 3FU2;[83] these were in the presence of the ligand, PreQ1 **50**,(TRAJ_LIG, approximately 18 ns) and the absence of the ligand (TRAJ_NOLIG, approximately 16 ns) using the AMBER[76] suite of programs. The main goal of this analysis was to find out as much information as possible about the system; however, there were a few specific questions to be answered.

PreQ1 **50** is significantly buried within the aptamer domain and therefore the scope for structural modification appears limited. The importance of the extensive hydrogen bonds that PreQ1 **50** makes with the aptamer domain (see section **1.2.2.4**) is one question that requires an answer; if certain hydrogen bond donors/acceptors are found to be unnecessary then they could be potential sites for modification. Another important piece of information that is required pertains to the exocyclic amine of PreQ1 **50**. In all of the crystal structures in the literature this primary amine points into a relatively solvent exposed area; this presents a problem as this amine is the most synthetically tractable point of modification in the molecule and expansion into solvent exposed regions is not particularly favourable. There is, however, a more suitable pocket in the opposite side of the aptamer domain that would be more suitable to build into and hence the structural flexibility of this amine was to be scrutinised to discover if it is able to orient itself towards the more desirable pocket (fig. 113).

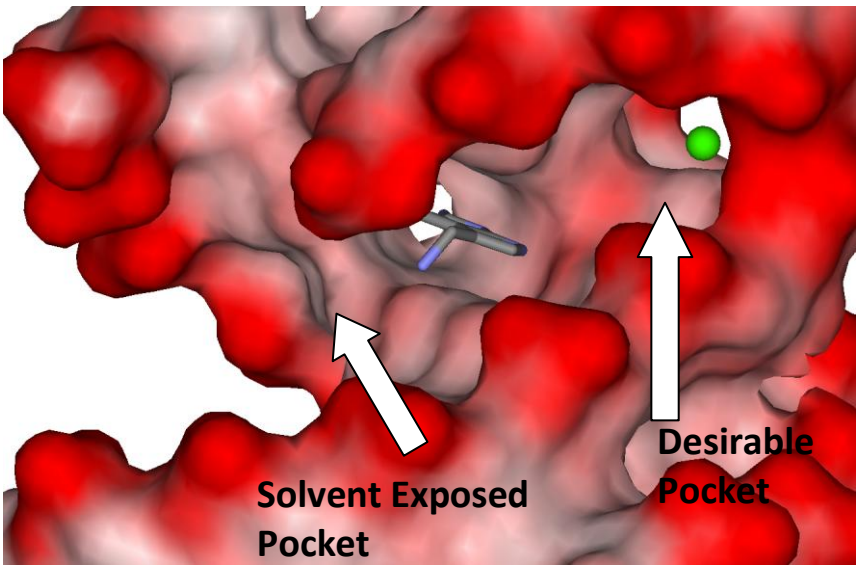

Figure 113: Two pockets in the riboswitch adjacent to PreQ1.

3.2.2.1 RMSD Trajectory Analysis

In order to gain some insight into the motion of the ribowistch comparing the binding site with the rest of the structure, an analysis into the root mean squared deviation (RMSD) was undertaken. Residues that possessed an atom within 5 Å of PreQ1 **50** were defined as being within the binding site of the riboswitch. The heavy atom RMSD, with reference to the crystallographic structure, of both the binding site and the entire riboswitch was calculated for both trajectories (fig. 114 and 115). Each snapshot from the trajectory has been superimposed on the crystallographic coordinates to ensure the removal of rotational and translational motion.

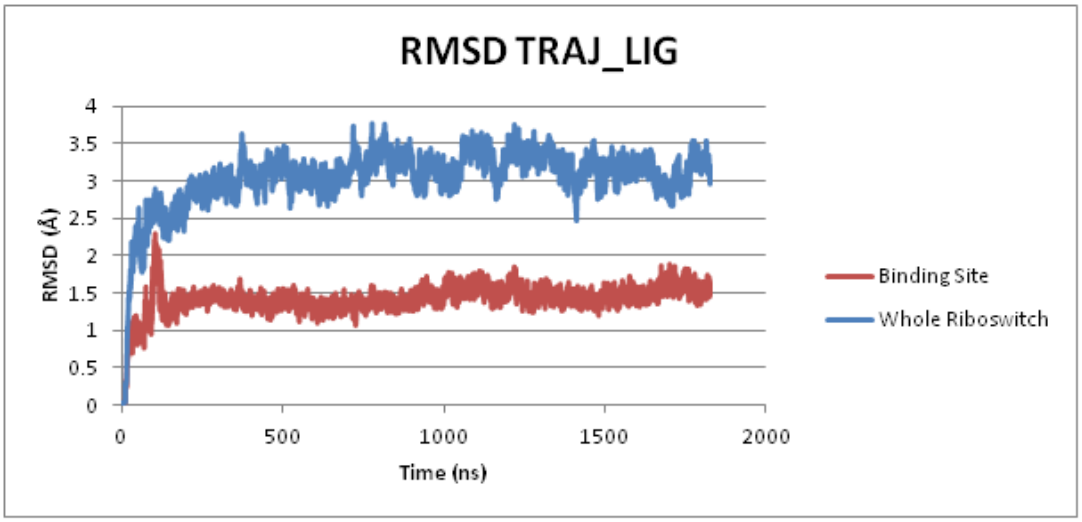

Figure 114: RMSD of TRAJ_LIG showing differences between the PreQ1 binding site and the whole riboswitch.

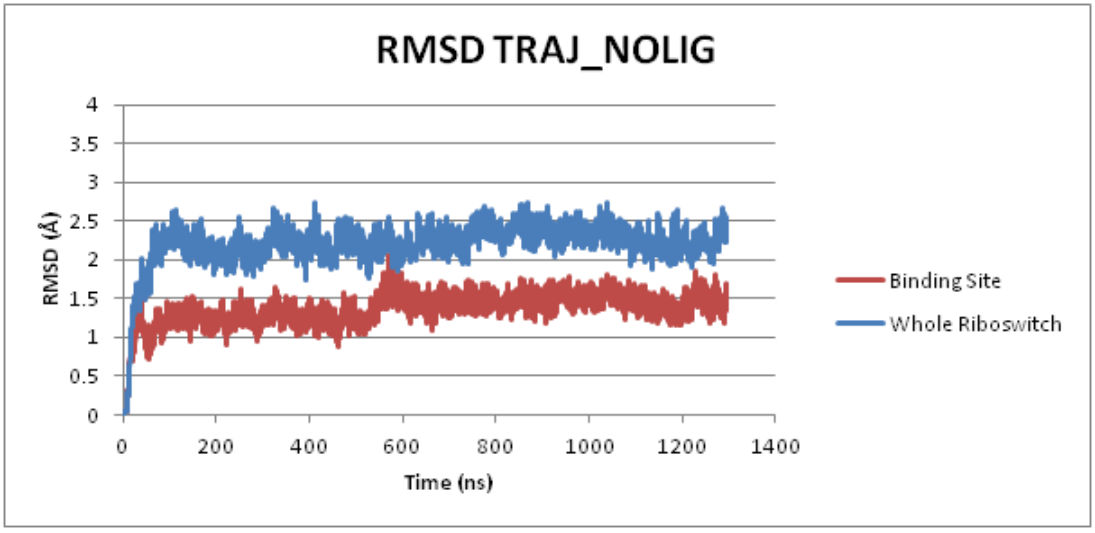

Figure 115: RMSD of TRAJ_NOLIG showing differences between the PreQ1 binding site and the whole riboswitch.

A comparison of the RMSDs of only the binding sites of the two trajectories shows a stable deviation of approximately 1.5 Å is achieved in both the trajectory with the ligand and that without. This indicates that the artificial removal of the ligand from the fully formed riboswitch does not significantly affect the overall stability of the structure. Further evidence to this can be seen in the RMSDs of the whole riboswitch in both trajectories. TRAJ_LIG reaches a stable deviation of approximately 3.2 Å; whereas, TRAG_NOLIG reaches a smaller deviation of

approximately 2.4 Å. The presence of PreQ1 **50** within the formed riboswitch structures imparts more fluctuation in the riboswitch structure.

It is well known that ions can have a profound effect on the control of riboswitches and they often work synergistically with the ligand, preorganising the mRNA. Throughout the course of both trajectories there is a Ca^{2+} ion that stays associated with the same region of the riboswitch and it was thought that this ion could be working in tandem with PreQ1 **50** (fig. 116). To this end, the residues containing the phosphates that coordinate to this Ca^{2+} ion (fig. 116) were subjected to an RMSD analysis using both TRAJ_LIG and TRAJ_NOLIG (fig. 117 and 118).

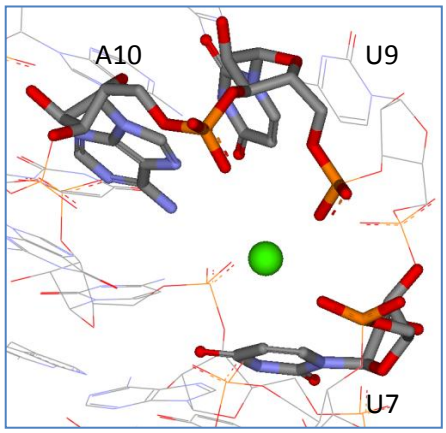

Figure 116: U7, U9 and A10 in proximity to the Ca^{2+} ion.

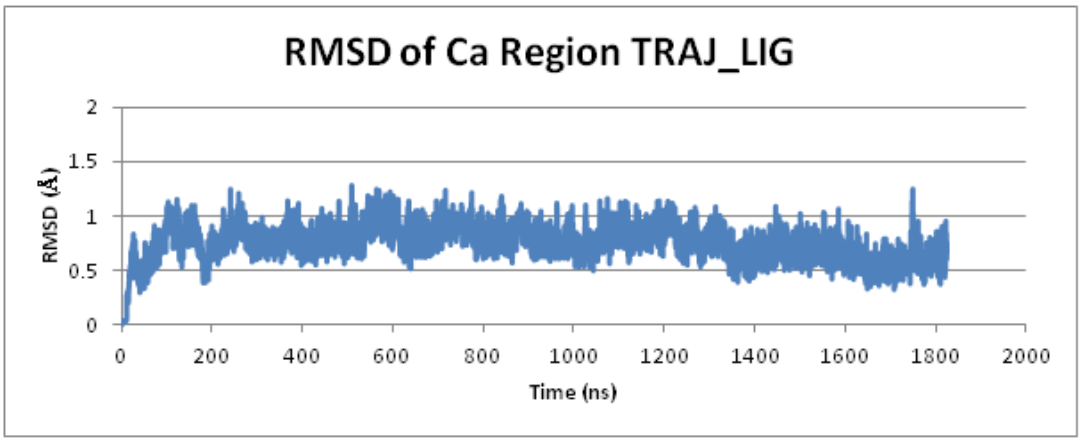

Figure 117: RMSD of U7, U9 and A10 in TRAJ_LIG.

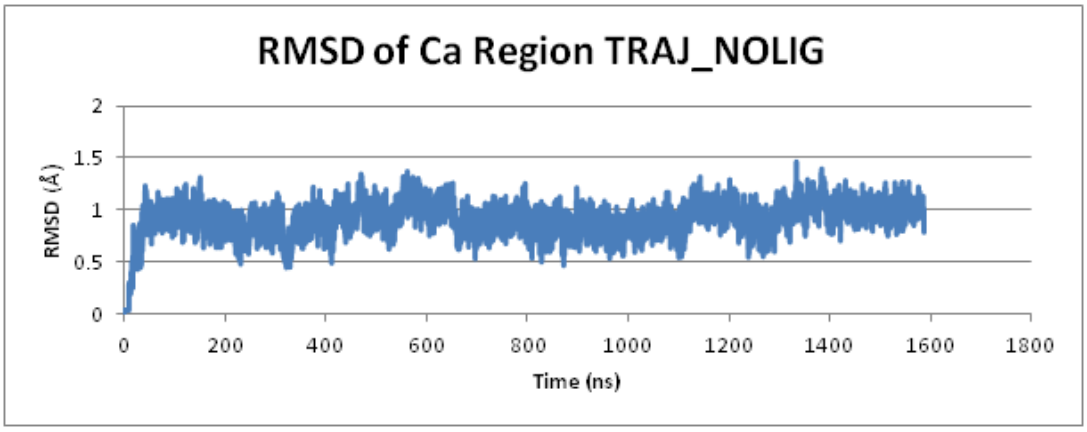

Figure 118: RMSD of U7, U9 and A10 in TRAJ_NOLIG.

Both RMSDs are very similar, showing no clear correlation between the Ca^{2+} ion and PreQ1 **50**. If presence or absence of PreQ1 **50** were having an effect on the Ca^{2+} ion then one would expect to see a significantly larger or smaller RMSD for the Ca^{2+} ion. Although this suggests that PreQ1 **50** does not influence the Ca^{2+} ion it does not preclude the Ca^{2+} ion from influencing the binding of PreQ1 **50**. It is possible that the Ca^{2+} ion may preorganise the riboswitch in some way to assist the binding of PreQ1 **50**. This is useful as it suggests that, in designing new structures to bind to the riboswitch, the interactions of the Ca^{2+} should either not be interfered with or perhaps the Ca^{2+} could be replaced by a suitably positively charged moiety.

3.2.2.2 Cross Correlation Matrices

Further information with regards to the motion of the riboswitch was sought; this time interest was placed in the correlated motions of the residues. The cross-correlation coefficients of each residue compared with all other residues was calculated for both TRAJ_LIG and TRAJ_NOLIG. Figures 119 and 120 show the normalised correlation matrix plots for both positive and negative correlated motions between each residue in the PreQ1 riboswitch for each trajectory. A positive correlated motion between two residues indicates that as one moves, the other moves in the same direction. If there is a negative correlation between two residues then as one moves, the other moves in the opposite direction.

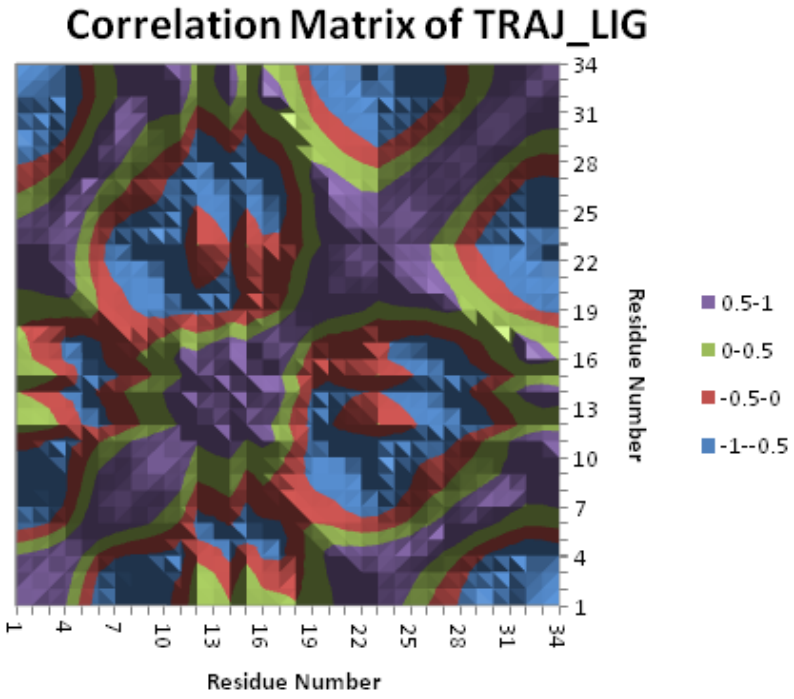

Figure 119: Correlated motions of the residues in TRAJ_LIG. Correlation coefficients of 0.5 to 1 are purple, those 0 to 0.5 are green, those -0.5 to 0 are red and those -1 to -0.5 are blue.

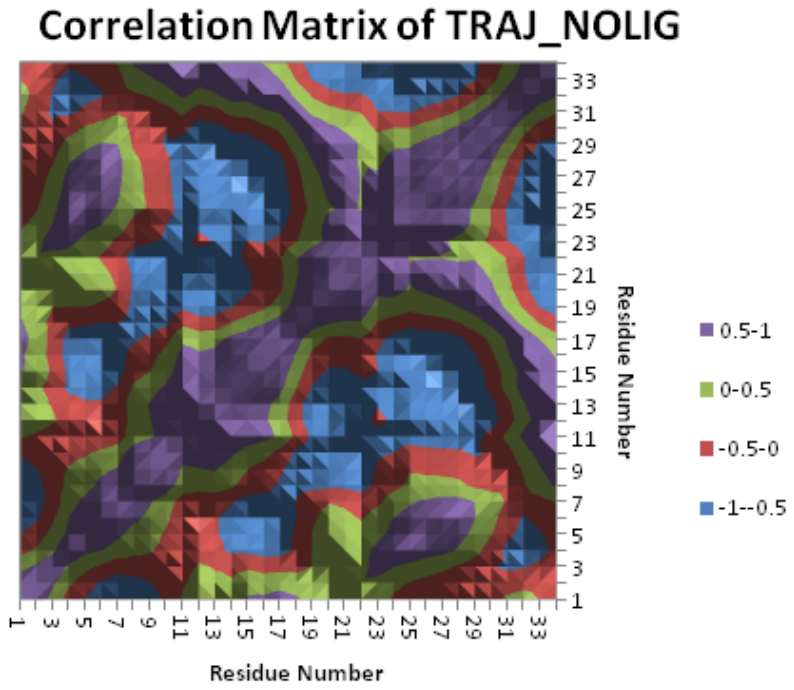

Figure 120: Correlated motions of the residues in TRAJ_NOLIG. Correlation coefficients of 0.5 to 1 are purple, those 0 to 0.5 are green, those -0.5 to 0 are red and those -1 to -0.5 are blue.

One would expect to see large correlations between residues that are on the same section of secondary structure or those that are directly interacting with each other, e.g. bases pairing, and these are seen, for example in figure 119 the left to right upwards diagonal line of purple indicates highly correlated base pairs. An extensive analysis of each plot individually reveals nothing unexpected, which is not surprising given that this riboswitch is so small and compact. If the two matrices are compared there is one major difference between them: for the TRAJ_LIG trajectory the residues around 8 are positively correlated with those around 31 whereas for the TRAJ_NOLIG trajectory, there is a negative correlation. This result will be discussed at the end of this section (section **3.2.3**).

3.2.2.3 Examination of Hydrogen Bonds

It is known from the crystal structure that PreQ1 **50** makes an extensive array of hydrogen bonds in the binding site of the riboswitch (see section **1.2.2.4**); however, the persistence of these and thus the importance of these is of intrinsic interest for designing potential non-natural ligands. To examine this all hydrogen bond donors and acceptors of PreQ1 **50** were monitored using the *hbond* command of *ptraj* in the AMBER suite. For convenience, these hydrogen bonds can be conceptually grouped into two: those of the pyrrolopyrimidine base and those of the primary amine.

There are six hydrogen bonding interactions between the heterocyclic core of PreQ1 **50** and the binding site of the riboswitch (figs. 121 to 127). All of these interactions persist throughout the trajectory.

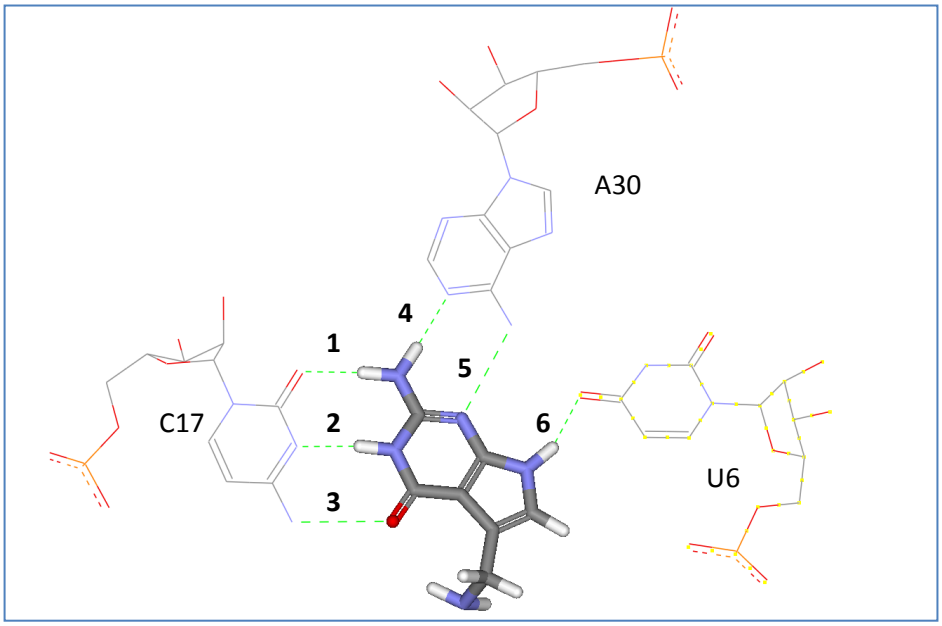

Figure 121: Hydrogen bonding pattern of PreQ1, 50.

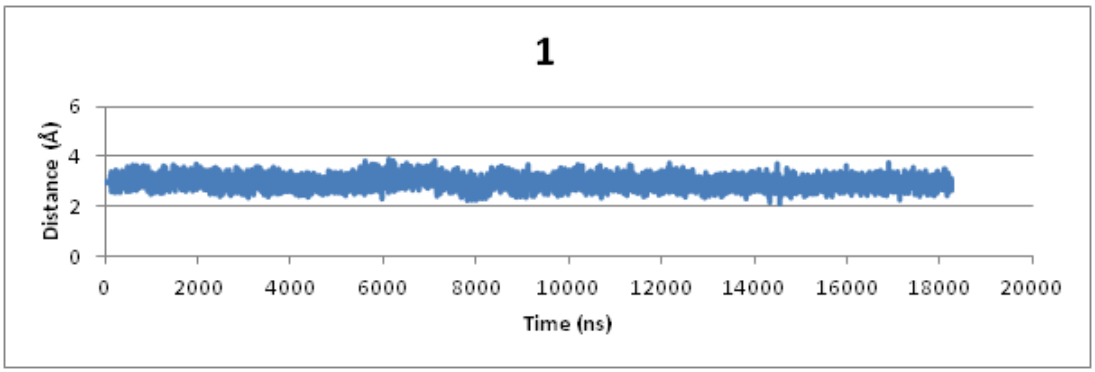

Figure 122: Hydrogen bond 1 as depicted in figure 121.

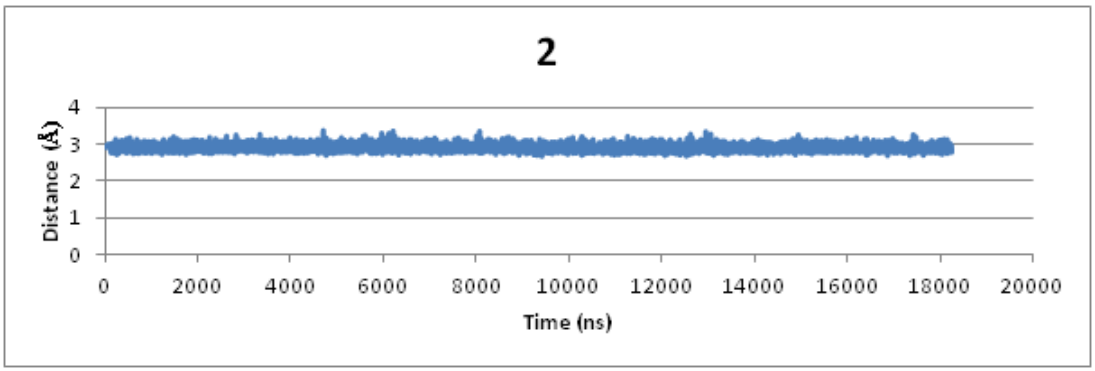

Figure 123: Hydrogen bond 2 as depicted in figure 121.

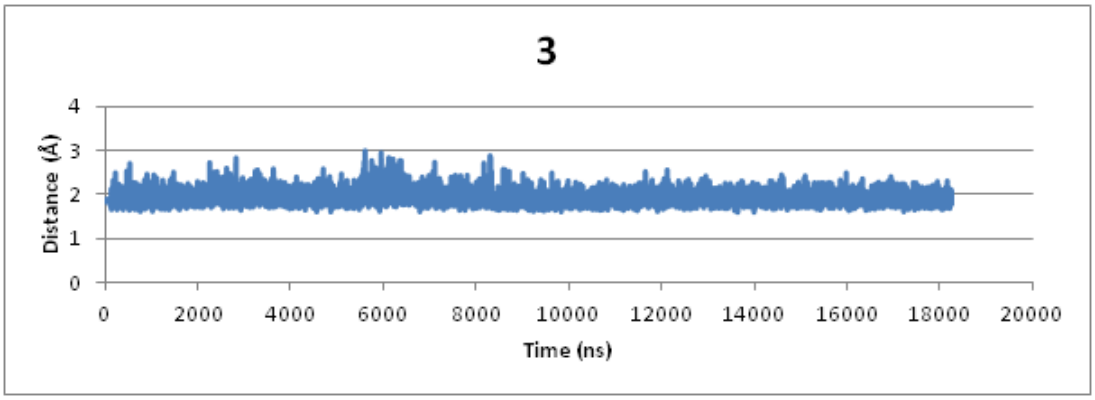

Figure 124: Hydrogen bond 3 as depicted in figure 121.

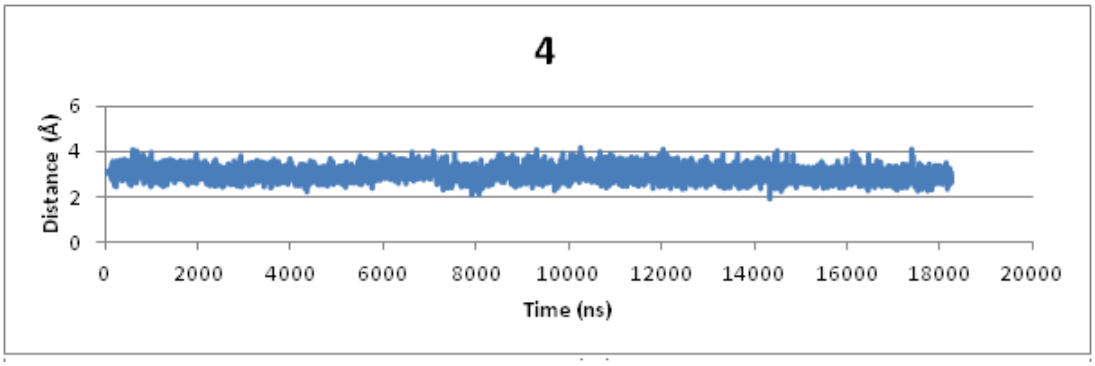

Figure 125: Hydrogen bond 4 as depicted in figure 121.

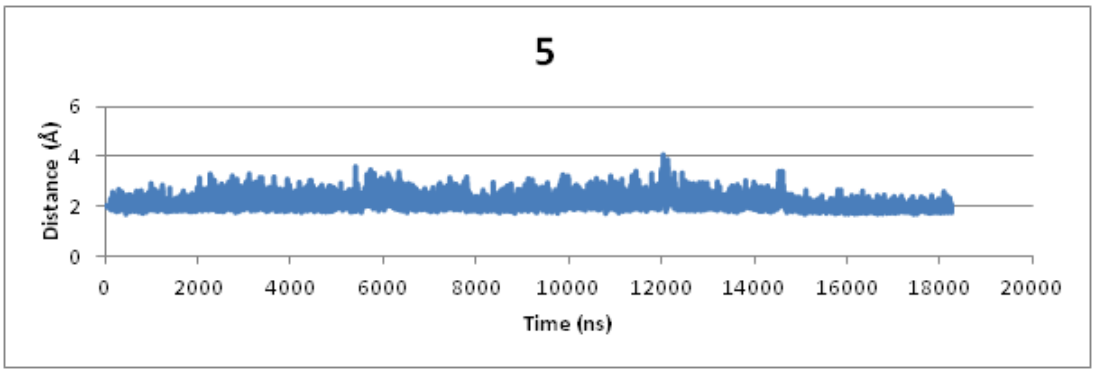

Figure 126: Hydrogen bond 5 as depicted in figure 121.

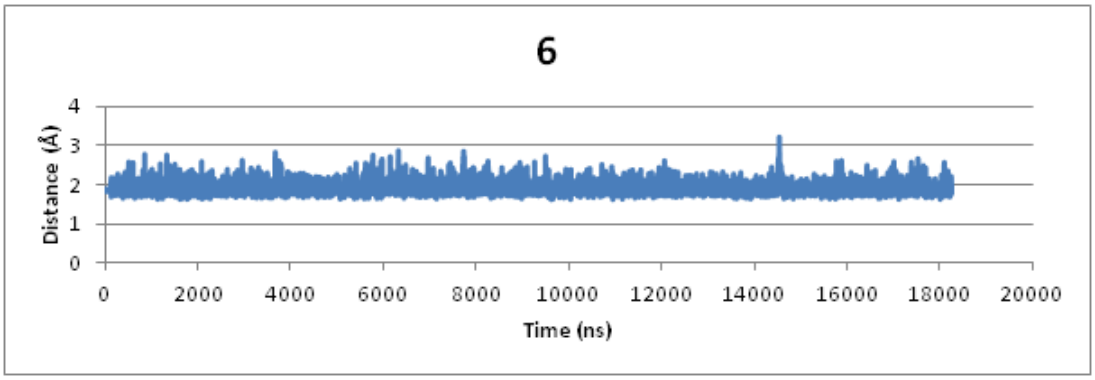

Figure 127: Hydrogen bond 6 as depicted in figure 121.

In contrast to the above hydrogen bonding interactions, those of the primary amine exhibit more dynamic behaviour (figs. 128 to 132).

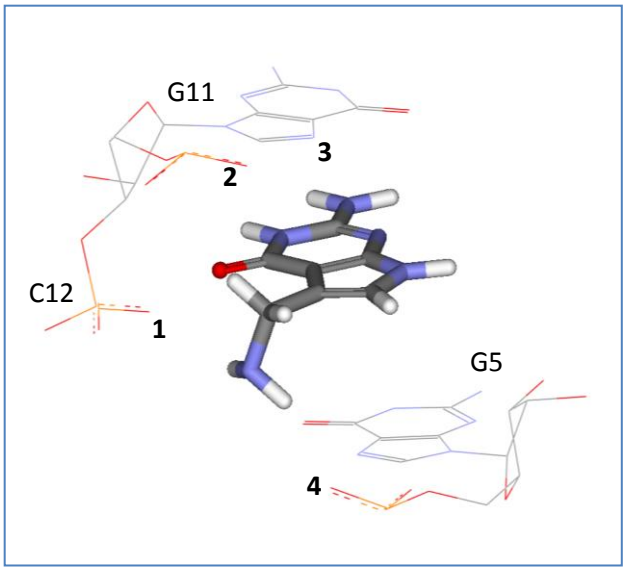

Figure 128: Monitored hydrogen bonds between primary amine of PreQ1 and the riboswitch. Atoms of riboswitch that are monitored are numbered.

A cursory glance at the graphs of the four possible hydrogen bonding interactions (in particular interaction 4) would show that there are perhaps two different conformations in this region of the riboswitch; there appears to be a bimodal distribution in figure 132. Closer inspection of figures 129 to 132 reveals that there is in fact another consistently occurring conformation. For example figure 129, shows three regularly occupied interaction distances: 3 Å, 5 Å and 6 Å, approximately.

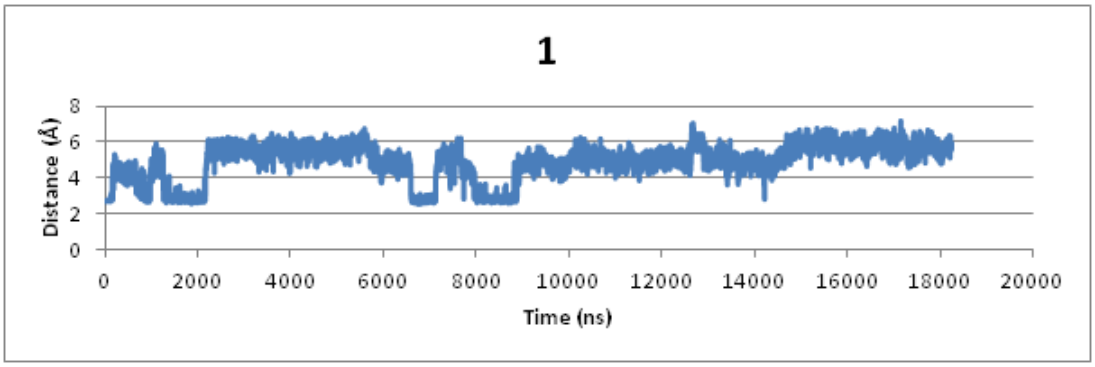

Figure 129: Hydrogen bond 1 as depicted in figure 128.

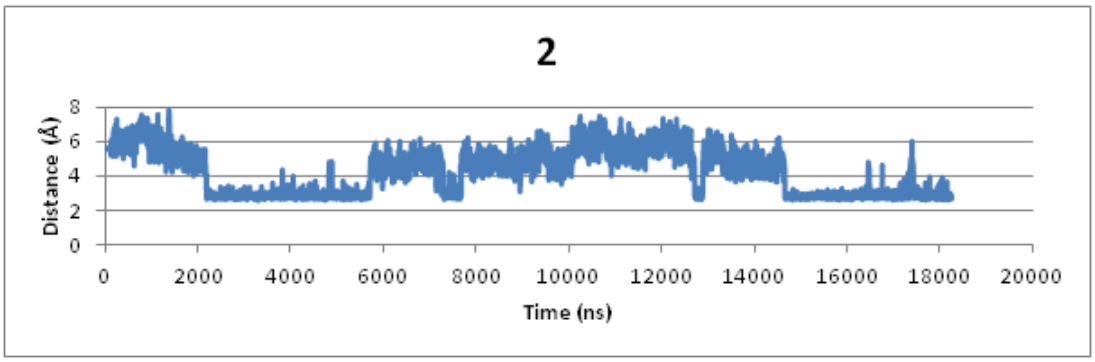

Figure 130: Hydrogen bond 2 as depicted in figure 128.

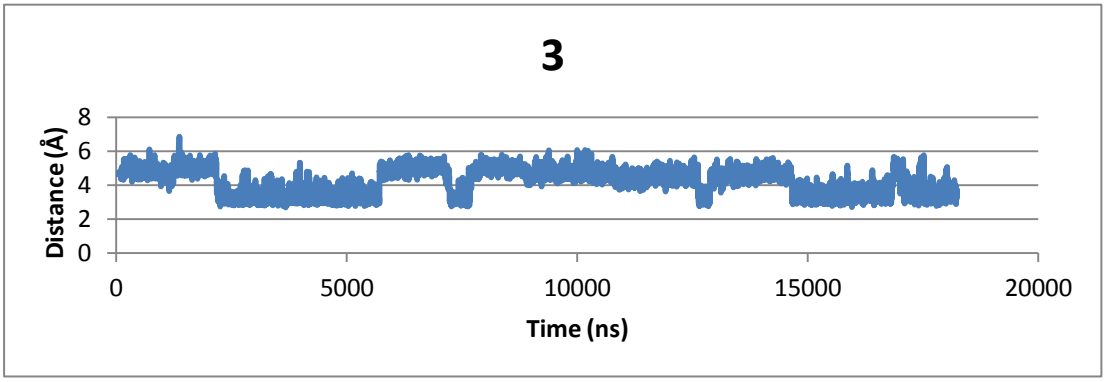

Figure 131: Hydrogen bond 3 as depicted in figure 128.

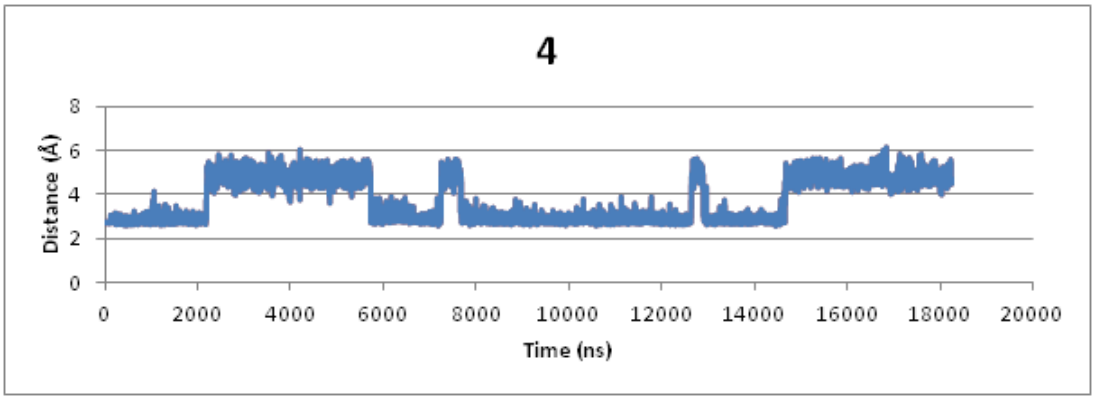

Figure 132: Hydrogen bond 4 as depicted in figure 128.

An example time segment of each of the three identified conformations was extracted from the trajectory and an average .pdb structure obtained. These were 1000-2000 ns (Pose 1); 2200 -5400 ns (Pose 2); and 10000-12000 ns (Pose 3) (fig. 133).

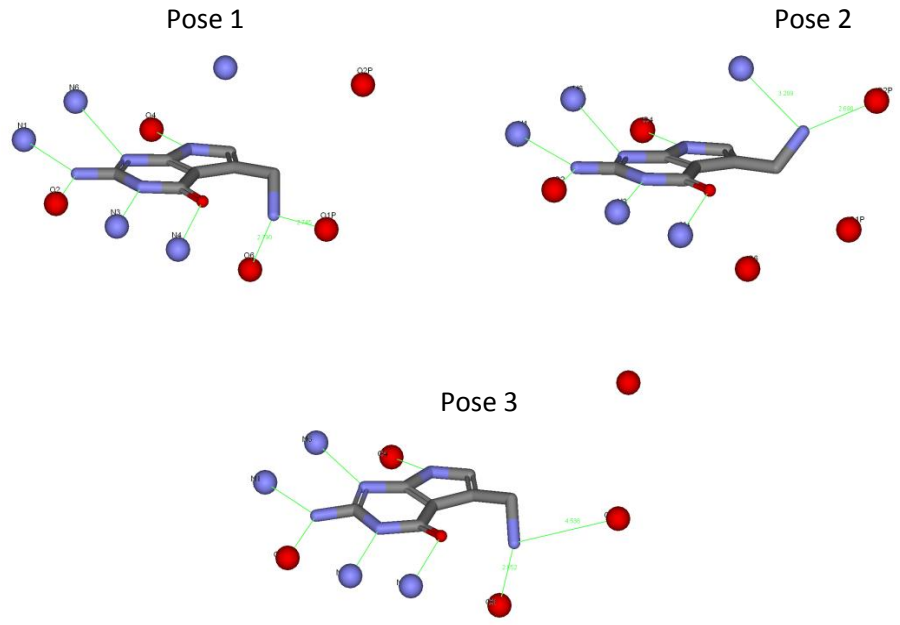

Figure 133: Diagram showing the three captured poses of the primary amino group of PreQ1, 50, and the surrounding atoms of the riboswitch involved in hydrogen bonding.

These conformations are particularly insightful as it can be seen in pose 2 that the primary amino group is able to rotate and point towards the less solvent exposed pocket. In fact, the amine points to this pocket for approximately 40% of the

trajectory. In achieving this, the nucleotide pocket around the primary amine must expand and contract (cf. pose 1 and pose 3) to allow the rotation to occur.

3.2.3 PreQ1 Conclusions

A number of general features of the aptamer domain of the PreQ1 riboswitch have been illuminated. It would seem that PreQ1 **50** does not afford any considerable stabilisation to the aptamer domain once it has formed; in fact the removal of the ligand appears to afford some stabilisation. This places the role of the ligand not on stabilisation of the overall complex but instead on facilitating the formation of the "closed" form of the aptamer domain. It is known that the control of genes by this riboswitch (from *Bacillus subtilus*) occurs during the transcription of the mRNA strand that contains the riboswitch sequence and hence once the aptamer domain has been transcribed, if the relevant ligand is sufficiently present it will bind and induce a discontinuation of transcription. This means that the rate of formation of the "closed" form of the aptamer domain is more important than the overall stability of the fold once it is formed; it need only exist for a short time for its effects to occur. It has been previously established that for this type II, class I PreQ1 riboswitch, kinetics are particularly important and this MD study supports this claim.[85, 86]

The cross-correlation matrices showed no unusual coupled motions within each trajectory; however, there was a noticeable difference between them. Although no definitive conclusion can be made from the change in correlation in the aforementioned region, it may be interesting to note that in the class I PreQ1 riboswitch, the Shine-Delgarno sequence begins around residue 33. It has been previously shown that this region is more solvent exposed in the "open" PreQ1 class I crystal structure compared with the "closed" crystal structure and that this more solvent exposed SD sequence would likely allow ribosome binding to occur. The MD analysis that has been carried out might tentatively suggest that although the class II PreQ1 riboswitch operates through kinetic control of transcription, the mechanism for translational control may exist given an appropriately located SD sequence. [85, 86]

There are also some answers to the initially posed questions. All of the hydrogen bonds that the pyrrolopyrimidine core of PreQ1 **50** makes with the riboswitch are very stable over time and thus likely to be of great importance. Pleasingly, the primary amino group does occupy the desired position, towards the less exposed pocket, for a significant portion of the trajectory. This finding would suggest that designing analogues of PreQ1 **50**, in which an extension is made into this pocket, could be a potential strategy to be explored.

This analysis has been very useful in terms of the compound screen that is to be carried out. Given the importance of the hydrogen bonding around the pyrollopyrimidine of PreQ1 **50**, structures which would eliminate the hydrogen bonds of the Watson-Crick face can be removed from the screen. This leaves a selection of compounds exemplified by those in figure 134. There remains a series of different substitution patterns on the pyrrole ring which will likely be sterically tolerated. The compounds containing the hydroxyl ethyl chain have been included in this set as it is possible that this substitution may point into the less solvent exposed pocket.

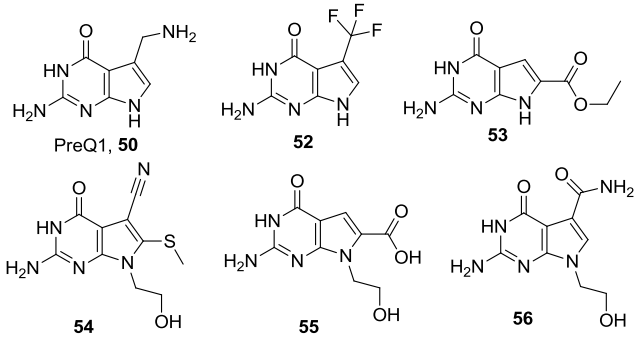

Figure 134: Examples of molecules of interest for PreQ1 riboswitch screen.

3.2.4 PreQ1 Future Work

Our existing compound library will be screened *in silico* to determine if we posses any molecular architectures that are capable of binding to this riboswitch. Design and synthesis of PreQ1 **50** analogues will follow taking note of the flexibility of the amino group and with a view to building the molecular architectures into the less solvent exposed pocket.

3.3 TPP Riboswitch

The most crucial feature in designing TPP **63** analogues will be identifying effective isosteres for the pyrophosphate moiety. To achieve this and to ultimately create a small library of compounds a docking study was carried out. After which synthesis of a chosen group of compounds, indicated by the docking study, was initiated. Using our established collaboration with the University of Bonn the resultant molecules were assessed for their potential to bind to the riboswitch and "turn off" gene expression.

3.3.1 TPP Docking Study

In order to investigate the *in silico* binding of a library of TPP **63** analogues it was first necessary to select the most appropriate docking software from those available to the Institution. Crystal structures of the TPP Riboswitch from *Arabidopsis thaliana* with three different ligands bound (TPP, **63**, and two analogues: PTPP, **193**, and OTPP, **194**, (fig. 135)) were obtained from the PDB (codes 3D2G, 3D2V and 3D2X respectively).[87]

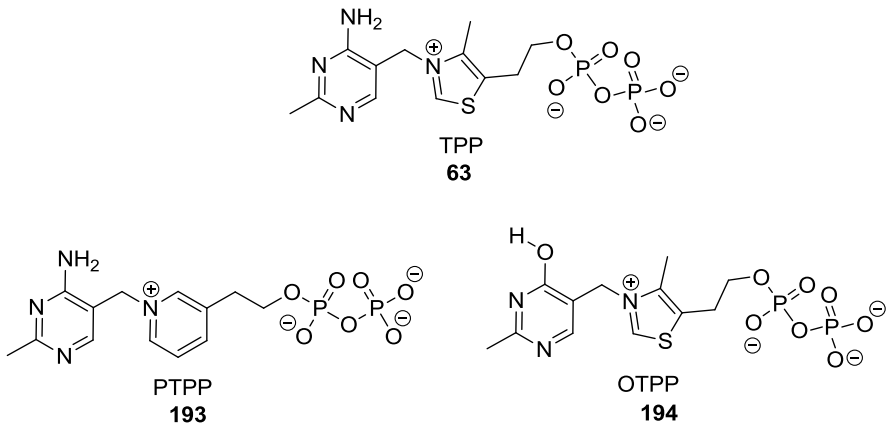

Figure 135: TPP and two analogues: PTPP and OTPP.

Using the Accelerys Suite, each ligand was removed and docked back into its respective riboswitch using both GOLD and CDocker. CDocker proved to be the superior docking algorithm for this application; in all three cases CDocker was found to have the best reproducibility of the native binding mode through assessment of the

route mean square deviation (RMSD) using the pose of the ligand in the crystal structure as a reference (table 14).

	GOLD RMSD	CDocker RMSD
TPP 63	2.54	0.97
PTPP 193	2.97	1.24
OTPP 194	3.81	2.01

Table 14: RMSDs of docked ligands.

Now that a suitable algorithm for docking was selected, the next task was the construction of a virtual library of compounds for docking. Five positions of variability were identified in the structure of TPP. These were positions 2 (B), 4 (A) and 6 (C) of the pyrimidine ring, the thiazole moiety (D), and the diphosphate (E) (fig. 136).

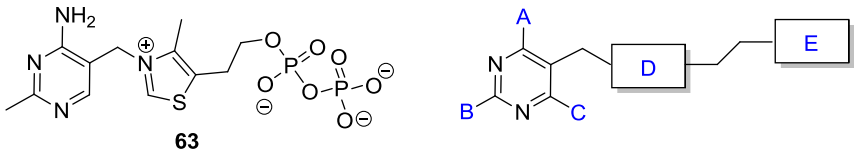

Figure 136: Positions of variability in TPP for libraary construction.

It was known from the literature and from examining available crystal structures that the amino group on position 4 of the pyrimidine ring is involved in hydrogen bonding to G28 of the riboswitch. The importance of this hydrogen bonding is exemplified by noting that in the crystal structure of the TPP analogue OTPP, **194**, in which the exocyclic amino is replaced by a carbonyl, the binding geometry is conserved. This implies that the less stable enol tautomer is found within the binding site of the riboswitch (fig. 137).[87] In response to this it was decided that our library of compounds for docking would only contain the amino or carbonyl (hydroxyl) groups at position 4' of the pyrimidine.

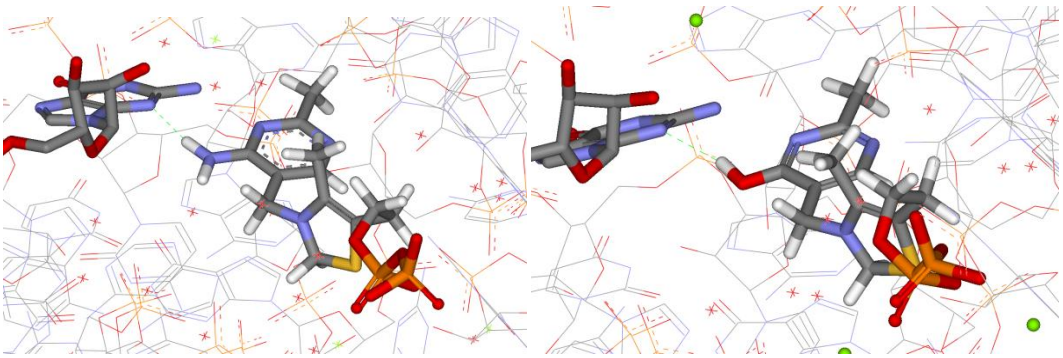

Figure 137: Left: Hydrogen bond between 6-amino of TPP and G28 of Riboswitch. Right: Hydrogen bond between 6-hydroxy of OTPP and G28 of Riboswitch.

TPP, **63**, has a methyl group in position 2 of the pyrimidine and examination of the crystal structure reveals a small space that may accommodate an expansion (fig. 138) and as such it was decided to include SMe and Et groups at this position in the library. It was also decided that an amino group in this position was worth investigating as it is similarly sized but capable of facilitating hydrogen bonding interactions.

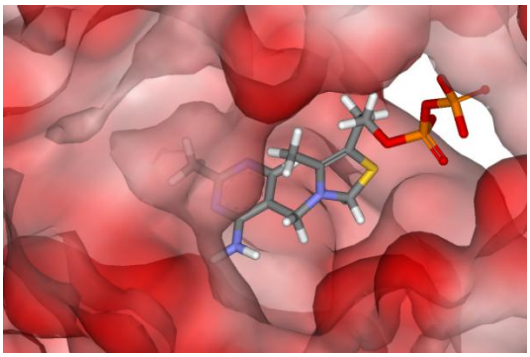

Figure 138: Pocket of Riboswitch available for expansion into.

The last position on the pyrimidine ring to be subject to variation was position 6' in which TPP **63** itself has hydrogen. Reference to the crystal structure again revealed a significant amount of space which could be utilised to increase bonding interactions (fig. 138 (above)) thus our library was to contain hydrogen, methyl, ethyl, amino and chlorine variations at this position.

The TPP analogue PTPP, **193**, differs only in the central linking moiety that connects the pyrimidine to the diphosphate and so continuing this notion, several

variations on the 4-methylthiazolium (D1) in TPP **63** were added to our library: 4-methylthiazolium (D1), thiazolium (D2), 2-methylpyridinium (D3) and pyridinium (D4) (fig. 140).

The final position of variability to introduce is the diphosphate moiety. For reasons of bioavailability it is necessary to design out this highly charged region whilst retaining its coordination capacity to the magnesium ions found in the riboswitch (fig. 139) in order to maintain both binding strength and activity of any resultant analogue. In light of this our library was to include three isosteres in addition to the diphosphate moiety (fig. 140).

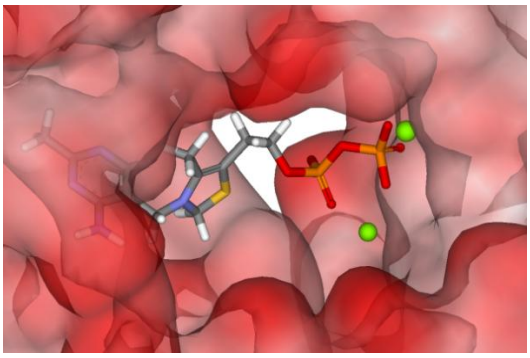

Figure 139: Location of MG ions in binding site.

A summary of the positions of variability and variations is shown in figure 61.

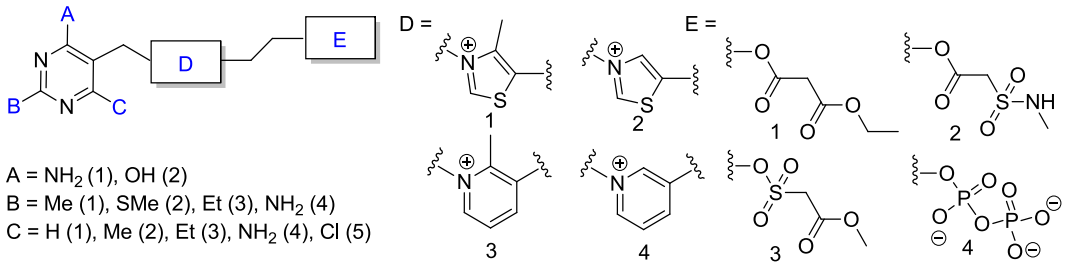

Figure 140: Summary of compound library.

This set of variations about the TPP scaffold results in 640 different molecules that were docked into the TPP riboswitch (PDB file: 3D2G) with tenfold repetition using the CDocker algorithm. In order to understand the scores generated

for each docked pose and to relate these to the variations within the set of molecules it was decided that linear regression would be carried out on the data using the positions of variability as factors and the output score from the docking as the response variate. The statistical program GenStat was used to carry out this analysis and the output is summarised in table 15.

Parameter	estimate	s.e.	t(16904)	t pr.
Constant	69.423	0.252	275.75	<.001
A 2	2.025	0.139	14.56	<.001
B 2	-0.942	0.171	-5.5	<.001
B 3	0.86	0.171	5.03	<.001
B 4	2.341	0.162	14.41	<.001
C 2	0.712	0.185	3.84	<.001
C 3	0.707	0.185	3.82	<.001
C 4	0.718	0.186	3.87	<.001
C 5	0.494	0.185	2.67	0.008
D 2	0.22	0.166	1.33	0.185
D 3	1.77	0.166	10.66	<.001
D 4	2.724	0.166	16.39	<.001
E 2	1.662	0.186	8.95	<.001
E 3	-3.148	0.185	-16.98	<.001
E 4	60.748	0.161	378.29	<.001

Table 15: Summary of GenStat output for linear regression on CDocker pose score based on the general compound structure in figure 137. The estimate gives the contribution of that parameter to the regression equation. S.e. refers to the standard error; t(16904) gives the t statistic; and t pr is the significance level of the estimate on that parameter.

Before attempting to rationalise these results it is important to realise that whilst the molecules have been docked in the TPP binding site, the poses obtained do not necessarily conform to that of TPP itself. This raises the question: "which molecules within the library best fit into the binding site of TPP?" and not the more pertinent question of "which molecules within the library best mimic the native binding mode of TPP?". Despite this, the data can still provide some relevant information. Firstly, and most obviously, the molecules with the diphosphate moiety (E4) have much higher scores than any other variation at this position. This may be to be expected as the multiple negative charges of the phosphates are particularly complementary to the positive charge of the magnesium ions to which they are bound. This perhaps highlights the difficulty that might be faced when trying to find

effective bio-isosteres for the diphosphate. It can also be seen that the data for variations investigated at position C suggest that there is enough space to accommodate groups other than hydrogen as none of the parameter estimates are negative.

In light of the ambiguity of this analysis, and in the hope of answering the second of the aforementioned questions, it was decided that the data generated from the docking study required further manipulation to yield significant insight into the binding of our TPP analogue library. The binding of TPP to its riboswitch can be thought of in a simplified way by the assumption that the central thiazolium moiety acts merely as a linker to the two regions primarily responsible for binding: the pyrimidine and the diphosphate. Literature precedent suggests this to be a valid assumption.[73] Thus if a TPP analogue that mimics the native binding mode is to be sought, then a sensible filter that could be applied to the data set, would be to remove any docked conformations that have significant positional deviation from the native binding mode at either of the two binding regions. With this in mind, a protocol was devised to reduce the vast number of docked conformations to those only of similar conformation to TPP. This protocol is detailed in figure 141.

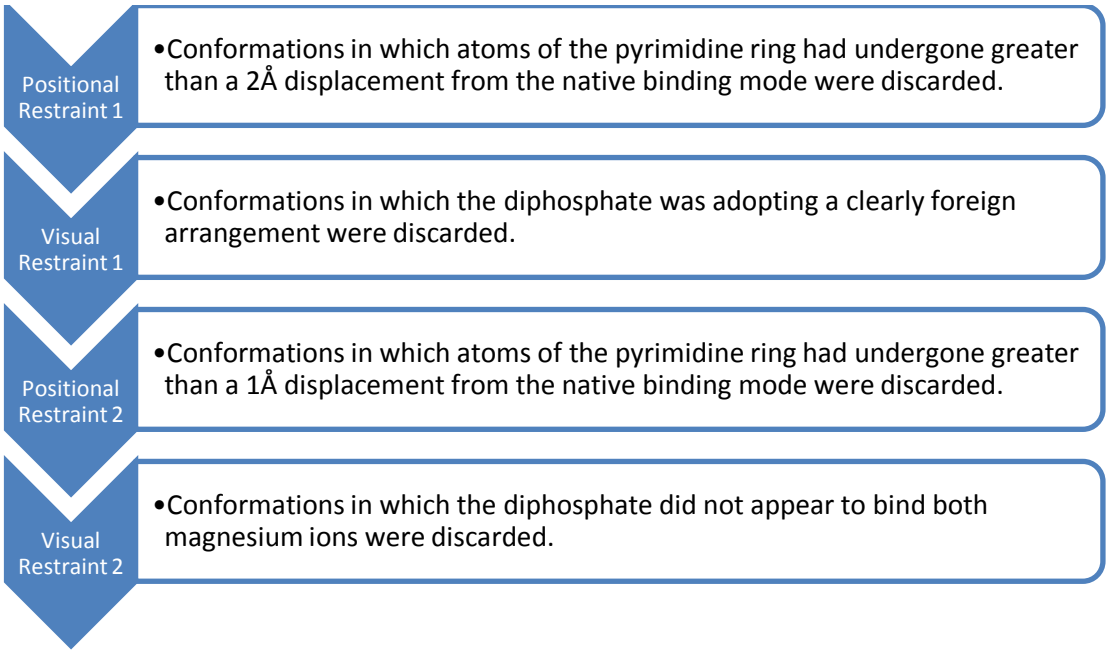

Figure 141: Protocol applied to data set to filter out non-native binding conformations.

The subsequently smaller data set was then subjected to the same linear regression as before to yield the results that are summarised in table 16.

Parameter	estimate	s.e.	t(140)	t pr.
Constant	81.47	2	40.73	<.001
A 2	3.36	1.01	3.32	0.001
B 2	-5.05	1.42	-3.55	<.001
B 3	-1.17	1.45	-0.81	0.422
B 4	-3.11	1.32	-2.36	0.02
C 2	2.32	1.65	1.41	0.162
C 3	4.3	1.55	2.77	0.006
C 4	1.51	1.42	1.06	0.291
C 5	-0.83	1.67	-0.5	0.618
D 2	1.31	1.47	0.89	0.374
D 3	1.45	1.5	0.96	0.339
D 4	2.64	1.39	1.9	0.06
E 2	-2.79	1.81	-1.54	0.126
E 3	-6.38	1.78	-3.59	<.001
E 4	52.43	1.57	33.49	<.001

Table 16: Summary of GenStat output for linear regression on CDocker pose score based on the general compound structure in figure 137. The estimate gives the contribution of that parameter to the regression equation. S.e. refers to the standard error; t(16904) gives the t statistic; and t pr is the significance level of the estimate on that parameter.

If only the most definite of conclusions are to be drawn from the data, thus considering only t pr values of 0.001 or less, then it can be seen that a high docking score is afforded by the 4-hydroxypyrimidine over the 4-aminopyrimidine as the A2 parameter is shown to have a positive value. It can also be seen, as expected and rationalised earlier, that the diphosphate (E4) has a profound effect in increasing the docking score. At the same position, the sulfonate ester (E3) is seen to decrease the docking score.

During the data set refinement protocol another variate was generated: namely the FitValue. This is a measure of similarity in the atoms of the pyrimidine ring in the TPP analogue to TPP itself; the higher the score the more similar the docked pose of the pyrimidine. Since this variate was available, a further linear regression was carried out and the results of this are summarised in table 17.

Parameter	estimate	s.e.	t(140)	t pr.
Constant	0.8697	0.0633	13.75	<.001
A 2	0.0584	0.032	1.83	0.07
B 2	-0.4052	0.045	-9	<.001
B 3	-0.3481	0.0459	-7.58	<.001
B 4	-0.0979	0.0417	-2.35	0.02
C 2	-0.0114	0.0521	-0.22	0.827
C 3	-0.1851	0.049	-3.78	<.001
C 4	0.0439	0.045	0.97	0.331
C 5	-0.08	0.0528	-1.52	0.132
D 2	0.0553	0.0464	1.19	0.236
D 3	-0.0228	0.0476	-0.48	0.632
D 4	0.0488	0.044	1.11	0.27
E 2	0.0308	0.0574	0.54	0.592
E 3	-0.0455	0.0563	-0.81	0.42
E 4	-0.1118	0.0495	-2.26	0.026

Table 17: Summary of GenStat output for linear regression on FitValue. The FitValue is a parameter that was generated from the docking study which measures the similarity of the pose to that of TPP.

If we make the same restriction on t pr value as per the previous analysis then we can see that both thiomethyl (B2) and ethyl groups (B3) in position B cause a shift in the position of the pyrimidine ring and, although to a lesser extent, so too does an ethyl (C3) in position C.

In summarising the statistical evaluation a few significant findings are brought to light. Position B of the pyrimidine ring is unlikely able to accommodate groups larger than a methyl as determined by a combination of a lower docking score and positional shifting of the pyrimidine ring. Of position C, a noteworthy result is the positional shifting of the pyrimidine when an ethyl (C3) is considered; larger groups are likely to have the same result. Finally, the sulfonyl ester (E3) appears to be the poorest choice as a diphosphate bio-isostere due to its negative contribution to the docking score.

It must be stated that the variations at position D yielded little information; however, perhaps this serves to illustrate the low level of importance this region of TPP plays in its binding.

Athough not highlighted by the statistical evaluation, the importance of amino groups around the pyrimidine ring is clearly demonstrated through several of the docked molecules showing extra hydrogen bonding to the riboswitch when subjected to a visual examination (fig. 142). As the statistical evaluation showed no negative outcomes in amino substituted pyrimidines, then it would be wise to take advantage of these potential hydrogen bonding opportunities.

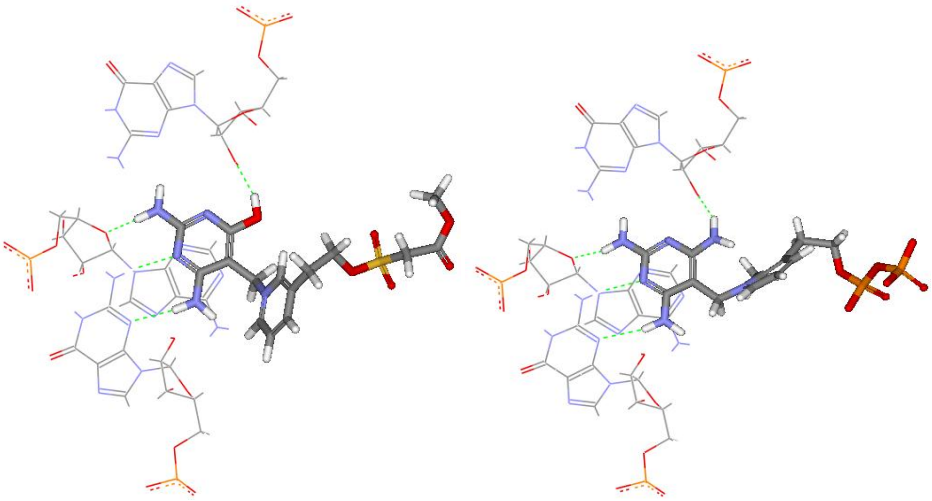

Figure 142: Two examples of amino substituted pyrimidine TPP analogues showing extra hydrogen bonds.

The above analysis has successfully directed the reduction in size of the molecular space to be explored through synthetic methods. Figure 143 summarises the molecules highlighted from this docking study.

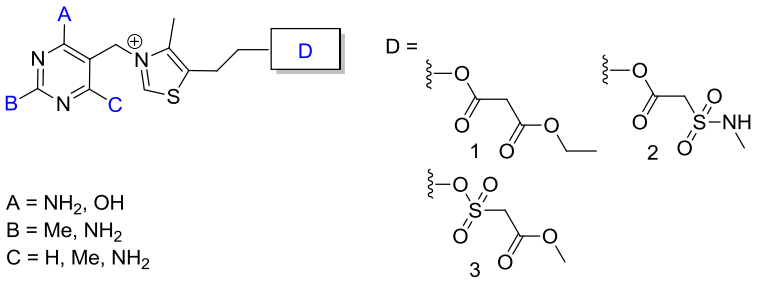

Figure 143: Molecules of Synthetic Interest.

3.3.2 Synthesis of TPP Analogues

It was decided to restrict the synthesis of TPP analogues to only one pyrimidine ring variation, that of TPP itself, for the initial synthetic programme to allow the synthetic viability to be explored. Thus the following diagram indicates the molecules that were to be synthesised (fig. 144). It should be noted that molecule **198** did not appear in the previous docking study but was added here as the starting materials for this were already available in the lab and 1,2-dicarbonyl compounds are known to chelate to metal ions in integrase inhibitors.[88]

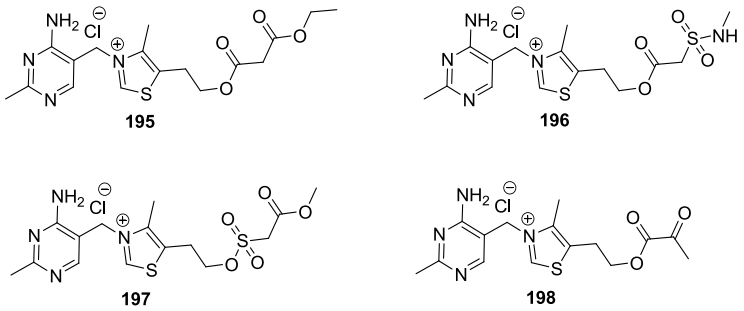

Figure 144: Target molecules.

The retrosynthetic analysis of these compounds, **195-198**, (scheme 25) begins with the formation of the thiazolium salt **199** via an alkylation of the functionalised thiazole **201** by the chloromethylpyrimidine **200**. This pyrimidine moiety should be easily obtained through simple functional group conversions: the chloro **200** can be obtained from the alcohol **204** by reaction with thionyl chloride; this can be obtained from the carboxylic acid **205** by reduction using lithium aluminium hydride; which can in turn be obtained from the nitrile **206** by oxidation using aqueous potassium hydroxide. The nitrile functionalised pyrimidine can be formed by reaction between acetamidine hydrochloride **208** and ethoxymethylene malonitrile **207**. In the other branch of this synthesis, the general thiazole ester **201** can be obtained via a coupling reaction between the alcohol **202** and appropriate acid **203**.

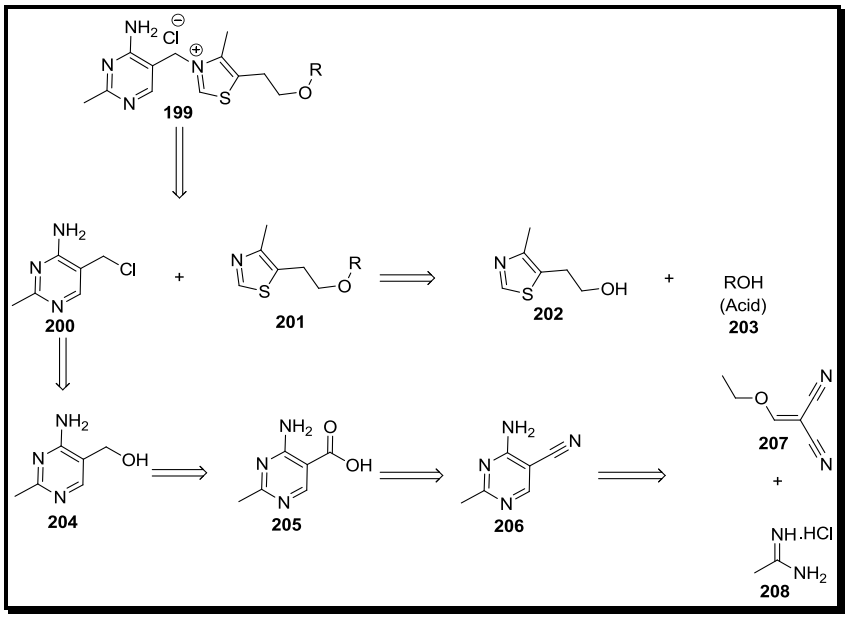

Scheme 25: Retrosynthetic analysis of target molecules.

Let us first consider the branch of the synthesis pertaining to the formation of the functionalised pyrimidine **200** (scheme 20). The first step was to construct the pyrimidine ring and this was achieved by the reaction of acetamidine hydrochloride **208** with sodium ethoxide in dry ethanol and ethoxymethylene malonitrile **208**. This afforded the desired nitrile pyrimidine **206** in 42 % yield. From here, **206** was hydrolysed to the carboxylic acid **205** via reaction with 10% potassium hydroxide solution to furnish the required material in 65 % yield. This was in turn reduced to the alcohol **204** using lithium aluminium hydride giving a yield of 89 %. The final step involved the conversion of the alcohol **204** into the chloro-functionalised pyrimidine **200** using neat thionyl chloride to give a yield of 86 %.

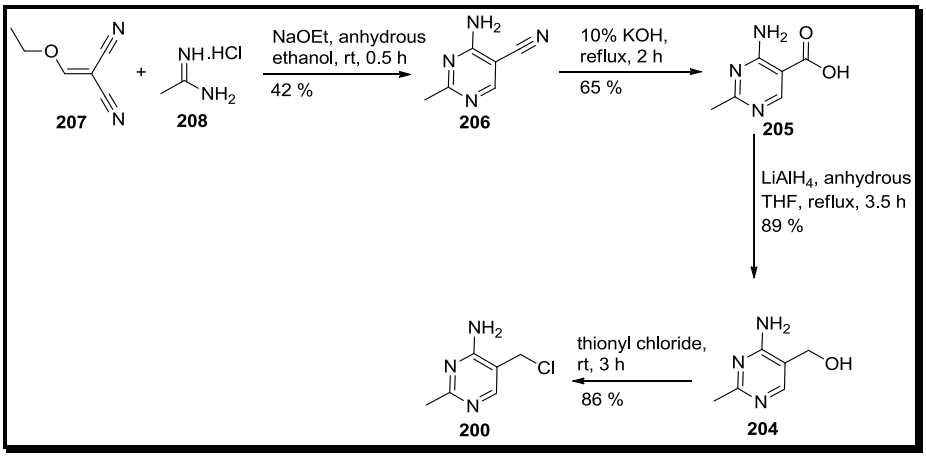

Scheme 26

In order to form the thiazole ester that is required to form compound **195**, monoethyl malonate **209** was converted into its acid chloride **211** by refluxing in neat thionyl chloride. The so formed acid chloride **211** was then coupled to 2-(4-methylthiazol-5-yl)ethanol **202** in anhydrous DCM and using NMM to quench the acid that was generated. After purification by column chromatography the desired product **213** was obtained in a low yield of 13 % (scheme 27). In order to form the thiazole ester **214** that is required to form the α-ketoester **198**, the same procedure was used as above with the exception that the acid used was pyruvic acid, **210**. This reaction produced a much lower yield of 3 % (scheme 27). Despite the low yield, enough of the material was obtained for future reactions.

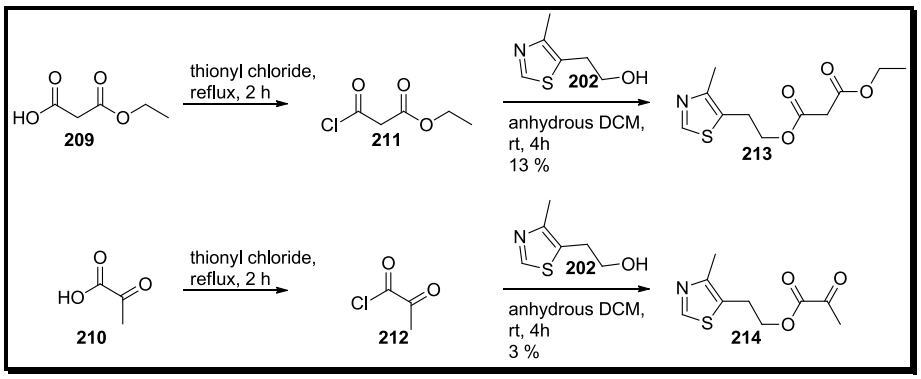

Scheme 27

The final step towards compound **195** is the *N*-alkylation of the thiazole **213** with the chloromethyl pyrimidine **200** (scheme 28). Both were dissolved in

anhydrous THF, with NMM acting as base, and heated to 70 ^{o}C with stirring for 8 hours. Neither NMR nor mass spectrometry could identify the desired material. This reaction was repeated using different conditions, in DCM or THF at 30 – 70 ^{o}C but unfortunately, none proved successful and a more thorough investigation into reaction conditions is required.

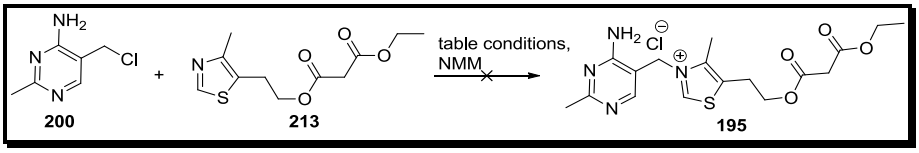

Scheme 28

An imminent visit from our collaborators in Bonn, who were to be carrying out the biological evaluation of the compounds obtained from this project, further stimulated the desire for testable compounds and to this end a new synthesis was developed which should furnish a number of compounds in a short space of time. The docking study had confirmed that the presence of the thiazole ring within the structure of the final compounds was not crucial since the thiazole does not evidently participate in any significant interactions within the binding site of the riboswitch. This, coupled with the fact that the *N*-alkylation of the thiazole was problematic, prompted a design change: the thiazole would be replaced with a more synthetically appealing triazole.

3.3.3 Synthesis of Panel 1 TPP Modulators

The new compounds that were synthesised via the triazole substitution are shown below (fig. 145). These compounds are simple variations of the structure of thiamine and at this stage did contain the pyrophosphate analogues. These were not included at this stage as it was thought prudent to assess some of the more fundamental biology of the system when using triazole analogues before moving to those that also contain groups that can interact with the magnesium ions in the riboswitch.

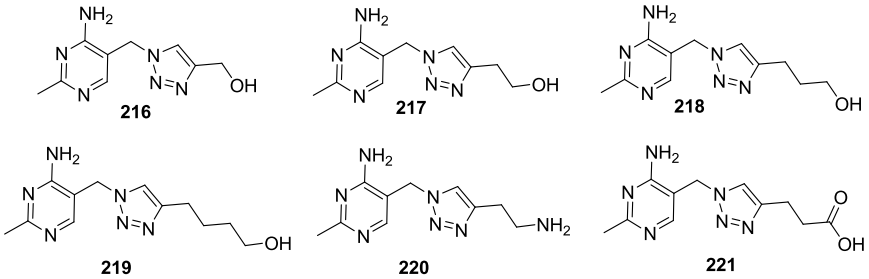

Figure 145: Proposed triazole structures.

Ironically, the first step in this synthesis (scheme 29) begins with the displacement of the thiazole moiety from thiamine **63** by reaction with sodium azide in water at 65 ^{o}C for 5 hours. This afforded the azide **222** in 63 % yield. "Click" chemistry was then used to form the triazole containing compounds. This involved a room temperature reaction of the azide **222** with respective alkyne in the presence of sodium ascorbate and copper sulfate in a tertiary butanol and water solvent system which afforded the triazole compounds **216-219** in 70-82 % yield.

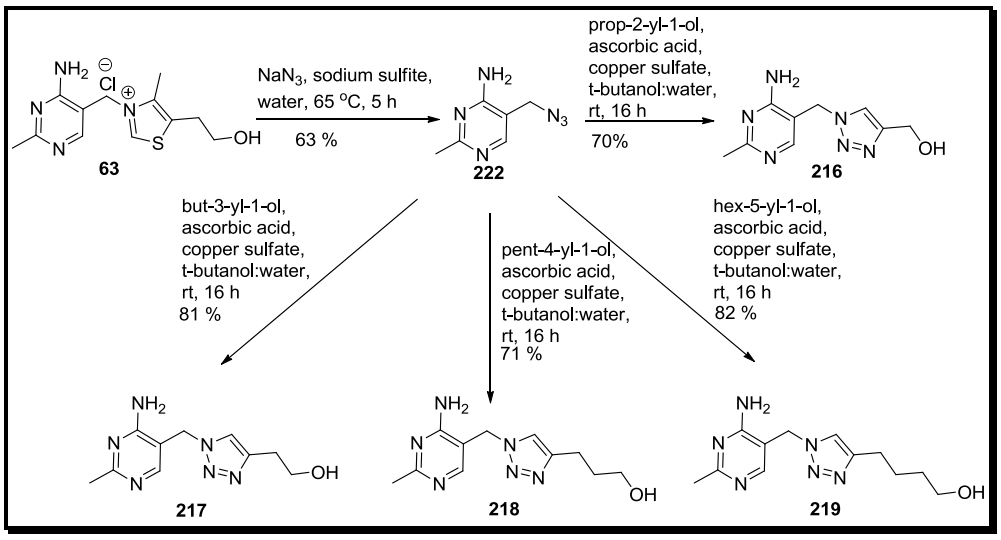

Scheme 29

The carboxylic acid containing analogue, **221**, was synthesised in a similar manner and purified by HPLC to give the desired material in a 39 % yield (scheme 30).

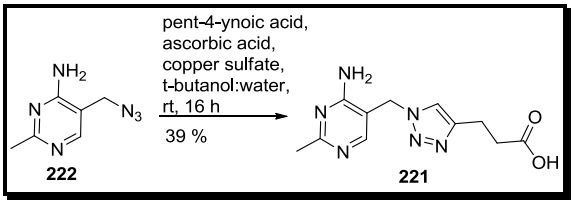

Scheme 30

In order to produce the amine analogue of compound **217**, the required amino alkyne had to be prepared. This was achieved by converting but-3-yl-1-ol, **223**, into its mesylate, **224**, by reaction with mesyl chloride, followed by a one-pot conversion to the amine, **225**, through the azide, by nucleophilic substitution using sodium azide and then a Staudinger reaction. This was then used in a "click" reaction, as before, using the azide functionalised pyrimidine **222** to give the required amino analogue **220** (scheme 31).

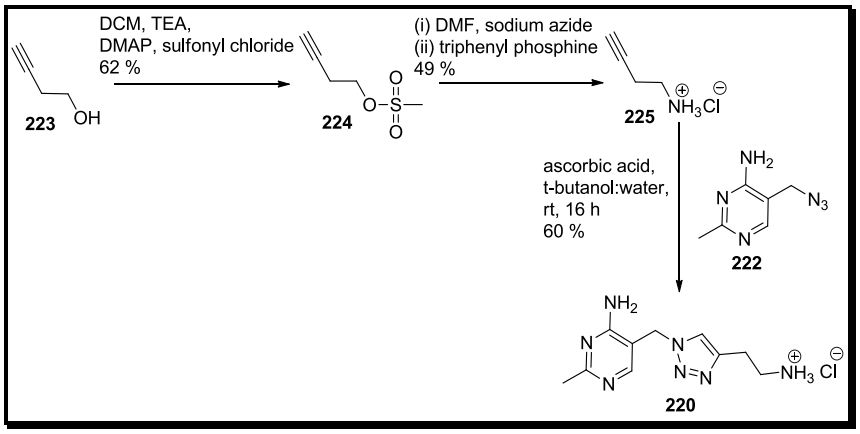

Scheme 31

3.3.4 Biological Evaluation Of Panel 1 TPP Modulators

Our collaborators at the University of Bonn have developed a β-galactosidase reporter gene assay to assess the activity of our compounds on the TPP riboswitch of *E. coli*. This reporter gene assay involves a pRS414.2 vector construct in which the *thi*-box riboswitch thiM from *E. coli* is cloned into the 5´-UTR of β-galactosidase. This plasmid was transformed into two *E. coli* strains, namely MG1566 and DH5αZ1. The β-galactosidase activity was monitored in the presence and absence of

thiamine **63** (T in figures), pyrithiamine **64** (PT in figures) or the newly synthesized thiazole analogues (figure 146).

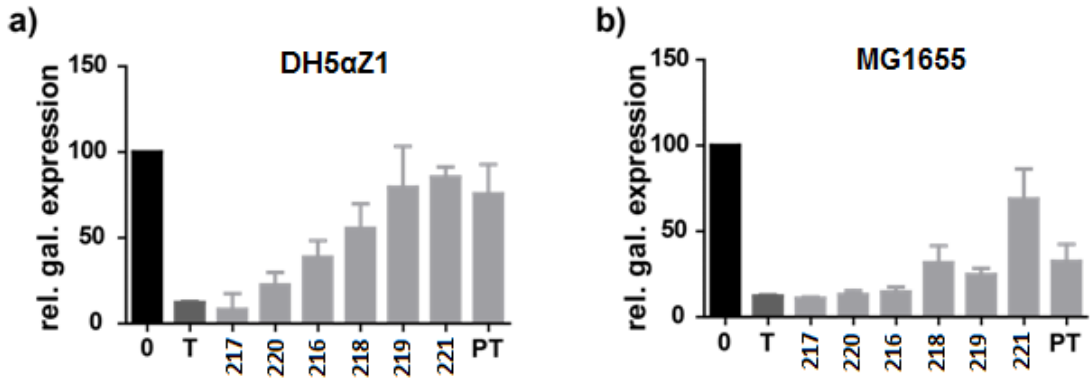

Figure 146: Relative β-galactosidase expression in the presence of either thiamine (T) [20µM] or compounds 216-221 and pyrithiamine (PT) [500µM] in *E. coli* DH5αZ1 pRS414.2 thiM wt (a), *E. coli* MG1655 pRS414.2 thiM wt (b).

It can be seen that pyrithiamine **64** (PT in figure) was only capable of ß-galactosidase repression in strain MG1655, but not in DH5αZ1 (figure 146). Figure 146a displays reporter gene activity in DH5αZ1 bacteria for thiamine **63** (T in figure), pyrithiamine **64** (PT in figure) or the synthesized thiamine analogues. These data indicate that **217** was able to repress reporter gene activity. **217**, just like PT, is likely to be phosphorylated *in vivo* and thus able to interact with the TPP riboswitch, and therefore induce the necessary conformational changes in the RNA to repress gene expression. This argument is strengthened by the observation that shortening (**216**) or elongating the alkyl side chain (**218** and **219**) resulted in a reduction of activity. This may be due to reduced uptake or phosphorylation of these compounds *in vivo*. Interestingly, the amine analogue of **217**, **220,** also repressed reporter gene activity.

Strong differences in the gene regulation efficiency of the thiamine analogues were observed the DH5αZ1 strain and the MG1655 strain. In contrast to the DH5αZ1 strain in which the compounds showed a clear structure-activity relationship (figure 146a) the MG1655 strain reveal that most compounds were active with a slight decrease of activity in elongation of the alkyl-side chain (Figure 146b).

The replacement of the hydroxyl group of **217** with a carboxylic acid (**221**) has reduced gene repression activity of the compared to **217** in the DH5αZ1 strain and also in the MG1655 strain.

In order to evaluate whether the observed effects on β-galactosidase expression were solely due to the riboswitch activation, our collaborators used a TPP riboswitch mutant (thiM-Mu) that had a base substitution in the aptamer domain disrupting the P2 helix. This prevented the riboswitch controlling β-galactosidase expression (scheme 147). Figure 148a and b show that thiamine **63** and the new thiamine analogues had little effect in both bacterial strains when the mutant TPP aptamer domain has been used. This clearly indicates that the observed repression of gene expression is due to interaction with the TPP riboswitch.

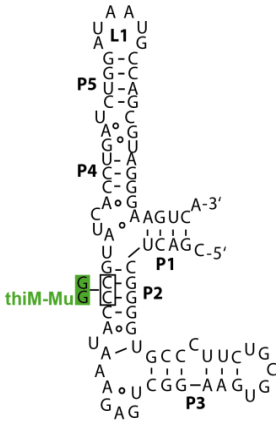

Figure 147: Secondary structure of the aptamer domain of the thiM riboswitch and the non-binding thiM mutant riboswitch (thiM-Mu). Mutations in P2 are shown in green.

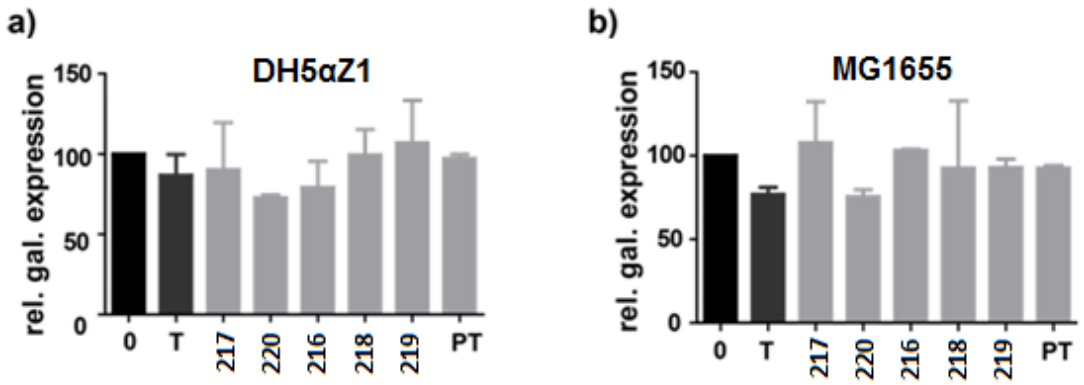

Figure 148: Relative β-galactosidase expression in the presence of either thiamine [20µM] or compounds 216-220 and pyrithiamine (PT) [500µM] in *E. coli* DH5αZ1' pRS414.2 thiM-Mu (a) and *E. coli* MG1655 pRS414.2 thiM-Mu (b).

These compounds have now been validated as TPP riboswitch activators *in vivo* and their impact on bacterial growth was next investigated. These data are presented in figure 149 and show that **217** inhibited bacterial growth in a concentration dependent manner (figure 149a). The shorter alkyl side chain variant, **216**, did not display this property (figure 149b). In contrast, lengthening of the alkyl side chain (**218** and **219**) appears to be more accomodating, as **219** also showed bacterial growth inhibition; however, its activity in repression of gene expression was less prominent (figure 149c and d). The amine-compound **220** slightly induced bacterial growth rather than inhibiting it (figure 149e).

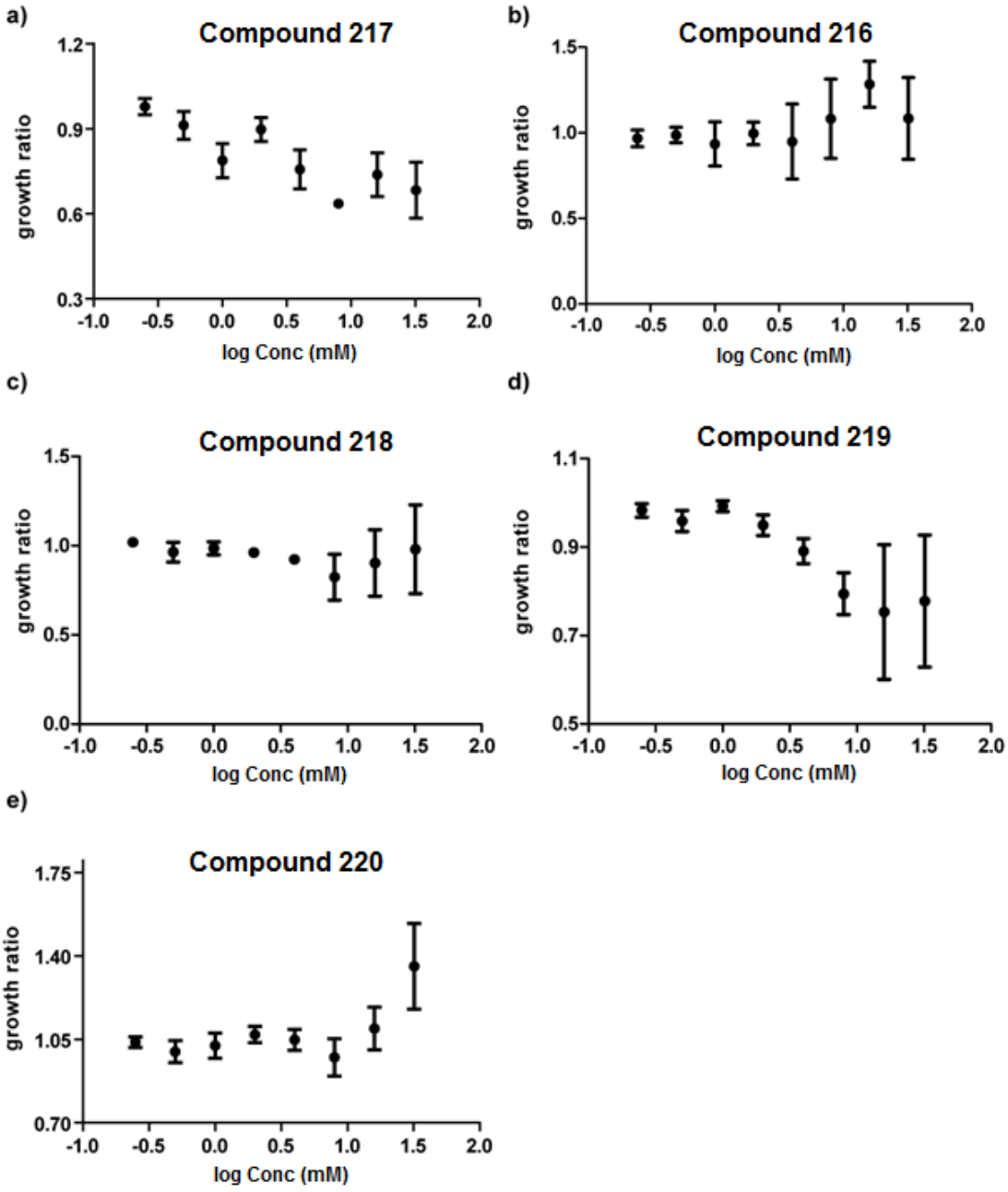

Figure 149: Bacterial growth of DH5αZ' in M9 minimal medium in the presence of compound 216-220 [0.25 mM-32 mM] (a-e). Graphs show bacterial growth at t = 495 min in the presence of compound in relation to same concentration of thiamine.

The data that has been obtained on this set of 6 thiamine analogues is both significant and comprehensive and indicates that TPP riboswitches are interesting and attractive target structures for developing antibacterial compounds. Replacing the thiazole heterocycle of thiamine with 1,2,3-triazole is a valuable strategy to

generate thiamine analogues that interact with the TPP riboswitch and, thus, induce repression of gene expression *in vivo*. It is important to note that their activity can differ significantly within bacterial strains and from *in vitro* experiments. This demonstrates that compounds acting on riboswitches have to be carefully investigated *in vivo* and that *in vitro* data alone may not be sufficient to predict behaviour. Since compound **217** is active *in vivo* and reveals superior activity when compared to pyrithiamine it represents a very promising starting point for developing novel antibacterial compounds that target TPP riboswitches.

3.3.5 Synthesis Of Panel 2 TPP Modulators

Given that the above simple thiamine analogues showed some very interesting biological properties attention was now turned to thiamine pyrophosphate analogues. With the aminoethyl compound **220** available in sufficient quantity it was now possible to introduce potential magnesium ion binding moieties in order to create a small library of compounds for biological evaluation. The intentions here were to use readily available and appropriate materials, in terms of knowledge of the binding site, whilst exploring the types of synthetic chemistry that compound **220** could be utilised in.

Methanesulfonyl chloride and *p*-toluenesulfonyl chloride were each reacted with **102**, after forming the free base, to generate the sulfonamides **226** and **227** (scheme 32).

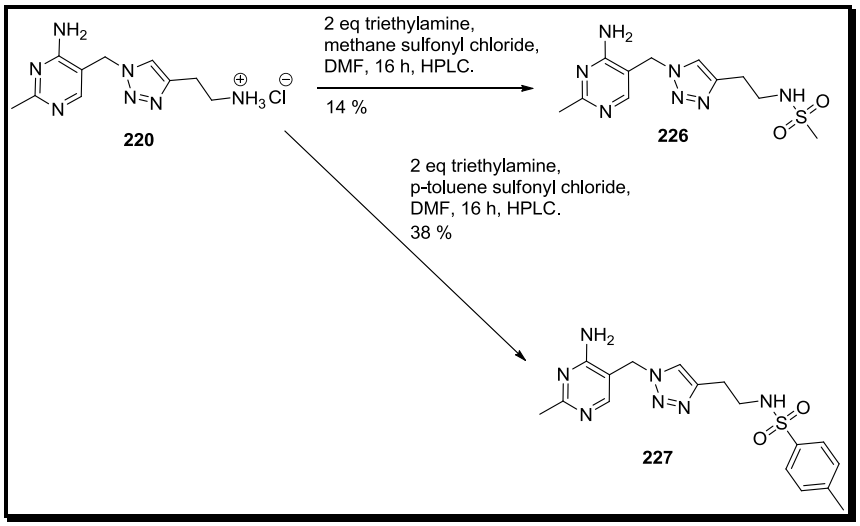

Scheme 32

DCC mediated amide couplings were employed on the free base of **220** using monoethyl malonate, pyruvic acid and salicylic acid forming compounds **228**, **229** and **230**, respectively (Scheme 25).

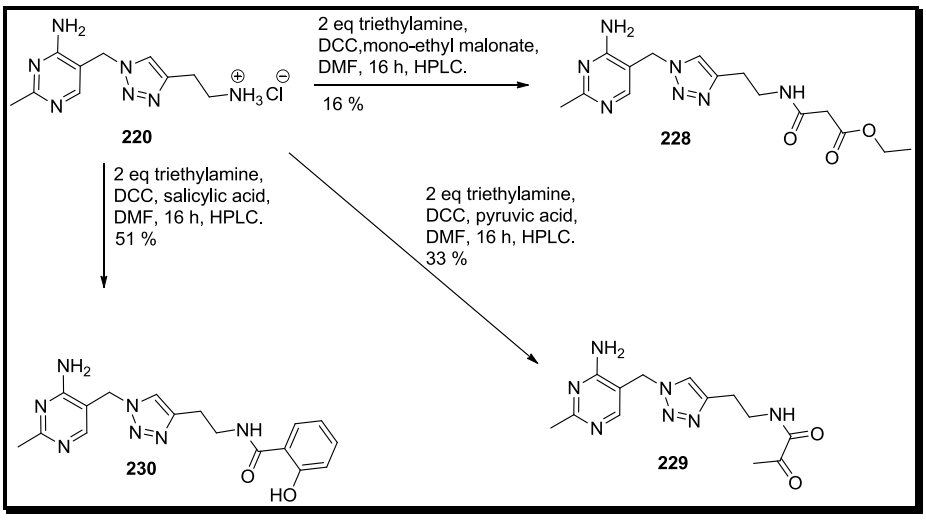

Scheme 33

The free base of compound **220** was also reacted with Michael acceptors **231** and **233** in a conjugate addition to yield the secondary amines **232** and **234**, respectively (scheme 34).

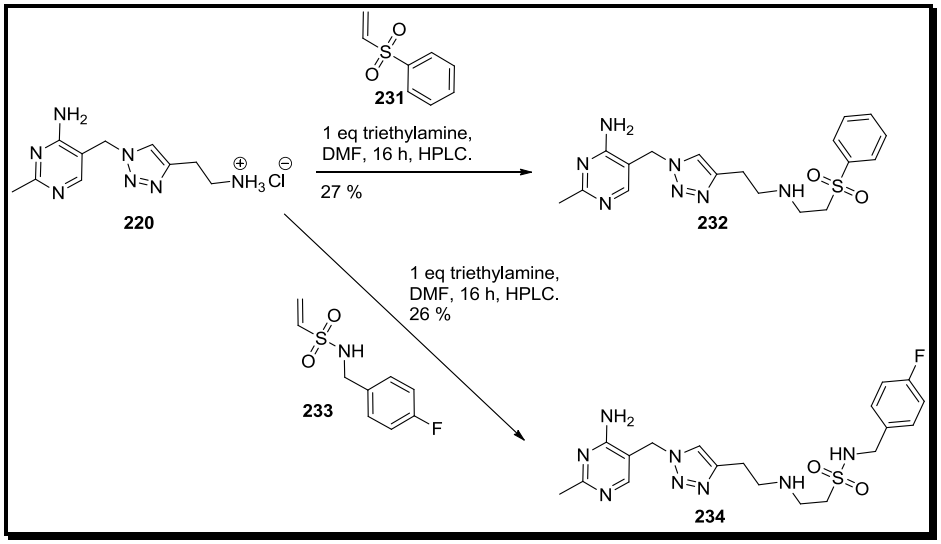

Scheme 34

The amine **220** was also reacted with **235** in an addition-elimination reaction to yield the nitroalkene **236** (scheme 35).

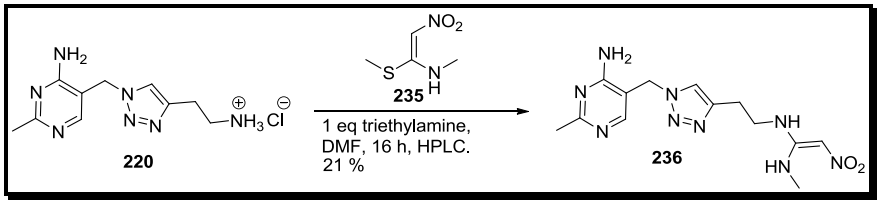

Scheme 35

Since the alkyne mesylate, **224**, was available it was reacted with the azide-functionalised pyrimide, **222**, in a similar "click" reaction as before to generate another analogue of interest **237** (scheme 36).

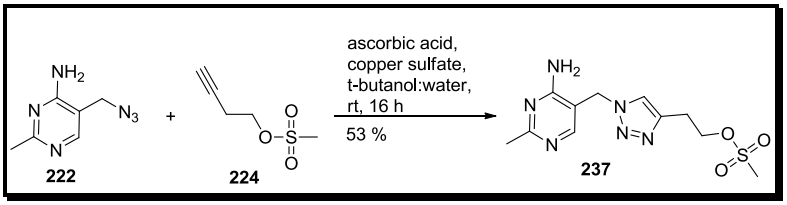

Scheme 36

The pyrimidyl azide **222** was also reacted with a precursor from our compound library in another "click" reaction. This produced compound **239**, and this

was hydrolysed with NaOH solution at reflux, to generate the 4-aminobenzolylglutamate analogue **240** (scheme 37).

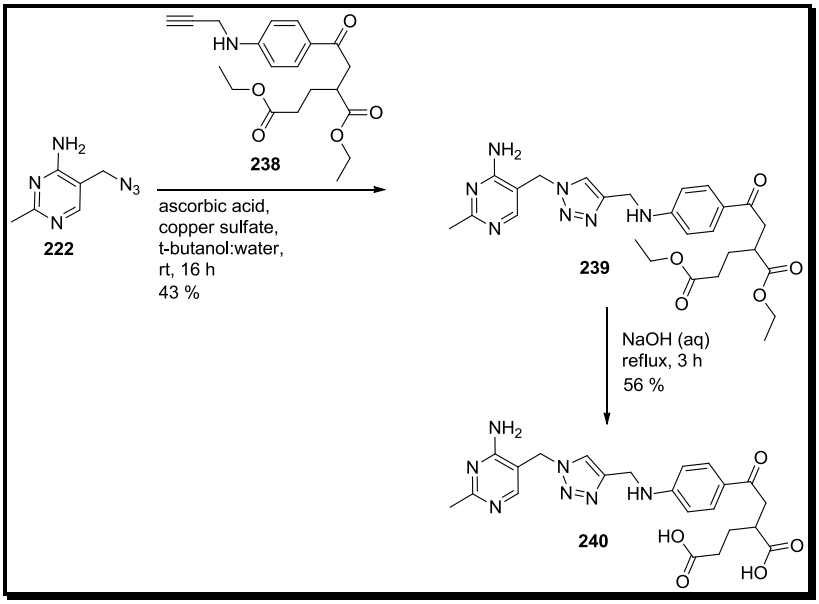

Scheme 37

A final "click" reaction with compound **222**, using a phosphate and ester containing alkyne fragment led to the production of compound **242**. The ester functionality of this compound was hydrolysed to the acid using NaOH solution at reflux, to obtain compound **243** (scheme 38).

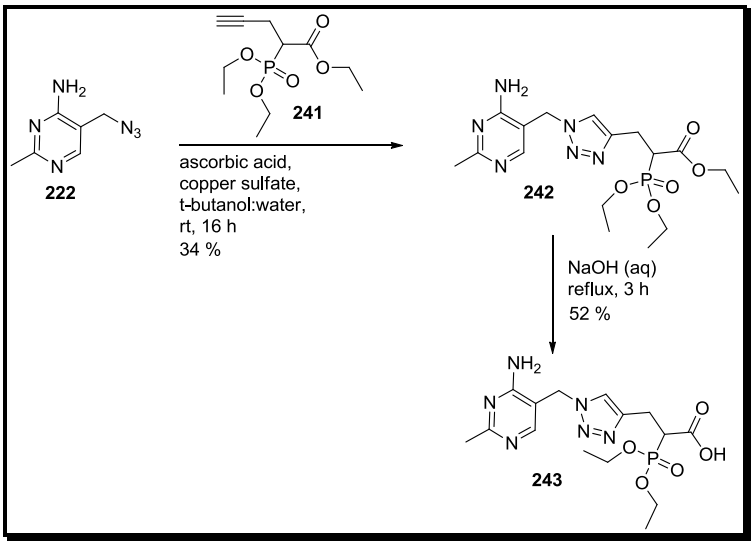

Scheme 38

In order to generate an example that did not contain the triazole moiety, compound **222** was reduced to amine **244** and then reacted with the trimethoxy benzene containing compound **245** in an HBTU-mediated coupling (scheme 39).

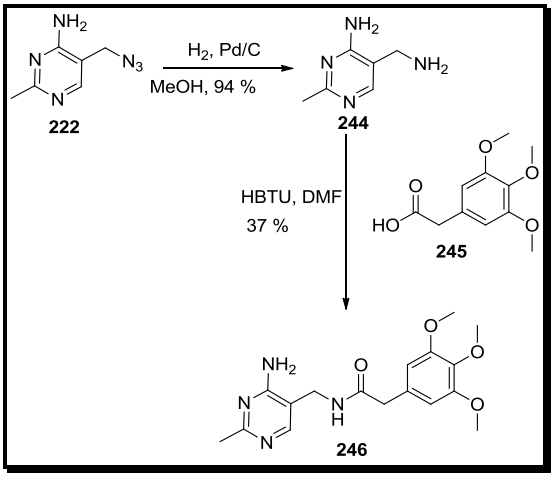

Scheme 39

3.3.6 Biological Evaluation Of Panel 2 TPP Modulators

This diverse set of thiamine analogues was subjected to the same set of β-galactosidase reporter gene assays to assess their activity against both the DH5αZ1 E.coli strain and the MG1655 strain (fig. 150 – 153).

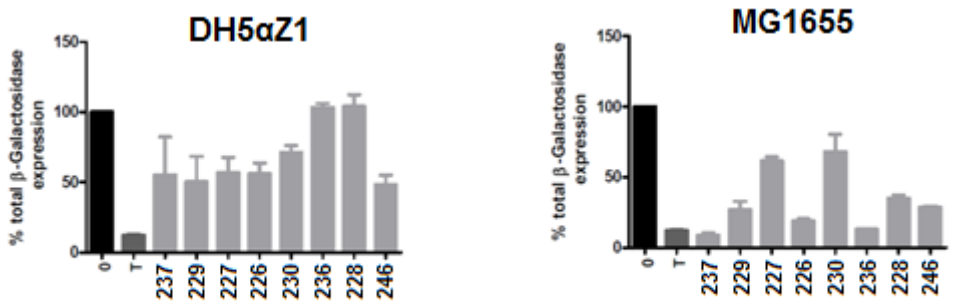

Figure 150: Relative β-galactosidase expression in the presence of either thiamine [20μM] or compounds [500μM] in *E. coli* DH5αZ' pRS414.2 thiM-Mu (a) and *E. coli* MG1655 pRS414.2 thiM-Mu (b).

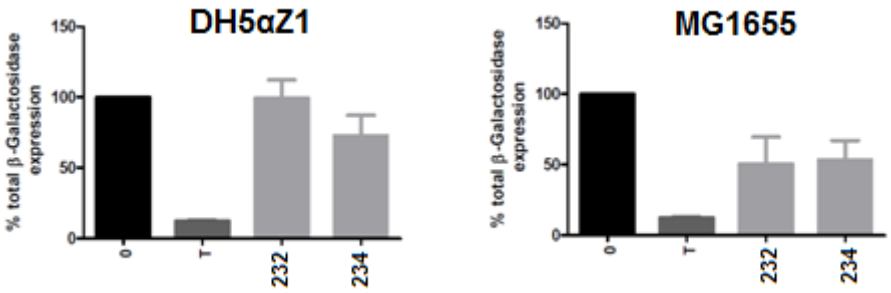

Figure 151: Relative β-galactosidase expression in the presence of either thiamine [20µM] or compounds 232 and 234 [500µM] in *E. coli* DH5αZ' pRS414.2 thiM-Mu (a) and *E. coli* MG1655 pRS414.2 thiM-Mu (b).

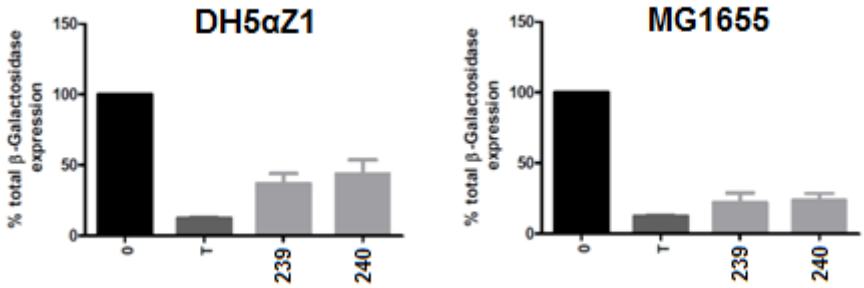

Figure 152: Relative β-galactosidase expression in the presence of either thiamine [20µM] or compounds 239 and 240 [500µM] in *E. coli* DH5αZ' pRS414.2 thiM-Mu (a) and *E. coli* MG1655 pRS414.2 thiM-Mu (b).

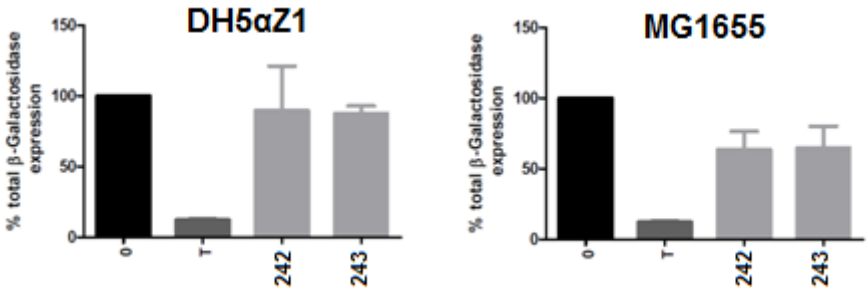

Figure 153: Relative β-galactosidase expression in the presence of either thiamine [20µM] or compounds 242 and 243 [500µM] in *E. coli* DH5αZ' pRS414.2 thiM-Mu (a) and *E. coli* MG1655 pRS414.2 thiM-Mu (b).

It can be seen that the sulfonamides, **226** and **227**, were both fairly inactive against the DH5αZ1 strain; however, **226** showed more significant activity in the MG1655 strain (fig. 150). The presence of the phenyl ring in **227** may indicate a lower tolerance to larger substiuents.

The malonate amide, **228**, showed negligible activity in the DH5αZ1 strain but the MG1655 strain showed a significant suppression in of β-galactosidase

expression. The pyruvate amide, **229**, displayed a significant activity in both strains although it is more pronounced in the MG1655 strain. The salicylate amide analogue **230** demonstrates some activity in both strains (fig. 150).

The nitroalkene **236** showed some interesting variation between the two strains. For the DH5αZ' strain this compound is one of the most inactive to be tested; however, it is one of the most active for the MG1655 strain (fig. 150).

The methyl sulfonate ester **237**, showed similar activity to its amide analogue. It showed appreciable activity in the DH5αZ1 strain and is one of the most active in the MG1655 strain, more so than the amide analogue **226** (fig. 150).

Compound **246**, the trimethoxy benzene derivative, had significant ability to suppress β-galactosidase expression in both strains. This compound was more active against the MG1655 strain (fig.150).

Compound **239**, and its hydrolysed analogue **240**, both demonstrated activity to both stains of E. coli. The activity against the MG1655 strain was appreciably high for both these compounds (fig.152).

The compounds obtained from the Michael addition reactions, **232** and **234**, both displayed a similar activity profile. They displayed little activity against the DH5αZ1 strain; however, they were significantly active against the MG1655 strain (fig. 151).

Both phosphonates, **242** and **243**, demonstrated little activity against the DH5αZ1 strain with both showing more significant activity against the MG1655 strain (fig. 153).

3.3.7 TPP Conclusion

Many important points can be deduced from the above data set and subsequent analysis. It has been demonstrated that a number of triazole containing thiamine analogues, utilising different moieties in place of the hydroxyethyl, can display significant suppression of β-galactosidase expression. It is significant that

many of these compounds are more active than pyrithiamine itself. As concluded previously, there can be significant differences between the activities against the two tested strains with the MG1655 strain displaying greater activities than the DH5αZ1 strain. One compound from this set did not contain the triazole moiety, compound **246**. This compound displayed appreciable activity against both strains, which is significant as it demonstrates further that the thiazole of thiamine can be replaced by a simple aliphatic chain, a fact that could prove significant in the long term with respect to drug discovery.

3.3.8 TPP Further Work

The utility of the TPP riboswitch as a novel target for antibiotic design has been confirmed. From here a larger and more diverse set of structures will be synthesised in order to explore both the interesting chemical biology and to move towards more drug like compounds. Given that the thiazole replacement strategy has afforded a number of active compounds containing a triazole ring it is intended that a variety of other replacements will be synthesised to explore the tolerance of this region.

4 Experimental

4.1 Instrumental

Reagents and Solvents: Used as supplied from Aldrich unless dry DCM or dry THF. These were provided by standard operating procedures for InnovativeTechnology Solvent Purification System.

Solvent Removal: This was carried out by evaporation using a rotary evaporator at reduced pressure (*ca* 20 mmHg) unless otherwise stated.

Thin Layer Chromatography: TLC was carried out using pre-coated silica plates (Alugram® Sil G/UV_{254}). Visualisation of TLC plates was achieved by UV (254 nm).

Melting Point: Reichert hot stage melting point apparatus and are uncorrected.

NMR: Bruker Spectrospin 400 MHz or 500 MHz operating frequency for ^{1}H NMR nuclei. δ quoted in ppm and measured relative to residual proton from the solvent. Coupling constants, *J,* are given in Hz. ^{13}C NMR run at 125 MHz and measured relative to the solvent.

IR: Mattson 1000 FTIR spectrometer (Unicam Analytical Systems). Spectrum software. Frequencies are quoted in cm^{-1}.

HR-MS-FAB:Recorded on a Jeol JMS-700 M STATION high resolution magnetic sector spectrometer. Samples were analysed by the technical staff at the Strathclyde Institute of Pharmacy and Biomedical Sciences.

Column Chromatography: Silica gel mesh size 230-400 (40-60μm).

HPLC:

Instrument Setup:

Waters 1525 Binary HPLC Pump
Waters 717plus Autosampler
Waters 2487 Dual λ Absorbance Detector

LC Conditions:

Column:	Luna 5µ C18(2) 100A
Dimensions:	60 × 21.1 mm
Injection Volume:	100 µL
Solvent Flow Rate:	1 mL/min
Detection wavelength:	254 nm

4.2 Synthesis

Synthesis of 1-amino-3-[({4-[({4-[({[amino(iminio)methyl]amino}acetyl)amino]-1-methyl-1*H*-pyrrol-2-yl}carbonyl)amino]-1-methyl-1*H*-pyrrol-2-yl}carbonyl)amino]-1-propaniminium bis(trifluoroacetate) **26**

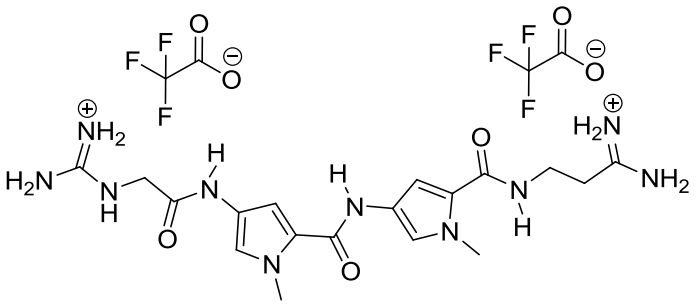

N-(5-{[(3-Amino-3-iminopropyl)amino]carbonyl}-1-methyl-1*H*-pyrrol-3-yl)-1-methyl-4-nitro-1*H*-pyrrole-2-carboxamide **111** (30 mg, 0.083 mmol) was dissolved in MeOH (3 mL) to which was added Pd/C-10 % (30 mg) and this was subjected to hydrogenation for 2 h. After this, the reaction mixture was filtered through Kieselguhr and the solvent removed by rotary evaporation. The resulting residue was dissolved in DMF (1 mL) and to this was added guanidine acetic acid (9.7 mg, 0.083 mmol) and HBTU (64 mg, 0.17 mmol). This was left to stir overnight and subjected to HPLC purification directly to yield the desired material (14 mg, 25 %).

HPLC Procedure

Flow rate: 6 mL/min.

Time (mins)	% Water (with 0.1% TFA)	% MeCN (with 0.1% TFA)
0	90	10
25	70	30
30	50	50
35	90	10

Retention time: 10 min.

Purity by HPLC: >96%.

Melting Point: >230 ^{o}C.

IR: 3262, 3094, 2965, 1701, 1675, 1660, 1636, 1627, 1587, 1574, 1565, 1546, 1532, 1518, 1433, 1267, 1202, 1177, 1125.

δ_H NMR (DMSO): 9.83 (1H, s), 9.63 (1H, s), 8.89 (2H, s), 8.52 (2H, s), 8.20 (1H, t, *J* = 6.0), 7.15 (1H, d, *J* = 1.5), 6.92 (1H, d, *J* = 1.5), 6.86 (1H, d, *J* = 1.5), 6.65 (1H, d, *J* = 1.5), 3.86 (3H, s), 3.81 (3H, s), 3.49 (2H, m), 3.02 (2H, s), 2.60 (2H, t, *J* = 6.0).

δ_C NMR (DMSO): insufficient material.

HR-MS-FAB: Found 430.2676 calculated for $C_{18}H_{26}N_{10}O_3^+$ (M) 430.2680.

Synthesis of 7-(Aminomethyl)-7-deazaguanine[83] **50**

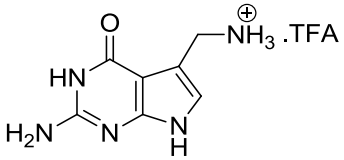

tert-Butyl [(2-amino-4,7-dihydro-4-oxo-1*H*-pyrrolo[2,3-*d*]pyrimidin-5-yl)methy]carbamate **192** (13 mg, 0.046 mmol) was dissolved at 0 ^{o}C in TFA (1 mL). The solution was stirred for 2 h at room temperature. MeOH (5 mL) was added dropwise at 0^{o}C, and the volatiles were evaporated under reduced pressure. The trifluoroacetate salt of **50** was obtained (19 mg, quant.).

Purity by HPLC: >95 %.

Melting Point: >230 ^{o}C.

IR: 3402, 1684, 1204, 802, 724.

δ_H NMR ($CDCl_3$): 11.18 (1H, s), 10.81 (1H, s), 8.15 (3H, s), 6.76 (1H, s), 6.30 (2H, s), 4.01 (2H, m).

δ_C NMR (DMSO): 163.5, 155.5, 154.7, 119.3, 112.6, 100.9, 38.2.

HR-MS-FAB: Found 180.0809 calculated for $C_7H_{10}N_5O^+$ (M+H) 180.0807.

Synthesis of 1-methyl-*N*-[2-(4-morpholinyl)ethyl]-4-nitro-1*H*-pyrrole-2-carboxamide[89] **67**

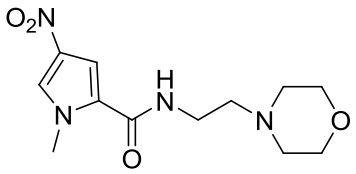

1-Methyl-4-nitro-1*H*-pyrrole-2-carboxylic acid **65** (102 mg, 0.60 mmol) was dissolved in thionyl chloride (4 mL) then the reaction mixture was heated to reflux and left for 3 h. Excess thionyl chloride was removed at 30 ^oC under reduced pressure and the acid chloride so formed was used without further purification. *N*-Aminoethyl morpholine **66** (125 µl, 0.95 mmol) was dissolved in DCM (20 mL, dry) to which NMM (125 µl, 1.14 mmol) was added. The acid chloride was dissolved in DCM (5 mL, dry) then added drop-wise to the aminoethylmorpholine solution with stirring. The reaction mixture was left stirring for 15 h. The crude product was extracted with a solution of sodium carbonate (540 mg, 5.09 mmol) in water (25 mL) and the organic layer was dried over magnesium sulfate, filtered and the solvent was removed under reduced pressure. The crude product obtained was purified by flash column chromatography using ethyl actetate as the mobile phase. Material with an R_f value of 0.09 was collected and the solvent removed at 30 ^oC under reduced pressure to afford the desired product as a pale yellow solid (73 mg, 43 % yield). The data obtained for this compound is consistent with previous preparations from this lab.[89]

Melting Point: 140-141 ^oC

IR: 3326, 3118, 2928, 2816, 1634, 1551, 1533, 1146, 1114

δ_H NMR (DMSO): 7.56 (1H, d, *J* = 1.9), 7.06 (1H, d, *J* = 1.9), 6.58 (1H, bs), 4.00 (3H, s), 3.76 (4H, t, *J* = 4.6), 3.49 (2H, m), 2.59 (2H, t, *J* = 6.0), 2.51 (4H, t, *J* = 4.6)

δ_C NMR (DMSO): 159.7, 133.7, 127.8, 126.4, 107.2, 66.15, 57.3, 53.2, 37.3, 35.9.

HR-MS-FAB: Found 283.1411 calculated for $C_{12}H_{19}O_4N_4^+$ (M+ H) 283.1406.

Synthesis of 1-Methyl-*N*-[1-methyl-5-({[2-(4-morpholinyl)ethyl]amino}carbonyl)-1*H*-pyrrol-3-yl]-4-nitro-1*H*-pyrrole-2-carboxamide[89] **68**

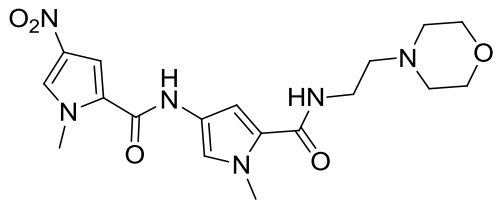

1-Methyl-*N*-[2-(4-morpholinyl)ethyl]-4-nitro-1*H*-pyrrole-2-carboxamide **67** (1.500 g, 5.31 mmol) was dissolved in methanol (35 mL) and cooled to 0 ^oC under nitrogen. Pd/C-10 % (0.600 g) was added portionwise then the reaction mixture was hydrogenated for 4 h at room temperature and atmospheric pressure. The catalyst was removed over kieselguhr and the solvent was removed under reduced pressure to give the amine (as grey oil) which was used without further purification. 1-Methyl-4-nitro-1*H*-pyrrole-2-carboxylic acid **65** (0.903 g, 5.84 mmol) was dissolved in thionyl chloride (6 mL) and the reaction mixture was heated under reflux for 3h. The volatile material was removed under reduced pressure and the acid chloride formed was dissolved in DCM (10 mL, dry). The amine was dissolved in DCM (25 mL, dry) to which NMM (1 mL, dry) was added. The solution of the acid chloride was added to the reaction mixture dropwise with stirring under nitrogen. The reaction mixture was left stirring at room temperature overnight. It was extracted with a saturated aqueous solution of sodium hydrogen carbonate. The organic layer was dried over $MgSO_4$, filtered and the solvent was removed under reduced pressure to give the crude product, which was triturated with ethyl acetate and filtered to give the required product as a pale yellow solid (1.496 g, 70 % yield). The data obtained for this compound is consistent with previous preparations from this lab. [89]

Melting Point: >230 ^{o}C.

IR: 1661, 1635, 1564, 1538, 1502, 1307, 1114.

δ_H NMR (DMSO): 10.21 (1H, s), 8.17 (1H, d, *J* =1.7), 7.95 (1H, t, *J* = 5.7), 7.57 (1H, d, *J* =1.7), 7.21 (1H, d, *J* =1.7), 6.82 (1H, d, *J* =1.7), 3.95 (3H, s), 3.80 (3H, s), 3.57 (4H, t, *J* =4.6), 3.0-3.28 (2H, m), 2.44-2.40 (6H, m).

δ_C NMR (DMSO): 161.0, 159.8, 133.7, 128.2, 126.3, 123.2, 121.3, 117.9, 107.5, 103.8, 66.2, 57.5, 53.3, 37.4, 36.0, 35.7.

HR-MS-FAB: Found 405.1889 calculated for $C_{18}H_{25}O_5N_6^+$ 405.1886.

Synthesis of 4-[(*E*)-2-(3-Methoxyphenyl)ethenyl]benzoic acid[89] **69**

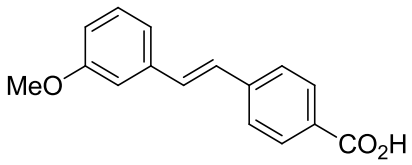

Methyl 4-[(*E*)-2-(3-methoxyphenyl)ethenyl]benzoate and 4-[(*E*)-2-(3-methoxyphenyl)ethenyl]benzoic acid **81** (5.930 g, 23.1 mmol) was dissolved in ethanol (15 mL) to which was added NaOH solution (1.6 g in 40 mL water). This was left to reflux for 3 h. The resulting solution was acidified with dil. HCl and the precipitate filtered and washed with water to afford the desired material (5.515 g, 98 % yield). The data obtained for this compound is consistent with previous preparations from this lab. [89]

Melting Point: 200-205 ^{o}C.

IR:1674, 1596, 1429, 1317, 1280, 1242, 1180, 1036, 948, 849, 770.

δ_H NMR (DMSO): 12.88 (1H, br), 7.94 (2H, d, *J* = 8.4), 7.72 (2H, d, *J* = 8.4), 7.37 (2H, m), 7.31 (1H, t, *J* = 8.0), 7.22 (2H, m), 6.88 (1H, m), 3.80 (3H, s).

δ_C NMR (DMSO): 167.0, 159.6, 141.3, 138.1, 130.9, 129.7, 129.5, 127.7, 126.4, 126.5, 119.4, 114.0, 111.9, 55.1.

HR-MS-FAB: Found 255.0945 calculated for $C_{16}H_{15}O_3^+$ (M+H) 255.0977.

Synthesis of 6-[(*E*)-2-(4-hydroxyphenyl)ethenyl]nicotinic acid[89] **70**

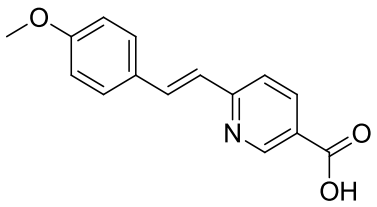

Methyl 6-[(*E*)-2-(4-methoxyphenyl)ethenyl]nicotinate **75** (5.925 g, 23.1 mmol) was dissolved in ethanol (15 mL) to which was added NaOH solution (1.6 g in 40 mL water). This was left to reflux for 3 h. The resulting solution was acidified with HCl and the precipitate filtered and washed with water to afford the desired material (5.509 g, 98.3 % yield). The data obtained for this compound is consistent with previous preparations from this lab. [89]

Melting Point: >230 ^oC.

IR: 3541, 3107, 2934, 1719, 1595, 1276.

δ_H NMR (DMSO): 9.00 (1H, d, *J* = 2.0), 8.37 (1H, dd, *J* = 8.0, 2.0), 7.91 (1H, d, *J* = 16.0), 7.83 (1H, d, *J* = 8.0), 7.66 (2H, d, *J* = 9.0), 7.32 (1H, d, *J* = 16.0), 7.01 (2H, d, *J* = 9.0), 3.85 (3H, s).

HR-MS-FAB: Found: 256.0972 Calculated for $C_{15}H_{14}O_3N^+$ (M+H) 256.0974.

Synthesis of 4-[(*E*)-2-(3-quinolinyl)ethenyl]benzoic acid[89] **71**

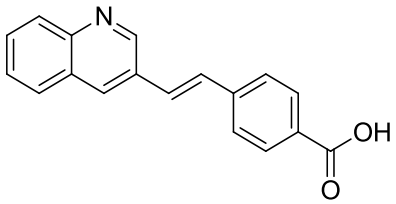

Methyl 4-[(*E*)-2-(3-quinolinyl)ethenyl]benzoate **80** (0.840 mg, 3.36 mmol) was suspended in methanol (10 mL) and water (20 mL) to which sodium hydroxide solution (0.580 g, 14.5 mmol in water 10 mL) was added with stirring. The reaction

mixture was heated under reflux for 2 h. At the beginning the starting material dissolved then white precipitate appeared. The reaction mixture was cooled in an ice bath then dilute HCl was added dropwise with vigorous stirring until pH 2. The product as a yellow solid material was filtered off, washed with water and dried under reduced pressure at 60 ^{o}C (0.640 g, 69 % yield). The data obtained for this compound is consistent with previous preparations from this lab. [89]

Melting Point: 286-289 ^{o}C.

IR: 3203, 1694, 1586, 1541, 1423, 1310, 1272, 1172, 962, 767, 687.

δ_H NMR (DMSO): 12.91 (1H, br), 9.25 (1H, d, *J* = 2.1), 8.54 (1H, d, *J* = 2.1), 8.03-7.97 (4H, m), 7.69-7.59 (6H, m).

δ_C NMR (DMSO): 166.9, 146.0, 140.5, 138.1, 132.3, 131.6, 130.8, 130.4, 129.9, 128.9, 128.8, 128.2, 126.8, 126.9, 126.0, 123.7.

HR-MS-FAB: found: 276.0948 calculated for $C_{18}H_{14}NO_2^+$ (M+H) 276.0946.

Synthesis of Methyl 3-methoxybenzenecarbimidothioate hydroiodide[89] **72**

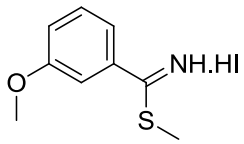

3-Methoxybenzenecarbothioamide **83** (605 mg, 4.41 mmol) was dissolved in acetone (15 mL,) to which methyl iodide (0.275 mL, 4.41 mmol) was added dropwise at 0 ^{o}C with stirring. The stirring was continued at room temperature overnight. The yellow solid material formed was filtered off, washed with small amount of acetone and dried under reduced pressure to give the required material (890 mg, 72 % yield). The data obtained for this compound is consistent with previous preparations from this lab. [89]

Melting Point: 157-159 ^{o}C.

IR: 2994, 1665, 1543, 1490, 1425, 1292, 1220, 1038, 906, 785.

δ_H NMR (DMSO): 11.71 (2H, br), 7.59-7.55 (1H, m), 7.44-7.37 (3H, m), 3.85 (3H, s), 2.82 (3H,s).

HR-MS-FAB: Found 182.0648 calculated for $C_9H_{12}NOS^+$ (M+H) 182.0639.

Synthesis of Methyl 6-[(*E*)-2-(4-methoxyphenyl)ethenyl]nicotinate[90] **75**

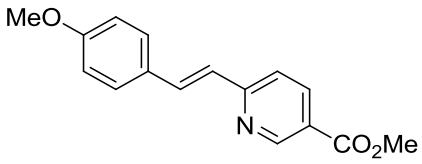

4-Methoxybenzaldehyde **73** (4.50 g, 33.07 mol), methyl 6-methylnicotinate **74** (5.00 g, 33.07 mmol), acetic anhydride (6.75 g, 66.14 mol) and catalytic amount of zinc chloride were heated at 140 ^oC with stirring for 48 h. The reaction mixture was triturated with ethyl acetate, small amount of methanol and brine. The required product as a light brown solid was obtained after filtration (6.200 g, 70%). The data obtained for this compound is consistent with previous preparations from this lab. [90]

Melting Point: 170-173 ^oC.

IR:1717, 1606, 1591, 1511, 1433, 1290, 1254, 1175, 1111, 1020, 844, 818, 760, 734.

δ_H NMR (DMSO): 9.04 (1H, d, *J* = 2.0), 8.25 (1H, dd, *J* = 8.2, *J* = 2.0), 7.81 (1H, d, *J* = 16.0), 7.67-7.62 (3H, m), 7.28 (1H, d, *J* = 16.0), 7.00 (2H, d, *J* = 8.8), 3.88 (3H, s), 3.80 (3H, s).

δ_C NMR (DMSO): 164.9, 160.2, 158.6, 149.3, 138.2, 137.5, 129.2, 128.3, 123.8, 123.6, 121.9, 114.4, 55.3, 52.3.

HR-MS-FAB: Found 270.1127 Calculated for $C_{16}H_{16}O_3N^+$ (M+H) 270.1130.

Synthesis of methyl 4-[(diethoxyphosphoryl)methyl]benzoate[89] **77**

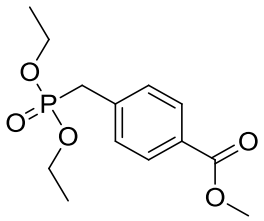

A mixture of methyl 4-(bromomethyl)benzoate **76** (2.51 g, 10.9 mmol) and triethylphosphite **75** (3.62 g, 21.8 mmol) was heated at 160 ^{o}C under nitrogen for 2 h. The excess of triethylphosphite was removed under reduced pressure to give the required product as a colourless oil (3.03 g, 97 % yield). The data obtained for this compound is consistent with previous preparations from this lab. [89]

Melting Point: Oil at room temperature.

δ_H NMR (DMSO): 7.91 (2H, d, *J* = 8.0), 7.44 (2H, dd, *J* = 8.0), 4.00 (4H, quintet, *J* = 6.8), 3.84 (3H, s), 3.36 (2H, d, *J* = 22.0), 1.16 (6H, t, *J* = 6.8).

HR-MS-FAB: Found 287.1062 Calculated for $C_{13}H_{20}O_5P^+$ (M+H) 287.1048.

Synthesis of Methyl 4-[(*E*)-2-(3-quinolinyl)ethenyl]benzoate[89] **80**

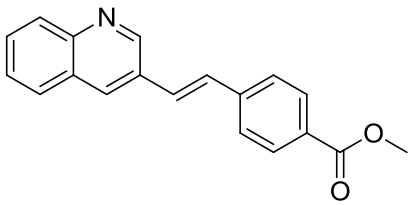

To a solution of methyl 4-[(diethoxyphosphoryl)methyl]benzoate **77** (0.911 g, 3.18 mmol) in THF (10 mL, dry) under nitrogen atmosphere was added sodium hydride (0.678 g, 60 %, 18.8 mmol). After cooling the reaction mixture to 0 ^{o}C, quinoline-3-aldehyde **78** (0.500 g, 3.18 mmol) in THF 10 mL, dry) was carefully added dropwise with stirring. The reaction mixture was stirred for 1 h at room temperature and then quenched with water. After neutralization with dilute HCl, the two layers were separated. The water layer was extracted with ethyl acetate (3 × 10 mL) and the

organic layers were combined, dried ($MgSO_4$), filtered and the solvent removed under reduced pressure to give white solid. The product was purified by silica gel column chromatography using 1:4; ethyl acetate:hexane (R_F = 0.50) to give the required material, as a white solid (0.900 g, 98 % yield). The data obtained for this compound is consistent with previous preparations from this lab. [89]

Melting Point: 93-95 ^oC.

IR: 1716, 1598, 1460, 1273, 1173, 750.

δ_H NMR (DMSO): 9.25 (1H, d, *J* = 2.0), 8.54 (1H, d, *J* = 2.0), 8.21-8.35 (4H, m), 7.82 (2H, d, *J* = 8.4), 7.75 (1H, t, *J* = 6.8), 7.64 (2H, d, *J* = 8.4), 7.63 (1H, t, *J* = 6.8), 3.87 (3H, s).

HR-MS-FAB: Found 290.1104 calculated for $C_{19}H_{16}NO_2^+$ (M+H) 290.1103.

Synthesis of Methyl 4-[(*E*)-2-(3-methoxyphenyl)ethenyl]benzoate[89] **81**

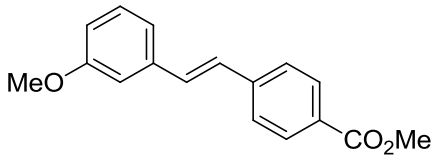

To a solution of methyl 4-[(diethoxyphosphoryl)methyl]benzoate **77** (3.03 g, 10.6 mmol) in THF (10 mL, dry) under nitrogen atmosphere was added sodium hydride (0.678 g, 60%, 18.8 mmol). After cooling the reaction mixture to 0 ^oC, *m*-anizaldehyde **79** (1.54 g, 11.3 mmol in THF 20 mL, dry) was carefully added dropwise with stirring. The reaction mixture was stirred for 1h at room temperature and then quenched with water. After neutralization with dilute HCl, the two layers were separated. The water layer was extracted with ethyl acetate and the organic layers were combined, dried ($MgSO_4$), filtered and the solvent removed under reduced pressure to give the desired material as white solid (1.57 g, 55 % yield). The data obtained for this compound is consistent with previous preparations from this lab. [89]

Melting Point: 92-94 ^oC.

IR:1708, 1595, 1438, 1280, 1244, 1174, 1105, 1033, 965, 865, 784, 697.

δ_H NMR (DMSO): 7.96 (2H, d, *J* = 8.4), 7.74 (2H, d, *J* = 8.4), 7.42-7.21 (5H, m), 6.88 (1H, m), 3.85 (3H, s), 3.80 (3H, s).

HR-MS-FAB: Found 269.1100 calculated for $C_{17}H_{17}O_3^+$ (M+H) 269.1099.

Synthesis of 3-Methoxybenzenecarbothioamide[91] **83**

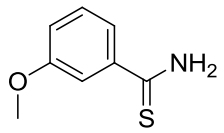

3-Methoxybenzamide **82** (1.5 g, 10.9 mmol) was dissolved in THF (50 mL, dry) to which Lawesson's reagent (5 g, 4.41 mmol) was added and heated at 55 ^oC for 3 h. The solvent was removed under reduced pressure and the resulting oil was recrystalised from acetone/water to give the desired material (1.03g, 62 % yield). The data obtained for this compound is consistent with previous preparations from this lab.[91]

Melting Point: 180-183 ^oC.

IR: 3284, 3134, 1632, 1590, 1466, 1418, 1278, 1240, 1026, 812, 690.

δ_H NMR (DMSO): 9.85 (1H, s), 9.45 (1H, s), 7.46 (1H, dd, *J* = 8.0, *J* = 2.0), 7.42 (1H, t, *J* = 2.0), 7.31 (1H, t, *J* = 8.0), 7.06 (1H, dd, *J* = 8.0, *J* = 2.0), 3.78 (3H, s).

δ_C NMR (DMSO): 189.3, 158.6, 140.7, 128.9, 119.6, 116.8, 112.5, 55.22.

HR-MS-FAB: Found 168.0407 calculated for $C_8H_{10}OSN^+$ (M+H) 168.0411.

Synthesis of 2,3,4,5,6-pentafluorophenyl 6-[(*E*)-2-(4-methoxyphenyl)ethenyl]nicotinate **84**

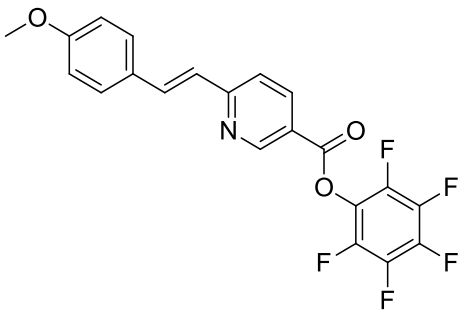

6-[(*E*)-2-(4-methoxyphenyl)ethenyl]nicotinic acid **70** (2.0 g, 7.81 mmol) was dissolved in DCM (60 mL, dry) to which was added DIC (1.8 g, 14.3 mmol) and this was left to stir for 30 min. Pentafluorophenol (1.7 g, 9.23mmol) was then added slowly and the reaction monitored by TLC (product has R_f of 0.41 on 1:1; ethylacetate: hexane). After 2 h the reaction mixture was washed with saturated potassium carbonate solution (3 × 10 mL) and the organic phase subjected to rotary evaporation to yield an off-white solid. This was washed with ether to yield the desired material in pure form (1.41 g, 50 % yield).

Melting Point: 152-154 ^{o}C.

IR: 3328, 3031, 2930, 2851, 1756, 1704, 1587, 1519, 1257, 1176, 1059, 991.

δ_H NMR (DMSO): 9.33 (1H, d, *J* = 2.0), 8.37 (1H, dd, *J* = 8.0, 2.0), 7.84 (1H, d, *J* = 16.0), 7.59 (1H, d, *J* = 8.0), 7.49 (2H, d, *J* = 9.0), 7.13 (1H, d, *J* = 16.0), 6.95 (2H, d, *J* = 9.0), 3.87 (3H, s).

δ_C NMR (DMSO): 161.5, 161.3, 160.7, 151.9, 142.1 (m), 140.0 (m), 139.1(m), 138.5, 137.0 (m), 136.7, 129.1, 128.6, 124.3, 121.3, 120.3, 114.3, 55.3. (See appendix 10).

HR-MS-FAB: Found 421.0739 calculated for $C_{21}H_{13}NO_3F_5^+$ (M) 421.0737.

Synthesis of 2,3,4,5,6-pentafluorophenyl 4-[(*E*)-2-(3-methoxyphenyl)ethenyl]benzoate **87**

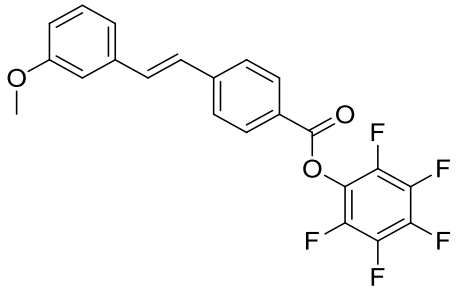

4-[(*E*)-2-(3-methoxyphenyl)ethenyl]benzoic acid **69** (1.486 g, 5.83 mmol) was dissolved in DCM (60 mL, anhydrous) to which was added DIC (1.35 g, 10.7 mmol) and this was left to stir for 30 min. Pentafluorophenol (1.125 g, 6.11 mmol) was then added slowly and the reaction monitored by TLC (product has R_f of 0.40 on 1:1; ethyl acetate:hexane). After 2 hours the reaction mixture was washed with saturated potassium carbonate solution (3 × 10 mL) and the organic phase subjected to rotary evaporation to yield an off-white solid. This was washed with ether to yield the desired material in pure form (1.482 g, 60 %).

Melting Point: 110-112 ^{o}C.

IR: 2962, 1755, 1604, 1578, 1520, 1284, 1258, 1227, 1049.

δ_H NMR (DMSO): 8.18 (2H, d, *J* = 8.4), 7.66 (2H, d, *J* = 8.4), 7.21-7.42 (3H, m), 7.12-7.19 (2H, m), 7.11 (1H, m), 6.90 (1H, dd, *J* = 7.8, *J* = 2.0), 3.88 (3H, s).

δ_C NMR (DMSO): 162.3, 160.0, 143.6, 142.2 (m), 140.5 (m), 138.9 (m), 137.8, 136.8 (m), 132.4, 131.2, 129.8, 127.3, 126.7, 125.4, 119.6, 114.2, 112.1, 55.3. (See appendix 10).

HR-MS-FAB: Found 420.0784 calculated for $C_{22}H_{14}O_3F_5^+$ (M) 420.0785.

Synthesis of 2,3,4,5,6-pentafluorophenyl 4-[(*E*)-2-(3-quinolinyl)ethenyl]benzoate **88**

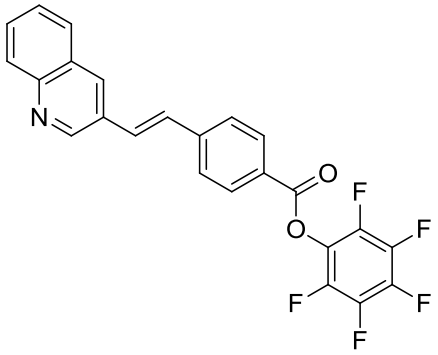

4-[(*E*)-2-(3-Quinolinyl)ethenyl]benzoic acid **71** (2.191 g, 10.14 mmol) was dissolved in DCM (60 mL, dry) to which was added DIC (1.920 g, 15.21 mmol) and this was left to stir for 30 mins. Pentafluorophenol (1.866 g, 10.14 mmol) was then added slowly and the reaction monitored by TLC (product has R_f of 0.38 on 1:1; ethylacetate: hexane). After 2 h the reaction mixture was washed with saturated aqueous potassium carbonate solution (3 × 10 mL) and the organic phase subjected to rotary evaporation to yield an off-white solid. This was washed with ether to yield the desired material in pure form (1.631 g, 48 % yield).

Melting Point: 102-105 ^{o}C.

IR: 3461, 3414, 1741, 1603, 1594, 1518, 1247, 1053.

δ_H NMR ($CDCl_3$): 9.18 (1H, d, *J* = 2.1), 8.2-8.3 (3H, m), 8.13 (1H, d, *J* = 8.5), 7.87 (1H, d, *J* = 8.5), 7.74 (3H, d, *J* = 8.5), 7.60 (1H, t, *J* = 8.5), 7.43 (2H, m).

δ_C NMR (DMSO): Insufficient solubility.

HR-MS-FAB: Found 441.0786 calculated for $C_{24}H_{13}NO_3F_5^+$ (M) 441.0788.

Synthesis of 4-({4-[(*E*)-2-(3-Methoxyphenyl)ethenyl]benzoyl}amino)-1-methyl-*N*-[1-methyl-5-({[2-(4-morpholinyl)ethyl]amino}carbonyl)-1*H*-pyrrol-3-yl]-1*H*-pyrrole-2-carboxamide[90] **BP1**

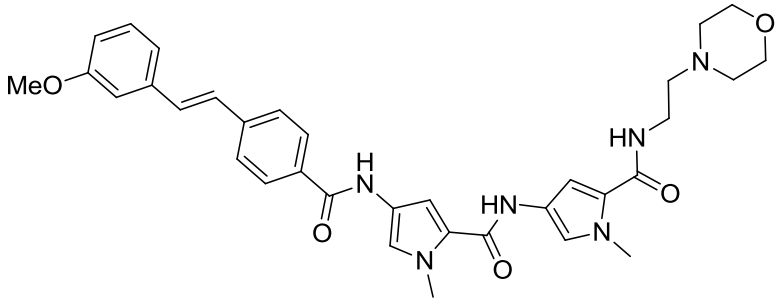

1-Methyl-*N*-[1-methyl-5-({[3-(4-morpholinyl)propyl]amino}carbonyl)-1*H*-pyrrol-3-yl]-4-nitro-1*H*-pyrrole-2-carboxamide **68** (160 mg, 0.396 mmol) was dissolved in methanol (35 mL) at 0 ^{o}C under nitrogen. Pd/C-10 % (110 mg) was added portionwise with stirring under nitrogen at 0 ^{o}C. The reaction mixture was hydrogenated for 3 h at room temperature and atmospheric pressure. The catalyst was removed over kieselguhr and the solvent was removed under reduced pressure to give the amine. This was dissolved in DMF (2 mL, dry) to which was added 2,3,4,5,6-pentafluorophenyl 4-[(*E*)-2-(3-methoxyphenyl)ethenyl]benzoate **87** (166 mg, 0.396 mmol). The reaction mixture was heated to 50 ^{o}C for 2 h then the reaction mixture was left stirring at room temperature overnight. DMF was removed under reduced pressure and the crude product was treated with ethyl acetate and saturated aqueous solution of potassium carbonate. The pale yellow solid precipitated was collected, washed with distilled water and dried to give the required product as a pale yellow solid (145 mg, 60 % yield). The data obtained for this compound is consistent with previous preparations from this lab. [90]

Melting Point: >230 ^{o}C.

IR: 1681, 1642, 1577, 1464, 1435, 1404, 1266, 1202, 1134.

δ_H NMR (DMSO): 10.32 (1H, s), 9.97 (1H, s), 9.68 (1H, br), 8.23 (1H, t, *J* = 5.6), 7.97 (2H, d, *J* = 8.4), 7.75 (2H, d, *J* = 8.4), 7.3-7.29 (4H, m), 7.22 (2H, m), 7.12 (1H,

d, *J* = 1.5), 7.00 (1H, d, *J* = 1.5), 6.90 (1H, dd, *J* = 3.7, *J* = 1.5), 3.99 (2H, m), 3.88 (3H, s), 3.83 (3H, s), 3.81 (3H, s), 3.67-3.55 (6H, m), 3.27 (2H, m), 3.14 (2H, m).

HR-MS-FAB: Found 611.2971 calculated for $C_{34}H_{40}N_6O_5^+$ (M+H) 611.2982.

Synthesis of 6-[(*E*)-2-(4-Methoxyphenyl)ethenyl]-*N*-[1-methyl-5-({[1-methyl-5-({[2-(4-morpholinyl)ethyl]amino}carbonyl)-1*H*-pyrrol-3-yl]amino}carbonyl)-1*H*-pyrrol-3-yl]nicotinamide[90] **BP2**

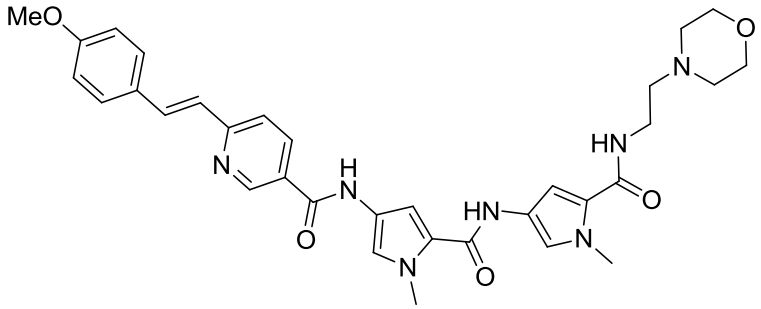

1-Methyl-*N*-[1-methyl-5-({[3-(4-morpholinyl)propyl]amino}carbonyl)-1*H*-pyrrol-3-yl]-4-nitro-1*H*-pyrrole-2-carboxamide **68** (200 mg, 0.495 mmol) was dissolved in methanol (35 mL) at 0 ^{o}C under nitrogen. Pd/C-10 % (100 mg) was added portionwise with stirring under nitrogen at 0 ^{o}C. The reaction mixture was hydrogenated for 4 h at room temperature and atmospheric pressure. The catalyst was removed over kieselguhr and the solvent was removed under reduced pressure to give the amine. This was dissolved in DMF (2 mL, dry) to which was added 2,3,4,5,6-pentafluorophenyl 6-[(*E*)-2-(4-methoxyphenyl)ethenyl]nicotinate **84** (140 mg, 0.332 mmol). The reaction mixture was heated to 50 ^{o}C for 2 h then the reaction mixture was left stirring at room temperature overnight. DMF was remover under reduced pressure and the crude product was treated with ethyl acetate and saturated solution of potassium carbonate. The pale yellow solid precipitated was collected, washed with distilled water and dried to give the required product as a pale yellow solid (146 mg, 72 % yield). The data obtained for this compound is consistent with previous preparations from this lab. [90]

Melting Point: >230 ^{o}C.

IR: 3427, 1673, 1588, 1402, 1253, 1202, 1174, 832, 720

δ_H NMR (DMSO): 10.48 (1H, s), 9.98 (2H, s & br), 9.07 (1H, s), 8.28 (1H, d, *J* = 2.3), 8.26 (1H, d, *J* = 2.3), 7.77 (1H, d, *J* = 16.0), 7.67 (3H, d, *J* = 8.8), 7.35 (1H, d, *J* = 1.6), 7.27 (1H, d, *J* = 16.0), 7.22 (1H, d, *J* = 1.6), 7.12 (1H, d, *J* = 1.6), 7.01 (3H, m), 4.01 (2H, m), 3.88 (3H, s), 3.83 (3H, s), 3.80 (3H, s), 3.73 (2H, m), 3.56 (4H, m), 3.27 (2H, m), 2.99 (2H, m).

HR-MS-FAB: Found 612.2990 calculated for $C_{34}H_{39}O_5N_6^+$ (M+H) 612.2982.

Synthesis of 1-methyl-*N*-[1-methyl-5-({[2-(4-morpholinyl)ethyl]amino}carbonyl)-1*H*-pyrrol-3-yl]-4-({4-[(*E*)-2-(3-quinolinyl)ethenyl]benzoyl}amino)-1*H*-pyrrole-2-carboxamide[90] **BP3**

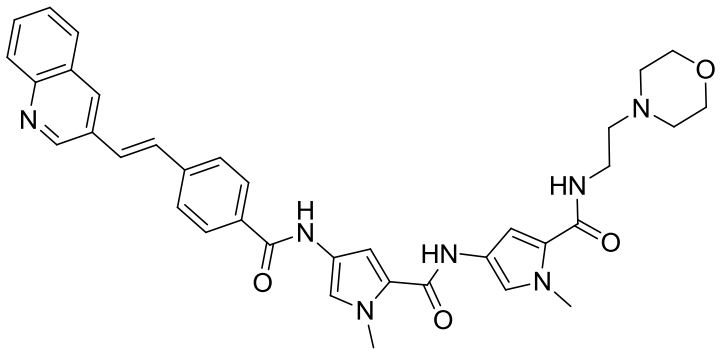

1-Methyl-*N*-[1-methyl-5-({[3-(4-morpholinyl)propyl]amino}carbonyl)-1*H*-pyrrol-3-yl]-4-nitro-1*H*-pyrrole-2-carboxamide **68** (0.300 g, 0.742 mmol) was dissolved in methanol (50 mL and DMF (10 mL) at 0 ^oC under nitrogen. Pd/C-10 % (178 mg) was added portionwise with stirring under nitrogen at 0 ^oC. The reaction mixture was hydrogenated for 4 h at room temperature and atmospheric pressure. The catalyst was removed over kieselguhr and the solvent was removed under reduced pressure to give the amine. To the DMF solution 2,3,4,5,6-pentafluorophenyl 4-[(*E*)-2-(3-quinolinyl)ethenyl]benzoate **88** (328 mg, 0.742 mmol) was added. The reaction mixture was heated to 50 ^oC for 2 h then the reaction mixture was left stirring at room temperature overnight. DMF was remover under reduced pressure and the crude product was treated with ethyl acetate containing 5% methanol and saturated solution of potassium carbonate. The pale yellow solid precipitated was collected,

washed with distilled water and dried to give the required product as a pale yellow solid (244 mg, 52 % yield). The data obtained for this compound is consistent with previous preparations from this lab. [90]

Melting Point: >230 ^{o}C.

IR: 1681, 1642, 1577, 1464, 1435, 1404, 1266, 1202, 1134.

δ_H NMR (DMSO): 10.35 (1H, s), 9.98 (1H, s), 9.55 (1H, br), 9.28 (1H, d, *J* = 2.0), 8.59 (1H, d, *J* = 2.0), 8.23 (1H, t, *J* = 8.0), 8.05-7.97 (5H, m), 7.83-7.75 (4H, m), 7.70-7.60 (4H, m), 7.34 (1H, d, *J* = 1.7), 7.21 (1H, d, *J* = 1.7), 7.13 (1H, d, *J* = 1.7), 7.01 (1H, d, *J* = 1.7), 4.03-3.99 (2H, m), 3.88 (3H, s), 3.83 (3H, s), 3.69-3.63 (2H, m), 3.59-3.54 (4H, m), 3.28 (2H, m), 3.15 (2H, m).

HR-MS-FAB: Found 632.2982 calculated for $C_{36}H_{38}N_7O_4^+$ (M+H) 632.2985.

Synthesis of 1-methyl-*N*-[1-methyl-5-({[2-(4-morpholinyl)ethyl]amino}carbonyl)-1*H*-pyrrol-3-yl]-4-({4-[(*E*)-2-(3-quinolinyl)ethenyl]benzoyl}amino)-1*H*-pyrrole-2-carboxamide[90] **BP3**

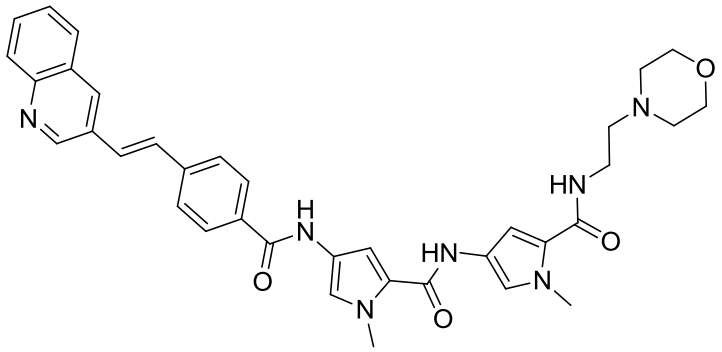

1-Methyl-*N*-[1-methyl-5-({[3-(4-morpholinyl)propyl]amino}carbonyl)-1*H*-pyrrol-3-yl]-4-nitro-1*H*-pyrrole-2-carboxamide **68** (0.300 g, 0.742 mmol) was dissolved in methanol (60 mL). Pd/C-10 % (160 mg) was added portionwise with stirring under nitrogen at 0 ^{o}C. The reaction mixture was hydrogenated for 4 h at room temperature and atmospheric pressure. The catalyst was removed over kieselguhr and the solvent was removed under reduced pressure to give the amine which was dissolved in DMF (4 mL, dry). 4-[(*E*)-2-(3-quinolinyl)ethenyl]benzoic acid **71** (204 mg, 0.742 mmol)

and HBTU (563 mg, 1.484 mmol) were added. The reaction mixture was left stirring at room temperature overnight. DMF was removed under reduced pressure and the crude product was treated with ethyl acetate containing 5% methanol and a solution of sodium hydroxide (60 mg, 1.484 mmol in water 10 mL). The organic layer was collected, dried (Na_2SO_4), filtered and the solvent removed under reduced pressure. The crude product was applied to a silica gel column chromatography using ethyl acetate/methanol/NMM (90/10/1; R_F = 0.2) to give the required product as a pale yellow solid (181 mg, 39 % yield). The data obtained for this compound is consistent with previous preparations from this lab. [90]

This material was identical to that reported above

Synthesis of 4-({4-[(*E*)-2-(3-methoxyphenyl)ethenyl]benzoyl}amino)-1-methyl-*N*-[1-methyl-5-({[2-(4-oxido-4-morpholinyl)ethyl]amino}carbonyl)-1*H*-pyrrol-3-yl]-1*H*-pyrrole-2-carboxamide **90**

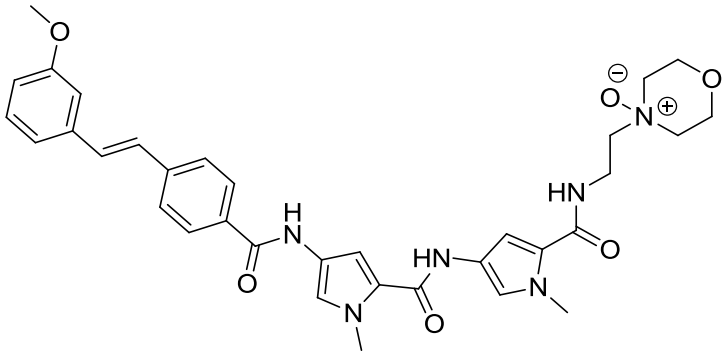

4-({4-[(*E*)-2-(3-Methoxyphenyl)ethenyl]benzoyl}amino)-1-methyl-*N*-[1-methyl-5-({[2-(4-morpholinyl)ethyl]amino}carbonyl)-1*H*-pyrrol-3-yl]-1*H*-pyrrole-2-carboxamide, **BP1**, (10 mg, 16.4 mmol) was dissolved in DMF (1 mL, anhydrous) to which was added *m*-CPBA (2.8 mg, 16.4 mmol). This was left to stir overnight afterwhich it was purified directly by HPLC to obtain the desired product (7 mg, 68 % yield).

HPLC Procedure

Flow rate: 6 mL/min.

Time (mins)	% Water (with 0.1% TFA)	% MeCN (with 0.1% TFA)
0	70	30
25	50	50
30	70	30
35	70	30

Retention time: 18 min.

Purity by HPLC: >95 %.

Melting Point: >230 ^{o}C.

IR: 3279, 2954, 2867, 1672, 1642, 1632, 1526, 1433, 1399, 1265, 1131.

δ_H NMR (DMSO): 12.41 (1H, s), 10.32 (1H, s), 9.97 (1H, s), 8.31 (1H, t, *J* = 5.8), 7.96 (2H, d, *J* = 8.4), 7.73 (2H, d, *J* = 8.4), 7.3-7.4 (4H, m), 7.20-7.25 (3H, m), 7.11 (1H, d, *J* = 1.5), 6.97 (1H, d, *J* = 1.5), 6.87 (1H, d, *J* = 1.5), 3.95-3.98 (2H, m), 3.87 (3H, s), 3.81-3.85 (2H, m), 3.83 (3H, s), 3.81 (3H, s), 3.65-3.72 (4H, m), 3.28 (2H, m), 3.15 (2H, m).

δ_C NMR: Insufficient material.

HR-MS-FAB: Found 627.2916 calculated for $C_{34}H_{39}O_6N_6^+$ (M+H) 627.2926.

Synthesis of 2-[(*E*)-2-(4-methoxyphenyl)ethenyl]-5-({[1-methyl-5-({[1-methyl-5-({[2-(4-oxido-4-morpholinyl)ethyl]amino}carbonyl)-1*H*-pyrrol-3-yl]amino}carbonyl)-1*H*-pyrrol-3-yl]amino}carbonyl)pyridinium trifluoroacetate **91**

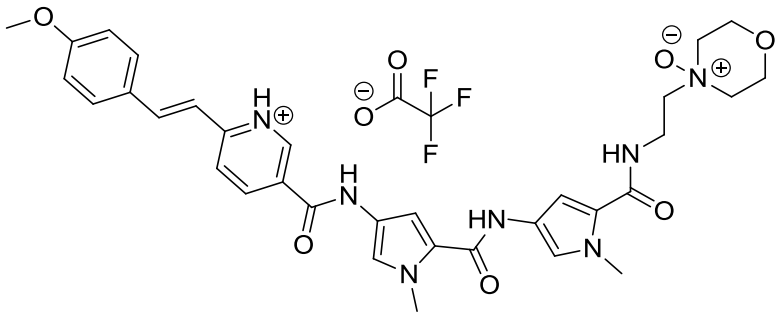

6-[(*E*)-2-(4-Methoxyphenyl)ethenyl]-*N*-[1-methyl-5-({[1-methyl-5-({[2-(4-morpholinyl)ethyl]amino}carbonyl)-1*H*-pyrrol-3-yl]amino}carbonyl)-1*H*-pyrrol-3-yl]nicotinamide, **BP2**, (10 mg, 16.4 mmol) was dissolved in DMF (1 mL, anhydrous) to which was added *m*-CPBA (2.8 mg, 16.4 mmol). This was left to stir overnight afterwhich it was purified directly by HPLC to obtain the desired product (10 mg, 82 % yield).

HPLC Procedure

Flow rate: 6 mL/min.

Time (mins)	% Water (with 0.1% TFA)	% MeCN (with 0.1% TFA)
0	70	30
25	50	50
30	70	30
35	70	30

Retention time: 10 min.

Purity by HPLC: >95 %.

Melting Point: >230 ^{o}C.

IR: 3262, 3116, 3042, 2911, 1867, 1668, 1591, 1513, 1409, 1200, 1131.

δ_H NMR (DMSO): 12.36 (1H, s), 10.47 (1H, s), 9.97 (1H, s), 9.06 (1H, s), 8.31 (1H, t, 5.8 Hz), 8.25 (1H, dd, *J* = 8.0, 2.5), 7.75 (2H, d, *J* = 16.0), 7.63-67 (3H, m), 7.34 (1H, d, *J* = 1.5), 7.2-7.27 (2H, m), 7.10 (1H, d, *J* = 1.5), 6.97-7.02 (3H, m), 3.95-3.98 (2H, m), 3.88 (3H, s), 3.81-3.85 (2H, m), 3.83 (3H, s), 3.80 (3H, s), 3.65-3.72 (4H, m), 3.28 (2H, m), 3.15 (2H, m).

δ_C NMR: Insufficient material.

HR-MS-FAB: Found 628.2872 calculated for $C_{33}H_{38}O_6N_7^+$ 628.2878.

Synthesis of 3-{(*E*)-2-[4-({[1-methyl-5-({[1-methyl-5-({[2-(4-oxido-4-morpholinyl)ethyl]amino}carbonyl)-1*H*-pyrrol-3-yl]amino}carbonyl)-1*H*-pyrrol-3-yl]amino}carbonyl)phenyl]ethenyl}quinolinium trifluoroacetate **92**

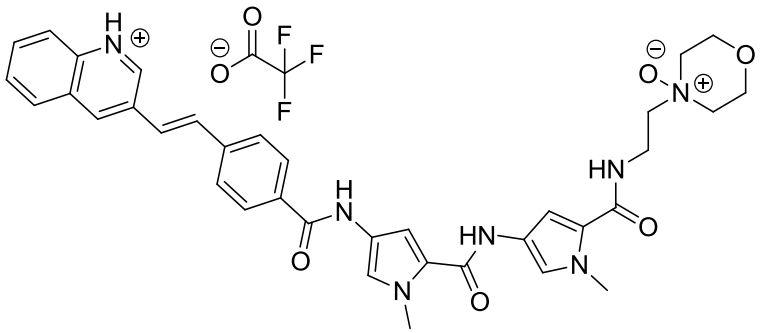

1-Methyl-*N*-[1-methyl-5-({[2-(4-morpholinyl)ethyl]amino}carbonyl)-1*H*-pyrrol-3-yl]-4-({4-[(*E*)-2-(3-quinolinyl)ethenyl]benzoyl}amino)-1*H*-pyrrole-2-carboxamide, **BP3**, (10 mg, 15.5 mmol) was dissolved in DMF (1 mL, anhydrous) to which was added *m*-CPBA (2.6 mg, 15.5 mmol). This was left to stir overnight after which it was purified directly by HPLC to obtain the desired product (8 mg, 68 % yield).

HPLC Procedure

Flow rate: 6 mL/min.

Time (mins)	% Water (with 0.1% TFA)	% MeCN (with 0.1% TFA)
0	70	30
25	50	50
30	70	30
35	70	30

Retention time: 8 min.

Purity by HPLC: >95 %.

Melting Point: >230 ^{o}C.

IR: 3414, 3126, 2923, 2846, 1676, 1648, 1631, 1582, 1541, 1464, 1435, 1203, 1131, 1011.

δ_H NMR (DMSO): 10.38 (1H, s), 9.98 (1H, s), 9.55 (1H, br), 8.41 (1H, d, *J* = 9.0), 8.22 (1H, t, *J* = 8.0), 7.87-8.03 (8H, m), 7.78 (1H, m), 7.56-7.66 (2H, m), 7.34 (1H, d, *J* = 1.7), 7.21 (1H, d, *J* = 1.7), 7.13 (1H, d, *J* = 1.7), 7.01 (1H, d, *J* = 1.7), 3.98-4.01 (2H, m), 3.88 (3H, s), 3.83 (3H, s), 3.62-3.69 (2H, m), 3.55-3.59 (4H, m), 3.27 (2H, m), 3.12 (2H, m).

δ_C NMR: Insufficient material.

HR-MS-FAB: Found 648.29 calculated for $C_{36}H_{38}O_5N_7^+$ (M+H) 648.29.

Synthesis of 3-((*E*)-2-{4-[({1-methyl-5-[({1-methyl-5-[({2-[(trifluoroacetyl)amino]ethyl}amino)carbonyl]-1*H*-pyrrol-3-yl}amino)carbonyl]-1*H*-pyrrol-3-yl}amino)carbonyl]phenyl}ethenyl)quinolinium trifluoroacetate **89**

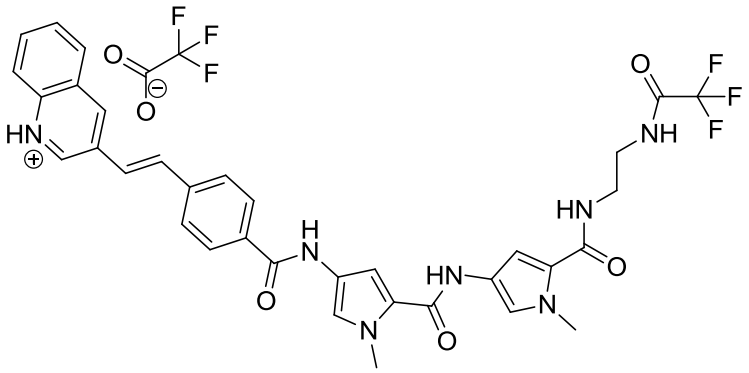

3-[(*E*)-2-(4-{[(5-{[(5-{[(2-Ammonioethyl)amino]carbonyl}-1-methyl-1*H*-pyrrol-3-yl)amino]carbonyl}-1-methyl-1*H*-pyrrol-3-yl)amino]carbonyl}phenyl)ethenyl] quinolinium bis(trifluoroacetate) **96** (50 mg, 0.063 mmol) was dissolved in DMF (1 mL, dry) and to this was added triethylamine (17.5 mL, 0.126 mmol). After 30 mins of stirring, trifluoroacetic acid anhydride (26.5 mg, 0.126 mmol) was added dropwise and left to stir for 16 h. The reaction mixture was subjected to HPLC purification to obtain the desired product (24 mg, 50 % yield).

HPLC Procedure

Flow rate: 6 mL/min.

Time (mins)	% Water (with 0.1% TFA)	% MeCN (with 0.1% TFA)
0	70	30
25	50	50
30	30	70
35	70	30
40	70	30

Retention time: 2.61 min.

Purity by HPLC: >97 %

Melting Point: >230 ^{o}C.

IR: 3421, 2961, 2928, 2851, 1706, 1682, 1650, 1440, 1204.

δ_H NMR (DMSO): 10.15 (1H, s), 9.75 (1H, s), 9.25 (1H, bs), 9.23 (1H, d, *J* = 2.0), 8.51 (1H, d, *J* = 2.0), 7.97-8.03 (5H, m), 7.92 (1H, m), 7.55-7.81 (5H, m), 7.30 (1H, d, *J* = 2.0), 7.17 (1H, d, *J* = 2.0), 7.09 (1H, d, *J* = 2.0), 6.97 (1H, d, *J* = 2.0), 3.88 (3H, s), 3.82 (3H, s), 3.35 (4H, m).

δ_C NMR: Insufficient material.

HR-MS-FAB: Found 658.2390 calculated for $C_{34}H_{31}O_4N_7F_3^+$ (M+H) 658.2384.

Synthesis of *tert*-butyl 2-({[1-methyl-4-({[1-methyl-4-({4-[(*E*)-2-(3-quinolinyl)ethenyl]benzoyl}amino)-1*H*-pyrrol-2-yl]carbonyl}amino)-1*H*-pyrrol-2-yl]carbonyl}amino)ethylcarbamate[89] **95**

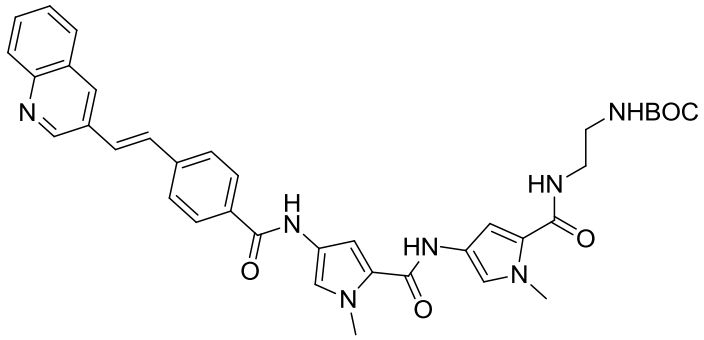

tert-Butyl 2-{[(1-methyl-4-{[(1-methyl-4-nitro-1*H*-pyrrol-2-yl)carbonyl]amino}-1*H*-pyrrol-2-yl)carbonyl]amino}ethylcarbamate **94** (0.300 g, 0.69 mmol) was taken up in methanol (10 mL) and cooled to 0 ˚C. Pd/C-10 % (10 %, 0.100 g) was then added in small portions and the suspension stirred under hydrogen for 3 h. The suspension was then filtered and the solvent removed under reduced pressure. The residue was dissolved in anhydrous DMF (5 mL), 4-[(*E*)-2-(3-quinolinyl)ethenyl]benzoic acid **71** (0.176 g, 0.69 mmol) was then added along with HBTU (0.525 g, 1.38 mmol). The

resulting solution was allowed to stir for 16 h before being reduced under vacuum to give a brown oil. Ethyl acetate (5 mL) and sat. aq NaOH (5ml) where added and after this the product precipitated as a light grey solid which was filtered, washed with cold ethyl acetate and water, before being dried in a dessicator (286 mg, 66 % yield). The data obtained for this compound is consistent with previous preparations from this lab.

Melting Point: > 230 ˚C.

IR: 3446, 3132, 2925, 1637, 1594, 1260.

δ_H NMR (DMSO): 10.50 (1H, s), 9.96 (1H, s), 9.06 (1H, d, *J* = 2.2), 8.27 (1H, dd, *J* = 8.2, 2.3), 7.98 (1H, t, *J* = 5.6), 7.76 (1H, d, *J* = 16.1), 7.66 (3H, m), 7.35 (1H, d, *J* = 1.8), 7.25 (1H, d, *J* = 16.1),7.20 (1H, d, *J* = 1.8), 7.08 (1H, d, *J* = 1.8), 6.99 (2H, d, *J* = 8.2), 6.88 (3H, m), 3.87 (3H, s), 3.82 (3H, s), 3.19 (2H, m), 3.05 (2H, m), 1.37 (9H, s).

HR-MS-FAB: Found 642.2991 calculated for $C_{34}H_{40}N_7O_6^+$ (M+H) 642.2995.

Synthesis of 3-[(*E*)-2-(4-{[(5-{[(5-{[(2-ammonioethyl)amino]carbonyl}-1-methyl-1*H*-pyrrol-3-yl)amino]carbonyl}-1-methyl-1*H*-pyrrol-3-yl)amino]carbonyl}phenyl)ethenyl]quinolinium bis(trifluoroacetate) **96**

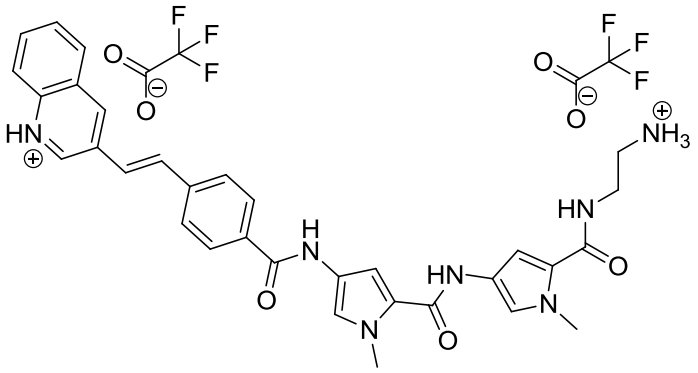

tert-Butyl 2-({[1-methyl-4-({[1-methyl-4-({4-[(*E*)-2-(3-quinolinyl)ethenyl]benzoyl}amino)-1*H*-pyrrol-2-yl]carbonyl}amino)-1*H*-pyrrol-2-yl]carbonyl}amino)ethylcarbamate **95** (20 mg, 0.03 mmol) was dissolved in DCM (2

mL) to which was added trifluoroacetic acid (1 mL) and this was heated to 40 ^{o}C for 1 h. After this, the solvents were removed under reduced pressure. The resultant residue was dissolved in DMF (1 mL) and subjected to HPLC purification to obtain the desired product (18 mg, 75 % yield).

HPLC Procedure

Flow rate: 6 mL/min.

Time (mins)	% Water (with 0.1% TFA)	% MeCN (with 0.1% TFA)
0	72	28
5	72	28
7	50	50
9	72	28

Retention time: 5.5 min.

Purity by HPLC: >95 %.

Melting Point: >230 ^{o}C.

IR: 3424, 2928, 2857, 1677, 1641, 1580, 1536, 1465, 1436, 1405, 1267, 1203, 1133.

δ_H NMR (DMSO): 10.35 (1H, s), 9.96 (1H, s), 9.26 (1H, d, *J* = 2.0), 8.55 (1H, d, *J* = 2.0), 8.11 (1H, t, *J* = 6.0), 7.98-8.04 (4H, m), 7.81 (2H, d, *J* = 9.0), 7.59-7.77 (8H, m), 7.34 (1H, d, *J* = 2.0), 7.19 (1H, d, *J* = 2.0), 7.12 (1H, d, *J* = 2.0), 6.98 (1H, d, *J* = 2.0), 3.87 (3H, s), 3.82 (3H, s), 3.14 (2H, q, *J* = 6.0), 2.92-2.97 (2H, m).

δ_C NMR: Insufficient material.

HR-MS-FAB: Found 562.2559 calculated for $C_{32}H_{32}O_3N_7^+$ (M+H) 562.2561.

Synthesis of 2-{[4-({4-[(*E*)-2-(3-methoxyphenyl)ethenyl]benzoyl}amino)-1-methyl-1*H*-pyrrol-2-yl]carbonyl}-1,1-dimethylhydrazinium trifluoroacetate **97**

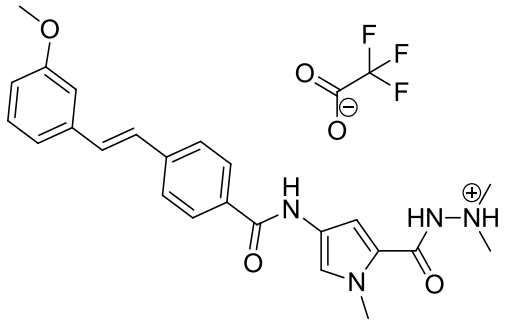

N',*N*',1-Trimethyl-4-nitro-1*H*-pyrrole-2-carbohydrazide **107** (30 mg, 0.14 mmol) was dissolved in MeOH (5 mL) and Pd/C-10 % was added under nitrogen (15 mg). This was subjected to hydrogenation for 3 h. After this the solution was filtered through kieselguhr, reduced under vacuum, and the resultant residue dissolved in DMF (1 mL, dry). 2,3,4,5,6-pentafluorophenyl 4-[(*E*)-2-(3-methoxyphenyl)ethenyl]benzoate **87** (60mg, 0.14 mmol) was then added to the solution and left for 16 h. The reaction mixture was subjected to HPLC purification to obtain the desired product (15 mg, 20 % yield).

HPLC Procedure

Flow rate: 6 mL/min.

Time (mins)	% Water (with 0.1% TFA)	% MeCN (with 0.1% TFA)
0	60	40
25	50	50
30	30	70
35	70	30
40	70	30

Retention time: 8.7 min.

Purity by HPLC: >96 %.

Melting Point: >230 ^{o}C.

IR: 3271, 2963, 2835, 1666, 1638, 1580, 1439, 1399, 1174, 1127.

δ_H NMR (DMSO): 10.32 (1H, s), 10.02 (1H, bs), 8.31 (1H, s), 7.96 (2H, d, *J* = 8.4), 7.74 (2H, d, *J* = 8.4), 7.31-7.38 (4H, m), 7.21-7.23 (2H, m), 7.03 (1H, bs), 6.89 (1H, dd, *J* = 8.0, *J* = 2.0), 3.85 (3H, s), 3.81 (3H, s), 2.80 (6H, s).

δ_C NMR: Insufficient material.

HR-MS-FAB: Found 419.2076 calculated for $C_{24}H_{27}O_3N_4^+$ (M+H) 419.2078.

Synthesis of 1-{[4-({4-[(*E*)-2-(3-methoxyphenyl)ethenyl]benzoyl}amino)-1-methyl-1*H*-pyrrol-2-yl]carbonyl}-4-methylpiperazin-4-ium trifluoroacetate **98**

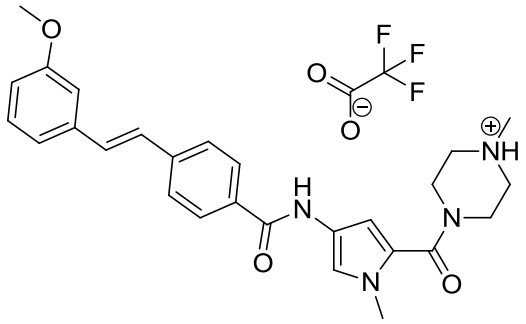

1-Methyl-4-[(1-methyl-4-nitro-1*H*-pyrrol-2-yl)carbonyl]piperazine **106** (40 mg, 0.16 mmol) was dissolved in MeOH (5 mL) and Pd/C-10 % was added under nitrogen (15 mg). This was subjected to hydrogenation for 3 h. After this the solution was filtered through Kieselguhr, reduced under vacuum, and the resultant residue dissolved in DMF (1 mL, dry). 2,3,4,5,6-Pentafluorophenyl 4-[(*E*)-2-(3-methoxyphenyl)ethenyl]benzoate **87** (60 mg, 0.14 mmol) was then added to the solution and left for 16 h. The reaction mixture was subjected to HPLC purification to obtain the desired product (12 mg, 15 % yield).

HPLC Procedure

Flow rate: 6 mL/min.

Time (mins)	% Water (with 0.1% TFA)	% MeCN (with 0.1% TFA)
0	66	34
25	50	50
30	30	70
35	70	30
40	70	30

Retention time: 10.5 min.

Purity by HPLC: >97 %.

Melting Point: >230 ^{o}C.

IR: 3425, 3274, 3026, 2940, 2836, 2722, 2614, 2481, 1677, 1638, 1606, 1575, 1464, 1445, 1413, 1399, 1258, 1201, 1125, 1048, 1026, 1015, 975.

δ_H NMR (DMSO): 10.29 (1H, s), 9.94 (1H, bs), 7.96 (2H, d, *J* = 8.4), 7.74 (2H, d, *J* = 8.4), 7.31-7.38 (4H, m), 7.21-7.23 (2H, m), 6.89 (1H, dd, *J* = 8.0, *J* = 2.0), 6.58 (1H, d, *J* = 1.6), 4.41-4.45 (2H, m), 3.81 (3H, s), 3.70 (3H, s), 3.46-3.49 (2H, m), 3.27-3.33 (2H, m), 3.07-3.10 (2H, m), 2.84 (3H, s).

δ_C NMR: Insufficient material.

HR-MS-FAB: Found 459.2386 calculated for $C_{27}H_{31}O_3N_4^+$ (M+H) 459.2391.

Synthesis of 1-({4-[({6-[(*E*)-2-(4-methoxyphenyl)ethenyl]-3-pyridiniumyl}carbonyl)amino]-1-methyl-1*H*-pyrrol-2-yl}carbonyl)-4-methylpiperazin-4-ium bis(trifluoroacetate) **99**

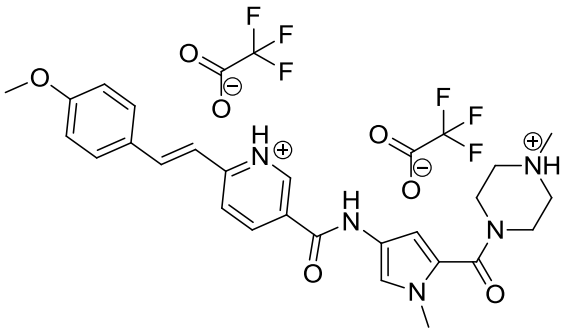

1-Methyl-4-[(1-methyl-4-nitro-1*H*-pyrrol-2-yl)carbonyl]piperazine **106** (40 mg, 0.16 mmol) was dissolved in MeOH (5 mL) and Pd/C-10 % was added under nitrogen (15 mg). This was subjected to hydrogenation for 3 h. After this the solution was filtered through kieselguhr, reduced under vacuum, and the resultant residue dissolved in DMF (1 mL, dry). 2,3,4,5,6-Pentafluorophenyl 6-[(E)-2-(4-methoxyphenyl)ethenyl]nicotinate **84** (30 mg, 0.14 mmol) was then added to the solution and left for 16 h. The reaction mixture was subjected to HPLC purification to obtain the desired product (16 mg, 17 % yield).

HPLC Procedure

Flow rate: 6 mL/min.

Time (mins)	% Water (with 0.1% TFA)	% MeCN (with 0.1% TFA)
0	70	30
25	50	50
30	30	70
35	70	30
40	70	30

Retention time: 10.4 min.

Purity by HPLC: >95 %.

Melting Point: >230 ^{o}C.

IR: 3262, 3114, 3051, 2939, 1698, 1668, 1591, 1573, 1446, 1192, 1127.

δ_H NMR (DMSO): 10.33 (1H, s), 9.78 (1H, bs), 9.04 (1H, d, *J* = 2.0), 8.24 (1H, dd, *J* = 8.0, *J* = 2.0), 7.63-7.76 (4H, m), 7.35 (1H, d, *J* = 1.6), 7.24 (1H, d, *J* = 16.0), 6.99 (2H, d, *J* = 8.0), 6.56 (1H, d, *J* = 1.6), 4.41-4.45 (2H, m), 3.79 (3H, s), 3.69 (3H, s), 3.46-3.49 (2H, m), 3.27-3.33 (2H, m), 3.07-3.10 (2H, m), 2.84 (3H, s).

δ_C NMR: Insufficient material.

HR-MS-FAB: Found 460.2340 calculated for $C_{26}H_{30}O_3N_5^+$ (M+H) 460.2343.

Synthesis of 3-((*E*)-2-{4-[({1-methyl-5-[(4-methylpiperazin-4-ium-1-yl)carbonyl]-1*H*-pyrrol-3-yl}amino)carbonyl]phenyl}ethenyl)quinolinium bis(trifluoroacetate) **100**

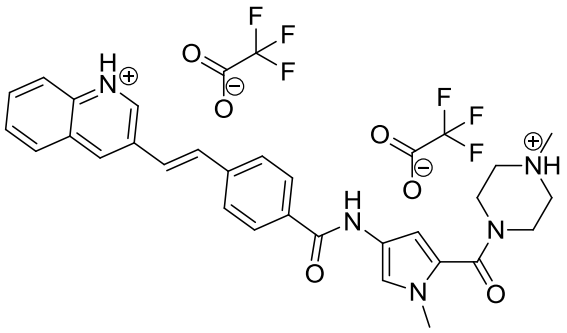

1-Methyl-4-[(1-methyl-4-nitro-1*H*-pyrrol-2-yl)carbonyl]piperazine **106** (40 mg, 0.16 mmol) was dissolved in MeOH (5 mL) and Pd/C-10 % was added under nitrogen (15 mg). This was subjected to hydrogenation for 3 h. After this the solution was filtered through kieselguhr, reduced under vacuum, and the resultant residue dissolved in DMF (1 mL, dry). 2,3,4,5,6-Pentafluorophenyl 4-[(*E*)-2-(3-quinolinyl)ethenyl]benzoate **88** (60 mg, 0.14 mmol) was then added to the solution and left for 16 h. The reaction mixture was subjected to HPLC purification to obtain the desired product (20 mg, 21 % yield).

HPLC Procedure

Flow rate: 6 mL/min.

Time (mins)	% Water (with 0.1% TFA)	% MeCN (with 0.1% TFA)
0	70	30
25	50	50
30	30	70
35	70	30
40	70	30

Retention time: 14.4 min.

Purity by HPLC: >95 %.

Melting Point: >230 ^{o}C.

IR: 3286, 2870, 2632, 2494, 1679, 1655, 1649, 1565, 1459, 1267, 1181.

δ_H NMR (DMSO): 10.34 (1H, s), 9.79 (1H, bs), 9.27 (1H, d, *J* = 2.0), 8.56 (1H, d, *J* = 2.0), 7.99-8.06 (4H, m), 7.75-7.84 (3H, m), 7.61-7.71 (3H, m), 7.39 (1H, d, *J* = 1.6), 6.59 (1H, d, *J* = 1.6), 4.43-4.47 (2H, m), 3.70 (3H, s), 3.48-3.51 (2H, m), 3.28-3.35 (2H, m), 3.08-3.13 (2H, m), 2.85 (3H, s).

δ_C NMR: Insufficient material.

HR-MS-FAB: Found 480.2395 calculated for $C_{29}H_{30}O_2N_5^+$ (M+H) 480.2394.

Synthesis of 4-[2-({[4-({4-[(*E*)-2-(3-methoxyphenyl)ethenyl]benzoyl}amino)-1-methyl-1*H*-pyrrol-2-yl]carbonyl}amino)ethyl]morpholin-4-ium trifluoroacetate **102**

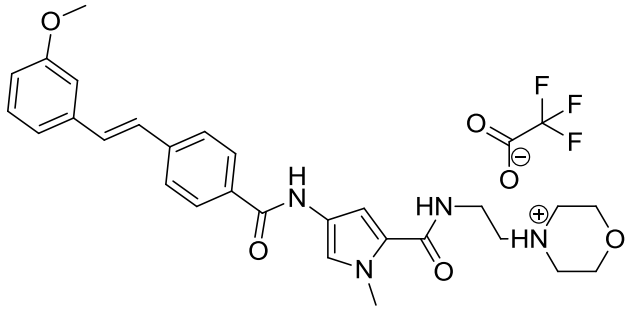

1-Methyl-*N*-[2-(4-morpholinyl)ethyl]-4-nitro-1*H*-pyrrole-2- carboxamide **67** (40 mg, 0.14 mmol) was dissolved in MeOH (5 mL) and Pd/C-10 % was added under nitrogen (15 mg). This was subjected to hydrogenation for 3 h. After this the solution was filtered through kieselguhr, reduced under vacuum, and the resultant residue dissolved in DMF (1 mL, dry). 2,3,4,5,6-Pentafluorophenyl 4-[(*E*)-2-(3-methoxyphenyl)ethenyl]benzoate **87** (60 mg, 0.14 mmol) was then added to the solution and left for 16 h. The reaction mixture was subjected to HPLC purification to obtain the desired product (40 mg, 47 % yield).

HPLC Procedure

Flow rate: 6 mL/min.

Time (mins)	% Water (with 0.1% TFA)	% MeCN (with 0.1% TFA)
Isocratic	50	50

Retention time: 4.3 min.

Purity by HPLC: >96 %.

Melting Point: >230 ^{o}C.

IR: 3424, 3026, 2928, 2857, 2604, 2483, 1675, 1650, 1606, 1577, 1559, 1536, 1464, 1437, 1402, 1274, 1202, 1131, 1045, 1015.

δ_H NMR (DMSO): 10.32 (1H, s), 9.72 (1H, bs), 8.27 (1H, m), 7.96 (2H, d, *J* = 8.4), 7.74 (2H, d, *J* = 8.4), 7.31-7.38 (4H, m), 7.21-7.23 (2H, m), 7.03 (1H, d, *J* = 1.6), 6.89 (1H, dd, *J* = 8.0, *J* = 2.0), 3.95-4.04 (2H, m), 3.86 (3H, s), 3.81 (3H, s), 3.63-3.67 (2H, m), 3.51-3.58 (4H, m), 3.26-3.29 (2H, m), 3.12-3.15 (2H, m).

δ_C NMR (DMSO): 163.2, 161.8, 159.6, 158.1, 139.8, 138.1, 133.2, 130.2, 129.7, 127.8, 126.3, 122.3, 122.2, 119.3, 118.8, 113.9, 111.7, 111.6, 104.9, 63.2, 55.6, 55.0, 51.3, 36.1, 33.2.

HR-MS-FAB: Found 489.2496 calculated for $C_{28}H_{33}O_4N_4^+$ (M+H) 489.2496.

Synthesis of 3-[(*E*)-2-(4-{[(1-methyl-5-{[(2-morpholin-4-ium-4-ylethyl)amino]carbonyl}-1*H*-pyrrol-3-yl)amino]carbonyl}phenyl)ethenyl]quinolinium bis(trifluoroacetate) **103**

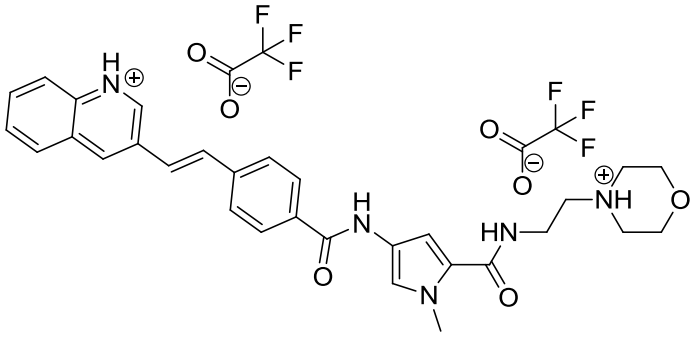

1-Methyl-*N*-[2-(4-morpholinyl)ethyl]-4-nitro-1*H*-pyrrole-2- carboxamide **67** (40 mg, 0.16 mmol) was dissolved in MeOH (5 mL) and Pd/C-10 % was added under nitrogen (15 mg). This was subjected to hydrogenation for 3 h. After this the solution was filtered through kieselguhr, reduced under vacuum, and the resultant residue dissolved in DMF (1 mL, dry). 2,3,4,5,6-Pentafluorophenyl 4-[(*E*)-2-(3-quinolinyl)ethenyl]benzoate **88** (69 mg, 0.16 mmol) was then added to the solution and left for 16 h. The reaction mixture was subjected to HPLC purification to obtain the desired product (21 mg, 20 % yield).

HPLC Procedure

Flow rate: 6 mL/min

Time (mins)	% Water (with 0.1% TFA)	% MeCN (with 0.1% TFA)
0	90	10
25	50	50
30	30	70
35	90	10
40	90	10

Retention time: 14.5 min

Purity by HPLC: >95 %.

Melting Point: >230 ^{o}C.

IR: 3414, 2956, 2925, 2851, 2186, 1677, 1651, 1632, 1603, 1533, 1438, 1403, 1389, 1337, 1282, 1204, 1133, 1016.

δ_H NMR (DMSO): 10.37 (1H, s), 9.52 (1H, br), 8.41 (1H, d, *J* = 8.5), 8.27 (1H, t, *J* = 8.0), 7.86-8.02 (8H, m), 7.77 (1H, m), 7.56-7.66 (2H, m), 7.31 (1H, d, *J* = 1.7), 7.04 (1H, d, *J* = 1.7), 3.98-4.03 (2H, m), 3.85 (3H, s), 3.62-3.68 (2H, m), 3.51-3.59 (4H, m), 3.27 (2H, m), 3.12 (2H, m).

δ_C NMR: Insufficient material.

HR-MS-FAB: Found 510.2499 calculated for $C_{30}H_{32}O_3N_5^+$ (M+H) 510.2500.

Synthesis of 1-methyl-4-[(1-methyl-4-nitro-1*H*-pyrrol-2-yl)carbonyl]piperazine **106**

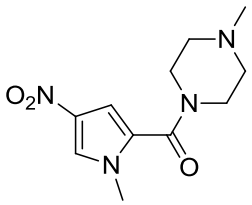

1-Methyl-4-nitro-1*H*-pyrrole-2-carboxylic acid **65** (100 mg, 0.64 mmol) was added to thionyl chloride (5 mL) and refluxed for 2 h. The excess thionyl chloride was then removed under reduced pressure and the residue dissolved in DCM (5 mL, dry); to this was added *N*-methyl piperazine **104** (128 mg, 0.64 mmol) and then left to stir for 3 h. The DCM was washed with water (2 × 5 mL) and the volume of the organic layer was reduced under reduced pressure and the resulting product was obtained by filtration (130 mg, 80 % yield).

Melting Point: >230 ^{o}C.

IR: 3375, 3176, 3025, 2496, 2427, 1625, 1588, 1547, 1508, 1461, 1427, 1299.

δ_H NMR (DMSO): 8.13 (1H, d, *J* = 2.0), 6.90 (1H, d, *J* = 2.0), 3.72 (3H, s), 3.60 (4H, m), 2.38 (4H, m), 2.23 (3H, s).

δ_C NMR (DMSO): 159.8, 134.0, 126.6, 126.3, 106.3, 54.3, 45.3, 35.9, 30.63

HR-MS-FAB: Found 253.1281 calculated for $C_{11}H_{17}N_4O_3^+$ (M+H) 253.1295.

Synthesis of *N*',*N*',1-trimethyl-4-nitro-1*H*-pyrrole-2-carbohydrazide **107**

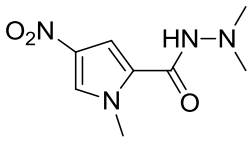

1-Methyl-4-nitro-1*H*-pyrrole-2-carboxylic acid **65** (50 mg, 0.32 mmol) was added to thionyl chloride (5 mL) and refluxed for 2 h. The excess thionyl chloride was then removed under reduced pressure and the residue dissolved in DCM (5 mL, dry), to this was added *N*,*N*-dimethyl hydrazine **105** (38.5 mg, 0.64 mmol) and then left to

stir for 3 h. The reaction mixture was washed with water (3 × 2 mL), organic layer was reduced in volume under reduced pressure and the resulting product was obtained by filtration (68 mg, 72 % yield).

Melting Point: >230 ^{o}C.

IR: 3180, 3139, 2835, 2792, 1677, 1651, 1560, 1532, 1494, 1310, 1075.

δ_H NMR (DMSO): 10.32 (1H, bs), 8.19 (1H, d, *J* = 2.0), 7.48 (1H, d, *J* = 2.0), 3.90 (3H, s), 2.74 (6H, s).

δ_C NMR (DMSO): 157.72, 133.8, 128.58, 123.95, 108.5, 46.35, 37.33.

HR-MS-FAB: Found 213.0988 calculated for $C_8H_{13}N_4O_3^+$ (M+H) 213.0982.

Synthesis of {amino[(2-{[5-({[5-({[3-(dimethylammonio)propyl]amino}carbonyl)-1-methyl-1*H*-pyrrol-3-yl]amino}carbonyl)-1-methyl-1*H*-pyrrol-3-yl]amino}-2-oxoethyl)amino]methylene}ammonium bis(trifluoroacetate) **108**

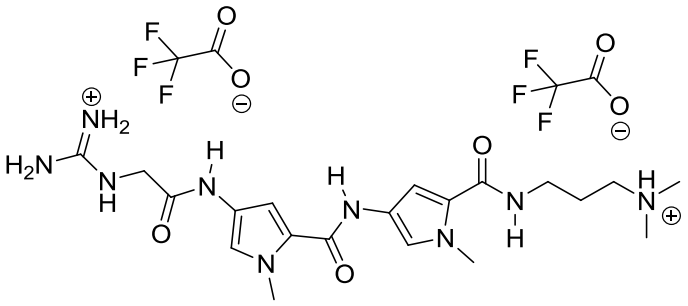

N-[5-({[3-(Dimethylamino)propyl]amino}carbonyl)-1-methyl-1*H*-pyrrol-3-yl]-1-methyl-4-nitro-1*H*-pyrrole-2-carboxamide **112** (30 mg, 0.080 mmol) was dissolved in MeOH (3 mL) to which was added Pd/C-10 % (30 mg) and this was subjected to hydrogenation for 2 h. After this, the reaction mixture was filtered through keisulghur and the solvent removed by rotary evaporation. The resulting residue was dissolved in DMF (1 mL) and to this was added guanidine acetic acid (9.4 mg, 0.080 mmol) and HBTU (64 mg, 0.17 mmol). This was left to stir overnight and subjected to HPLC purification directly to yield the desired material (13 mg, 24 %).

HPLC Procedure

Flow rate: 6 mL/min.

Time (mins)	% Water (with 0.1% TFA)	% MeCN (with 0.1% TFA)
0	92	8
20	70	30
30	50	50
35	90	10

Retention time: 12.1 min.

Purity by HPLC: >98%.

Melting Point: >230 ^{o}C.

IR: 3295, 2967, 2660, 2548, 1698, 1672, 1657, 1642, 1627, 1530, 1506, 1278, 1170.

δ_H NMR (DMSO): 9.84 (1H, s), 9.64 (1H, s), 9.27 (1H, bs), 8.15 (1H, t, *J* = 6.0), 7.16 (1H, d, *J* = 1.5), 6.93 (1H, d, *J* = 1.5), 6.88 (1H, d, *J* = 1.5), 6.66 (1H, d, *J* = 1.5), 3.87 (3H, s), 3.83 (3H, s), 3.24 (2H, m), 3.06 (4H, m), 2.77 (6H, s), 1.84 (2H, m).

δ_C NMR: Insufficient material.

HR-MS-FAB: Found 445.3037 calculated for $C_{20}H_{31}N_9O_3$ (M) 445.3028.

Synthesis of 4-{2-[({4-[({4-[({[amino(iminio)methyl]amino}acetyl)amino]-1-methyl-1*H*-pyrrol-2-yl}carbonyl)amino]-1-methyl-1*H*-pyrrol-2-yl}carbonyl)amino]ethyl}morpholin-4-ium bis(trifluoroacetate) **109**

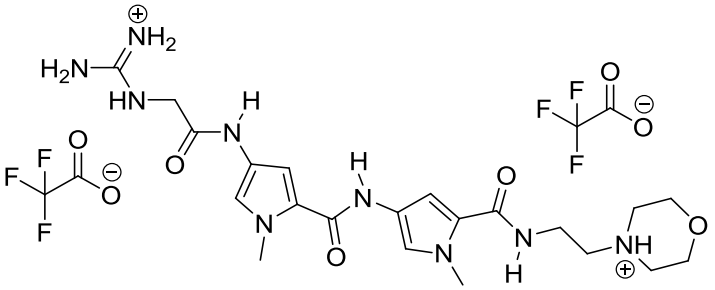

1-Methyl-*N*-[1-methyl-5-({[2-(4-morpholinyl)ethyl]amino}carbonyl)-1*H*-pyrrol-3-yl]-4-nitro-1*H*-pyrrole-2-carboxamide **68** (30 mg, 0.074 mmol) was dissolved in MeOH (3 mL) to which was added Pd/C-10 % (30 mg) and this was subjected to hydrogenation for 2 h. After this, the reaction mixture was filtered through keisulghur and the solvent removed by rotary evaporation. The resulting residue was dissolved in DMF (1 mL) and to this was added guanidine acetic acid (8.7 mg, 0.074 mmol) and HBTU (56 mg, 0.15 mmol). This was left to stir overnight and subjected to HPLC purification directly to yield the desired material (14 mg, 27%).

HPLC Procedure

Flow rate: 6 mL/min.

Time (mins)	% Water (with 0.1% TFA)	% MeCN (with 0.1% TFA)
0	90	10
25	70	30
30	50	50
35	90	10

Retention time: 14.9 min.

Purity by HPLC: >97 %.

Melting Point: >230 ^{o}C.

IR: 1686, 1673, 1656, 1638, 1563, 1545, 1524, 1507, 1457, 1438, 1198, 1181, 1144, 1110.

δ_H NMR (DMSO): 9.89 (1H, s), 9.82 (1H, br), 9.68 (1H, s), 8.24 (1H, m), 7.18 (1H, d, *J* = 1.5), 6.95 (1H, d, *J* = 1.5), 6.86 (1H, d, *J* = 1.5), 6.67 (1H, d, *J* = 1.5), 3.97-4.01 (2H, m), 3.86 (3H, s), 3.82 (3H, s), 3.62-3.68 (2H, m), 3.51-3.56 (4H, m), 3.26 (2H, m), 3.13 (2H, m), 3.02 (2H, s).

δ_C NMR: Insufficient material.

HR-MS-FAB: Found 473.2979 calculated for $C_{21}H_{31}N_9O_4$ (M) 473.2985.

Synthesis of 1-amino-3-[({4-[({4-[(4-methoxy-4-oxobutanoyl)amino]-1-methyl-1*H*-pyrrol-2-yl}carbonyl)amino]-1-methyl-1*H*-pyrrol-2-yl}carbonyl)amino]-1-propaniminium trifluoroacetate **121**

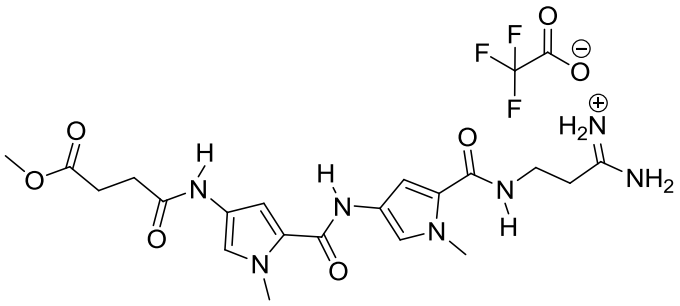

N-(5-{[(3-Amino-3-iminopropyl)amino]carbonyl}-1-methyl-1*H*-pyrrol-3-yl)-1-methyl-4-nitro-1*H*-pyrrole-2-carboxamide **111** (30 mg, 0.083 mmol) was dissolved in MeOH (3 mL) to which was added Pd/C-10 % (30 mg) and this was subjected to hydrogenation for 2 h. After this, the reaction mixture was filtered through keisulghur and the solvent removed by rotary evaporation. The resulting residue was dissolved in DMF (1 mL) and to this was added the monomethyl ester of succinic

acid (11 mg, 0.083 mmol) and HBTU (64 mg, 0.17 mmol). This was left to stir overnight and subjected to HPLC purification directly to yield the desired material (14 mg, 30 %).

HPLC Procedure

Flow rate: 6 mL/min.

Time (mins)	% Water (with 0.1% TFA)	% MeCN (with 0.1% TFA)
0	90	10
25	70	30
30	50	50
35	90	10

Retention time: 15.1 min.

Purity by HPLC: >95 %.

Melting Point: >230 ^{o}C.

IR: 3303, 3116, 2962, 1740, 1725, 1701, 1686, 1660, 1643, 1632, 1580, 1543, 1528, 1470, 1435, 1412, 1367, 1259, 1198, 1140.

δ_H NMR (DMSO): 9.89 (1H, s), 9.84 (1H, s), 8.88 (2H, s), 8.42 (2H, s), 8.17 (1H, t, *J* = 6.0), 7.14 (1H, d, *J* = 1.5), 7.11 (1H, d, *J* = 1.5), 6.93 (1H, bs), 6.87 (1H, d, *J* = 1.5), 3.81 (6H, m), 3.58 (3H, s), 3.48 (2H, m), 2.57-2.60 (2H, m), 2.51-2.54 (4H, m).

δ_C NMR: Insufficient material.

HR-MS-FAB: Found 446.2150 calculated for $C_{20}H_{28}O_5N_7^+$ (M+H) 446.2146.

Synthesis of 1-amino-3-[({4-[({4-[(3-carboxypropanoyl)amino]-1-methyl-1*H*-pyrrol-2-yl}carbonyl)amino]-1-methyl-1*H*-pyrrol-2-yl}carbonyl)amino]-1-propaniminium trifluoroacetate **122**

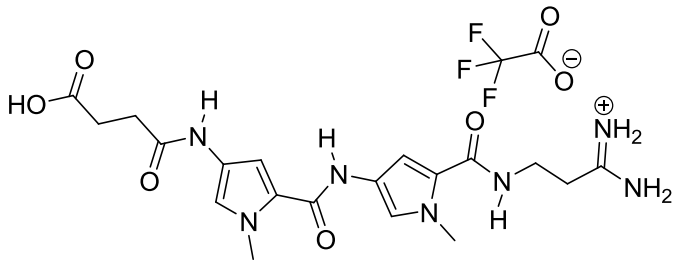

1-Amino-3-[({4-[({4-[(4-methoxy-4-oxobutanoyl)amino]-1-methyl-1*H*-pyrrol-2-yl}carbonyl)amino]-1-methyl-1*H*-pyrrol-2-yl}carbonyl)amino]-1-propaniminium trifluoroacetate **121** (8 mg, 0.014 mmol) was dissolved in LiOH solution (20 mg, 0.5 mL water) and left stirring for 48 h. The resulting reaction mixture was subjected to HPLC purification directly to yield the desired material (5 mg, 64 %).

HPLC Procedure

Flow rate: 6 mL/min.

Time (mins)	% Water (with 0.1% TFA)	% MeCN (with 0.1% TFA)
0	90	10
25	70	30
30	50	50
35	90	10

Retention time: 14.5 min.

Purity by HPLC: >95 %.

Melting Point: >230 ^{o}C.

IR: 3303, 3064, 2945, 1740, 1705, 1686, 1677, 1662, 1656, 1645, 1634, 1625, 1582, 1573, 1556, 1553, 1405, 1276, 1202, 1185.

δ_H NMR (DMSO): 12.07 (1H, bs), 9.83-9.86 (2H, m), 8.89 (2H, s), 8.44 (2H, s), 8.18 (1H, t, *J* = 6.0), 7.16 (1H, d, *J* = 1.5), 7.12 (1H, d, *J* = 1.5), 6.95 (1H, d, *J* = 1.5), 6.89 (1H, d, *J* = 1.5), 3.83 (6H, m), 3.49 (2H, m), 2.57-2.60 (2H, m), 2.51-2.54 (4H, m).

δ_C NMR: Insufficient material.

HR-MS-FAB: Found 432.1992 calculated for $C_{19}H_{26}O_5N_7^+$ (M+H) 432.1990.

Synthesis of 1-amino-3-{[(4-{[(4-{[4-(methoxycarbonyl)benzoyl]amino}-1-methyl-1*H*-pyrrol-2-yl)carbonyl]amino}-1-methyl-1*H*-pyrrol-2-yl)carbonyl]amino}-1-propaniminium trifluoroacetate **123**

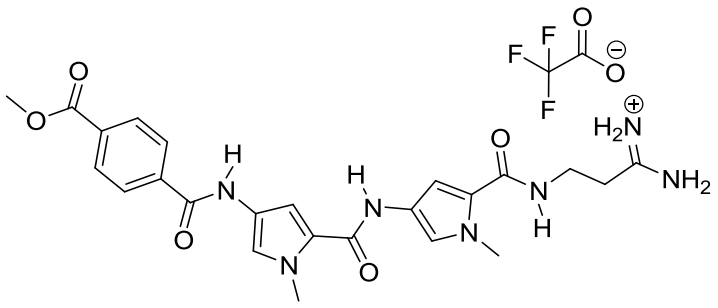

N-(5-{[(3-Amino-3-iminopropyl)amino]carbonyl}-1-methyl-1*H*-pyrrol-3-yl)-1-methyl-4-nitro-1*H*-pyrrole-2-carboxamide **111** (30 mg, 0.083 mmol) was dissolved in MeOH (3 mL) to which was added Pd/C-10 % (30 mg) and this was subjected to hydrogenation for 2 h. After this, the reaction mixture was filtered through keisulghur and the solvent removed by rotary evaporation. The resulting residue was dissolved in DMF (1 mL) and to this was added the monomethyl ester of terephthalic acid (15 mg, 0.083 mmol) and HBTU (64 mg, 0.17 mmol). This was left to stir overnight and subjected to HPLC purification directly to yield the desired material (17 mg, 34 %).

HPLC Procedure

Flow rate: 6 mL/min.

Time (mins)	% Water (with 0.1% TFA)	% MeCN (with 0.1% TFA)
0	90	10
25	80	20
30	50	50
35	90	10

Retention time: 20.8 min.

Purity by HPLC: >98 %.

Melting Point: >230 ^{o}C.

IR: 3299, 3103, 2943, 1707, 1688, 1675, 1660, 1645, 1634, 1623, 1580, 1565, 1539, 1530, 1507, 1494, 1440, 1435, 1407, 1394, 1280, 1187, 1121, 1058, 1015.

δ_H NMR (DMSO): 10.53 (1H, s), 9.95 (1H, s), 8.89 (2H, s), 8.43 (2H, s), 8.18 (1H, m), 8.04-8.10 (4H, m), 7.33 (1H, d, *J* = 1.5), 7.17 (1H, d, *J* = 1.5), 7.11 (1H, d, *J* = 1.5), 6.95 (1H, d, *J* = 1.5), 3.89 (3H, s), 3.87 (3H, s), 3.81 (3H, s), 3.46-3.52 (2H, m), 2.58-2.61 (2H, m).

δ_C NMR: Insufficient material.

HR-MS-FAB: Found 494.2148 calculated for $C_{24}H_{28}O_5N_7^+$ (M+H) 494.2146.

Synthesis of 1-amino-3-[({4-[({4-[(4-carboxybenzoyl)amino]-1-methyl-1*H*-pyrrol-2-yl}carbonyl)amino]-1-methyl-1*H*-pyrrol-2-yl}carbonyl)amino]-1-propaniminium trifluoroacetate **124**

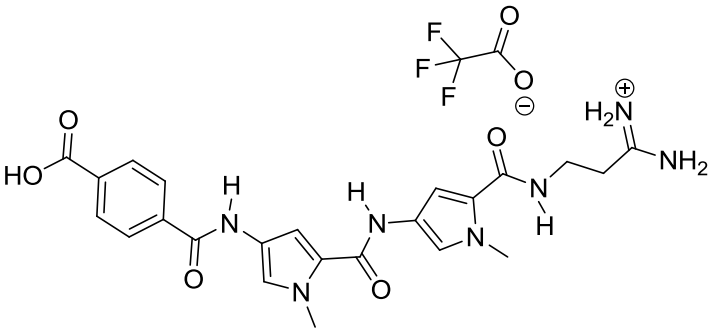

1-Amino-3-{[(4-{[(4-{[4-(methoxycarbonyl)benzoyl]amino}-1-methyl-1*H*-pyrrol-2-yl)carbonyl]amino}-1-methyl-1*H*-pyrrol-2-yl)carbonyl]amino}-1-propaniminium trifluoroacetate **123** (9 mg, 0.015 mmol) was dissolved in LiOH solution (20 mg, 0.5 mL water) and left stirring for 48 h. The resulting reaction mixture was subjected to HPLC purification directly to yield the desired material (6 mg, 68 %).

HPLC Procedure

Flow rate: 6 mL/min.

Time (mins)	% Water (with 0.1% TFA)	% MeCN (with 0.1% TFA)
0	90	10
25	80	20
30	50	50
35	90	10

Retention time: 18.2 min.

Purity by HPLC: >96 %.

Melting Point: >230 ^{o}C.

IR: 3305, 3193, 2939, 1703, 1668, 1653, 1634, 1576, 1545, 1515, 1477, 1464, 1435, 1405, 1289, 1261, 1203, 1131, 1114, 1062, 1023.

δ_H NMR (DMSO): 13.20 (1H, bs), 10.50 (1H, s), 9.94 (1H, s), 8.03-8.09 (4H, m), 7.98 (1H, m), 7.35 (1H, s, *J* = 1.5), 7.33 (2H, m), 7.21 (1H, d, *J* = 1.5), 7.10 (1H, ds, *J* = 1.5), 6.84 (1H, d, *J* = 1.5), 6.81 (2H, m), 3.88 (3H, s), 3.81 (3H, s), 3.34-3.38 (2H, m), 2.31-2.35 (2H, m).

δ_C NMR: Insufficient material.

HR-MS-FAB: Found 480.1995 calculated for $C_{23}H_{26}O_5N_7^+$ (M+H) 480.1990.

Synthesis of 3-[({4-[({4-[(4-methoxy-4-oxobutanoyl)amino]-1-methyl-1*H*-pyrrol-2-yl}carbonyl)amino]-1-methyl-1*H*-pyrrol-2-yl}carbonyl)amino]-*N*,*N*-dimethyl-1-propanaminium trifluoroacetate **125**

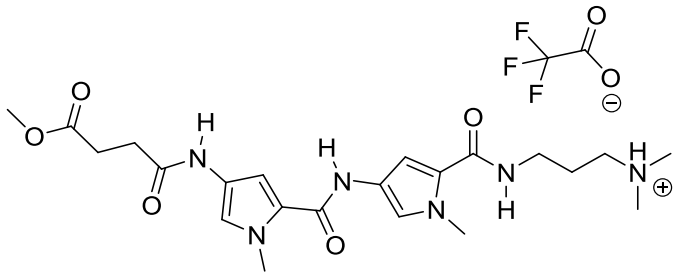

N-[5-({[3-(Dimethylamino)propyl]amino}carbonyl)-1-methyl-1*H*-pyrrol-3-yl]-1-methyl-4-nitro-1*H*-pyrrole-2-carboxamide **112** (30 mg, 0.080 mmol) was dissolved in MeOH (3 mL) to which was added Pd/C-10 % (30 mg) and this was subjected to hydrogenation for 2 h. After this, the reaction mixture was filtered through keisulghur and the solvent removed by rotary evaporation. The resulting residue was dissolved in DMF (1 mL) and to this was added the monomethyl ester of succinic acid (10.6 mg, 0.080 mmol) and HBTU (64 mg, 0.17 mmol). This was left to stir overnight and subjected to HPLC purification directly to yield the desired material (15 mg, 32 %).

HPLC Procedure

Flow rate: 6 mL/min.

Time (mins)	% Water (with 0.1% TFA)	% MeCN (with 0.1% TFA)
0	90	10
25	70	30
30	50	50
35	90	10

Retention time: 15.9 min.

Purity by HPLC: >97 %.

Melting Point: >230 ^{o}C.

IR: 3279, 2958, 2686, 2563, 1720, 1696, 1681, 1651, 1647, 1638, 1580, 1560, 1206, 1133.

δ_H NMR (DMSO): 9.86 (1H, s), 9.84 (1H, s), 9.21 (1H, bs), 8.14 (1H, t, *J* = 6.0), 7.16 (1H, d, *J* = 1.5), 7.12 (1H, d, *J* = 1.5), 6.93 (1H, bs), 6.88 (1H, d, *J* = 1.5), 3.81 (6H, m), 3.60 (3H, s), 3.24 (2H, m), 3.08 (2H, m), 2.79 (6H, s), 2.54-2.59 (4H, m), 1.84 (2H, m).

δ_C NMR: Insufficient material.

HR-MS-FAB: Found 461.2506 calculated for $C_{22}H_{33}O_5N_6^+$ (M+H) 461.2507.

Synthesis of 3-[({4-[({4-[(3-carboxypropanoyl)amino]-1-methyl-1*H*-pyrrol-2-yl}carbonyl)amino]-1-methyl-1*H*-pyrrol-2-yl}carbonyl)amino]-*N*,*N*-dimethyl-1-propanaminium trifluoroacetate **126**

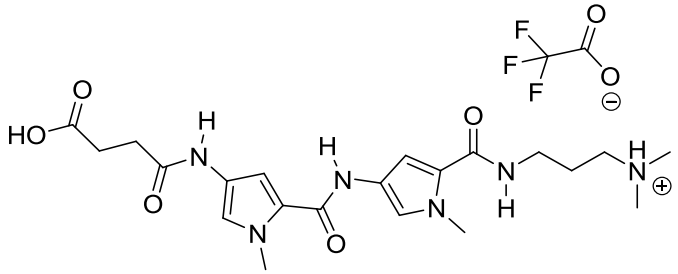

3-[({4-[({4-[(4-Methoxy-4-oxobutanoyl)amino]-1-methyl-1*H*-pyrrol-2-yl}carbonyl)amino]-1-methyl-1*H*-pyrrol-2-yl}carbonyl)amino]-*N*,*N*-dimethyl-1-propanaminium trifluoroacetate **125** (8 mg, 0.014 mmol) was dissolved in LiOH solution (20 mg, 0.5 mL water) and left stirring for 48 h. The resulting reaction mixture was subjected to HPLC purification directly to yield the desired material (4.5 mg, 58 %).

HPLC Procedure

Flow rate: 6 mL/min.

Time (mins)	% Water (with 0.1% TFA)	% MeCN (with 0.1% TFA)
0	90	10
25	70	30
30	50	50
35	90	10

Retention time: 15.1 min.

Purity by HPLC: >98 %.

Melting Point: >230 ^{o}C.

IR: 3256, 2956, 2660, 2566, 1720, 1698, 1685, 1647, 1636, 1575, 1534, 1414, 1282, 1196, 1109.

δ_H NMR (DMSO): 12.08 (1H, s), 9.83 (2H, bs), 9.21 (1H, bs), 8.14 (1H, t, *J* = 6.0), 7.16 (1H, d, *J* = 1.5), 7.12 (1H, d, *J* = 1.5), 6.93 (1H, bs), 6.88 (1H, d, *J* = 1.5), 3.83 (6H, m), 3.24 (2H, m), 3.07 (2H, m), 2.79 (6H, s), 2.54-2.59 (4H, m), 1.84 (2H, m).

δ_C NMR: Insufficient material.

HR-MS-FAB: Found 447.2351 calculated for $C_{21}H_{31}O_5N_6^+$ (M+H) 447.2350.

Synthesis of 3-{[(4-{[(4-{[4-(methoxycarbonyl)benzoyl]amino}-1-methyl-1*H*-pyrrol-2-yl)carbonyl]amino}-1-methyl-1*H*-pyrrol-2-yl)carbonyl]amino}-*N*,*N*-dimethyl-1-propanaminium trifluoroacetate **127**

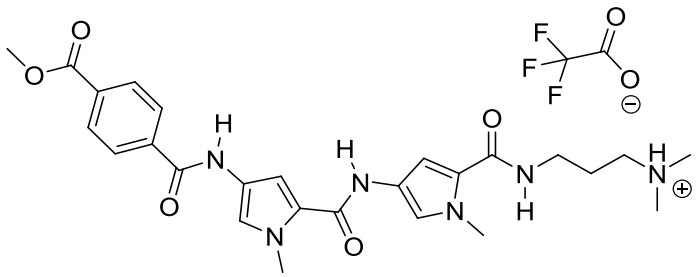

N-[5-({[3-(Dimethylamino)propyl]amino}carbonyl)-1-methyl-1*H*-pyrrol-3-yl]-1-methyl-4-nitro-1*H*-pyrrole-2-carboxamide **112** (30 mg, 0.080 mmol) was dissolved in MeOH (3 mL) to which was added Pd/C-10 % (30 mg) and this was subjected to hydrogenation for 2 h. After this, the reaction mixture was filtered through keisulghur and the solvent removed by rotary evaporation. The resulting residue was dissolved in DMF (1 mL) and to this was added the monomethyl ester of terephthalic acid (14 mg, 0.080 mmol) and HBTU (64 mg, 0.17 mmol). This was left to stir overnight and subjected to HPLC purification directly to yield the desired material (17 mg, 32 %).

HPLC Procedure

Flow rate: 6 mL/min.

Time (mins)	% Water (with 0.1% TFA)	% MeCN (with 0.1% TFA)
0	90	10
20	70	30
25	50	50
30	90	10

Retention time: 22.1 min.

Purity by HPLC: >95 %.

Melting Point: >230 ^{o}C.

IR: 3323, 2945, 2880, 2658, 2499, 1701, 1683, 1668, 1629, 1619, 1558, 1496, 1196, 1135.

δ_H NMR (DMSO): 10.53 (1H, s), 9.96 (1H, s), 9.18 (1H, m), 8.15 (1H, m), 8.04-8.10 (4H, m), 7.34 (1H, d, *J* = 1.5), 7.18 (1H, d, *J* = 1.5), 7.12 (1H, d, *J* = 1.5), 6.96 (1H, d, *J* = 1.5), 3.91 (3H, s), 3.89 (3H, s), 3.83 (3H, s), 3.24 (2H, m), 3.08 (2H, m), 2.80 (6H, s), 1.85 (2H, m).

δ_C NMR: Insufficient material.

HR-MS-FAB: Found 509.2511 calculated for $C_{26}H_{33}O_5N_6^+$ (M+H) 509.2507.

Synthesis of 3-[({4-[({4-[(4-carboxybenzoyl)amino]-1-methyl-1*H*-pyrrol-2-yl}carbonyl)amino]-1-methyl-1*H*-pyrrol-2-yl}carbonyl)amino]-*N*,*N*-dimethyl-1-propanaminium trifluoroacetate **128**

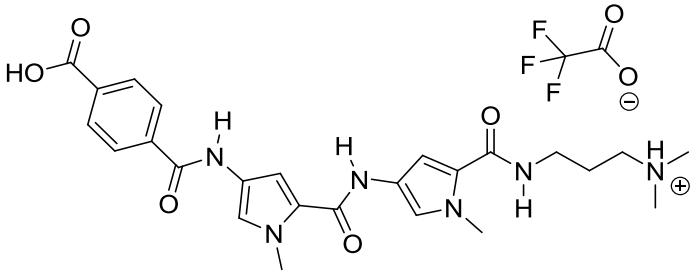

3-{[(4-{[(4-{[4-(Methoxycarbonyl)benzoyl]amino}-1-methyl-1*H*-pyrrol-2-yl)carbonyl]amino}-1-methyl-1*H*-pyrrol-2-yl)carbonyl]amino}-*N*,*N*-dimethyl-1-propanaminium trifluoroacetate **127** (10 mg, 0.016 mmol) was dissolved in LiOH solution (20 mg, 0.5 mL water) and left stirring for 48 h. The resulting reaction mixture was subjected to HPLC purification directly to yield the desired material (5 mg, 51 %).

HPLC Procedure

Flow rate: 6 mL/min.

Time (mins)	% Water (with 0.1% TFA)	% MeCN (with 0.1% TFA)
0	90	10
20	70	30
25	50	50
30	90	10

Retention time: 20.7 min.

Purity by HPLC: >95 %.

Melting Point: >230 ^{o}C.

IR: 3327, 2956, 2660, 2553, 1733, 1701, 1687, 1575, 1541, 1468, 1407, 1206, 1114.

δ_H NMR (DMSO): 10.50 (1H, s), 9.95 (1H, s), 9.18 (1H, m), 8.15 (1H, m), 8.03-8.09 (4H, m), 7.34 (1H, d, *J* = 1.5), 7.19 (1H, d, *J* = 1.5), 7.12 (1H, d, *J* = 1.5), 6.95 (1H, d, *J* = 1.5), 3.89 (3H, s), 3.83 (3H, s), 3.25 (2H, m), 3.08 (2H, m), 2.79 (6H, s), 1.85 (2H, m).

δ_C NMR: Insufficient material.

HR-MS-FAB: Found 495.2350 calculated for $C_{25}H_{31}O_5N_6^+$ (M+H) 495.2324.

Synthesis of 4-{2-[({4-[({4-[(4-methoxy-4-oxobutanoyl)amino]-1-methyl-1*H*-pyrrol-2-yl}carbonyl)amino]-1-methyl-1*H*-pyrrol-2-yl}carbonyl)amino]ethyl}morpholin-4-ium trifluoroacetate **129**

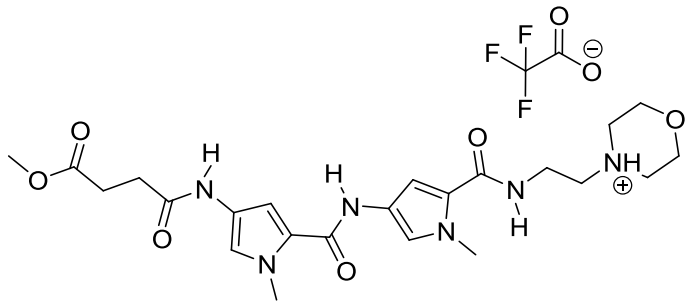

1-Methyl-*N*-[1-methyl-5-({[2-(4-morpholinyl)ethyl]amino}carbonyl)-1*H*-pyrrol-3-yl]-4-nitro-1*H*-pyrrole-2-carboxamide **68** (30 mg, 0.074 mmol) was dissolved in MeOH (3 mL) to which was added Pd/C-10 % (30 mg) and this was subjected to hydrogenation for 2 h. After this, the reaction mixture was filtered through keisulghur and the solvent removed by rotary evaporation. The resulting residue was dissolved in DMF (1 mL) and to this was added the monomethyl ester of succinic acid (9.8 mg, 0.074 mmol) and HBTU (56 mg, 0.15 mmol). This was left to stir overnight and subjected to HPLC purification directly to yield the desired material (16 mg, 36 %).

HPLC Procedure

Flow rate: 6 mL/min.

Time (mins)	% Water (with 0.1% TFA)	% MeCN (with 0.1% TFA)
0	90	10
20	70	30
25	50	50
30	90	10

Retention time: 17.5 min.

Purity by HPLC: >95 %.

Melting Point: >230 ^{o}C.

IR: 3278, 2952, 2879, 1720, 1658, 1645, 1584, 1526, 1468, 1433, 1405, 1373, 1263, 1200, 1174, 1127, 1101.

δ_H NMR (DMSO): 9.86 (1H, s), 9.48 (1H, br), 8.20 (1H, m), 7.17 (1H, d, *J* = 1.5), 7.11 (1H, d, *J* = 1.5), 6.98 (1H, bs), 6.88 (1H, d, *J* = 1.5), 3.98-4.02 (2H, m), 3.86 (6H, m), 3.62-3.68 (2H, m), 3.583 (3H, s), 3.52-3.56 (4H, m), 3.26 (2H, m), 3.12 (2H, m), 2.51-2.54 (4H, m).

δ_C NMR: Insufficient material.

HR-MS-FAB: Found 489.2450 calculated for $C_{23}H_{33}O_6N_6^+$ (M+H) 489.2456.

Synthesis of 4-{2-[({4-[({4-[(3-carboxypropanoyl)amino]-1-methyl-1*H*-pyrrol-2-yl}carbonyl)amino]-1-methyl-1*H*-pyrrol-2-yl}carbonyl)amino]ethyl}morpholin-4-ium trifluoroacetate **130**

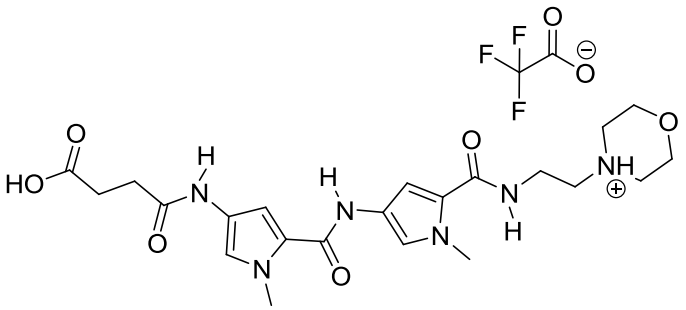

4-{2-[({4-[({4-[(4-Methoxy-4-oxobutanoyl)amino]-1-methyl-1*H*-pyrrol-2-yl}carbonyl)amino]-1-methyl-1*H*-pyrrol-2-yl}carbonyl)amino]ethyl}morpholin-4-ium trifluoroacetate **129** (8 mg, 0.013 mmol) was dissolved in LiOH solution (20 mg, 0.5 mL water) and left stirring for 48 h. The resulting reaction mixture was subjected to HPLC purification directly to yield the desired material (4.5 mg, 58 %).

HPLC Procedure

Flow rate: 6 mL/min.

Time (mins)	% Water (with 0.1% TFA)	% MeCN (with 0.1% TFA)
0	90	10
20	70	30
25	50	50
30	90	10

Retention time: 16.1 min.

Purity by HPLC: >96 %.

Melting Point: >230 ^{o}C.

IR: 3265, 3129, 2939, 2613, 2497, 1700, 1688, 1657, 1645, 1638, 1627, 1582, 1539, 1511, 1127.

δ_H NMR (DMSO): 12.08 (1H, bs), 9.87 (1H, s), 9.83 (1H, s), 9.56 (1H, bs), 8.20 (1H, m), 7.17 (1H, s), 7.11 (1H, d, *J* = 1.5), 6.98 (1H, s), 6.88 (1H, s), 3.98-4.02 (2H, m), 3.81 (3H, m), 3.62-3.68 (2H, m), 3.583 (3H, s), 3.52-3.56 (4H, m), 3.24 (2H, m), 3.13 (2H, m), 2.51-2.54 (4H, m).

δ_C NMR: Insufficient material.

HR-MS-FAB: Found 475.2300 calculated for $C_{22}H_{31}O_6N_6^+$ (M+H) 475.2300.

Synthesis of 4-(2-{[(4-{[(4-{[4-(methoxycarbonyl)benzoyl]amino}-1-methyl-1*H*-pyrrol-2-yl)carbonyl]amino}-1-methyl-1*H*-pyrrol-2-yl)carbonyl]amino}ethyl)morpholin-4-ium trifluoroacetate **131**

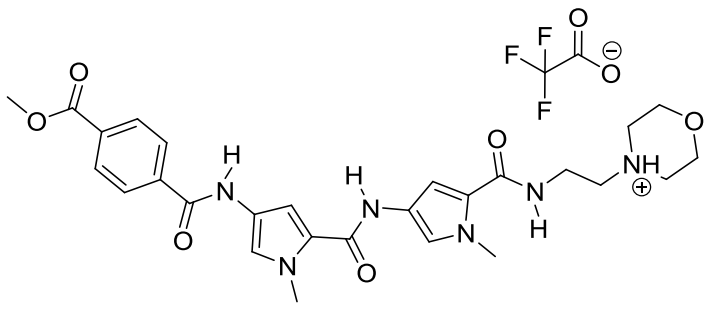

1-Methyl-*N*-[1-methyl-5-({[2-(4-morpholinyl)ethyl]amino}carbonyl)-1*H*-pyrrol-3-yl]-4-nitro-1*H*-pyrrole-2-carboxamide **68** (30 mg, 0.074 mmol) was dissolved in MeOH (3 mL) to which was added Pd/C-10 % (30 mg) and this was subjected to hydrogenation for 2 h. After this, the reaction mixture was filtered through keisulghur and the solvent removed by rotary evaporation. The resulting residue was dissolved in DMF (1 mL) and to this was added the monomethyl ester of terephthalic acid (13.3 mg, 0.074 mmol) and HBTU (56 mg, 0.15 mmol). This was left to stir overnight and subjected to HPLC purification directly to yield the desired material (14 mg, 29%).

HPLC Procedure

Flow rate: 6 mL/min.

Time (mins)	% Water (with 0.1% TFA)	% MeCN (with 0.1% TFA)
0	90	10
20	70	30
25	50	50
30	90	10

Retention time: 22.0 min.

Purity by HPLC: >95 %.

Melting Point: >230 ^{o}C.

IR: 3299, 2965, 1675, 1645, 1623, 1580, 1533, 1468, 1433, 1407, 1280, 1198, 1183, 1129, 1092, 1015, 1011.

δ_H NMR (DMSO): 10.53 (1H, s), 9.98 (1H, s), 9.50 (1H, bs), 8.22 (1H, m), 8.04-8.10 (4H, m), 7.33 (1H, s), 7.20 (1H, s), 7.11 (1H, s), 7.00 (1H, s), 3.98-4.02 (2H, m), 3.89 (3H, s), 3.87 (3H, s), 3.83 (3H, s), 3.62-3.68 (2H, m), 3.52-3.56 (4H, m), 3.24 (2H, m), 3.13 (2H, m).

δ_C NMR: Insufficient material.

HR-MS-FAB: Found 537.2450 calculated for $C_{27}H_{33}O_6N_6^+$ (M+H) 537.2456.

Synthesis of 4-{2-[({4-[({4-[(4-carboxybenzoyl)amino]-1-methyl-1*H*-pyrrol-2-yl}carbonyl)amino]-1-methyl-1*H*-pyrrol-2-yl}carbonyl)amino]ethyl}morpholin-4-ium trifluoroacetate **132**

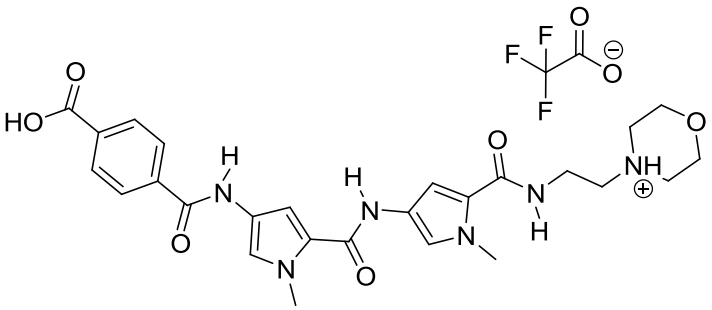

4-(2-{[(4-{[(4-{[4-(Methoxycarbonyl)benzoyl]amino}-1-methyl-1*H*-pyrrol-2-yl)carbonyl]amino}-1-methyl-1*H*-pyrrol-2-yl)carbonyl]amino}ethyl)morpholin-4-ium trifluoroacetate **131** (8 mg, 0.012 mmol) was dissolved in LiOH solution (20 mg, 0.5 mL water) and left stirring for 48 h. The resulting reaction mixture was subjected to HPLC purification directly to yield the desired material (5 mg, 64 %).

HPLC Procedure

Flow rate: 6 mL/min.

Time (mins)	% Water (with 0.1% TFA)	% MeCN (with 0.1% TFA)
0	90	10
20	70	30
25	50	50
30	90	10

Retention time: 20.6 min.

Purity by HPLC: >97 %.

Melting Point: >230 ^{o}C.

IR: 3223, 2945, 2889, 1675, 1643, 1584, 1530, 1464, 1438, 1410, 1263, 1177, 1129, 1092, 1052, 1009.

δ_H NMR (DMSO): 13.21 (1H, s), 10.49 (1H, s), 9.98 (1H, s), 9.49 (1H, bs), 8.22 (1H, m), 8.02-8.07 (4H, m), 7.33 (1H, s), 7.20 (1H, s), 7.12 (1H, s), 7.00 (1H, s), 3.99-4.03 (2H, m), 3.88 (3H, s), 3.83 (3H, s), 3.62-3.68 (2H, m), 3.52-3.56 (4H, m), 3.23 (2H, m), 3.12 (2H, m).

δ_C NMR: Insufficient material.

HR-MS-FAB: Found 523.2294 calculated for $C_{26}H_{31}O_6N_6^+$ (M+H) 523.2300.

Synthesis of 4-{2-[({4-[({4-[(4-{[iminio(3-methoxyphenyl)methyl]amino}benzoyl)amino]-1-methyl-1*H*-pyrrol-2-yl}carbonyl)amino]-1-methyl-1*H*-pyrrol-2-yl}carbonyl)amino]ethyl}morpholin-4-ium bis(trifluoroacetate) **135**

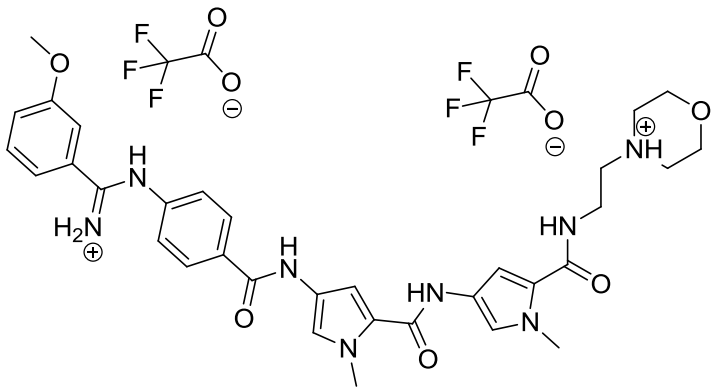

1-Methyl-*N*-[1-methyl-5-({[2-(4-morpholinyl)ethyl]amino}carbonyl)-1*H*-pyrrol-3-yl]-4-nitro-1*H*-pyrrole-2-carboxamide **68** (28 mg, 0.080 mmol) was dissolved in MeOH (3 mL) to which was added Pd/C-10 % (30 mg) and this was subjected to hydrogenation for 2 h. After this, the reaction mixture was filtered through keisulghur and the solvent removed by rotary evaporation. The resulting residue was dissolved in DMF (1 mL) and to this was added 4-{[imino(3-methoxyphenyl)methyl]amino}benzoic acid **146** (22 mg, 0.080 mmol) and HBTU

(64 mg, 0.17 mmol). This was left to stir overnight and subjected to HPLC purification directly to yield the desired material (17 mg, 27 %).

HPLC Procedure

Flow rate: 6 mL/min.

Time (mins)	% Water (with 0.1% TFA)	% MeCN (with 0.1% TFA)
0	90	10
25	70	30
30	50	50
35	90	10

Retention time: 12.5 min.

Purity by HPLC: >97 %.

Melting Point: >230 ^{o}C.

IR: 3258, 2936, 2660, 2466, 1562, 1524, 1511, 1148, 1032, 969.

δ_H NMR (DMSO): 11.56 (1H, s), 10.46 (1H, s), 9.92-9.95 (2H, m), 9.65 (1H, bs), 9.20 (1H, bs), 8.13-8.22 (2H, m), 7.45-7.72 (5H, m), 7.35 (2H, m), 7.16 (1H, d, *J* = 1.5), 7.12 (1H, s), 6.96 (1H, d, *J* = 1.5), 3.99-4.02 (2H, m), 3.88 (6H, s), 3.83 (3H, s), 3.62-3.67 (2H, m), 3.51-3.56 (4H, m), 3.27 (2H, m), 3.13 (2H, m).

δ_C NMR: Insufficient material.

HR-MS-FAB: Found 627.3047 calculated for $C_{33}H_{39}O_5N_8^+$ (M+H) 627.3038.

Synthesis of 5-({[5-({[4-({[3-(dimethylammonio)propyl]amino}carbonyl)-5-isopentyl-1,3-thiazol-2-yl]amino}carbonyl)-1-methyl-1*H*-pyrrol-3-yl]amino}carbonyl)-2-[(*E*)-2-(4-methoxyphenyl)ethenyl]pyridinium bis(trifluoroacetate) **136**

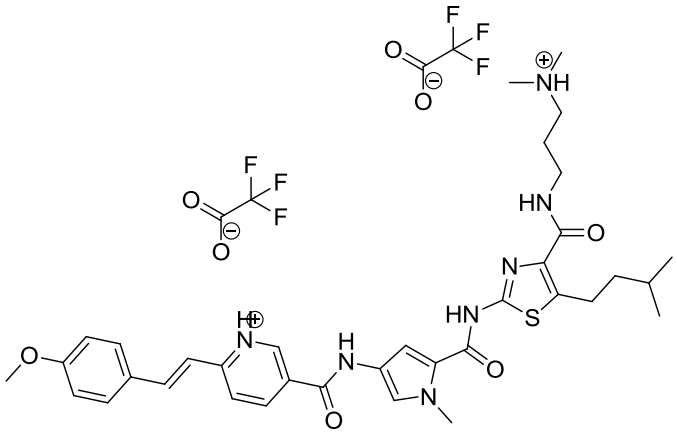

N-[3-(Dimethylamino)propyl]-5-isopentyl-2-{[(1-methyl-4-nitro-1*H*-pyrrol-2-yl)carbonyl]amino}-1,3-thiazole-4-carboxamide **144** (30 mg, 0.067 mmol) was dissolved in MeOH (3 mL) to which was added Pd/C-10 % (30 mg) and this was subjected to hydrogenation for 2 h. After this, the reaction mixture was filtered through keisulghur and the solvent removed by rotary evaporation. The resulting residue was dissolved in DMF (1 mL) and to this was added 6-[(*E*)-2-(4-hydroxyphenyl)ethenyl]nicotinic acid **70** (17 mg, 0.067 mmol) and HBTU (64 mg, 0.17 mmol). This was left to stir overnight and subjected to HPLC purification directly to yield the desired material (15 mg, 13 %).

HPLC Procedure

Flow rate: 6 mL/min.

Time (mins)	% Water (with 0.1% TFA)	% MeCN (with 0.1% TFA)
0	90	10
25	70	30
30	50	50
35	90	10

Retention time: 18.2 min.

Purity by HPLC: >96 %.

Melting Point: >230 ^{o}C.

IR: 2945, 2915, 1735, 1703, 1675, 1602, 1582, 1559, 1518, 1485, 1449, 1433, 1399, 1375, 1366, 1349, 1312, 1298, 1265, 1181, 1116, 1060.

δ_H NMR (DMSO): 12.11 (1H, s) 10.55 (1H, s), 9.08 (1H, s), 8.27 (1H, dd, *J* = 8.0, *J* = 2.5), 7.95 (1H, m), 7.63-7.78 (4H, m), 7.53 (1H, m), 7.45 (1H, m), 7.26 (1H, d, *J* = 16.0), 7.00 (2H, d, *J* = 8.5), 3.93 (3H, s), 3.82 (3H, s), 3.07-3.22 (4H, m), 2.79 (6H, d, *J* = 6.5), 1.85-1.91 (2H, m), 1.52-1.60 (3H, m), 1.29-1.32 (2H, m), 0.93 (6H, d, *J* = 8.0).

δ_C NMR: Insufficient material.

HR-MS-FAB: Found 658.3163 calculated for $C_{35}H_{44}O_4N_7S^+$ (M+H) 658.3170.

Synthesis of 5-({[5-({[5-({[3-(dimethylammonio)propyl]amino}carbonyl)-1-methyl-1*H*-pyrrol-3-yl]amino}carbonyl)-1-methyl-1*H*-pyrrol-3-yl]amino}carbonyl)-2-[(*E*)-2-(4-methoxyphenyl)ethenyl]pyridinium bis(trifluoroacetate) **137**

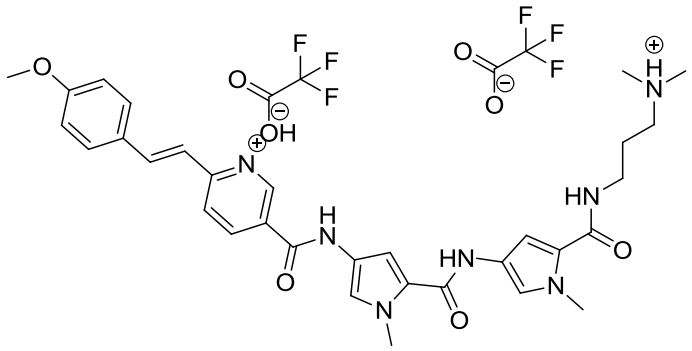

N-[5-({[3-(Dimethylamino)propyl]amino}carbonyl)-1-methyl-1*H*-pyrrol-3-yl]-1-methyl-4-nitro-1*H*-pyrrole-2-carboxamide **112** (30 mg, 0.080 mmol) was dissolved in MeOH (3 mL) to which was added Pd/C-10 % (30 mg) and this was subjected to hydrogenation for 2 h. After this, the reaction mixture was filtered through keisulghur and the solvent removed by rotary evaporation. The resulting residue was dissolved in DMF (1 mL) and to this was added 6-[(*E*)-2-(4-hydroxyphenyl)ethenyl]nicotinic acid **70** (20 mg, 0.080 mmol) and HBTU (64 mg, 0.17 mmol). This was left to stir overnight and subjected to HPLC purification directly to yield the desired material (15 mg, 23 %).

HPLC Procedure

Flow rate: 6 mL/min.

Time (mins)	% Water (with 0.1% TFA)	% MeCN (with 0.1% TFA)
0	90	10
25	70	30
30	50	50
35	90	10

Retention time: 25.1 min.

Purity by HPLC: >97 %.

Melting Point: >230 ^{o}C.

IR: 3251, 2981, 2961, 1688, 1675, 1655, 1638, 1593, 1543, 1511, 1466, 1435, 1407, 1259, 1203, 1174, 1127.

δ_H NMR (DMSO): 10.46 (1H, s), 9.94 (1H, s), 9.17 (1H, bs), 9.06 (1H, s), 8.24 (1H, dd, *J* = 8.0, *J* = 2.5), 8.15 (1H, m), 7.63-7.77 (4H, m), 7.33 (1H, m), 7.24 (1H, d, *J* = 16.0), 7.18 (1H, d, *J* = 1.5), 7.10 (1H, d, *J* = 1.5), 6.99 (2H, d, *J* = 8.5), 6.94 (1H, d, *J* = 1.5), 6.85 (1H, s), 3.87 (3H, s), 3.82 (3H, s), 3.80 (3H, s), 3.24-3.26 (2H, m), 3.04-3.09 (2H, m), 2.79 (6H, s), 1.83 (2H, m).

δ_C NMR: Insufficient material.

HR-MS-FAB: Found 584.2975 calculated for $C_{32}H_{38}O_4N_7^+$ (M+H) 584.2980.

Synthesis of 5-({[5-({[4-({[3-(dimethylammonio)propyl]amino}carbonyl)-5-isopropyl-1,3-thiazol-2-yl]amino}carbonyl)-1-methyl-1*H*-pyrrol-3-yl]amino}carbonyl)-2-[(*E*)-2-(4-methoxyphenyl)ethenyl]pyridinium bis(trifluoroacetate) **138**

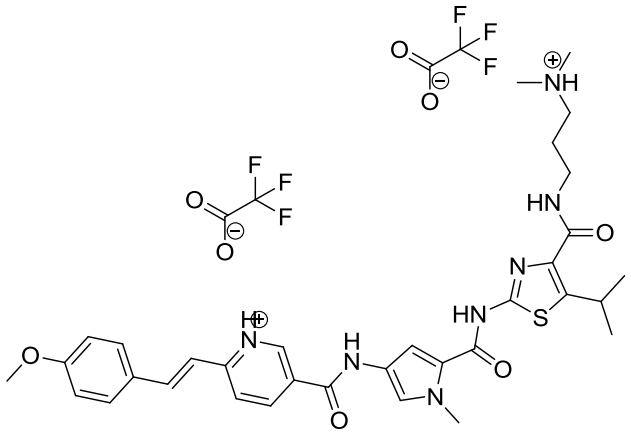

N-[3-(Dimethylamino)propyl]-5-isopropyl-2-{[(1-methyl-4-nitro-1*H*-pyrrol-2-yl)carbonyl]amino}-1,3-thiazole-4-carboxamide **143** (30 mg, 0.071 mmol) was dissolved in MeOH (3 mL) to which was added Pd/C-10 % (30 mg) and this was subjected to hydrogenation for 2 h. After this, the reaction mixture was filtered through keisulghur and the solvent removed by rotary evaporation. The resulting residue was dissolved in DMF (1 mL) and to this was added 6-[(*E*)-2-(4-hydroxyphenyl)ethenyl]nicotinic acid **70** (18 mg, 0.071 mmol) and HBTU (64 mg, 0.17 mmol). This was left to stir overnight and subjected to HPLC purification directly to yield the desired material (17 mg, 28 %).

HPLC Procedure

Flow rate: 6 mL/min.

Time (mins)	% Water (with 0.1% TFA)	% MeCN (with 0.1% TFA)
0	90	10
25	70	30
30	50	50
35	90	10

Retention time: 17.4 min.

Purity by HPLC: >96 %.

Melting Point: >230 ^{o}C.

IR: 2962, 1673, 1640, 1595, 1548, 1509, 1477, 1427, 1399, 1369, 1289, 1261, 1202, 1174, 1134, 1026, 1002.

δ_H NMR (DMSO): 12.11 (1H, s) 10.56 (1H, s), 9.19 (1H, bs), 9.08 (1H, d, *J* = 2.5), 8.28 (1H, dd, *J* = 8.0, *J* = 2.5), 7.97 (1H, t, *J* = 7.5), 7.64-7.78 (4H, m), 7.53 (1H, m), 7.46 (1H, m), 7.27 (1H, d, *J* = 16.0), 7.00 (2H, d, *J* = 8.5), 4.21 (1H, m), 3.93 (3H, s), 3.82 (3H, s), 3.34-3.37 (2H, m), 3.07-3.22 (2H, m), 2.79 (6H, d, *J* = 6.5), 1.85-1.91 (2H, m), 1.29 (6H, d, *J* = 8.0).

δ_C NMR: Insufficient material.

HR-MS-FAB: Found 630.2848 calculated for $C_{33}H_{40}O_4N_7S^+$ (M+H) 630.2857.

Synthesis of [[4-({[5-({[5-({[3-(dimethylammonio)propyl]amino}carbonyl)-1-methyl-1*H*-pyrrol-3-yl]amino}carbonyl)-1-methyl-1*H*-pyrrol-3-yl]amino}carbonyl)anilino](3-methoxyphenyl)methylene]ammonium bis(trifluoroacetate) **139**

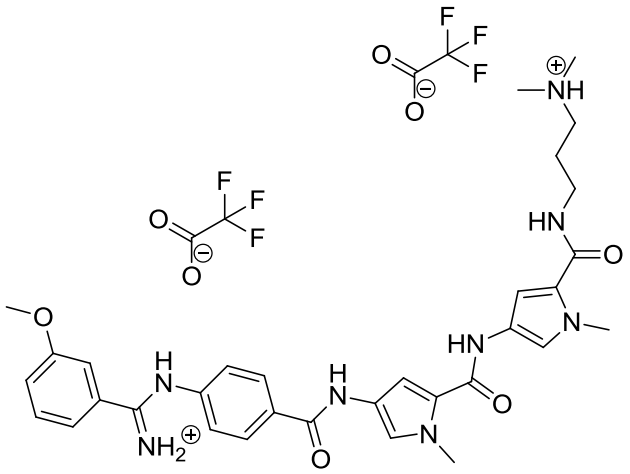

N-[5-({[3-(Dimethylamino)propyl]amino}carbonyl)-1-methyl-1*H*-pyrrol-3-yl]-1-methyl-4-nitro-1*H*-pyrrole-2-carboxamide **112** (30 mg, 0.080 mmol) was dissolved in MeOH (3 mL) to which was added Pd/C-10 % (30 mg) and this was subjected to hydrogenation for 2 h. After this, the reaction mixture was filtered through keisulghur and the solvent removed by rotary evaporation. The resulting residue was dissolved in DMF (1 mL) and to this was added 4-{[imino(3-methoxyphenyl)methyl]amino}benzoic acid **146** (22 mg, 0.080 mmol) and HBTU (64 mg, 0.17 mmol). This was left to stir overnight and subjected to HPLC purification directly to yield the desired material (18 mg, 27 %).

HPLC Procedure

Flow rate: 6 mL/min.

Time (mins)	% Water (with 0.1% TFA)	% MeCN (with 0.1% TFA)
0	90	10
25	75	25
30	50	50
35	90	10

Retention time: 11.1 min.

Purity by HPLC: >97%.

Melting Point: >230 ^{o}C.

IR: 3072, 2986, 2367, 1720, 1651, 1616, 1578, 1543, 1528, 1509, 1478, 1457, 1433, 1416, 1398, 1368, 1316, 1293, 1226, 1194, 1135, 1131, 1079.

δ_H NMR (DMSO): 11.54 (1H, s), 10.45 (1H, s), 9.92-9.95 (2H, m), 9.24 (2H, m), 8.13-8.22 (2H, m), 7.45-7.72 (5H, m), 7.35 (2H, m), 7.16 (1H, d, *J* = 1.5), 7.12 (1H, s), 6.96 (1H, d, *J* = 1.5), 6.85 (1H, s), 3.88 (6H, s), 3.82 (3H, s), 3.24-3.26 (2H, m), 3.04-3.07 (2H, m), 2.79 (6H, s), 1.83 (2H, m).

δ_C NMR: Insufficient material.

HR-MS-FAB: Found 599.3084 calculated for $C_{32}H_{39}O_4N_8^+$ (M+H) 599.3089.

Synthesis of 3-({[4-({[4-({4-[(*E*)-2-(3-methoxyphenyl)ethenyl]benzoyl}amino)-1-methyl-1*H*-pyrrol-2-yl]carbonyl}amino)-1-methyl-1*H*-pyrrol-2-yl]carbonyl}amino)-*N*,*N*-dimethyl-1-propanaminium trifluoroacetate **140**

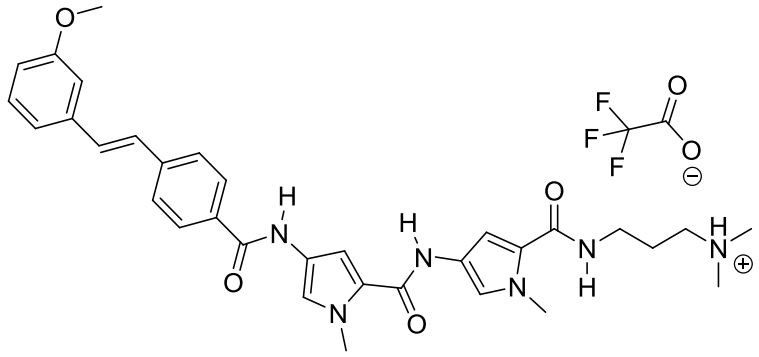

N-[5-({[3-(Dimethylamino)propyl]amino}carbonyl)-1-methyl-1*H*-pyrrol-3-yl]-1-methyl-4-nitro-1*H*-pyrrole-2-carboxamide **112** (30 mg, 0.080 mmol) was dissolved in MeOH (3 mL) to which was added Pd/C-10 % (30 mg) and this was subjected to hydrogenation for 2 h. After this, the reaction mixture was filtered through keisulghur and the solvent removed by rotary evaporation. The resulting residue was dissolved in DMF (1 mL) and to this was added 4-[(*E*)-2-(3-methoxyphenyl)ethenyl]benzoic acid **69** (20 mg, 0.080 mmol) and HBTU (64 mg, 0.17 mmol). This was left to stir overnight and subjected to HPLC purification directly to yield the desired material (17 mg, 31 %).

HPLC Procedure

Flow rate: 6 mL/min.

Time (mins)	% Water (with 0.1% TFA)	% MeCN (with 0.1% TFA)
0	70	30
25	50	50
30	70	30
35	70	30

Retention time: 21.7 min.

Purity by HPLC: >95 %.

Melting Point: >230 ^{o}C.

IR: 3284, 2945, 2650, 1687, 1644, 1627, 1584, 1539, 1427, 1401, 1260, 1202, 1172, 1120.

δ_H NMR (DMSO): 10.32 (1H, s), 9.94 (1H, s), 9.19 (1H, bs), 8.16 (1H, t, *J* = 5.5), 7.97 (2H, d, *J* = 8.5), 7.74 (2H, d, *J* = 8.5), 7.29-8.37 (4H, m), 7.21-7.23 (2H, m), 7.18 (1H, d, *J* = 1.5), 7.10 (1H, d, *J* = 1.5), 6.95 (1H, d, *J* = 1.5), 6.88 (1H, m), 3.89 (3H, s), 3.83 (3H, s), 3.82 (3H, s), 3.24-3.27 (2H, m), 3.09 (2H, m), 2.80 (6H, s), 1.85 (2H, m).

δ_C NMR: Insufficient material.

HR-MS-FAB: Found 583.3036 calculated for $C_{33}H_{39}O_4N_6^+$ (M+H) 583.3027.

Synthesis of 5-{[(5-{[(5-{[(3-amino-3-iminiopropyl)amino]carbonyl}-1-methyl-1*H*-pyrrol-3-yl)amino]carbonyl}-1-methyl-1*H*-pyrrol-3-yl)amino]carbonyl}-2-[(*E*)-2-(4-methoxyphenyl)ethenyl]pyridinium bis(trifluoroacetate) **141**

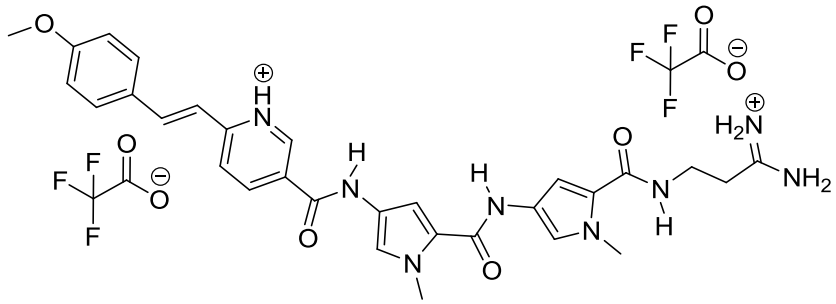

N-(5-{[(3-Amino-3-iminopropyl)amino]carbonyl}-1-methyl-1*H*-pyrrol-3-yl)-1-methyl-4-nitro-1*H*-pyrrole-2-carboxamide **111** (30 mg, 0.083 mmol) was dissolved in MeOH (3 mL) to which was added Pd/C-10 % (30 mg) and this was subjected to hydrogenation for 2 h. After this, the reaction mixture was filtered through keisulghur and the solvent removed by rotary evaporation. The resulting residue was dissolved in DMF (1 mL) and to this was added 6-[(*E*)-2-(4-hydroxyphenyl)ethenyl]nicotinic acid **70** (21 mg, 0.083 mmol) and HBTU (64 mg, 0.17 mmol). This was left to stir overnight and subjected to HPLC purification directly to yield the desired material (21 mg, 32 %).

HPLC Procedure

Flow rate: 6 mL/min.

Time (mins)	% Water (with 0.1% TFA)	% MeCN (with 0.1% TFA)
0	90	10
25	70	30
30	50	50
35	90	10

Retention time: 12.3 min.

Purity by HPLC: >98 %.

Melting Point: >230 ^{o}C.

IR: 3295, 3094, 2935, 1677, 1655, 1640, 1612, 1578, 1558, 1543, 1530, 1472, 1433, 1408, 1386, 1261, 1196, 1183, 1134, 1064, 1013, 965.

δ_H NMR (DMSO): 10.35 (1H, s), 9.95 (1H, s), 9.26 (1H, d, *J* = 2.0), 8.89 (2H, s), 8.54 (1H, m), 8.43 (2H, s), 8.19 (1H, m), 7.99-8.03 (4H, m), 7.59-7.82 (6H, m), 7.34 (1H, d, *J* = 1.5), 7.18 (1H, d, *J* = 1.5), 7.12 (1H, d, *J* = 1.5), 6.97 (1H, d, *J* = 1.5), 3.88 (3H, s), 3.82 (6H, s), 3.48-3.51 (2H, m), 2.58-2.62 (2H, m).

δ_C NMR: Insufficient material.

HR-MS-FAB: Found 569.2618 calculated for $C_{30}H_{33}O_4N_8^+$ (M+H) 569.2619.

Synthesis of 1-amino-3-({[4-({[4-({4-[(*E*)-2-(3-methoxyphenyl)ethenyl]benzoyl}amino)-1-methyl-1*H*-pyrrol-2-yl]carbonyl}amino)-1-methyl-1*H*-pyrrol-2-yl]carbonyl}amino)-1-propaniminium trifluoroacetate **142**

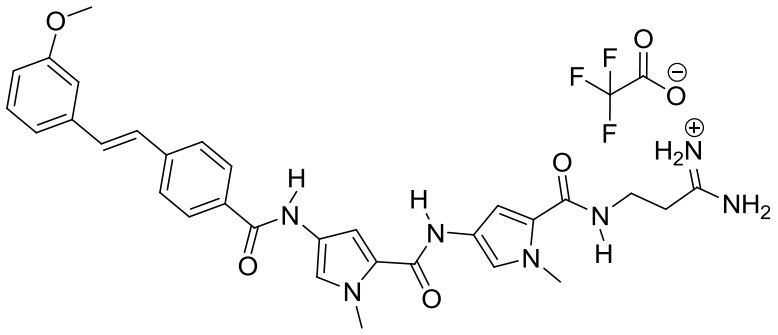

N-(5-{[(3-Amino-3-iminopropyl)amino]carbonyl}-1-methyl-1*H*-pyrrol-3-yl)-1-methyl-4-nitro-1*H*-pyrrole-2-carboxamide **111** (30 mg, 0.083 mmol) was dissolved in MeOH (3 mL) to which was added Pd/C-10 % (30 mg) and this was subjected to hydrogenation for 2 h. After this, the reaction mixture was filtered through keisulghur and the solvent removed by rotary evaporation. The resulting residue was dissolved in DMF (1 mL) and to this was added 4-[(*E*)-2-(3-

methoxyphenyl)ethenyl]benzoic acid **69** (21 mg, 0.083 mmol) and HBTU (64 mg, 0.17 mmol). This was left to stir overnight and subjected to HPLC purification directly to yield the desired material (22 mg, 39 %).

HPLC Procedure

Flow rate: 6 mL/min.

Time (mins)	% Water (with 0.1% TFA)	% MeCN (with 0.1% TFA)
0	90	10
25	70	30
30	50	50
35	90	10

Retention time: 19.1 min.

Purity by HPLC: >97 %.

Melting Point: >230 ^{o}C.

IR: 3295, 3068, 2948, 2824, 1703, 1673, 1655, 1632, 1614, 1582, 1561, 1546, 1532, 1513, 1502, 1489, 1470, 1436, 1403, 1390, 1276, 1198, 1174, 1121, 1051, 1008.

δ_H NMR (DMSO): 10.31 (1H, s), 9.94 (1H, s), 8.89 (2H, s), 8.48 (2H, s), 8.19 (1H, t, *J* = 5.5), 7.95 (2H, d, *J* = 8.5), 7.73 (2H, d, *J* = 8.5), 7.29-8.37 (4H, m), 7.21-7.23 (2H, m), 7.18 (1H, d, *J* = 1.5), 7.10 (1H, d, *J* = 1.5), 6.95 (1H, d, *J* = 1.5), 6.88 (1H, m), 3.87 (3H, s), 3.81 (3H, s), 3.80 (3H, s), 3.48-3.51 (2H, m), 2.58-2.62 (2H, m).

δ_C NMR: Insufficient material.

HR-MS-FAB: Found 568.2672 calculated for $C_{31}H_{34}O_4N_7^+$ (M+H) 568.2667.

Synthesis of 4-{[imino(3-methoxyphenyl)methyl]amino}benzoic acid **146**

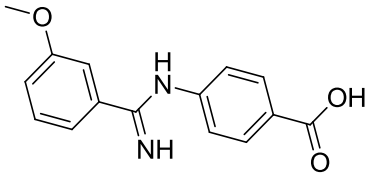

Methyl 3-methoxybenzenecarbimidothioate hydroiodide **72** (50 mg, 0.16 mmol) and 4-aminobenzoic acid **145** (22 mg, 0.16 mmol) were dissolved in methanol (5 mL).This was left to stir overnight after which the desired material precipitated and was obtained by filtration (35 mg, 80 %).

Purity by HPLC: > 95 %.

Melting Point: >230 ^{o}C.

IR: 3293, 3144, 3029, 2937, 2835, 1703, 1668, 1577, 1362, 1261, 1189, 1172.

δ_H NMR (DMSO): 13.20 (1H, bs), 11.59 (1H, s), 9.98 (1H, s), 9.27 (1H, s), 8.12 (2H, d, *J* = 6.8), 7.36-7.61 (5H, m), 3.88 (3H, s).

δ_C NMR (DMSO): 166.5, 163.0, 159.2, 138.6, 131.2, 131.0, 130.3, 129.8, 125.4, 120.9, 119.8, 114.1, 55.6.

HR-MS-FAB: Found 271.1076 calculated for $C_{15}H_{15}O_2N_3^+$ (M+H) 271.1077.

Synthesis of 4-[2-({[4-({[4-({4-[(*E*)-2-(3-methoxyphenyl)ethenyl]benzoyl}amino)-1-methyl-1*H*-pyrrol-2-yl]carbonyl}amino)-1-methyl-1*H*-pyrrol-2-yl]carbonyl}amino)ethyl]-4-methylmorpholin-4-ium trifluoroacetate **147**

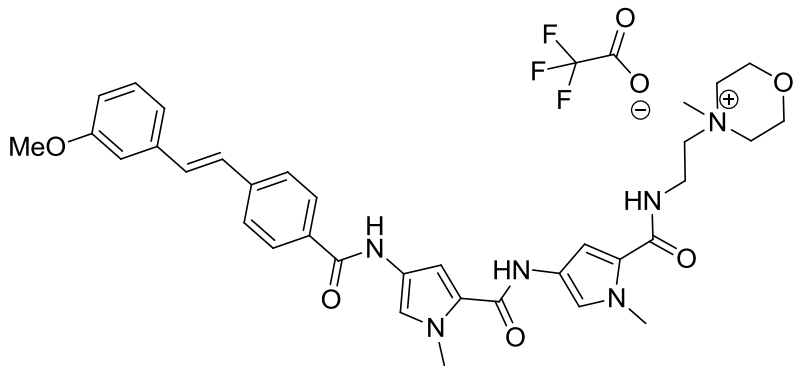

4-({4-[(*E*)-2-(3-Methoxyphenyl)ethenyl]benzoyl}amino)-1-methyl-*N*-[1-methyl-5-({[2-(4-morpholinyl)ethyl]amino}carbonyl)-1*H*-pyrrol-3-yl]-1*H*-pyrrole-2-carboxamide **BP1** (10 mg, 16.4 mmol) was dissolved in DMF (1 mL, anhydrous) to which was added dimethyl sulfate (1.2 mg, 16.4 mmol). This was left to stir overnight after which it was purified directly by HPLC to obtain the desired product (8 mg, 66 % yield).

HPLC Procedure

Flow rate: 6 mL/min.

Time (mins)	% Water (with 0.1% TFA)	% MeCN (with 0.1% TFA)
0	90	10
25	70	30
30	50	50
35	90	10

Retention time: 17.7 min.

Purity by HPLC: >98 %.

Melting Point: >230 ^{o}C.

IR: 3305, 3073, 2995, 1670, 1651, 1640, 1593, 1524, 1429, 1411, 1458, 1170, 1109.

δ_H NMR (DMSO): 10.32 (1H, s), 9.97 (1H, s), 8.23 (1H, m), 7.95 (2H, d, *J* = 8.4), 7.71 (2H, d, *J* = 8.4), 7.27-7.33 (4H, m), 7.16-7.21 (3H, m), 7.10 (1H, d, *J* = 1.5), 6.98 (1H, d, *J* = 1.5), 6.87 (1H, d, *J* = 1.5), 3.94-3.97 (2H, m), 3.88 (3H, s), 3.84 (3H, s), 3.82 (3H, s), 3.61-3.66 (4H, m), 3.49-3.55 (6H, m), 3.40 (3H, s).

δ_C NMR: Insufficient material.

HR-MS-FAB: Found 625.3135 calculated for $C_{35}H_{41}O_5N_6^+$ (M) 625.3133.

Synthesis of 4-{2-[({4-[({4-[({6-[(*E*)-2-(4-methoxyphenyl)ethenyl]-3-pyridiniumyl}carbonyl)amino]-1-methyl-1*H*-pyrrol-2-yl}carbonyl)amino]-1-methyl-1*H*-pyrrol-2-yl}carbonyl)amino]ethyl}-4-methylmorpholin-4-ium bis(trifluoroacetate) **148**

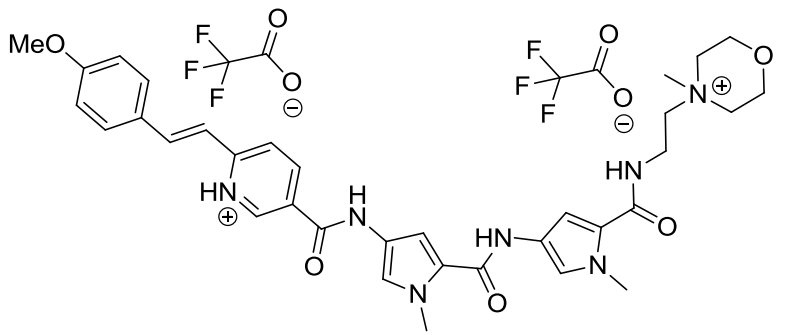

6-[(*E*)-2-(4-Methoxyphenyl)ethenyl]-*N*-[1-methyl-5-({[1-methyl-5-({[2-(4-morpholinyl)ethyl]amino}carbonyl)-1*H*-pyrrol-3-yl]amino}carbonyl)-1*H*-pyrrol-3-yl]nicotinamide **BP2** (10 mg, 16.4 mmol) was dissolved in DMF (1 mL, anhydrous) to which was added dimethyl sulfate (1.2 mg, 16.4 mmol). This was left to stir overnight after which it was purified directly by HPLC to obtain the desired product (9 mg, 64 % yield).

HPLC Procedure

Flow rate: 6 mL/min.

Time (mins)	% Water (with 0.1% TFA)	% MeCN (with 0.1% TFA)
0	90	10
25	70	30
30	50	50
35	90	10

Retention time: 12.6 min.

Purity by HPLC: >96 %.

Melting Point: >230 ^{o}C.

IR: 3258, 3079, 2954, 2880, 1672, 1644, 1627, 1534, 1433, 1265, 1200, 1174, 1122.

δ_H NMR (DMSO): 10.89 (1H, s), 10.03 (1H, s), 9.34 (1H, s), 8.89 (1H, d, *J* = 8.0), 8.65 (1H, d, *J* = 8.0), 8.29 (1H, m), 8.10 (1H, d, *J* = 16.0), 7.90 (2H, d, 8.0), 7.51 (1H, d, *J* = 16.0), 7.39 (1H, d, *J* = 1.5 Hz), 7.22 (1H, d, *J* = 1.5 Hz), 7.2-7.27 (3H, m), 7.01 (1H, d, *J* = 1.5 Hz), 3.94-3.98 (2H, m), 3.91 (3H, s), 3.87 (3H, s), 3.85 (3H, s), 3.61-3.66 (4H, m), 3.49-3.55 (6H, m), 3.25 (3H, s).

δ_C NMR: Insufficient material.

HR-MS-FAB: Found 626.3099 calculated for $C_{34}H_{40}O_5N_7^+$ (M) 626.3085.

Synthesis of 3-{(*E*)-2-[4-({[1-methyl-5-({[1-methyl-5-({[2-(4-methylmorpholin-4-ium-4-yl)ethyl]amino}carbonyl)-1*H*-pyrrol-3-yl]amino}carbonyl)-1*H*-pyrrol-3-yl]amino}carbonyl)phenyl]ethenyl}quinolinium bis(trifluoroacetate) **149**

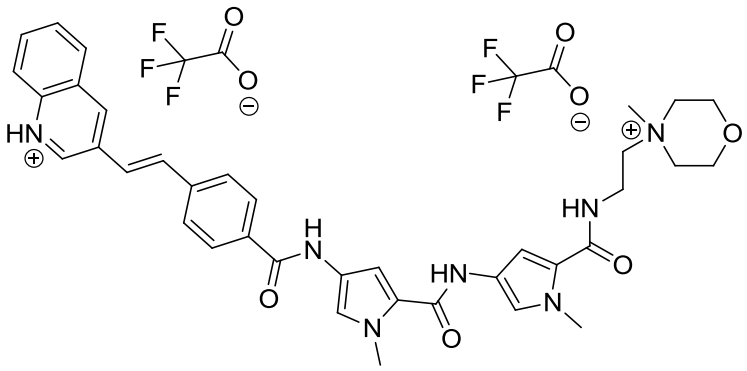

1-Methyl-*N*-[1-methyl-5-({[2-(4-morpholinyl)ethyl]amino}carbonyl)-1*H*-pyrrol-3-yl]-4-({4-[(*E*)-2-(3-quinolinyl)ethenyl]benzoyl}amino)-1*H*-pyrrole-2-carboxamide **BP3** (10 mg, 15.5 mmol) was dissolved in DMF (1 mL, anhydrous) to which was added dimethyl sulfate (1.1 mg, 15.5 mmol). This was left to stir overnight after which it was purified directly by HPLC to obtain the desired product (5 mg, 37 % yield).

HPLC Procedure

Flow rate: 6 mL/min.

Time (mins)	% Water (with 0.1% TFA)	% MeCN (with 0.1% TFA)
0	90	10
25	70	30
30	50	50
35	90	10

Retention time: 11.1 min.

Purity by HPLC: >95 %.

Melting Point: >230 ^{o}C.

IR: 3284, 3101, 2954, 1673, 1659, 1644, 1593, 1519, 1422, 1401, 1260, 1172, 1015.

δ_H NMR (DMSO): 10.39 (1H, s), 9.95 (1H, s), 9.56 (1H, br), 8.43 (1H, d, *J* = 8.0), 8.23 (1H, t, *J* = 8.0), 7.87-8.04 (7H, m), 7.79 (1H, m), 7.56-7.69 (2H, m), 7.34 (1H, d, *J* = 1.7), 7.21 (1H, d, *J* = 1.7), 7.12 (1H, d, *J* = 1.7), 7.05 (1H, d, *J* = 1.7), 3.98-4.01 (2H, m), 3.88 (3H, s), 3.82 (3H, s), 3.79 (3H, s), 3.62-3.69 (2H, m), 3.55-3.59 (4H, m), 3.27 (2H, m), 3.12 (2H, m).

δ_C NMR: Insufficient material.

HR-MS-FAB: Found 646.3143 calculated for $C_{37}H_{40}O_4N_7^+$ (M) 646.3136.

Synthesis of [{[5-({[5-({[5-isopentyl-4-({[3-(trimethylammonio)propyl]amino}carbonyl)-1,3-thiazol-2-yl]amino}carbonyl)-1-methyl-1*H*-pyrrol-3-yl]amino}carbonyl)-1-methyl-1*H*-pyrrol-3-yl]amino}(3-methoxyphenyl)methylene]ammonium bis(trifluoroacetate) **150**

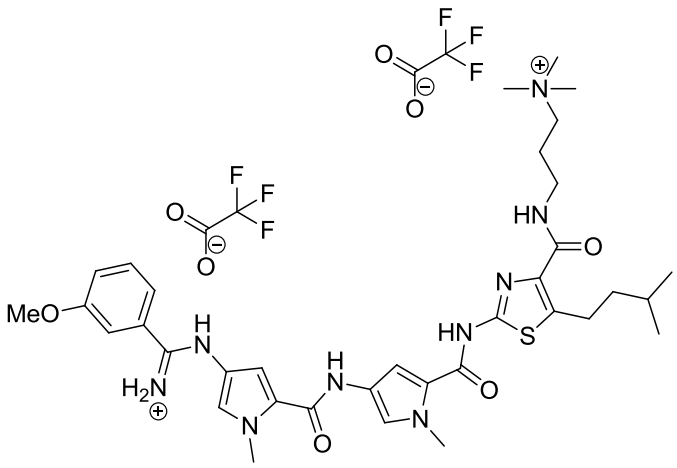

[{[5-({[5-({[4-({[3-(Dimethylammonio)propyl]amino}carbonyl)-5-isopentyl-1,3-thiazol-2-yl]amino}carbonyl)-1-methyl-1*H*-pyrrol-3-yl]amino}carbonyl)-1-methyl-1*H*-pyrrol-3-yl]amino}(3-methoxyphenyl)methylene]ammonium bis(trifluoroacetate) **BP4** (8 mg, 0.009 mmol) was dissolved in DMF (1 mL) to which was added TEA (2

mg, 0.018 mmol) dimethyl sulfate (1.1 mg 0.009 mmol) and this was left to stir for 4 h. This was subjected to HPLC purification directly to yield the desired material (5 mg, 62 %).

HPLC Procedure

Flow rate: 6 mL/min.

Time (mins)	% Water (with 0.1% TFA)	% MeCN (with 0.1% TFA)
0	90	10
25	70	30
30	50	50
35	90	10

Retention time: 12.9 min.

Purity by HPLC: >98 %.

Melting Point: >230 ^{o}C.

IR: 3137, 2958, 1876, 1699, 1686, 1669, 1655, 1642, 1587, 1561, 1546, 1489, 1477, 1431, 1403, 1293, 1198, 1174, 1127.

δ_H NMR (DMSO): 12.08 (1H, s) 11.11 (1H, s), 10.09 (1H, s), 9.77 (1H, s), 8.82 (1H, s), 7.91 (1H, m), 7.58 (1H, m), 7.33-7.45 (4H, m), 7.29 (1H, s), 7.08 (1H, s), 6.50 (1H, s), 3.95 (3H, s), 3.89 (3H, s), 3.87 (3H, s), 3.32-3.35 (2H, m), 3.17-3.22 (2H, m), 3.04 (9H, s), 1.85-1.91 (2H, m), 1.92-1.95 (2H, m), 1.48-1.59 (3H, m), 0.91 (6H, d, J = 8.0).

δ_C NMR: Insufficient material.

HR-MS-FAB: Found 690.3538 calculated for $C_{35}H_{48}O_4N_9S^+$ (M) 690.3544.

Synthesis of 3-Phthalimidopropanal[83] **190**

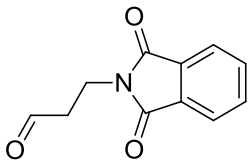

To a solution of oxalyl chloride (5 g, 3.94 mmol) in DCM (25 mL, dry) at -78 ^{o}C was slowly added a solution of DMSO (10.374 mL, 150 mmol) in DCM (25 mL, anhydrous). After stirring for 1 hour at this temperature the alcohol **189** (2.4 g, 11.7 mmol) in DCM (15 mL, dry) was slowly added to the above solution. After 0.5 h Hünig's base (30 mL) was introduced by syringe. The reaction was then stirred, at -78 ^{o}C, for 0.5 h and further at -50 ^{o}C for 20 mins. The reaction was quenched with saturated aqueous ammonium chloride solution (50 mL). The organic phase was separated and then washed with saturated $NaHCO_3$ solution (2 × 15 mL) and dried over $MgSO_4$. The solvent was removed under reduced pressure and the resulting solid was purified by flash column chromatography (hexane:ethyl acetate; 1:1, R_f 0.40) to afford the desired material as a white solid (1.820g, 76 %).

Melting Point: 118-120 ^{o}C. lit: 121-123 ^{o}C.

IR: 3456, 1768, 1706, 1441, 1403, 1369, 1324, 1031, 721, 532.

δ_H NMR (DMSO): 9.82 (1H, t, *J* = 1.5), 7.86-7.72 (4H, m), 4.04 (2H, t, *J* = 7.0), 2.88 (2H, td, *J* = 7.0, *J* = 1.5).

δ_C NMR (DMSO): 199.5, 168.1, 134.1, 132.1, 123.5, 42.5, 31.8.

HR-MS-FAB: Found 204.0573 calculated for $C_{11}H_{10}NO_3^+$ (M+H) 204.0582.

Synthesis of 2-[(2-Amino-4,7-dihydro-4-oxo-1*H*-pyrrolo[2,3-*d*]pyrimidin-5-yl)methyl]-1,3-dihydro-2*H*-isoindole-1,3-dione[83] **191**

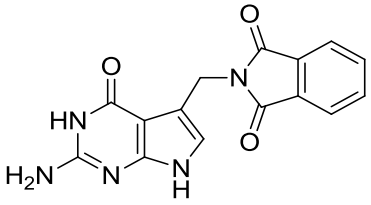

A solution of 3-phthalimidopropanal **190** (5 g, 24.6 mmol) in MeCN (80 mL) was cooled to 0 ^{o}C. DMSO (1.84 mL, 25.9 mmol) was added dropwise, and Me_3SiBr (3.35 mL, 35.9 mmol) was added slowly. The yellow coloured solution was stirred for 4 h at room temperature. A suspension of 2,6-diaminopyrimidin-4-one (3.1 g, 24.6 mmol) and AcONa· 3 H_2O (3.5 g, 25.1 mmol) in water (80 mL) was added slowly. The mixture was stirred overnight. A yellow precipitate was formed. The bright yellow suspension was filtered and washed with acetone (3×80 mL) and water (3×80 mL). The solid was dried to yield the desired material as a yellow solid (6.5 g, 85 % yield).

Melting Point: >230 ^{o}C.

IR: 3387, 2926, 1770, 1711, 1627, 1444, 1361, 1116, 950, 719, 532.

δ_H NMR (DMSO): 10.79 (1H, s), 10.17 (1H, s), 7.87-7.79 (4H, m), 6.35 (1H, s), 6.07 (2H, s), 4.83 (2H, s).

δ_C NMR (DMSO): 168.2, 163.7, 152.8, 151.7, 134.6, 132.1, 123.4, 123.2, 114.0, 98.4, 37.9.

HR-MS-FAB: Found 310.0943 calculated for $C_{11}H_9NO_3^+$ (M+H) 310.0940.

Synthesis of *tert*-Butyl [(2-Amino-4,7-dihydro-4-oxo-1*H*-pyrrolo[2,3-*d*]pyrimidin-5-yl)methy]carbamate[83] **192**

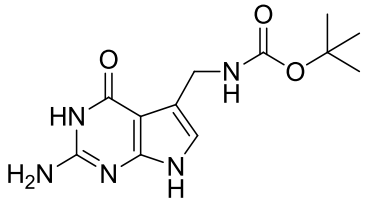

2-[(2-Amino-4,7-dihydro-4-oxo-1*H*-pyrrolo[2,3-*d*]pyrimidin-5-yl)methyl]-1,3-dihydro-2*H*-isoindole-1,3-dione **191** (800 mg, 2.64 mmol) was suspended in ethanol (30 mL), and $NH_2NH_2 \cdot H_2O$ (1.3 mL, 26.4 mmol) was added. The suspension was heated at reflux for 2 h at 80 ^oC and stirred for another 8 h at room temperature. The solvent was evaporated, and 7-(aminomethyl)-7-deazaguanine **50** (crude) was obtained as a white solid. 7-(Aminomethyl)-7-deazaguanine **50** (crude; 200 mg, 1.12 mmol) was suspended in DMF (8 mL), Et_3N (93 mL, 0.67 mmol) and $(Boc)_2O$ (146 mg, 0.67 mmol) were added. After stirring for 8 h at room temperature, more $(Boc)_2O$ (146 mg, 0.67 mmol) and Et_3N (93 mL, 0.67 mmol) were added. After 16 h, the solution was washed with sat. aqueous $NaHCO_3$ (50 mL), and the aqueous phase was re-extracted with CH_2Cl_2 (4×50 mL). The combined organic fractions were extracted with brine (40 mL) and dried ($MgSO_4$). The solvent was evaporated, and, after column chromatography (MeOH:$CHCl_3$; 1 : 10, R_f 0.40), the desired material was obtained as a light brown solid (50 mg, 31 % yield).

Melting Point: >230 ^oC.

IR: 3429, 2978, 2933, 1673, 1592, 1535, 1249, 1169.

δ_H NMR ($CDCl_3$): 10.78 (1H, s), 10.31 (1H, s), 7.04 (1H, s), 6.46 (1H, t, J = 1.0), 6.07 (2H, s), 4.13 (2H, d, J = 1.0), 1.36 (9H, s).

δ_C NMR (DMSO): 160.1, 155.5, 152.7, 151.9, 116.3, 113.7, 98.9, 78.1, 37.0, 27.7.

HR-MS-FAB: Found 280.1359 calculated for $C_{12}H_{18}N_5O_3^+$ (M+H) 280.1331.

Synthesis of 5-(chloromethyl)-2-methyl-4-pyrimidinaminium chloride **200**

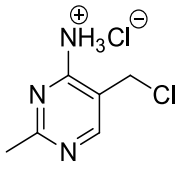

(4-amino-2-methyl-5-pyrimidinyl)methanol **204** (250 mg, 1.80 mmol) was dissolved in thionyl chloride (5 mL) and left to stir for 3 h under nitrogen. The solvent was removed under reduced pressure and the resulting solid was washed with THF to afford the desired material (300 mg, 86 % yield).

Melting Point: >230 ^{o}C.

IR: 3188, 1601, 1566, 1421, 1388, 1311, 1236, 823.

δ_H NMR (DMSO): 9.52 (3H, s), 8.71 (1H, s), 3.83 (2H, s), 2.53 (3H, s).

δ_C NMR (DMSO): 165.5, 163.5, 163.0, 148.8, 103.7, 22.0.

HR-MS-FAB: Found 158.0462 calculated for $C_6H_9ClN_3^+$ (M+H) 158.0480.

Synthesis of (4-amino-2-methyl-5-pyrimidinyl)methanol[91] **204**

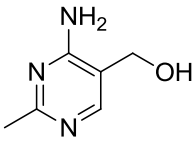

4-amino-2-methyl-5-pyrimidinecarboxylic acid **205** (333 mg, 2.18 mmol) was dissolved in THF (10 mL, dry), under nitrogen, and to this was added $LiAlH_4$ (164.7 mg, 4.34 mmol) in THF (6 mL, dry) via a dropping funnel with addition taking place over one hour. The reaction was then heated to reflux and left for 3 h. The mixture was cooled to room temperature and then quenched by the sequential, drop wise addition of water (1 mL), 15 % NaOH solution (1 mL) and then water (5 mL). The mixture was stirred for 15 mins then filtered, and the filtrate subjected to rotary evaporation to give the desired material (270 mg, 89 % yield).

Melting Point: 197-199 ^{o}C; lit 198-200 ^{o}C. [91]

IR: 3338, 3124, 1614, 1565, 1420, 1379, 1310, 1235.

δ_H NMR (DMSO): 9.08 (2H, bs), 8.44 (1H, s), 6.81 (1H, bs), 3.89 (2H, s) 2.25 (3H, s).

δ_C NMR (DMSO): 169.2, 166.9, 163.8, 158.0, 110.6, 25.9.

HR-MS-FAB: Found 140.0835 calculated for $C_6H_{10}N_3O^+$ (M+H) 140.0818.

Synthesis of 4-amino-2-methyl-5-pyrimidinecarboxylic acid[92] **205**

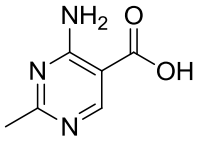

4-amino-2-methyl-5-pyrimidinecarbonitrile **206** (450 mg, 3.35 mmol) was refluxed at 110 ^{o}C for 2 h in 10 % aqueous KOH solution (15 mL). The mixture was allowed to cool and acidified with glacial acetic acid and the resulting solid was removed by filtration, washed with ether and dried overnight under reduced pressure. This gave the desired material (333 mg, 65 % yield).

Melting Point: >230 ^{o}C.

IR: 3327, 3129, 1710, 1636, 1562, 1420, 1366, 1138.

δ_H NMR (DMSO): 8.55 (1H, s), 8.17 (2H, bs), 7.51 (1H, bs), 2.34 (3H, s).

δ_C NMR (DMSO): 168.7, 167.9, 162.8, 158.0, 104.8, 25.3.

HR-MS-FAB: Found 154.0612 calculated for $C_6H_8N_3O_2^+$ (M+H) 154.0611.

Synthesis of 4-amino-2-methyl-5-pyrimidinecarbonitrile[91] **206**

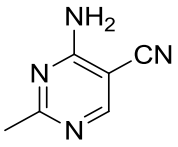

Acetamidine hydrochloride **208** (3.2 g, 34 mmol) was added to a solution of sodium ethoxide in ethanol (2.27 M, 10 mL). The solution was filtered and the filtrate mixed with ethoxymethylene malonitrile **207** (2 g, 16.4 mmol). The dense precipitate which formed immediately was filtered off and crystallised from ethanol to afford the desired material as a yellow solid, without further purification (927 mg, 42 %).

Melting Point: 245-247 ^{o}C. lit 246-248 ^{o}C. [91]

IR: 3326, 3120, 2210, 1610, 1562, 1421, 1366, 1139.

δ_H NMR (DMSO): 8.49 (1H, s), 7.76 (2H, bs), 2.37 (3H, s).

δ_C NMR (DMSO): 170.0, 162.3, 161.0, 115.6, 86.6, 25.8.

HR-MS-FAB: Found 135.0665 calculated for $C_6H_7N_4^+$ (M+H) 135.0668.

Synthesis of 1-ethyl 3-[2-(4-methyl-1,3-thiazol-5-yl)ethyl] malonate **213**

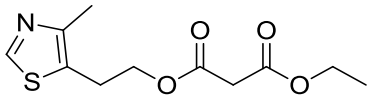

Monoethyl malonate **209** (1.062 mL, 9.00 mmol) was refluxed in thionyl chloride (5 mL) for 2 hours, excess thionyl chloride was removed under reduced pressure and the residue was dissolved in DCM (10 mL, dry). To this was added NMM (950 μL, 8.64 mmol) and 4-methylthiazoethanol **202** (836 μL, 7.18 mmol) in DCM (10 mL, dry) whilst stirring. Stirring continued for 16 hours. The solvent was removed under reduced pressure and the resulting yellow oil was dissolved in DCM (10 mL) and washed with sat. aqueous $NaHCO_3$ (3 x10 mL). The organic layer was dried over magnesium sulfate and the solvent removed at 50 ^{o}C under reduced pressure to yield a yellow oil. The crude product was purified by flash column chromatography using

an 1:1 ethyl acetate:hexane as eluent. Material with an R_f value of 0.28 was collected and the solvent removed at 50 ^oC under reduced pressure to afford a yellow oil (230 mg, 13 %).

Melting Point: Oil at room temperature.

IR: 2983, 2928, 1742, 1739, 1343, 1379, 1270, 1187, 1149, 1023.

δ_H NMR ($CDCl_3$): 8.62 (1H, s), 4.32 (2H, t, *J* = 6.5), 4.20 (2H, q, *J* = 7.0), 3.38 (2H, s), 3.13 (2H, t, *J* = 6.5), 2.42 (3H, s), 1.27 (3H, t, *J* = 7.0).

δ_C NMR ($CDCl_3$):166.3, 166.2, 149.9, 149.9, 126.4, 64.9, 61.6, 41.5, 25.6, 14.8, 14.0.

HR-MS-FAB: Found 258.0711 calculated for $C_{11}H_{16}NO_4S^+$ (M+H) 258.0712.

Synthesis of 2-(4-methyl-1,3-thiazol-5-yl)ethyl 2-oxopropanoate **214**

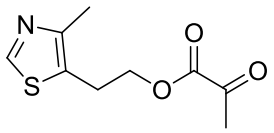

Pyruvic acid **210** (500 μL, 7.18 mmol) was refluxed in thionyl chloride (5 mL) for 2 h, the excess thionyl chloride was evaporated and the residue dissolved in DCM (10 mL, dry). To this was added NMM (950 μL, 8.64 mmol) and 4-methylthiazoethanol **202** (836 μL, 7.18 mmol) in DCM (10 mL, dry) whilst stirring. Stirring continued for 16 hours. The solvent was removed under reduced pressure and the resulting yellow oil was dissolved in DCM (10 mL) and washed with $NaHCO_3$ (saturated, 3x10 mL). The organic layer was dried over magnesium sulfate and the solvent removed at 50 ^oC under reduced pressure to yield a yellow oil. The crude product was purified by flash column chromatography using an 1:1 ethyl acetate:hexane as eluent. Material with an R_f value of 0.58 was collected and the solvent removed at 50 ^oC under reduced pressure to afford a yellow oil (45 mg, 3 %).

Melting Point: Oil at room temperature.

IR: 2987, 2920, 1742, 1721, 1343, 1380, 1270, 1187, 1149, 1033.

δ_H NMR ($CDCl_3$): 8.59 (1H, s), 4.24 (2H, t, *J* = 6.5), 3.10 (2H, t, *J* = 6.5), 2.42 (3H, s), 2.06 (3H, s).

δ_C NMR ($CDCl_3$): 171.1, 170.7, 149.9, 149.8, 126.6, 64.0, 25.7, 20.8, 14.9.

HR-MS-FAB: Found 214.0463 calculated for $C_9H_{12}NO_3S^+$ (M+H) 214.0460.

Synthesis of {1-[(4-amino-2-methyl-5-pyrimidinyl)methyl]-1*H*-1,2,3-triazol-4-yl}methanol **216**

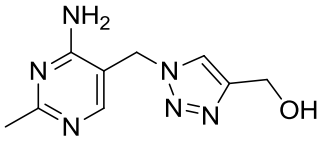

To a stirred solution of propargyl alcohol (170 mg, 3.1 mmol) and 5-azidomethyl-2-methylpyrimidin-4-ylamine **222** (500 mg, 3.04 mmol) in *tert*-butanol/ water (10 mL; 2 : 1) were added sodium ascorbate (60 mg, 0.30 mmol) and $CuSO_4 \cdot 5H_2O$ (8 mg, 0.32 mmol). The reaction mixture was stirred at room temperature for 16 h. The crude mixture was evaporated under reduced pressure and the solid residue was purified by flash column chromatography (MeOH:EtOAc; 10:90, R_f 0.15). The desired material was obtained as an off white powder (468 mg, 70 % yield).

Purity by HPLC: >95%.

Melting Point: >230 °C.

IR: 3402, 3329, 3138, 2879, 2778, 2678, 2431, 2176, 2011, 1922, 1663, 1597, 1564, 1482, 1461, 1430, 1033, 1012.

δ_H NMR (DMSO): 7.97 (1H, bs), 7.94 (1H, s), 6.89 (2H, bs), 5.40 (2H, s), 5.14 (1H, bs), 4.48 (2H, s), 2.29 (3H, s).

δ_C NMR (DMSO): 167.4, 161.9, 156.6, 148.6, 123.2, 109.0, 55.5, 47.0, 25.6.

HR-MS-FAB: Found 221.1144 calculated for $C_9H_{13}ON_7$ (M+H) 221.1145.

Synthesis of 2-[1-(4-Amino-2-methylpyrimidin-5-ylmethyl)-1*H*-[1,2,3]triazol-4-yl]ethanol[93] **217**

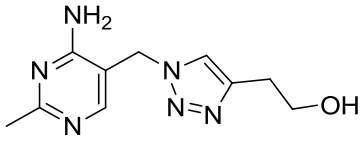

To a stirred solution of 3-butynol (907 µL, 12.0 mmol) and 5-azidomethyl-2-methylpyrimidin-4-ylamine **222** (1.968 g, 12.0 mmol) in *tert*-butanol/ water (12 mL; 2 : 1) were added sodium ascorbate (238 mg, 1.2 mmol) and $CuSO_4 \cdot 5H_2O$ (30 mg, 0.12 mmol). The reaction mixture was stirred at room temperature for 16 h. The crude mixture was evaporated under reduced pressure and the solid residue was dissolved in 1-butanol (10 mL). The organic layer was washed with aqueous potassium carbonate (0.1 M) and then with brine, dried ($MgSO_4$) and evaporated under reduced pressure to give a white solid. Recrystallisation from 2-propanol/hexane gave the triazole as fine needles (2.27 g, 81 % yield).

Purity by HPLC: >95%.

Melting Point: 163-164 ^{o}C lit: 164-165 ^{o}C. [93]

IR: 3313, 3139, 2947, 2885, 2812, 2620, 2473, 211, 2111, 1916, 1847, 1682, 1604, 1562, 1489, 1438, 1352, 1068, 1055, 1026.

δ_H NMR (DMSO): 7.93 (1 H, s), 7.83 (1 H, s), 6.85 (2 H, s), 5.35 (2 H, s), 4.65 (1 H, s), 3.58 (2 H, t, *J* = 6.8), 2.74 (2 H, t, *J* = 6.8), 2.28 (3 H, s).

δ_C NMR (DMSO): 167.3, 161.9, 156.5, 145.1, 122.9, 108.9, 60.7, 46.95, 29.5, 25.7.

HR-MS-FAB: Found 235.1310 calculated for $C_{10}H_{15}N_6O^+$ (M+H) 235.1307.

Synthesis of 3-{1-[(4-amino-2-methyl-5-pyrimidinyl)methyl]-1*H*-1,2,3-triazol-4-yl}-1-propanol **218**

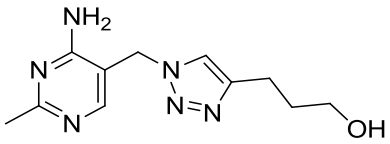

To a stirred solution of 4-pentynol (150 µL, 1.61 mmol) and 5-azidomethyl-2-methylpyrimidin-4-ylamine **222** (250 mg, 1.52 mmol) in *tert*-butanol/ water (5 mL; 2 : 1) were added sodium ascorbate (30 mg, 0.15 mmol) and $CuSO_4 \cdot 5H_2O$ (4 mg, 0.016 mmol). The reaction mixture was stirred at room temperature for 16 h. The crude mixture was evaporated under reduced pressure and the solid residue was purified by flash column chromatography (MeOH:EtOAc; 10:90, R_f 0.17). The desired material was obtained as a white powder (310 mg, 71 % yield).

Purity by HPLC: >95%.

Melting Point: 188-190 ^{o}C.

IR: 3417, 3343, 3246, 3122, 2950, 2924, 2777, 2430, 2193, 1671, 1599, 1567, 1487, 1431, 1376, 1067, 1054.

δ_H NMR (DMSO): 7.93 (1H, s), 7.84 (1H, s), 6.87 (2H, bs), 5.41 (2H, s), 4.47 (1H, t, *J* = 5.0), 3.40 (2H, m), 2.61 (2H, t, *J* = 7.5), 2.29 (3H, s), 1.70 (2H, m)

δ_C NMR (DMSO): 167.3, 161.9, 156.4, 147.3, 122.4, 109.0, 60.5, 46.9, 32.7, 25.6, 22.1.

HR-MS-FAB: Found 249.1459 calculated for $C_{11}H_{17}N_6O^+$ (M+H) 249.1464.

Synthesis of 4-{1-[(4-amino-2-methyl-5-pyrimidinyl)methyl]-1*H*-1,2,3-triazol-4-yl}-1-butanol **219**

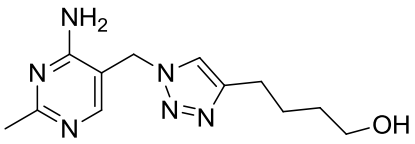

To a stirred solution of 5-hexynol (300 µL, 3.0 mmol) and 5-azidomethyl-2-methylpyrimidin-4-ylamine **222** (500 mg, 3.04 mmol) in *tert*-butanol/ water (5 mL; 2 : 1) were added sodium ascorbate (60 mg, 0.30 mmol) and $CuSO_4 \cdot 5H_2O$ (8 mg, 0.32 mmol). The reaction mixture was stirred at room temperature for 16 h. The crude mixture was evaporated under reduced pressure and the solid residue was purified by flash column chromatography (MeOH:EtOAc; 10:90, R_f 0.19). The desired material was obtained as a white powder (644 mg, 82 % yield).

Purity by HPLC: >95 %.

Melting Point: 138-139 ^{o}C.

IR: 3397, 3334, 3132, 2934, 2859, 2752, 2670, 2417, 2183, 2113, 1661, 1601, 1563, 1484, 14451062, 1052.

δ_H NMR (DMSO): 7.92 (1H, s), 7.82 (1H, s), 6.85 (2H, bs), 5.40 (2H, s), 4.34 (1H, t, *J* = 5.0), 3.38 (2H, m), 2.58 (2H, t, *J* = 7.5), 2.29 (3H, s), 1.57 (2H, m), 1.41 (2H, m).

δ_C NMR (DMSO): 167.3, 161.8, 156.3, 147.5, 122.3, 108.9, 60.8, 46.9, 32.4, 26.0, 25.6, 25.2.

HR-MS-FAB: Found 263.1622 calculated for $C_{12}H_{19}N_6O^+$ (M+H) 263.1620.

Synthesis of 2-{1-[(4-amino-2-methyl-5-pyrimidinyl)methyl]-1*H*-1,2,3-triazol-4-yl}ethanaminium chloride **220**

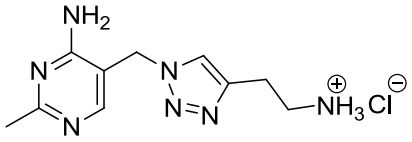

To a stirred solution of 3-butyn-1-aminium chloride **225** (400 mg, 3.79 mmol) and 5-azidomethyl-2-methylpyrimidin-4-ylamine **222** (500 mg, 3.04 mmol) in *tert*-butanol/ water (5 mL; 2 : 1) were added sodium ascorbate (60 mg, 0.30 mmol) and $CuSO_4 \cdot 5H_2O$ (8 mg, 0.32 mmol). The reaction mixture was stirred at room temperature for 16 h. This was evaporated under reduced pressure to give the crude material as a brown residue. This was purified by flash column chromatography (MeOH:EtOAc; 10:90, R_f 0.12) to give the required material as a brown solid (512 mg, 60 % yield).

Purity by HPLC: >95 %.

Melting Point: > 230 ^oC.

IR: 3412, 3210, 2910, 2884, 2812, 2620, 2473, 211, 2111, 1916, 1847, 1682, 1604, 1562, 1489, 1438, 1352, 1068, 1055, 1026.

δ_H NMR (DMSO): 8.06 (3H, bs), 8.02 (1H, s), 7.98 (1H, s), 7.05 (2H, bs), 5.43 (2H, s), 3.04-3.08 (2H, m), 2.91-2.95 (2H, m), 2.30 (3H, s).

δ_C NMR (DMSO): 167.2, 161.9, 156.3, 143.1, 123.4, 108.8, 47.1, 38.7, 25.6, 23.8.

HR-MS-FAB: Found 234.1458 calculated for $C_{10}\ H_{16}\ N_7^+$ (M+H) 234.1462.

Synthesis of 4-amino-5-{[4-(2-carboxyethyl)-1H-1,2,3-triazol-1-yl]methyl}-2-methylpyrimidin-1-ium trifluoroacetate **221**

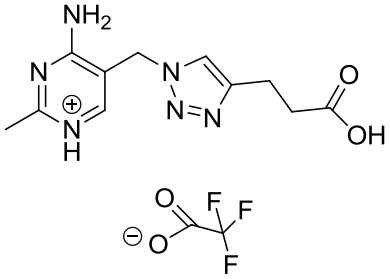

To a stirred solution of pent-4-ynoic acid (50 mg, 0.51 mmol) and 5-azidomethyl-2-methylpyrimidin-4-ylamine **222** (50 mg, 0.31 mmol) in *tert*-butanol/ water (3 mL; 2 : 1) were added sodium ascorbate (10 mg, 0.05 mmol) and $CuSO_4 \cdot 5H_2O$ (1 mg, 0.04 mmol). The reaction mixture was stirred at room temperature for 16 h. The crude mixture was evaporated under reduced pressure and the solid residue was purified by HPLC using the method outlined below. The desired material was obtained as an off white solid (40 mg, 39 % yield).

HPLC Procedure

Flow rate: 6 mL/min.

Time (mins)	% Water (with 0.1% TFA)	% MeCN (with 0.1% TFA)
0	90	10
25	50	50
30	30	70
35	90	10

Retention time: 4.1 min.

Purity by HPLC: >95 %.

Melting Point: > 230 ^{o}C.

IR: 3087, 2594, 1724, 1655, 1631, 1547, 1502, 1200, 1168, 1135.803, 715.

δ_H NMR (DMSO): 8.5-9.1 (2H, bs), 8.27 (1H, s), 7.95 (1H, s), 5.49 (1H, s), 2.85 (2H, t, *J* = 7.2), 2.58 (2H, t, *J* = 7.2, 2.49 (3H, s).

δ_C NMR (DMSO): 173.5, 163.0, 161.8, 145.9, 144.8, 122.4, 109.6, 45.4, 33.0, 21.5, 20.6.

HR-MS-FAB: Found 263.1247 calculated for $C_{11}H_{15}O_2N_6^+$ (M+H) 263.1251.

Synthesis of 5-Azidomethyl-2-methylpyrimidin-4-ylamine[93] **222**

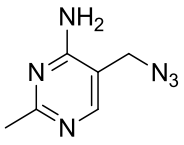

To a solution of thiamine chloride **63** (10.3 g, 30.6 mmol) and sodium azide (4.9 g, 75.4 mmol) in water (100 mL) was added sodium sulfite (0.38 g, 3.0 mmol) and the mixture was stirred at 65 ^{o}C for 5 h. Citric acid (21.0 g, 100 mmol, to pH ≈ 4) was added and the aqueous solution was washed with dichloromethane. Solid potassium carbonate (to pH ≈ 8) was added and this was extracted with ethyl acetate (3×10 mL) and the combined organic layers were washed with brine, dried ($MgSO_4$) and evaporated under reduced pressure. The solid residue recrystallised from ethyl acetate/hexane to give the azide as fine needles (3.15g, 63 % yield).

Purity by HPLC: >95%.

Melting Point: 150-152 ^{o}C. lit: 150-153 ^{o}C. [93]

IR: 3300, 2086, 2107, 1668, 1587, 1561.

δ_H NMR ($CDCl_3$): 8.08 (1H, s), 5.19 (2H, br), 4.23 (2H, s), 2.53 (3H, s).

δ_C NMR ($CDCl_3$): 168.5, 161.6, 155.5, 108.1, 49.7, 25.7.

HR-MS-FAB: Found 165.0889 calculated for $C_6H_9N_6^+$ (M+H) 165.0881.

Synthesis of 3-butynylmethanesulfonate[94] **224**

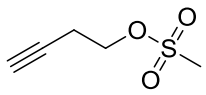

3-Butyn-1-ol **223** (11.72 g, 0.17 mol) was dissolved in DCM (80 mL) and cooled to 0 °C, and Et_3N (35.3 mL, 0.25 mol) and 4-dimethylaminopyridne (DMAP, 800 mg) was added in one portion, followed by addition of methanesulfonyl chloride (19.5 mL, 0.25 mol). The reaction mixture was stirred for 2 h at 0 ^oC and for another 3 h at 25 ^oC. The reaction was cooled again to 0 ^oC, quenched with addition of water (50 mL), and extracted with Et_2O (100 mL × 3). The combined organic phase was washed with aqueous NH_4Cl, aqueous $NaHCO_3$, brine, and dried over Na_2SO_4 overnight. After removal of volatile solvents by rotary evaporation, the residue was subjected to silica gel flash column chromatography to furnish the desired mesylate (14.8 g, 62 % yield).

Melting Point: liquid at room temperature.

IR: 2904, 2858, 2670, 2425, 2193, 2066, 1664, 1140, 1061, 920.

δ_H NMR ($CDCl_3$): 4.32 (2H, t, *J* = 6.9), 3.07 (3H, s), 2.67 (2H, td, *J* = 6.9, 2.7), 2.08 (1H, t, *J* = 2.7).

δ_C NMR ($CDCl_3$): 77.9, 70.5, 66.6, 37.2, 19.3.

Synthesis of 3-butyn-1-aminium chloride[94] **225**

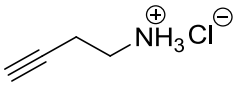

3-Butynylmethanesulfonate **224** (5.5 g, 24.5 mmol) was dissolved in anhydrous dimethylformamide (DMF, 100 mL), and sodium azide (4 g, 61.4 mmol) added in

portions. The reaction mixture was heated to 70 °C and stirred for 3.5 h, cooled to 25 °C and extracted with Et_2O (50 mL × 3). The combined organic phase was washed with water, brine, and dried over Na_2SO_4. Volatile solvents were removed by rotary evaporation. The resulting residue containing 3-butyn-1-azide was used without further purification and was mixed with triphenyl phosphine (6.44 g, 24.4 mmol) in Et_2O (100 mL) at 0° C and stirred for 2 h. Water (3.9 mL) was added and the resulting mixture stirred for an additional 20 h at 25 °C. The mixture was poured into 1N HCl (25 mL) and the aqueous layer extracted with Et_2O (10 mL × 3). The remaining aqueous layer was concentrated under reduced pressure rotary evaporation to give the desired product **101** as a light brown solid (1.25 g, 49 % yield for two steps).

Melting Point: > 230^{o}C.

IR: 3267, 2911, 2852, 2669, 2475, 2190, 2065, 1664, 1150.

δ_H NMR (D_2O): 3.02-3.08 (2H, m), 2.46-2.53 (2H, m), 2.53-2.39 (1H, m).

δ_C NMR (D_2O): 79.44, 72.58, 38.18, 16.85.

Synthesis of 4-amino-2-methyl-5-[(4-{2-[(methylsulfonyl)amino]ethyl}-1*H*-1,2,3-triazol-1-yl)methyl]pyrimidin-1-ium trifluoroacetate **226**

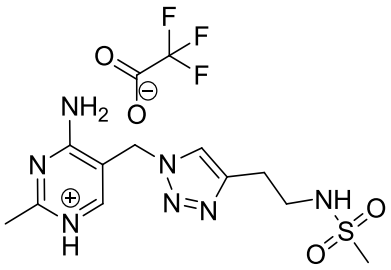

2-{1-[(4-Amino-2-methyl-5-pyrimidinyl)methyl]-1*H*-1,2,3-triazol-4-yl}ethanaminium chloride **220** (100 mg, 0.43 mmol) was dissolved in DMF (2 mL, dry) to which was added triethylamine (44 mg, 0.43 mmol). Methanesulfonyl chloride (49 mg, 0.43 mmol) was added dropwise and left to stir for 16 h. The

resulting solution was subjected to HPLC purification to obtain the desired product (25 mg, 14 % yield).

HPLC Procedure

Flow rate: 6 mL/min.

Time (mins)	% Water (with 0.1% TFA)	% MeCN (with 0.1% TFA)
0	100	0
20	70	30

Retention time: 8 min.

Purity by HPLC: >96 %.

Melting Point: > 230 ^{o}C.

IR: 3412, 3210, 2910, 2884, 2812, 2620, 2473, 211, 2111, 1916, 1847, 1682, 1604, 1562, 1489, 1438, 1352, 1068, 1055, 1026, 911.

δ_H NMR (DMSO): 8.61-8.81 (3H, bs), 8.18 (1H, s), 7.91 (1H, s), 7.02 (1H, t, *J* = 6.0), 5.47 (2H, s), 3.19-3.24 (2H, m), 2.85 (3H, s), 2.81 (2H, t, *J* = 7.0), 2.46 (3H, s).

δ_C NMR (DMSO): 163.4, 162.2, 145.5, 144.6, 123.3, 110.1, 46.2, 45.9, 42.5, 26.6, 22.0.

HR-MS-FAB: Found 312.1231 calculated for $C_{11}H_{18}N_7O_2S^+$ (M+H) 312.1237.

Synthesis of 4-amino-2-methyl-5-{[4-(2-{[(4-methylphenyl)sulfonyl]amino}ethyl)-1*H*-1,2,3-triazol-1-yl]methyl}pyrimidin-1-ium trifluoroacetate **227**

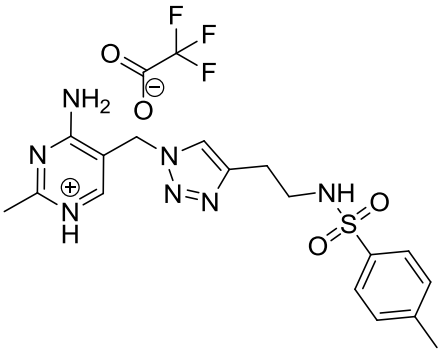

2-{1-[(4-Amino-2-methyl-5-pyrimidinyl)methyl]-1*H*-1,2,3-triazol-4-yl}ethanaminium chloride **220** (100 mg, 0.43 mmol) was dissolved in DMF (2 mL, dry) to which was added triethylamine (44 mg, 0.43 mmol). *p*-Toluenesulfonyl chloride (82 mg, 0.43 mmol) was added in small portions and left to stir for 16 h. The resulting solution was subjected to HPLC purification to obtain the desired product (82 mg, 38 % yield).

HPLC Procedure

Flow rate: 6 mL/min.

Time (mins)	% Water (with 0.1% TFA)	% MeCN (with 0.1% TFA)
0	100	0
8	70	30
20	70	30

Retention time: 11 min.

Purity by HPLC: >95 %.

Melting Point: > 230 ^{o}C.

IR: 3141, 3075, 1656, 1653, 1619, 1589, 1458, 1500, 1461, 1397, 1319, 1304, 1129, 1077.

δ_H NMR (DMSO): 8.4-9.0 (3H, bs), 8.20 (1H, s), 7.93 (1H, s), 7.64-7.67 (3H, m), 7.38 (2H, d, *J* = 8.0), 5.46 (2H, s), 2.92-2.96 (2H, m), 2.74 (2H, t, *J* = 8.0), 2.46 (3H, s), 2.38 (3H, s).

δ_C NMR (DMSO): 163.3, 162.2, 144.4, 143.2, 137.9, 137.2, 130.1, 127.0, 123.3, 110.1, 46.2, 45.9, 42.5, 26.6, 22.0.

HR-MS-FAB: Found 388.1557 calculated for $C_{17}H_{22}N_7O_2S^+$ (M+H) 388.1556.

Synthesis of ethyl 3-[(2-{1-[(4-amino-2-methyl-5-pyrimidinyl)methyl]-1H-1,2,3-triazol-4-yl}ethyl)amino]-3-oxopropanoate **228**

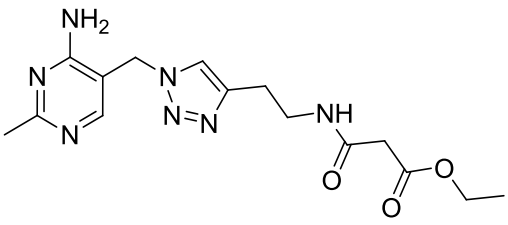

2-{1-[(4-Amino-2-methyl-5-pyrimidinyl)methyl]-1*H*-1,2,3-triazol-4-yl}ethanaminium chloride **220** (100 mg, 0.428 mmol) was dissolved in DMF (2 mL, dry) to which was added triethylamine (44 mg, 0.430 mmol). Monoethyl malonate (113.52 mg, 0.86 mmol) was dissolved in DMF (2 mL, dry) and cooled to 0 ^oC and to this was added DCC (178 mg, 0.86 mmol). The cooled monoethyl malonate and DCC mixture was slowly added to the cooled pyrimidinyl triazole mixture and left to stir for 4 h. The solid dicyclohexylurea was filtered off and the resulting solution was subjected to HPLC purification to obtain the desired product (24 mg, 16 % yield).

HPLC Procedure

Flow rate: 6 mL/min.

Time (mins)	% Water (with 0.1% Formic Acid)	% MeCN (with 0.1% Formic Acid)
0	95	5
10	80	20
15	70	30
20	70	30

Retention time: 6 min.

Purity by HPLC: >95 %.

Melting Point: > 230 ^{o}C.

IR: 3292, 3094, 2987, 1748, 1703, 1675, 1647, 1563, 1535, 1509, 1459, 1429, 1390, 1377, 1347, 1174, 1123, 1067, 1047, 1024.

δ_H NMR (DMSO): 8.4-8.9 (2H, bs), 8.17-8.19 (2H, m), 7.95 (1H, s), 5.47 (2H, s), 4.05 ((2H, q, *J* = 7.0), 3.92-3.33 (2H, m), 3.18 (2H, s), 2.76 (2H, t, *J* = 7.5), 2.46 (3H, s), 1.16 (3H, t, *J* = 7.0).

δ_C NMR (DMSO): 168.3, 165.6, 163.3, 162.5, 162.4, 144.8, 123.3, 110.1, 60.8, 46.0, 42.9, 38.9, 25.8, 22.1, 14.5.

HR-MS-FAB: Found 348.1776 calculated for $C_{15}H_{22}O_3N_7^+$ (M+H) 348.1779.

Synthesis of N-(2-{1-[(4-amino-2-methyl-5-pyrimidinyl)methyl]-1H-1,2,3-triazol-4-yl}ethyl)-2-oxopropanamide **229**

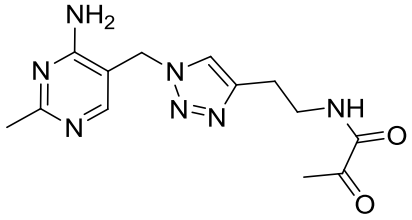

2-{1-[(4-Amino-2-methyl-5-pyrimidinyl)methyl]-1*H*-1,2,3-triazol-4-yl}ethanaminium chloride **220** (50 mg, 0.214 mmol) was dissolved in DMF (1 mL, dry) to which was added triethylamine (22 mg, 0.214 mmol). Pyruvic acid (38 mg, 0.43 mmol) was dissolved in DMF (1 mL, dry) and cooled to 0 ^{o}C and to this was added DCC (88.6 mg, 0.43 mmol). The cooled pyruvic acid and DCC mixture was slowly added to the cooled pyrimidinyl triazole mixture and left to stir for 4 h. The solid dicyclohexylurea was filtered off and the resulting solution was subjected to HPLC purification to obtain the desired product (21 mg, 33 % yield).

HPLC Procedure

Flow rate: 6 mL/min.

Time (mins)	% Water (with 0.1% Formic Acid)	% MeCN (with 0.1% Formic Acid)
0	95	5
10	80	20
15	70	30
20	70	30

Retention time: 3 min.

Purity by HPLC: >95 %.

Melting Point: > 230 ^{o}C.

IR: 3291, 3090, 2987, 1750, 1702, 1690, 1644, 1564, 1380, 1371, 1348, 1171, 1123, 1067, 1047, 1022.

δ_H NMR (DMSO): 8.4-8.9 (3H, m), 8.17 (1H, s), 7.95 (1H, s), 5.46 (2H, s), 3.33-3.38 (2H, m), 2.81 (2H, t, *J* = 7.5), 2.45 (3H, s), 2.32 (3H, s).

δ_C NMR: Insufficient material.

HR-MS-FAB: Found 304.1515 calculated for $C_{13}H_{18}O_2N_7^+$ (M+H) 304.1516.

Synthesis of 4-amino-5-[(4-{2-[(2-hydroxybenzoyl)amino]ethyl}-1*H*-1,2,3-triazol-1-yl)methyl]-2-methylpyrimidin-1-ium trifluoroacetate **230**

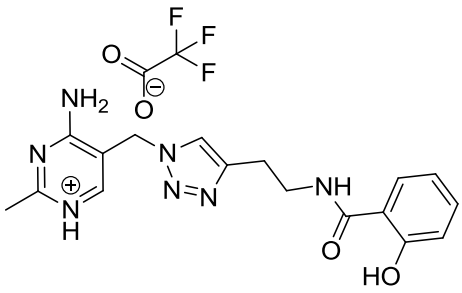

2-{1-[(4-Amino-2-methyl-5-pyrimidinyl)methyl]-1*H*-1,2,3-triazol-4-yl}ethanaminium chloride **220** (100 mg, 0.43 mmol) was dissolved in DMF (2 mL, dry) to which was added triethylamine (44 mg, 0.43 mmol). In a separate flask, the salicylic acid (70 mg, 0.51 mmol) was dissolved in DMF (1 mL, dry) and to this was added DCC (90 mg, 0.43 mmol) and triethylamine (44 mg, 0.43 mmol). The pyrimidinyl triazole solution was then slowly added to the salicylic acid solution at 0 ^oC and left stirring at room temperature for 16 h. The resulting solution was subjected to HPLC purification to obtain the desired product (100 mg, 51 % yield).

HPLC Procedure

Flow rate: 6 mL/min.

Time (mins)	% Water (with 0.1% TFA)	% MeCN (with 0.1% TFA)
0	85	15
5	85	15
10	70	30
20	70	30

Retention time: 10.1 min.

Purity by HPLC: >96 %.

Melting Point: > 230 ^{o}C.

IR: 3075, 2984, 2951, 1643, 1321, 1595, 1543, 1492, 1401, 1362, 1326, 1192, 1175, 1125, 1041.

δ_H NMR (DMSO): 12.50 (1H, s), 8.92 (1H, t, *J* = 5.5), 8.23 (1H, s), 8.00 (1H, s), 7.79 (1H, d, *J* = 8.0), 7.38 (1H, t, *J* = 8.0), 6.85-6.89 (2H, m), 5.48 (2H, s), 3.54 (2H, m), 2.91 (2H, t, *J* = 7.0), 2.48 (3H, s).

δ_C NMR (DMSO): 168.9, 162.9, 161.7, 159.93, 144.7, 144.4, 133.6, 127.6, 122.8, 118.5, 117.3, 115.1, 109.5, 45.4, 39.8, 25.1, 21.5.

HR-MS-FAB: Found 354.1665 calculated for $C_{17}H_{20}O_2N_7^+$ (M+H) 354.1673.

Synthesis of 4-amino-2-methyl-5-{[4-(2-{[2-(phenylsulfonyl)ethyl]ammonio}ethyl)-1*H*-1,2,3-triazol-1-yl]methyl}pyrimidin-1-ium bis(trifluoroacetate) **232**

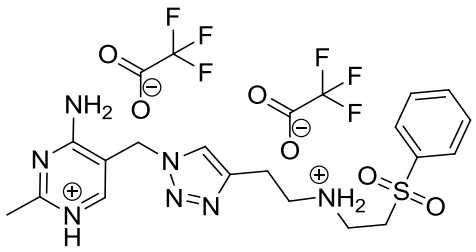

2-{1-[(4-Amino-2-methyl-5-pyrimidinyl)methyl]-1*H*-1,2,3-triazol-4-yl}ethanaminium chloride **220** (50 mg, 0.214 mmol) was dissolved in DMF (1 mL, dry) to which was added triethylamine (22 mg, 0.214 mmol) and after 30 min of stirring phenylvinyl sulfone **231** (36 mg, 0.214 mmol) was added. The reaction mixture was left for 16 h. The reaction mixture was subjected to HPLC purification to obtain the desired product (36 mg, 27 % yield).

HPLC Procedure

Flow rate: 6 mL/min.

Time (mins)	% Water (with 0.1% TFA)	% MeCN (with 0.1% TFA)
0	95	5
10	80	20
15	70	30
20	70	30

Retention time: 7.1 min.

Purity by HPLC: >97 %.

Melting Point: > 230 ^{o}C.

IR: 3075, 2985, 1651, 1545, 1509, 1448, 1422, 1315, 1198, 1181, 1127, 1086, 1054, 985.

δ_H NMR (DMSO): 8.71-8.91 (3H, bs), 8.42-8.71 (2H, bs), 8.30 (1H, s), 8.23 (1H, s) 7.93-7.96 (2H, m), 7.80-7.85 (1H, m), 7.71-7.75 (2H, m), 5.51 (2H, s), 3.71-3.76 (2H, m), 3.22-3.32 (4H, m), 2.96 (2H, t, *J* = 7.0), 2.46 (3H, s).

δ_C NMR (DMSO): 162.7, 161.9, 158.3, 142.3, 138.1, 134.5, 129.7, 127.7, 123.1, 109.3, 50.9, 46.1, 45.7, 40.4, 22.0, 21.9.

HR-MS-FAB: Found 402.1700 calculated for $C_{18}H_{24}O_2N_7S^+$ 402.1707.

Synthesis of 4-amino-5-[(4-{2-[(2-{[(4-fluorobenzyl)amino]sulfonyl}ethyl)ammonio]ethyl}-1*H*-1,2,3-triazol-1-yl)methyl]-2-methylpyrimidin-1-ium bis(trifluoroacetate) **234**

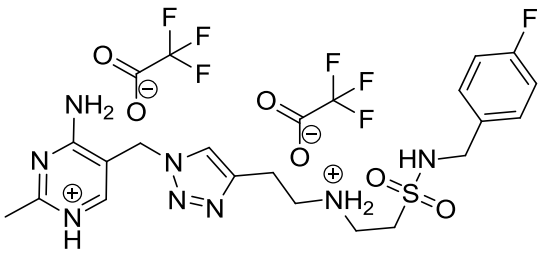

2-{1-[(4-Amino-2-methyl-5-pyrimidinyl)methyl]-1*H*-1,2,3-triazol-4-yl}ethanaminium chloride **220** (50 mg, 0.214 mmol) was dissolved in DMF (1 mL, dry) to which was added triethylamine (22 mg, 0.214 mmol) and after 30 min of stirring *N*-(4-fluorobenzyl)ethylenesulfonamide **233** (40 mg, 0.214 mmol) was added. The reaction mixture was heated to 50 ^oC and left for 16 h. The reaction mixture was subjected to HPLC purification to obtain the desired product (30 mg, 26 % yield).

HPLC Procedure

Flow rate: 6 mL/min.

Time (mins)	% Water (with 0.1% TFA)	% MeCN (with 0.1% TFA)
0	95	5
10	80	20
15	70	30
20	70	30

Retention time: 12.5 min.

Purity by HPLC: >97 %.

Melting Point: > 230 ^{o}C.

IR: 3319, 3139, 3072, 1658, 1636, 1539, 1509, 1459, 1425, 1362, 1323, 1200, 1177, 1127, 1051.

δ_H NMR (DMSO): 8.7-8.9 (3H, bs), 8.4-8.7 (2H, bs), 8.23 (1H, s), 8.01-8.06 (2H, m) 7.32-7.39 (2H, m), 7.15-7.21 (2H, m), 5.51 (2H, s), 4.16 (2H, d, *J* = 6.0), 3.25-3.51 (6H, m), 2.98 (2H, t, *J* = 6.0), 2.45 (3H, s).

δ_C NMR (DMSO): 163.3, 162.9, 160.9, 158.6 (d, *J* = 32.7), 142.8, 134.6, 130.1 (d, *J* = 8.2), 123.7, 115.7 (d, *J* = 21.4), 109.8, 48.1, 46.5, 46.1, 45.5, 42.9, 41.8, 22.4.

HR-MS-FAB: Found 449.1873 calculated for $C_{19}H_{26}O_2N_8FS^+$ (M+H) 449.1878.

Synthesis of 4-amino-2-methyl-5-{[4-(2-{[(*E*)-1-(methylamino)-2-nitroethenyl]amino}ethyl)-1*H*-1,2,3-triazol-1-yl]methyl}pyrimidin-1-ium trifluoroacetate **236**

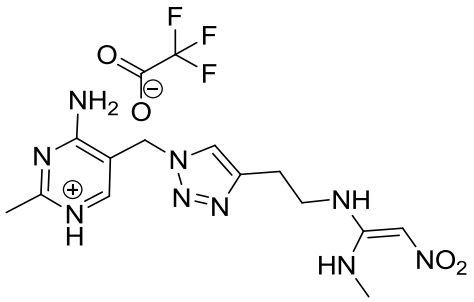

2-{1-[(4-Amino-2-methyl-5-pyrimidinyl)methyl]-1*H*-1,2,3-triazol-4-yl}ethanaminium chloride **220** (50 mg, 0.214 mmol) was dissolved in DMF (1 mL, dry) to which was added triethylamine (22 mg, 0.214 mmol) and after 30 min of stirring (*E*)-*N*-methyl-1-(methylthio)-2-nitroethenamine **235** (31 mg, 0.214 mmol) was added and the reaction left for 16 h. The reaction mixture was subjected to HPLC purification to obtain the desired product (20 mg, 21 % yield).

HPLC Procedure

Flow rate: 6 mL/min.

Time (mins)	% Water (with 0.1% TFA)	% MeCN (with 0.1% TFA)
0	99	1
10	80	20
15	70	30
20	70	30

Retention time: 5.1 min.

Purity by HPLC: >95 %.

Melting Point: > 230 ^{o}C.

IR: 3062, 2587, 1652, 1632, 1547, 1502, 1350, 1168, 1141, 804.

δ_H NMR (D_2O): 7.87 (1H, s), 7.84 (1H, s), 5.43 (2H, s), 3.21-3.28 (2H, m), 3.06 (3H, s), 3.0-3.05 (2H, m), 2.45 (3H, s).

δ_C NMR: Insufficient material.

HR-MS-FAB: Found 334.1738 calculated for $C_{13}H_{20}N_9O_2^+$ (M+H) 334.1735.

Synthesis of 2-{1-[(4-amino-2-methyl-5-pyrimidinyl)methyl]-1*H*-1,2,3-triazol-4-yl}ethyl methanesulfonate **237**

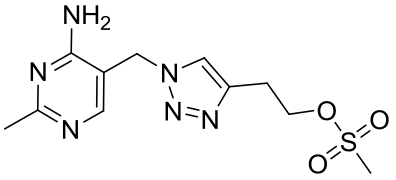

To a stirred solution of 3-butynyl methanesulfonate **224** (700 mg, 3.11 mmol) and 5-azidomethyl-2-methylpyrimidin-4-ylamine **222** (500 mg, 3.04 mmol) in *tert*-butanol/ water (5 mL; 2: 1) were added sodium ascorbate (60 mg, 0.30 mmol) and $CuSO_4 \cdot 5H_2O$ (8 mg, 0.32 mmol). The reaction mixture was stirred at room temperature for 16 h. The crude mixture was evaporated under reduced pressure and the solid residue was purified by flash column chromatography (MeOH:EtOAc; 10:90, R_f 0.15). The desired material was obtained as a white powder (500 mg, 53 % yield).

HPLC Procedure

Flow rate: 6 mL/min.

Time (mins)	% Water (with 0.1% TFA)	% MeCN (with 0.1% TFA)
0	95	5
10	80	20
15	70	30
20	70	30

Retention time: 12.0 min.

Purity by HPLC: >95 %.

Melting Point: > 230 ^{o}C.

IR: 3335, 3130, 1661, 1568, 1348, 1174, 1023, 905.

δ_H NMR (DMSO): 7.96 (1 H, s), 7.95 (1 H, s), 6.88 (2 H, bs), 5.40 (2 H, s), 4.41 (2 H, t, *J* = 7.0), 3.30 (3H, s), 3.04 (2 H, t, *J* = 7.0), 2.29 (3 H, s).

δ_C NMR (DMSO): 167.3, 161.9, 156.5, 143.2, 123.4, 108.7, 69.5, 47.1, 37.1, 25.9, 25.7.

HR-MS-FAB: Found 313.1087 calculated for $C_{11}H_{17}N_6O_3S^+$ (M+H) 313.1083.

Synthesis of 4-amino-5-{[4-({4-[6-ethoxy-3-(ethoxycarbonyl)-6-oxohexanoyl]anilino}methyl)-1*H*-1,2,3-triazol-1-yl]methyl}-2-methylpyrimidin-1-ium trifluoroacetate **239**

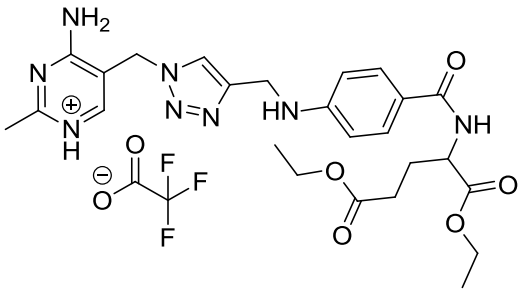

To a stirred solution of diethyl 2-(2-oxo-2-(4-(prop-2-yn-1-ylamino)phenyl)ethyl)pentanedioate **238** (50 mg, 0.22 mmol) and 5-azidomethyl-2-methylpyrimidin-4-ylamine **222** (35 mg, 0.22 mmol) in *tert*-butanol/ water (5 mL; 2 : 1) were added sodium ascorbate (4.3 mg, 0.02 mmol) and $CuSO_4 \cdot 5H_2O$ (0.6 mg, 0.02 mmol). The reaction mixture was stirred at room temperature for 16 h. The crude mixture was evaporated under reduced pressure and the solid residue was dissolved in DMF (1 mL) and purified by HPLC. The desired material was obtained as a white powder (50 mg, 43 % yield).

HPLC Procedure

Flow rate: 6 mL/min.

Time (mins)	% Water (with 0.1% TFA)	% MeCN (with 0.1% TFA)
0	75	25
15	70	30
20	70	30

Retention time: 15.5 min.

Purity by HPLC: >96 %.

Melting Point: > 230 ^{o}C.

IR: 3347, 3225, 2982, 2935, 2342, 1731, 1635, 1607, 1541, 1515, 1445, 1375, 1330, 1271, 1190, 1134, 1100, 1023.

δ_H NMR (DMSO): 8.22 (1H, d, *J* = 7.5), 7.98 (1H, s), 7.64 (2H, d, *J* = 9.0), 6.95 (2H, bs), 6.62-6.65 (3H, m), 5.44 (2H, s), 4.33-4.37 (4H, m), 4.01-4.09 (5H, m), 2.40 (2H, t, *J* = 7.5), 2.31 (3H, bs), 1.96-2.07 (2H, m), 1.16 (6H, q, *J* = 7.0).

HR-MS-FAB: Found 524.2618 calculated for $C_{26}H_{34}N_7O_5^+$ (M+H) 524.2616.

Synthesis of 4-amino-5-[(4-{[4-(3,5-dicarboxypentanoyl)anilino]methyl}-1*H*-1,2,3-triazol-1-yl)methyl]-2-methylpyrimidin-1-ium trifluoroacetate **240**

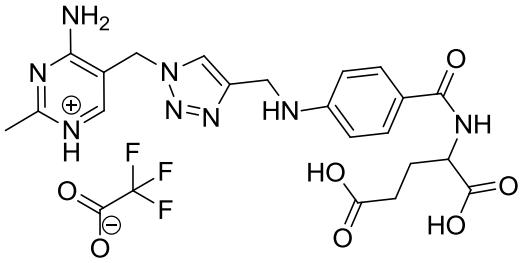

4-Amino-5-{[4-({4-[6-ethoxy-3-(ethoxycarbonyl)-6-oxohexanoyl]anilino}methyl)-1*H*-1,2,3-triazol-1-yl]methyl}-2-methylpyrimidin-1-ium trifluoroacetate **239** (30 mg, 0.057 mmol) was dissolved in NaOH solution (10 mg, 1 mL water) and refluxed for 3 hours. The solvent was removed by rotary evaporation, the resulting residue dissolved in DMF (1 mL) and purified by HPLC. The desired material was obtained as a white powder (15 mg, 56 % yield).

HPLC Procedure

Flow rate: 6 mL/min.

Time (mins)	% Water (with 0.1% TFA)	% MeCN (with 0.1% TFA)
0	75	25
15	70	30
20	70	30

Retention time: 11.5 min.

Purity by HPLC: >96 %.

Melting Point: > 230 ^{o}C.

IR: 3417, 2925, 2851, 1658, 1637, 1610, 1542, 1515, 1405, 1332, 1203, 1138, 1056.

δ_H NMR (DMSO): 12.37-12.45 (2H, m), 8.26 (1H, s), 8.10 (1H, d, *J* = 7.5), 8.05 (1H, s), 7.65 (2H, d, *J* = 9.0), 6.63 (2H, d, *J* = 9.0), 5.48 (2H, s), 4.33-4.37 (3H, m), 2.44 (3H, s), 2.31 (2H, t, *J* = 7.5), 1.90-2.07 (2H, m).

δ_C NMR (DMSO): 173.9, 173.7, 166.4, 163.1, 161.6, 150.9, 145.5, 144.31, 128.9, 123.2, 120.1, 111.0, 109.6, 51.7, 45.5, 37.9, 30.4, 26.0, 21.3.

HR-MS-FAB: Found 469.1942calculated for $C_{21}H_{25}O_5N_8^+$ (M+H) 469.1940.

Synthesis of 4-amino-5-({4-[2-(diethoxyphosphoryl)-3-ethoxy-3-oxopropyl]-1*H*-1,2,3-triazol-1-yl}methyl)-2-methylpyrimidin-1-ium trifluoroacetate **242**

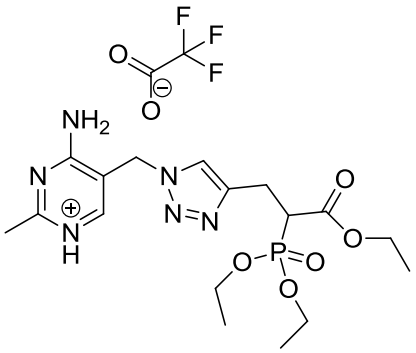

To a stirred solution of ethyl 2-(diethoxyphosphoryl)pent-4-ynoate **241** (57 mg, 0.22 mmol) and 5-azidomethyl-2-methylpyrimidin-4-ylamine **222** (35 mg, 0.22 mmol) in *tert*-butanol/ water (5 mL; 2 : 1) were added sodium ascorbate (4.3 mg, 0.02 mmol) and $CuSO_4 \cdot 5H_2O$ (0.6 mg, 0.02 mmol). The reaction mixture was stirred at room temperature for 16 h. The crude mixture was evaporated under reduced pressure and the solid residue was dissolved in DMF (1 mL) and purified by HPLC. The desired material was obtained as a white powder (40 mg, 34 % yield).

HPLC Procedure

Flow rate: 6 mL/min.

Time (mins)	% Water (with 0.1% TFA)	% MeCN (with 0.1% TFA)
0	75	25
15	70	30
20	70	30

Retention time: 8.5 min.

Purity by HPLC: >95 %.

Melting Point: > 230 ^{o}C.

IR: 3258, 2936, 2660, 2466, 1562, 1524, 1511, 1148, 1032, 969.

δ_H NMR (DMSO): 9.81 (2H, bs), 8.24 (1H, s), 7.98 (1H, s), 5.50 (2H, s), 4.01-4.11 (6H, m), 3.37-3.47 (1H, m), 3.15-3.24 (1H, m), 3.00-3.08 (1H, m), 2.48 (3H, s), 1.22-1.27 (6H, m), 1.11 (3H, t, *J* = 7.2).

δ_C NMR (DMSO): 167. 9, 162.9, 161.9, 145.0, 143.8, 122.9, 109.5, 62.4, 60.9, 45.5, 43.9, 22.9, 21.5, 16.2, 13.8.

HR-MS-FAB: Found 427.1851 calculated for $C_{17}H_{28}O_5N_6P^+$ (M+H) 427.1853.

Synthesis of 4-amino-5-({4-[2-carboxy-2-(diethoxyphosphoryl)ethyl]-1*H*-1,2,3-triazol-1-yl}methyl)-2-methylpyrimidin-1-ium trifluoroacetate **243**

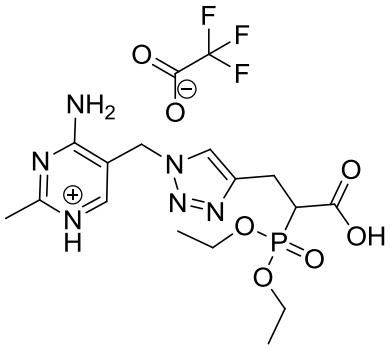

4-Amino-5-({4-[2-(diethoxyphosphoryl)-3-ethoxy-3-oxopropyl]-1*H*-1,2,3-triazol-1-yl}methyl)-2-methylpyrimidin-1-ium trifluoroacetate **242** (30 mg, 0.056 mmol) was dissolved in NaOH solution (20 mg, 1 mL water) and refluxed for 3 hours. The solvent was removed by rotary evaporation, the resulting residue dissolved in DMF (1 mL) and purified by HPLC. The desired material was obtained as a white powder (15 mg, 52 % yield).

HPLC Procedure

Flow rate: 6 mL/min.

Time (mins)	% Water (with 0.1% TFA)	% MeCN (with 0.1% TFA)
0	75	25
15	70	30
20	70	30

Retention time: 8.0 min.

Purity by HPLC: >95 %.

Melting Point: > 230 ^{o}C.

IR: 3112, 3050, 2986, 1726, 1687, 1655, 1651, 1621, 1562, 1543, 1508, 1437, 1420, 1398, 1364, 1230, 1189, 1140, 1103.

δ_H NMR (DMSO): 12.74 (1H, bs), 8.21 (1H, s), 7.95 (1H, s), 5.46 (2H, s), 4.01-4.08 (4H, m), 3.29-3.36 (1H, m), 3.12-3.19 (1H, m), 2.97-3.01 (1H, m), 2.48 (3H, s), 1.21-1.24 (6H, m).

δ_C NMR (DMSO): 169.1, 162.9, 161.9, 144.9, 144.2, 122.9, 109.5, 62.2, 45.5, 43.9, 22.9, 21.5, 16.16.

HR-MS-FAB: Found 399.1531 calculated for $C_{15}H_{24}O_5N_6P^+$ (M+H) 399.1540.

Synthesis of 4-amino-5-(ammoniomethyl)-2-methylpyrimidin-1-ium dichloride **244**

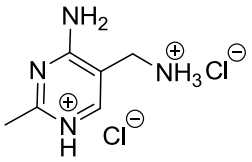

5-Azidomethyl-2-methylpyrimidin-4-ylamine **222** (50 mg, 0.30 mmol) was dissolved in 1:1; MeOH: 0.1 N HCl and to this was added Pd/C-10 % (30 mg) under nitrogen. This was subjected to hydrogenation for 6 hours then the catalyst was removed by filtration through keisulghur. The solvent was removed by rotary evaporation leaving the desired material as a light brown solid (60 mg, 94 % yield).

HPLC Procedure

Flow rate: 6 mL/min.

Time (mins)	% Water (with 0.1% TFA)	% MeCN (with 0.1% TFA)
0	90	10
15	70	30
20	70	30

Retention time: 9.5 min.

Purity by HPLC: >95 %.

Melting Point: > 230 ^{o}C.

IR: 3313, 3129, 2959, 2621, 2404, 2092, 1665, 1602, 1568, 1525, 1487, 1420, 1289.

δ_H NMR (DMSO): 8.06 (1H, s), 7.89 (2H, bs), 7.03 (2H, bs), 3.85 (2H, s), 2.32 (3H, s).

δ_C NMR (DMSO): 166.8, 161.8, 156.9, 106.7, 36.0, 25.24.

HR-MS-FAB: Found 139.0710 calculated for $C_6H_{11}N_4^+$ (M+H) 139.0978.

Synthesis of 4-amino-2-methyl-5-({[(3,4,5-trimethoxyphenyl)acetyl]amino}methyl)pyrimidin-1-ium trifluoroacetate **246**

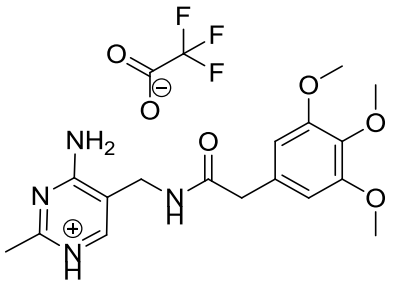

4-Amino-5-(ammoniomethyl)-2-methylpyrimidin-1-ium dichloride **244** (10 mg, 0.047 mmol) was dissolved in DMF (1 mL, anhydrous) and to this was added 2-(3,4,5-trimethoxyphenyl)acetic acid **245** (15 mg, 0.066 mmol) and HBTU (35 mg, 0.094 mmol). This was left to stir for 14 hours and purified directly by HPLC. The desired material was obtained as a white powder (8 mg, 37 % yield).

HPLC Procedure

Flow rate: 6 mL/min.

Time (mins)	% Water (with 0.1% TFA)	% MeCN (with 0.1% TFA)
0	85	15
15	70	30
20	70	30

Retention time: 11.5 min.

Purity by HPLC: >97 %.

Melting Point: > 230 ^{o}C.

IR: 3320, 3260, 3066, 2937, 1662, 1647, 1621, 1595, 1552, 1507, 1464, 1446, 1420, 1362, 1330, 1237, 1198, 1170, 1112.

δ_H NMR (DMSO): 9.02 (1H, bs), 8.46 (1H, t, *J* = 6.0), 8.31 (1H, bs), 8.01 (1H, s), 6.55 (2H, s), 4.11 (2H, d, *J* = 6.0), 3.73 (6H, s), 3.62 (3H, s), 3.44 (2H, s), 2.46 (3H, s).

δ_C NMR (DMSO): 171.5, 163.1, 160.9, 158.2, 152.7, 136.2, 131.2, 112.6, 106.3, 59.9, 55.7, 42.4, 36.0, 21.4.

HR-MS-FAB: Found 347.1709 calculated for $C_{17}H_{23}O_4N_4^+$ (M+H) 347.1714.

4.3 Stability Studies

Solutions of the test compounds (2 mg/mL), **BP1** – **BP5** were prepared in aqueous sodium phosphate buffer (pH 7.4, 10 mM). These were incubated at 37.5 ^{o}C in a water bath. Samples (100 µL) were injected into the HPLC at 0 h, 2 h 5 min, 4 h 15 min and 27 h. Significant precipitation had occurred during the course of the injections and the resultant precipitate was filtered, dried, re-dissolved in buffer and re-injected to ensure that the precipitate was the starting species.

LC Conditions:

Column:	Luna 5µ C18(2) 100A
Dimensions:	60 × 21.1 mm
Injection Volume:	100 µL

Retention times

MGB-BP-1: 19.7 min
MGB-BP-2: 6.8 min
MGB-BP-3: 5.5 min
MGB-BP-4: 20.8 min
MGB-BP-5: 18.0 min

HPLC Protocols

BP1, ***BP2*** *and* ***BP3****:*

Eluent: Acetonitrile/water 0.1% TFA

Time min	Flow mL/min	% Acetonitrile	% Water
0	6	60	40
25	6	50	50
30	6	30	70
35	6	60	40
40	0	60	40
40.1	0	60	40

BP4*:*

Eluent: Acetonitrile/water 0.1% TFA

Time min	Flow mL/min	% Acetonitrile	% Water
0	6	60	40
25	6	50	50
30	6	30	70
35	6	60	40
40	0	60	40
40.1	0	60	40

BP5*:*

Eluent: Acetonitrile/water 0.1% TFA

Time min	Flow mL/min	% Acetonitrile	% Water
0	6	60	40
25	6	50	50
30	6	30	70
35	6	60	40
40	0	60	40
40.1	0	60	40

Sample Traces:

BP1

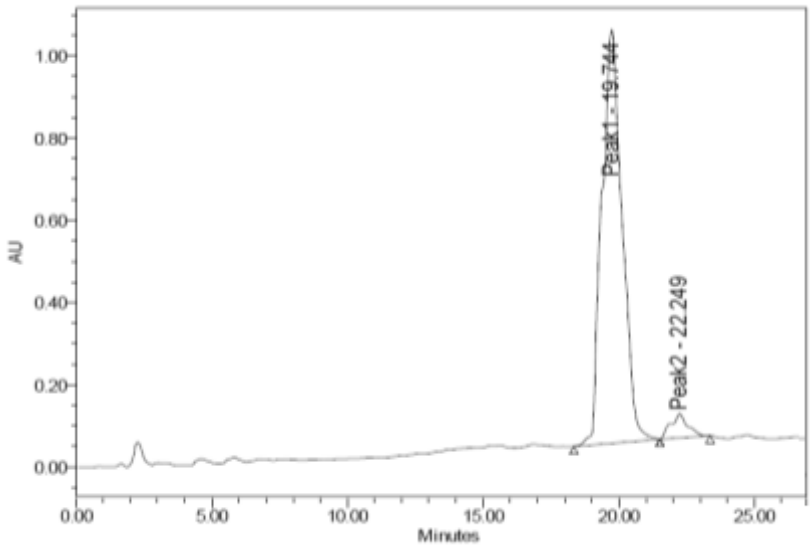

BP2

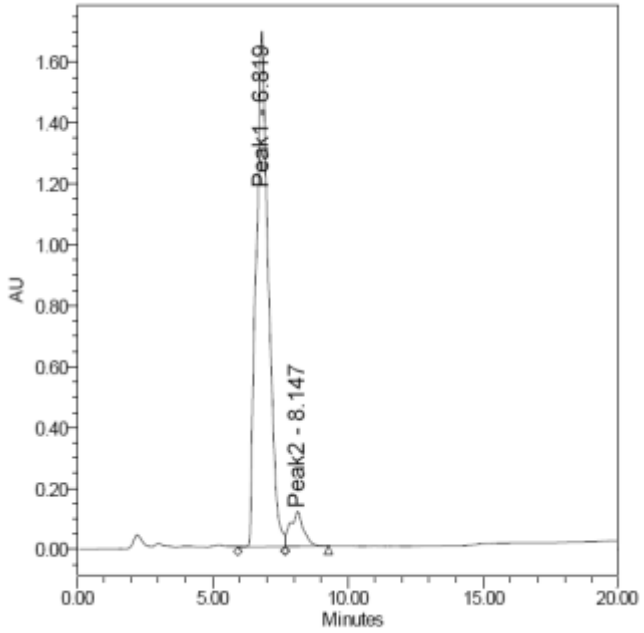

BP3

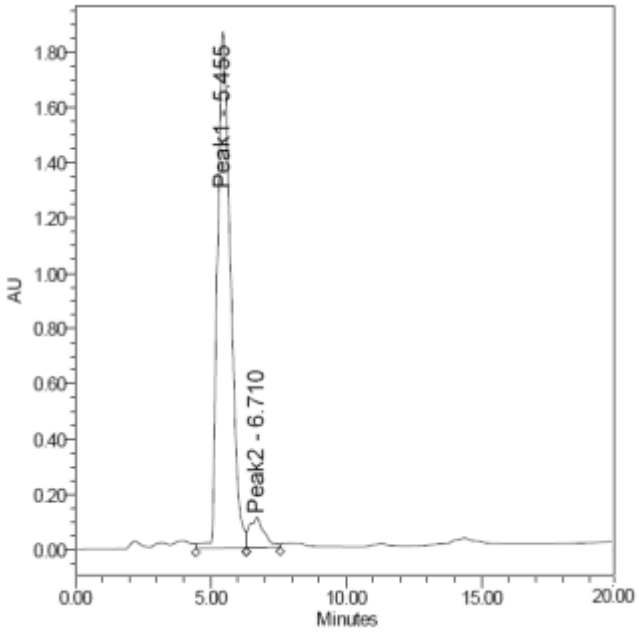
Peak1 - 5.455
Peak2 - 6.710
AU
Minutes
1.80
1.60
1.40
1.20
1.00
0.80
0.60
0.40
0.20
0.00
0.00
5.00
10.00
15.00
20.00

BP4

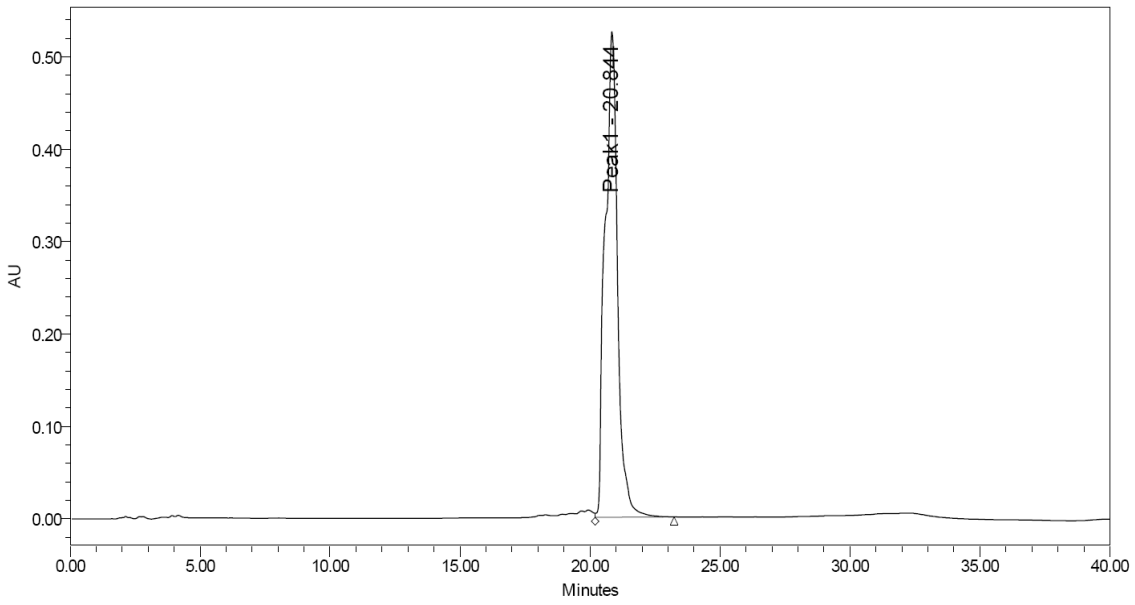
Peak1 - 20.844
AU
Minutes
0.50
0.40
0.30
0.20
0.10
0.00
0.00
5.00
10.00
15.00
20.00
25.00
30.00
35.00
40.00

BP5

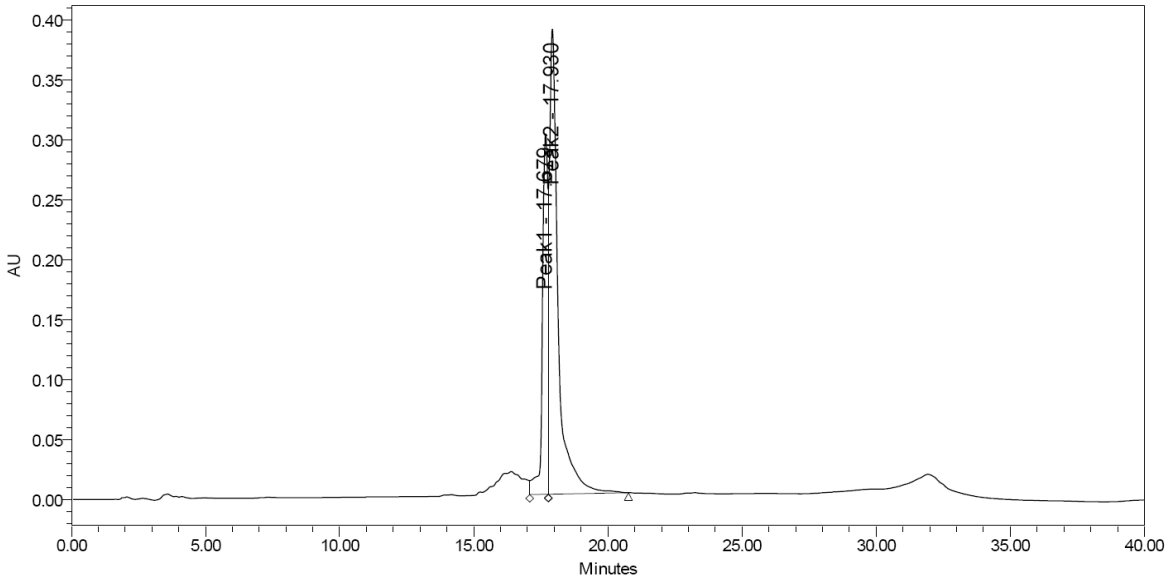
0.40
0.35
0.30
0.25
0.20
0.15
0.10
0.05
0.00
AU
0.00
5.00
10.00
15.00
20.00
25.00
30.00
35.00
40.00
Minutes

4.4 Microsome Stability Study

Procedure

Each of the test compounds, along with paracetamol as a positive control, were subjected to the following protocol:

A test compound stock solution was prepared (10 mM). The NADPH Regenerating System (NRS) was prepared by first preparing a 2 % aqueous $NaHCO_3$ solution (2 % w/v). To this was added NADP (1.7 mg), glucose-6-phosphate (7.8 mg) and glucose-6-phosphate dehydrogenase (6 units). To check that NAPDH was present, an aliquot of the solution was placed in a 37 ^{o}C water bath for 5 min and the UV spectrum of the solution was obtained, the absorption at 340 nm indicates the presence of NAPDH.

Tris buffer (pH 7.4, 50 mM) was prepared and the supplied microsomes (Male ICR/CD-1 mouse, Female ICR/CD-1 mouse, Celsis in Vitro GmbH) were diluted (2.5 mg, 500 µL of Tris buffer). A test tube was placed into an ice bath and to this was added diluted microsomes (100 µL), Tris buffer (640 µL) and the test compound stock (10 µL). This test tube along with another containing the NRS were placed into a 37 ^{o}C water bath and left for 5 min. NRS (250 µL) was then added to the test compound test tube and the time noted. At 0, 6 and 20 h an aliquot of the reaction mixture was subjected to analysis by mass spectrometry to determine the presence of any test compound metabolites.

Note that in each case, after 6 h the analysis by mass spectrometry of the paracetamol control showed no mass due to paracetamol, indicating that that system was functioning.

An aliquot of the reaction mixture was then injected into the HPLC system to determine the concentration of the test compound left in the mixture.

Analytical Procedure

LC Conditions:

Column:	Waters Spherisorb ODS-2 µm
Dimensions:	250 × 3.2mm
Injection Volume:	20 µL
Solvent Flow Rate:	1 mL/min
Detection wavelength:	254 nm

Pump Program for **BP1**:

Time	% Water (with 0.1% TFA)	% MeCN (with 0.1% TFA)
0	70	30
25	10	90
30	10	90

Pump Program for **BP2** and **BP3**:

Time	% Water (with 0.1% TFA)	% MeCN (with 0.1% TFA)
0	70	30
25	10	90
35	10	90

Calibration Curves:

50 µM, 100 µM and 200 µM standards of each compound were prepared. The preparation of a standard was followed by an immediate 20 µM injection into the HPLC system as precipitation of the compounds is time sensitive. Mass spectrometry was used to confirm the identity of the peaks.

Sample Injection

20 µM of the solution obtained from the microsome mixture was injected into the HPLC system and again mass spectrometry was used to confirm the identity of the peaks.

Enhanced Analysis of **BP3**

As previous except that for the calibration curve the injections were now in triplicate and at 100 µL. Sample injection was also at 100 µL

Sample HPLC Traces

BP1
Rt: 22.9 min

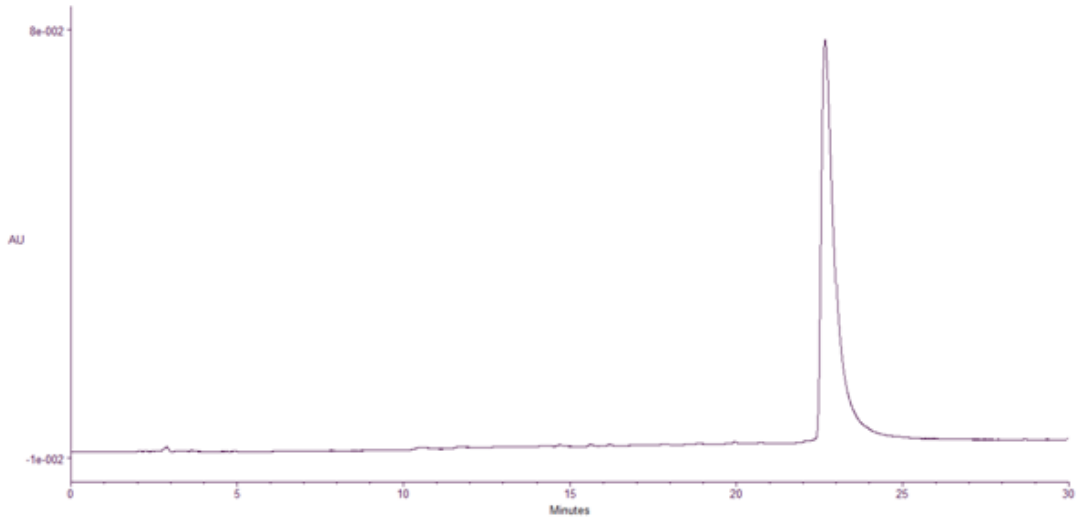

BP2
Rt: 25.3 min

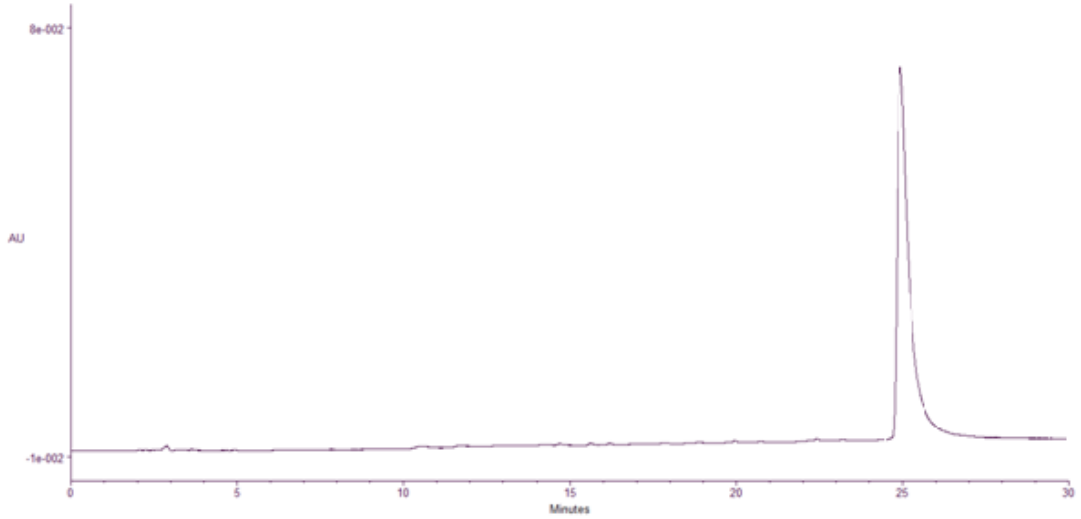

BP3
Rt: 21.0 min

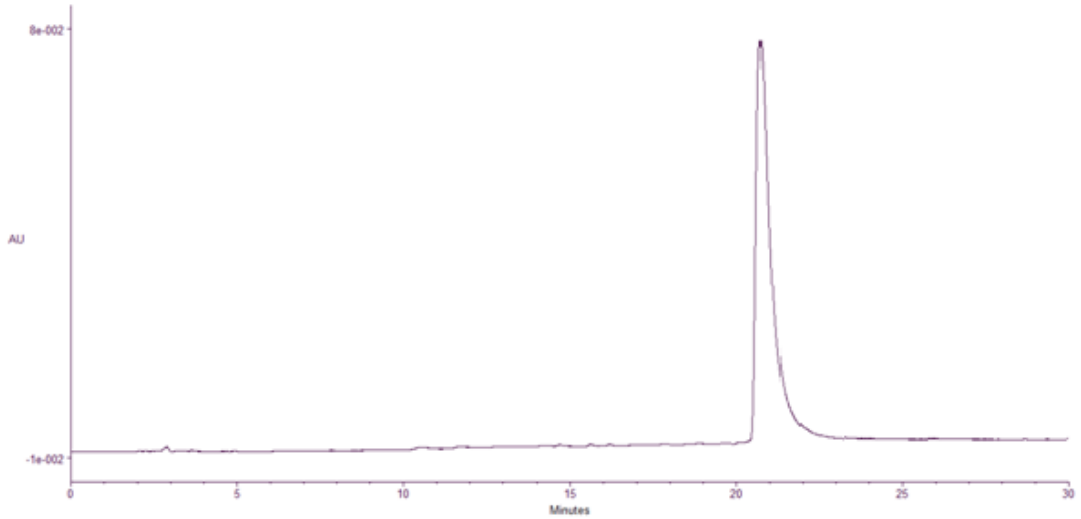

Enhanced Analysis of ***BP3***
Rt: 21.0 min

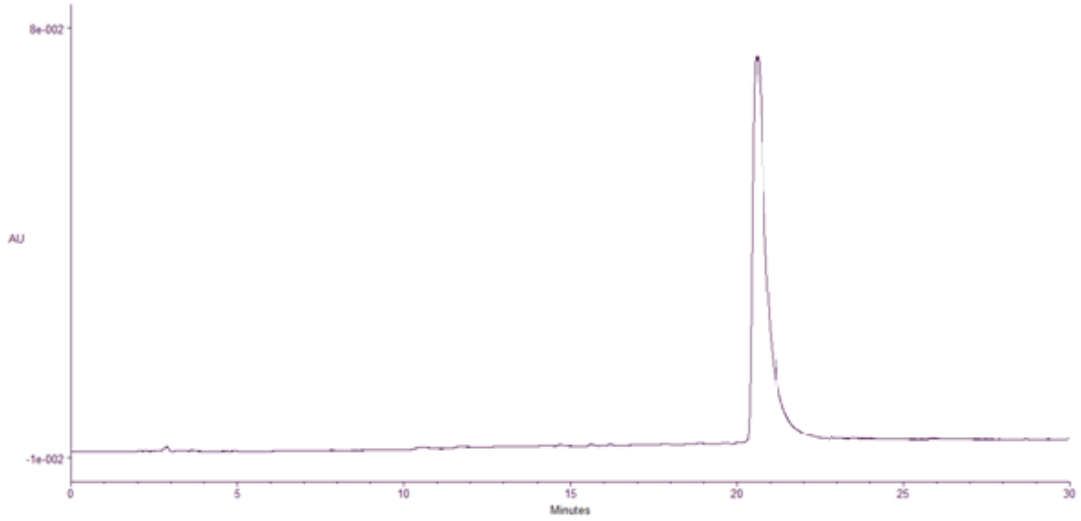

Microsome Stability Study Expanded Results

BP1

Male Microsomes

Time (hours)	Predominant Mass	New Masses
0	612.00 (M+1)	No
6	612.40 (M+1)	No
20	612.27 (M+1)	No

Female Microsomes

Time (hours)	Predominant Mass	New Masses
0	611.93 (M+1)	No
6	612.00 (M+1)	No
20	612.00 (M+1)	No

Analytical HPLC

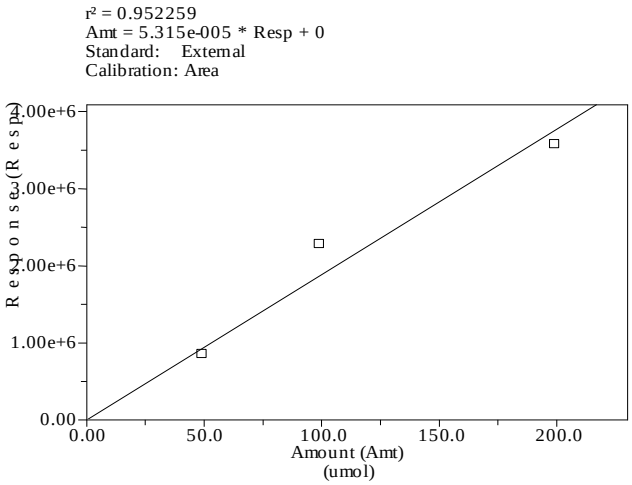

Percentage concentration of **BP1** from male microsomes: 90 ± 9
Percentage concentration of **BP1** from female microsomes: 92 ± 9

BP2

Male Microsomes

Time (hours)	Predominant Mass	New Masses
0	647.13 (M+Na)	No
6	646.93 (M+Na)	No
20	646.93 (M+Na)	No

Female Microsomes

Time (hours)	Predominant Mass	New Masses
0	647.00 (M+Na)	No
6	647.47 (M+Na)	No
20	647.12 (M+Na)	No

Analytical HPLC

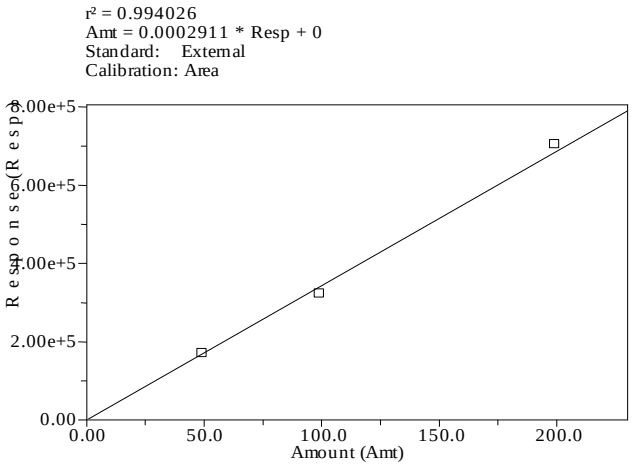

Percentage concentration of **BP2** from male microsomes: 99 ± 8
Percentage concentration of **BP2** from female microsomes: 93 ± 8

BP3

Male Microsomes

Time (hours)	Predominant Mass	New Masses
0	632.80 (M+1)	No
6	632.67 (M+1)	No
20	633.07 (M+1)	No

Female Microsomes

Time (hours)	Predominant Mass	New Masses
0	633.20 (M+1)	No
6	632.87 (M+1)	No
20	633.14 (M+1)	No

Analytical HPLC

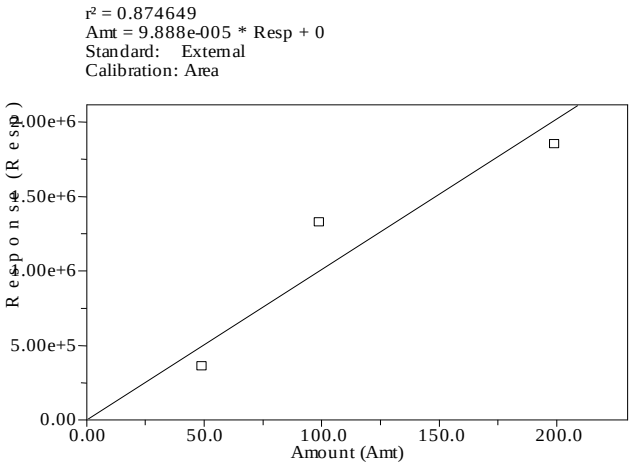

Percentage concentration of **BP3** from male microsomes: 90 ± 10
Percentage concentration of **BP3** from female microsomes: 101 ± 10

Further Developed Analytical HPLC

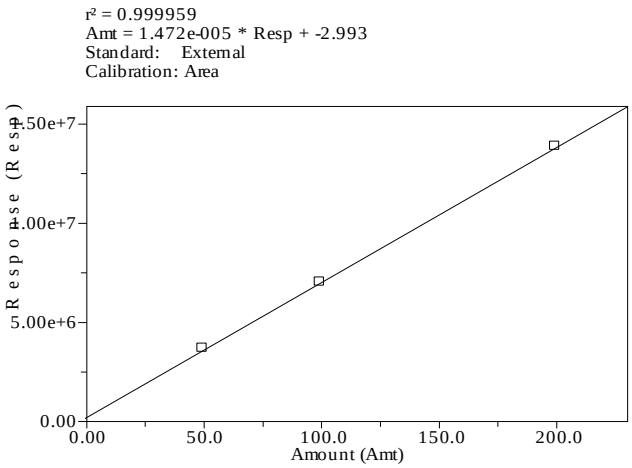

Standard Concentration	Precision (n = 3)
50µM	5.7
100µM	3.5
200µM	4.4

Percentage concentration of **BP3** from male microsomes: 97 ± 5.5
Percentage concentration of **BP3** from female microsomes: 100 ± 5.5

4.5 Microbiology Methods

Pseudomonas aerugenosa Growth Assay

A fresh culture of *Pseudomonas aerugenosa* was prepared by inoculating one loopful from the stock agar plate into LB broth (5 mL). This was incubabted, with shaking, at 37 ^{o}C for 18 hours. An aliquot of this culture (100 µL) was inoculated into LB broth (50 mL) and incubated, with shaking, at 37 ^{o}C until the optical density measured at 600 nm reached 0.3. An aliquot of this culture (25 µL) was added into M63 media (50 mL) and an aliquot of this (100 µL) was added into the appropriate wells of a microtitre plate. Solutions of the test compounds (5 µL, 30 µg/mL DMSO) were added to the appropriate wells and the plate was laminated. The plate was incubated at 37 ^{o}C for 18 hours. After this time the absorbance of each well was measured at 600 nm using a microplate reader. Wells containing culture (100 µL) and DMSO (5 µL) were used as a negative control and gentamycin (30 µg/mL DMSO) was used at as a positive control. All assays were carried out in triplaicate and were repeated twice.

Pseudomonas aerugenosa Growth Assay with EPI

This assay followed the same procedure as the assay with no EPI except that the working culture (25 µL) was added into M63 (46 mL) media and to this was added the PAβN solution (4 mg, 4 mL DMSO), giving a final concentration of 76.2 µg/mL of PAβN in each well once the test compounds were added. The concentration of PAβN did not affect the bacterial growth.

5 References

1 N.A. Campbell, J.B. Reece, Biology, 6th edition, **2002**, Pearson Education Inc, chapter 5.

2 J.D. Watson, The Double Helix, 1st edition, Penguin Books Ltd.

3 J.D. Watson, F.H.C. Crick, Nature, **1953**, *3*, 694-967.

4 G.L. Patrick, *An Introduction to Medicinal Chemistry*, 3rd edn., Oxford University Press Inc., New York, **2005**.

5 P.B. Dervan, *Bioorg. Med. Chem.*, **2001**, *9*, 2215-2231.

6 E.H. Bayne, R.C. Allshire, *Trends Genet.*, **2005**, *21*, 370.

7 M. Jovanovic, M.O. Hengartner, *Oncogene*, **2006**, *25*, 6176.

8 L. Manche, S.R. Green, C. Schmedt, M.B. Mathews, *Mol. Cell Biol.*, **1992**, *12*, 5238.

9 M.J. Fedor, J.R. Williamson, *Nature Rev. Mol. Cell Biol.*, **2005**, *6*, 399.

10 K.M. Weeks, D.M. Crothers, *Science*, **1993**, *261*, 1574.

11 C.B. Carlson, O.M. Stephens, P.A. Beal, *Biopolymers*, **2003**, *70*, 86

12 J. R. Thomas, P. J. Hergenrother, *Chem. Rev.*, **2008**, *108*, 1171-1224.

13 S. Yoshizawa, D. Fourmy, J.D. Puglisi, *Science*, **1999**, *285*, 1722.

14 A.P. Carter, W.M. Clemons, D.E. Brodersen, R.J. Morgan-Warren, B.T. Wimberly, V. Ramakrishnan, Nature, **2000**, *407*, 340.

15 N.E. Mikkelsen, K. Johansson, A. Virtanen, L.A. Kirsebom, *Nat. Struct. Biol.*, **2001**, *8*, 510.

16 R. Caswell, L. Bryant, J. Sinclair, *J. Virol.*, **1996**, *70*, 4028-4037.

17 T.M. Henkin, B.L. Glass, F.J. Grundy, *Bacteriol.*, **1992**, *174*, 1299.

18 M.S. Gerdeman, T.M. Henkin, J.V. Hines, *Nucleic Acids Res.*, **2002**, *30*, 1065.

19 P. Lombardi, A. Crisanti, *Pharmacol. Ther.*, **1997**, *76*, 125-133.

20 M.L. Kopka, C. Yoon, D. Goodsell, P. Pjura, R.E. Dickerson, *Proc. Natl. Acad. Sci. USA*, **1985**, *82*, 1376-1380.

21 A. Dimarco , M. Gaetani , P. Orezzi, T. Scotti , F. Arcamone, *Cancer Chemother. Rep.*, **1962**, *18*, 15-19.

22 R.P. Austin, A.M. Davis, C.N. Manners, *J. Pharm. Sci.*, **1995**, *54*, 1180-1183.

23 J.G. Pelton, D.E. Wemmer, *Biochem.*, **1988**, *27*, 8088-8096.

24 Y. Miao, PhD Thesis, *Shape-Dependent Molecular Recognition of Specific Sequences of DNA by Heterocyclic Cations*, College of Arts and Sciences Georgia State University, **2006**.

25 S.A. Khedkar, A.K. Malde, E. C. Coutinho, *J. Mol. Model*, **2007**, *13*, 1099–1108.

26 C.J. Suckling, *J. Phys. Org. Chem.* **2008**, *21*, 575-583.

27 P.B. Dervan, U. Ellernik, C.C.C. Wang, *J. Am. Chem. Soc.*, **2000**, *122*, 9354.

28 N.G. Anthony, B.F. Johnston, A.I. Khalaf, S.P. MacKay, J.A. Parkinson, C.J. Suckling, R.D. Waigh, *J. Am. Chem. Soc.*, **2004**, *126*, 11338-11349.

29 G. Burkhardt, H. Simon, K. Storl, *J. Biomol. Struct. Dyn.*, **1997**, *15*, 81.

30 C.J. Suckling, A.I. Khalaf, A.R. Pitt, M. Scobie, *Tetrahedron*, **2000**, *56*, 5225.

31 P.B. Dervan, D.M. Herman, J.M. Turner, E.E. Baird, *J. Am. Chem. Soc.*, **1999**, *121*, 11621.

32 P.G. Baraldi, D. Preti, F. Fruttarolo, M.A. Tabrizi, R. Romagnoli, *Bioorg. Med. Chem.*, **2007**, *15*, 17–35

33 C. Geroni, S. Marchini, P. Cozzi, *Cancer Res.*, **2002**, *62*, 2332-2336.

34 S. Pezzola, G. Antonini, C. Geroni, I. Beria, M. Colombo, M. Broggini, N. Mongelli, L. Leboffe, R. MacArthur, A. F. Mozzi, G. Federici and A. M. Caccuri, *Biochemistry*, **2010**, *49*, 226–235.

35 M.C. Sanguinetti, M. Tristani-Firouzi, *Nature*, **2006**, *440*, 463–9.

36 H. Choe, K.H. Nah, S.N. Lee, H.S. Lee, H.S. Lee, S.H. Jo, C.H. Leem and Y.J. Jang, *Biochem. Biophys. Res. Comm.*, **2006**, *344*, 72-78.

37 M.J. Waring and C. Johnstone, *Bioorg. Med. Chem. Lett.*, **2007**, *17*, 1759-1764.

38 T. Schirmer, *J. Struc. Biol.*, **1998**, *121*, 100-109.

39 R. Benz, K. Bauer, *Eur. J. Biochem.*, **1988**, *176*, 1-19.

40 C.J. Law, P.C. Maloney, D. Wang, *Ann. Rev. Microbiol.*, **2008**, *62*, 289–305.

41 J. Fernandez-Recio, F. Walas, L. Federici, J.V. Pratap, V.N. Bavro, *FEBS Letters*, **2004**, *578*, 5–9.

42 X. Zhang, F. Kiechle, *Ann. Clin. Lab. Sci.,* **2001**, *31*, 187-98.

43 S. Bansal, U. Tawar, M. Singh, A. Nikravesh, L.Good, V. Tandon, *Int. J. Antimicrob. Agents*, **2010**, *35*, 186-190.

44 A. Roth, R. R. Breaker, *Ann. Rev. Biochem*. **2009**, *78*, 305.

45 W.C. Winkler, *Arch. Microbiol*. **2005**, *183*, 151–159.

46 N. Sudarsan, J. E. Barrick, R. R. Breaker, *RNA*, **2003**, *9*, 644.

47 A. Serganov, *Curr. Op. Str. Bio.*, **2009**, *19*, 251.

48 K. F. Blount, R. R. Breaker, *Nature Biotech.*, **2006**, *24*, 1558.

49 C. A. Wakeman, W. C. Winkler, C. E, Dann III, *Trends BioChem. Sci.*, **2007**, *32*, 415.

50 M. Mandal, R. R. Breaker, *Nat. Struct. Mol. Biol.,* **2004**, *11*, 29–35.

51 A.R. Ferre, D. Amare, J.A. Doudna, *Ann. Rev. Biophys. Biomol. Struct.* **1999**, *28*, 57-73.

52 W. Winkler, A. Nahvi, R.R. Breaker, *Nature*, **2002**, *419*, 952-956.

53 W.C. Winkler, R.R. Breaker, *Chem. Bio. Chem.*, **2003**, *4*, 1024-1032.

54 K.S. Wilson, P.H. von Hippel, *Proc. Natl. Acad. Sci. U.S.A.*, **1995**, *92*, 8793–7.

55 J. Shine, L. Dalgarno, *Nature*, **1975**, *254*, 34–8.

56 M. Kozak, *Nucleic Acids Res.*, **1987**, *15*, 8125–8148.

57 F. Crick, *J. Mol. Biol.*, **1966**, *19*, 548–55.

58 D. Iwata-Reuyl, *BioOrg. Chem*., **2003**, *31*, 24.

59 N. Okada, S. Noguchi, H. Kasai, N. Shindo-Okada, T. Ohgi, T. Goto, S. Nishimura, *J. Biol. Chem.*, **1979**, 254**,** 3067–3073.

60 G. Phillips, B. El Yacoubi, B. Lyons, S. Alvarez, D. Iwata-Reuyl, V. de Crécy-Lagard, *J. Bacteriol*., **2008**, *190*, 7876–7884.

61 R.C. Morris, M.S. Elliott, *Mol. Gene Meta*., **2001**, *74*, 147–159.

62 U. Gunduz, J.R. Katze, *J. Biol. Chem.*, **1984**, *259*, 1110–1113.

63 M.M. Meyer, A. Roth, S.M. Chervin, G.A. Garcia, R.R. Breaker, *RNA*, **2008**, *14*, 685-695.

64 A. Roth, W.C. Winkler, E.E. Regulski, B.W. Lee, J. Lim, I. Jona, J.E. Barrick, A. Ritwik, J.N. Kim, R. Welz, D. Iwata-Reuyl, R.R. Breaker, *Nat. Struct. Mol. Biol.,* **2007**, *14*, 308–317.

65 M. Kang, R. Peterson, J. Feigon, *Mol. Cell*, **2009**, *33*, 784–790.

66 K. Agyei-Owusu, F.J. Leeper, *FEBS Journal*, **2009**, *276*, 2905–2916.

67 N. Sudarsan, S. Cohen-Chalamish, S. Nakamura, G. Mitchell Emilsson, R.R. Breaker, *Chem. and Bio.*, **2005**, *12*, 1325–1335.

68 N. Sudarsan, J.E. Barrick, R.R. Breaker, *RNA*, **2003**, *9*, 644.

69 E. Nudler, *Cell*, **2006**, *126*, 19-22.

70 S.Thore, M. Leibundgut, N. Ban, *Science*, **2006**, *312*, 1208-1211.

71 D.G. Sashital and S.E. Butcher, *Chem. Bio*., **2006**, *1*, 341–345.

72 T. Yamauchia, D. Miyoshia, T. Kuboderab, A. Nishimurab, S. Nakaib, N.Sugimoto, *FEBS Lett*., **2005**, *579*, 2583–2588.

73 W.Winkler, A. Nahvi, R.R. Breaker, *Nature*, **2002**, *419*, 952.

74 R.W. Bürli, P. Jones, J.A. Kaizermann, W. Hu, United States Patent, *Isoquinoline Compounds Having Antiinfective Activity*, GeneSoft Pharmaceuticals, San Francisco, **2004**.

75 D. Breen, A.R. Kennedy and C.J. Suckling, *Org. Biomol. Chem.*, **2009**, *7*, 178-186.

76 S. Xu, F.D. Orro, A.E. Mather, *Can. J. Chem*., **1993**, *71*, 1048.

77 D.A. Case, T.A. Darden, T.E. Cheatham, III, C.L. Simmerling, J. Wang, R.E. Duke, R. Luo, R.C. Walker, W. Zhang, K.M. Merz, B. Roberts, B. Wang, S. Hayik, A. Roitberg, G. Seabra, I. Kolossvai, K.F. Wong, F. Paesani, J. Vanicek, J. Liu, X. Wu, S.R. Brozell, T. Steinbrecher, H. Gohlke, Q. Cai, X. Ye, J. Wang, M.-J. Hsieh, G. Cui, D.R. Roe, D.H. Mathews, M.G. Seetin, C. Sagui, V. Babin, T. Luchko, S. Gusarov, A. Kovalenko, and P.A. Kollman (2010), *AMBER 11*, University of California, San Francisco.

78 H.Y. Alniss, N.G. Anthony , A.I. Khalaf, S.P. Mackay , C.J. Suckling, R.D. Waigh, N. J. Wheate, J.A. Parkinson, *Chem. Sci.*, **2012**, *3*, 711-722.

79 P. Lombardi, A. Crisantit, *Pharmacol. Ther.*, **1997**, *76*, 125-133.

80 J.M.T. Hamilton-Miller, *Int. J. Antimicrobial Agents*, **2008**, *31*, 189-192.

81 P. Nordmann, G. Cuzon, T. Naas, *Lancet Infect. Dis.*, **2009**, *9*, 228–236.

82 B. Rouveix, *J. Antimicrob. Chemo.*, **2007**, *59*, 1208 – 1209

83 F. Klepper, K. Polborn, T. Carell, *Helv. Chem. Acta*, **2005**, *88*, 2610.

84 D.J. Klein, T.E. Edwards, A. R. Ferre-D'Amare, *Nat. Struct. Mol. Biol.*, **2009,** *16*, 343-344.

85 J. Feng, N. G. Walter, C. L. Brooks, *J.A.C.S*., **2011**, *133*, 4196-4199.

86 J.L. Jenkins, J. Krucinska, R.M. McCarty, V.Bandarian, J.E. Wedekind, *J. Biol. Chem.*, **2011**, *286*, 24626-24637.

87 S. Thore, C. Frick, N. Ban, *J. Am. Chem. Soc.* **2008**, *130*, 8116–8117.

88 H.J. Stellbrink, *Eur. J. Med. Res.*, **2007**, *12*, 483–95.

89 A.I. Khalaf, N. Anthony, D. Breen, G. Donoghue, S.P. Mackay, F.J. Scott, C.J. Suckling, *Euro. J. Med. Chem.***, 2011,** *46*, 5343–5355.

90 N.G. Anthony , D. Breen , J. Clarke, G. Donoghue , A. J. Drummond , E.M. Ellis , C.G. Gemmell , J. Helesbeux , I.S. Hunter , A.I. Khalaf , S.P. Mackay , J.A. Parkinson , C.J. Suckling, R.D. Waigh, *J. Med. Chem.***, 2007,** *50*, 6116-6125.

91 K .Walczynski, H. Timmerman, O.P. Zuiderveld, M.Q. Zhang, R. Glinka, *Farmaco*, **1999**, *54*, 533-541.

92 R.L. Baxter, A.B. Hanley, H.W.S. Chan, *J. Chem. Soc. Perkin Trans.1*, **1990**, *1*, 2963-2966.

93 K. M. Erixon, C.L. Dabalos and F.J. Leeper, *Org. Biomol. Chem.*, **2008**, *6*, 3561–3572.

94 Y. Wang, S. Hu, W. Fast, *J. Am. Chem. Soc.*, **2009**, *131*, 15096–15097.

6 Appendices

Appendix 1

License Number	2950220945596
License date	Jul 15, 2012
Licensed content publisher	Nature Publishing Group
Licensed content publication	Nature
Licensed content title	Molecular Configuration in Sodium Thymonucleate
Licensed content author	ROSALIND E. FRANKLIN, R. G. GOSLING
Licensed content date	Apr 25, 1953
Type of Use	reuse in a thesis/dissertation
Volume number	171
Issue number	4356
Requestor type	academic/educational
Format	print and electronic
Portion	figures/tables/illustrations
Number of figures/tables/illustrations	1
Figures	1
Author of this NPG article	no
Your reference number	
Title of your thesis / dissertation	An investigation into nucleic acid binding compounds
Expected completion date	Aug 2012
Estimated size (number of pages)	250
Total	0.00 GBP

Appendix 2

License Number	2942020951529
License date	Jul 04, 2012
Licensed content publisher	Elsevier
Licensed content publication	Bioorganic & Medicinal Chemistry
Licensed content title	Molecular recognition of DNA by small molecules
Licensed content author	Peter B. Dervan
Licensed content date	September 2001
Licensed content volume number	9
Licensed content issue number	9
Number of pages	21
Type of Use	reuse in a thesis/dissertation
Portion	figures/tables/illustrations
Number of figures/tables/illustrations	2
Format	both print and electronic
Are you the author of this Elsevier article?	No
Will you be translating?	No
Order reference number	
Title of your thesis/dissertation	An investigation into nucleic acid binding compounds
Expected completion date	Aug 2012
Estimated size (number of pages)	250
Elsevier VAT number	GB 494 6272 12
Permissions price	0.00 GBP
VAT/Local Sales Tax	0.0 USD / 0.0 GBP
Total	0.00 GBP

Appendix 3

Licensed content publisher	Elsevier
Licensed content publication	FEBS Letters
Licensed content title	A model of a transmembrane drug-efflux pump from Gram negative bacteria
Licensed content author	Juan Fernandez-Recio,Fabien Walas,Luca Federici,J. Venkatesh Pratap,Vassiliy N. Bavro,Ricardo Nunez Miguel,Kenji Mizuguchi,Ben Luisi
Licensed content date	3 December 2004
Licensed content volume number	578
Licensed content issue number	1–2
Number of pages	5
Type of Use	reuse in a thesis/dissertation
Portion	figures/tables/illustrations
Number of figures/tables/illustrations	2
Format	both print and electronic
Are you the author of this Elsevier article?	No
Will you be translating?	No
Order reference number	
Title of your thesis/dissertation	An investigation into nucleic acid binding compounds
Expected completion date	Aug 2012
Estimated size (number of pages)	250
Elsevier VAT number	GB 494 6272 12
Permissions price	0.00 GBP
VAT/Local Sales Tax	0.00 USD / 0.00 GBP
Total	0.00 GBP

Appendix 4

Requestor type	Academic institution
Format	Print, Electronic
Portion	image/photo
Number of images/photos requested	1
Title or numeric reference of the portion(s)	Figure 1
Editor of portion(s)	N/A
Author of portion(s)	Christopher J. Law, Peter C. Maloney, Da-Neng Wang
Volume of serial or monograph	62
Page range of portion	293
Publication date of portion	June 6, 2008
Rights for	Main product
Duration of use	Life of current/future editions
Creation of copies for the disabled	no
With minor editing privileges	no
For distribution to	Worldwide
In the following language(s)	Original language of publication
With incidental promotional use	no
Lifetime unit quantity of new product	0 to 499
Made available in the following markets	Education
The requesting person/organization	Fraser Scott
Order reference number	
Author/Editor	Fraser Scott
Title	An investigation into nucleic acid binding compounds
Publisher	University of Strathclyde
Expected publication date	Aug 2012
Estimated size (pages)	250

Appendix 5

Licensed content publisher	Elsevier
Licensed content publication	Bioorganic Chemistry
Licensed content title	Biosynthesis of the 7-deazaguanosine hypermodified nucleosides of transfer RNA
Licensed content author	Dirk Iwata-Reuyl
Licensed content date	February 2003
Licensed content volume number	31
Licensed content issue number	1
Number of pages	20
Type of Use	reuse in a thesis/dissertation
Portion	figures/tables/illustrations
Number of figures/tables/illustrations	2
Format	both print and electronic
Are you the author of this Elsevier article?	No
Will you be translating?	No
Order reference number	
Title of your thesis/dissertation	An investigation into nucleic acid binding compounds
Expected completion date	Aug 2012
Estimated size (number of pages)	250
Elsevier VAT number	GB 494 6272 12
Permissions price	0.00 GBP
VAT/Local Sales Tax	0.00 USD / 0.00 GBP
Total	0.00 GBP

Appendix 6

Licensed content publisher	Elsevier
Licensed content publication	Molecular Cell
Licensed content title	Structural Insights into Riboswitch Control of the Biosynthesis of Queuosine, a Modified Nucleotide Found in the Anticodon of tRNA
Licensed content author	Mijeong Kang,Robert Peterson,Juli Feigon
Licensed content date	27 March 2009
Licensed content volume number	33
Licensed content issue number	6
Number of pages	7
Type of Use	reuse in a thesis/dissertation
Portion	figures/tables/illustrations
Number of figures/tables/illustrations	4
Format	both print and electronic
Are you the author of this Elsevier article?	No
Will you be translating?	No
Order reference number	
Title of your thesis/dissertation	An investigation into nucleic acid binding compounds
Expected completion date	Aug 2012
Estimated size (number of pages)	250
Elsevier VAT number	GB 494 6272 12
Permissions price	0.00 GBP
VAT/Local Sales Tax	0.00 USD / 0.00 GBP
Total	0.00 GBP

Appendix 7

Licensed content publisher	Elsevier
Licensed content publication	Molecular Cell
Licensed content title	Prospects for Riboswitch Discovery and Analysis
Licensed content author	Ronald R. Breaker
Licensed content date	16 September 2011
Licensed content volume number	43
Licensed content issue number	6
Number of pages	13
Type of Use	reuse in a thesis/dissertation
Portion	figures/tables/illustrations
Number of figures/tables/illustrations	3
Format	both print and electronic
Are you the author of this Elsevier article?	No
Will you be translating?	No
Order reference number	
Title of your thesis/dissertation	An investigation into nucleic acid binding compounds
Expected completion date	Aug 2012
Estimated size (number of pages)	250
Elsevier VAT number	GB 494 6272 12
Permissions price	0.00 GBP
VAT/Local Sales Tax	0.00 USD / 0.00 GBP
Total	0.00 GBP

Appendix 8

Licensed content publisher	Elsevier
Licensed content publication	Cell
Licensed content title	Flipping Riboswitches
Licensed content author	Evgeny Nudler
Licensed content date	14 July 2006
Licensed content volume number	126
Licensed content issue number	1
Number of pages	4
Type of Use	reuse in a thesis/dissertation
Portion	figures/tables/illustrations
Number of figures/tables/illustrations	3
Format	both print and electronic
Are you the author of this Elsevier article?	No
Will you be translating?	No
Order reference number	
Title of your thesis/dissertation	An investigation into nucleic acid binding compounds
Expected completion date	Aug 2012
Estimated size (number of pages)	250
Elsevier VAT number	GB 494 6272 12
Permissions price	0.00 GBP
VAT/Local Sales Tax	0.00 USD / 0.00 GBP
Total	0.00 GBP

Appendix 9

Licensed content publisher	The American Association for the Advancement of Science
Licensed content publication	Science
Licensed content title	Structure of the Eukaryotic Thiamine Pyrophosphate Riboswitch with Its Regulatory Ligand
Licensed content author	Stéphane Thore, Marc Leibundgut, Nenad Ban
Licensed content date	May 26, 2006
Volume number	312
Issue number	5777
Type of Use	Thesis / Dissertation
Requestor type	Scientist/individual at a research institution
Format	Print and electronic
Portion	Figure
Number of figures/tables	2
Order reference number	
Title of your thesis / dissertation	An investigation into nucleic acid binding compounds
Expected completion date	Aug 2012
Estimated size(pages)	250
Total	0.00 GBP

Appendix 10

The multiplicities of the carbons of the pentafluorophenol esters **84** and **87** in their ^{13}C NMR spectra have been defined as multiplets as the intensity is particularly low and the multiplicities difficult to assign. As an example, a zoomed view of the ^{13}C NMR spectrum of **87** is shown below where the signals due to the pentafluorophenol appear in the region 136-143 ppm.